A toolkit to visualise and interfere with ubiquitin-dependent DNA damage bypass

Dissertation

submitted to attain the academic degree

Doctor of Natural Sciences (Dr. rer. nat.)

Department of Biology

Johannes Gutenberg University Mainz

George Yakoub

April 2020

Declaration

Herewith I, George Yakoub, declare that the work presented in this thesis is my very own. I confirm that any information or data that have been derived from other sources are referred to and correctly cited in the thesis.

Abstract

Genome replication is a fundamental process for growth and proliferation. Therefore, timely resolution of replication problems protects daughter cells from genomic instability. In eukaryotes, DNA damage bypass safeguards cells against replication stress. This pathway is regulated by ubiquitylation of the replicative clamp, proliferation cell nuclear antigen (PCNA). Monoubiquitylation of PCNA activates error-prone translesion synthesis. Alternatively, attachment of K63-linked polyubiquitin chains on PCNA promotes error-free template switching. Whereas the specifics of translesion synthesis are well characterised, activation of template switching is still puzzling. In this project, I was interested to understand how cells choose one pathway over the other in response to genotoxic stress and discover yet unknown factors involved in polyubiquitin-dependent template switching. Our collaborator developed PCNA-specific reagents that bind to mono- and polyubiquitylated PCNA *in vitro*. These probes contain a PCNA-interacting peptide box and ubiquitin-binding domains (UBD) that selectively recognise ubiquitin modification with a relevant geometry. I adapted the probes for *in vivo* tools using various experimental strategies, e.g. microscopy, genomics, and genetic screening in the budding yeast *Saccharomyces cerevisiae*.

In the first approach, I converted the probes into fluorescent sensors to perform live-cell imaging. By using an inducible system in wild type and mutant yeast cells deficient in PCNA ubiquitylation, I showed that these sensors bind PCNA exclusively and act in a pathway-specific manner. Upon replication stress, ubiquitylated PCNA forms distinct nuclear foci that emerge during early S phase and resolve later in the G2/M phase. Analysis of the localisation and appearance of ubiquitylated PCNA by tracing fluorescently tagged replisomes and repair factors revealed that PCNA ubiquitylation is activated mainly behind replication forks and close to postreplicative repair territories (PORTs). Unlike DNA double-strand breaks and collapsed replication forks, damaged DNA marked by ubiquitylated PCNA does not reside at the nuclear pores or the nuclear periphery. Moreover, by studying the relative distribution of ubiquitylated PCNA between nuclei and nucleoli, I demonstrated that bypass events are less frequent in nucleoli.

In the second experimental strategy, I used the novel PCNA sensors in a genomics approach to investigate the genome-wide association of ubiquitylated PCNA. Although the sensors enriched on chromatin in a DNA damage specific manner, their enrichment was independent of PCNA ubiquitylation. I showed that UBDs of the sensors were responsible for the unspecific binding to damaged chromatin.

In the third and complementary approach, I utilised the probes to search for interactors of polyubiquitylated PCNA. Overexpression of the polyubiquitin-specific probe inhibited error-free template switching and rendered cells sensitive to DNA damage, likely by competing with factors that bind to polyubiquitinated PCNA. I expected that an overexpression genetic screen would identify factors that suppress the sensitising effects of the probe. Performing such a screen unveiled that Rad5's ubiquitin ligase and helicase functions were necessary to suppress the probe.

Zusammenfassung

Die Genomreplikation ist ein wesentlicher Prozess für das Wachstum und die Proliferation. Eine rechtzeitige Auflösung von Replikationsproblemen bewahrt Tochterzellen vor genomischer Instabilität. In Eukaryoten beschützt der so genannte "DNA Schadenstoleranz" die Zellen vor Replikationsstress. Dieser biologische Signalweg wird durch Ubiquitylierung von PCNA reguliert. Die Monoubiquitylierung von PCNA aktiviert die fehleranfällige Transläsionssynthese. Hingegen fördert die Konjugation von K63-verknüpften Polyubiquitin-Ketten auf PCNA das fehlerfreie Strang-Austausch. Im Gegenteil zur gut erforschten Transläsionssynthese, bleibt die Aktivierung des Strang-Austausch immer noch rätselhaft. Das Ziel meinem Projekt war zu verstehen, wie Zellen, die unter genotoxischem Stress leiden, zwischen den beiden Arten von DNA Schadenstoleranz wählen. Ebenso neue Faktoren des Strang-Austausch zu identifizieren. Unserer Kollaborateur entwickelte PCNA-spezifische Reagenzien, welche *in vitro* selektiv an mono- und polyubiquityliertes PCNA binden. Diese Sonden enthalten eine PCNA-interagierende Peptidbox und Ubiquitin-Bindungsdomänen (UBD), welche Ubiquitin-Modifikationen einer relevanten Geometrie spezifisch erkennen. Ich habe die Sonden als *in vivo* Werkzeuge angepasst, um sie in verschiedenen experimentellen Anwendungen einzusetzen, wie zum Beispiel in Mikroskopie, Genomik und im genetischen Screening in der Bäckerhefe *Saccharomyces cerevisiae*.

Im ersten Ansatz habe ich die Sonden als fluoreszierende Sensoren verwendet, um eine Lebendanalyse von Zellen durchführen zu können. Durch die Verwendung eines induzierbaren Systems in Wildtyp und mutierten Hefezellen, denen die PCNA-Ubiquitylierung fehlt, habe ich nachgewiesen, dass diese Sensoren ausschließlich an PCNA binden und spezifisch in diesem Signalweg wirken. Während des Replikationsstresses bildet ubiquityliertes PCNA ausgeprägte Foci im Zellkern. Diese Foci entstehen früh in der S-Phase und lösen sich später in der G2/M-Phase auf. Eine zeitlich-aufgelöste Analyse mit fluoreszenzmarkierten Replisom- und Reparaturfaktoren ergab, dass die PCNA-Ubiquitylierung überwiegend nach der Replikation und in der Nähe von postreplikativen Reparatur-Territorien aktiviert wird. Im Gegensatz zu DNA-Doppelstrang Schäden und kollabierten Replikationsgabeln werden die durch ubiquityliertes PCNA markierte DNA Schäden, nicht an die Kernporen oder die Kernperipherie rekrutiert. Darüber hinaus habe ich durch die Untersuchung der relativen Verteilung von ubiquityliertem PCNA zwischen Zellkernen und Nukleoli nachgewiesen, dass DNA Schadenstoleranz in Nukleoli weniger häufig verwendet wird.

Im zweiten Abschnitt meiner Arbeit habe ich die PCNA-Sensoren verwendet, um die Verteilung von ubiquityliertem PCNA genomweit zu untersuchen. Obwohl eine schadensspezifische Anreicherung der Sensoren an Chromatin gemessen werden konnte, geschah dies unabhängig von der PCNA-Ubiquitylierung. Ich konnte zeigen, dass die UBDs der Sensoren für diese unspezifische Bindung an beschädigtes Chromatin verantwortlich waren.

In der dritten und komplementären Strategie nutzte ich die Sonden, um Interaktoren von polyubiquityliertem PCNA zu identifizieren. Die Überexpression der Polyubiquitin-spezifischen Sonde

hemmte das Strang-Austausch und machte die Zellen empfindlich gegen DNA-Schäden. Wahrscheinlich geschah dies durch die Kompetition mit zelleigenen Faktoren, die an polyubiquityliertes PCNA binden. Ich erwartete, dass ein genetisches Überexpression-Screening Interaktoren, die sensibilisierenden Wirkungen der Sonde unterdrücken, identifizieren könnte. Dieser Screen enthüllte, dass die Ubiquitin-Ligase und Helikase Funktionen von Rad5 notwendig waren, um den inhibitorischen Effekt der Sonde zu unterdrücken.

Acknowledgments

I would like to extend my gratitude to everyone who supported me throughout my time as a PhD student. First, I want to express my warm thanks to my PhD supervisor for offering me an exciting project that let me grew as an independent scientist, learning a multitude of techniques and gaining confidence on the way. Thank you very much, for believing in me, supporting and giving ceaseless advice, regardless of all the hurdle that the project went through.

I would like to acknowledge all the members of my thesis advisory committee for their valuable advice and input in bringing my project further to its current diverse and exciting stage. A big thanks goes to our neighbour lab for allowing me to overuse the ROTOR, providing protocols, strains, the ORF library, and for all the fun collaborations.

I want to take a moment to thank all my colleagues, who were there to hear my complains, encourage and support me during the ups and downs of my project, teaching me yeast genetics, and building up a cheerful working atmosphere. A huge thanks to my family and friends in Germany and abroad for always being there to help and support me pursuing my PhD.

Furthermore, I am thankful for all the support that I received from IMB's core facilities and the scientific management, in particular, the grants office and IPP coordinators for their encouragements. I sincerely acknowledge the Boehringer Ingelheim Fonds not only for the financial support but also for the excellent training and networking opportunities.

Contents

List of Figures

List of Tables

Chapter 1

Introduction

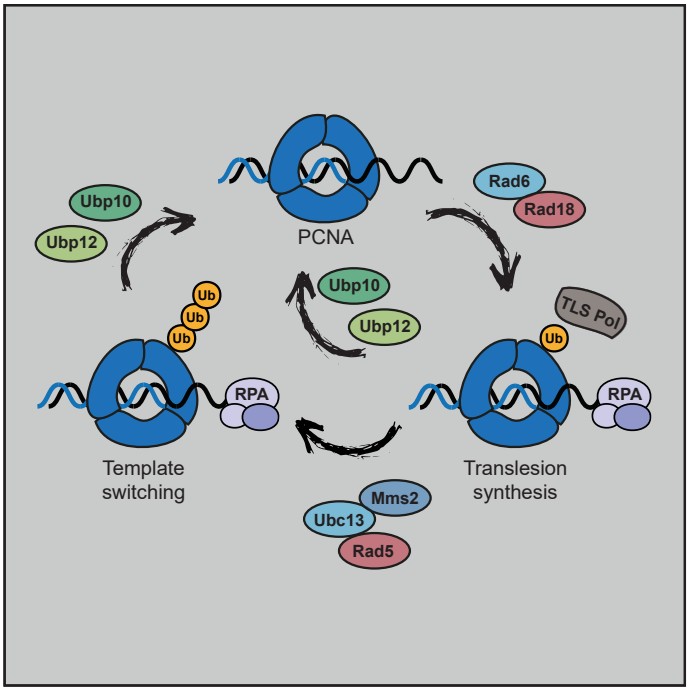

In a nutshell

This introductory chapter aims to make the reader familiar with the concepts, terminology, and fundamentals of post-translational modification with ubiquitin and DNA damage bypass, to pave the way into the objectives of the study and review some of the discovered and unexplored aspects of ubiquitylation and DNA damage bypass.

1.1 Signalling by ubiquitin

Almost every protein in a eukaryotic cell encounters a post-translational modification (PTM) during its lifetime. PTMs extend the chemical repertoire of the 20 standard amino acids by modifying an existing functional group or introducing a new one. The reversible nature of PTMs makes them act as cost and energy-efficient mechanisms for modulating and regulating protein function in contrast to *de novo* protein turnover. PTMs include alterations in protein secondary structure, like cleavage of precursor proteins by specific proteases or formation of disulphide bridges; addition of small functional groups, such as phosphorylation, acetylation, and methylation; and attachment of larger molecules or even whole proteins, like glycosylation, glycation, ubiquitylation, SUMOylation, and NEDDylation [1]. Among these PTMs, ubiquitylation has a particular structural and functional flexibility and controls a myriad of essential biological processes [2, 3].

1.1.1 Ubiquitin structure

Ubiquitin (Ub) is an evolutionarily conserved small protein containing 76 amino acids with a 96% sequence identity between human and yeast [4]. *Saccharomyces cerevisiae* has four ubiquitin-coding loci in which *UBI1*, *UBI2*, and *UBI3* are ubiquitin-ribosomal fusions, whereas *UBI4* is a polyubiquitin precursor consisting of five head-to-tail repeats [5]. Mammalian cells have a similar organisation of the ubiquitin genes. Cleavage of the ubiquitin fusions and the precursor proteins release the N- and C-termini that refold and create the mature monomeric ubiquitin with a compact globular structure [6, 7]. The prominent secondary structures of ubiquitin include an α-helix with three and a half turns, a short piece of 3_{10}-helix, a mixed β-sheet that contains five strands, and seven reverse turns (Figure 1.1.1 A) [8]. Ubiquitin is stable over a wide range of pH and temperatures and against protease digestion, although it contains seven lysine and four arginine residues [9]. The C-terminus of ubiquitin containing the LRGG motif is the only part that protrudes out of the protein. This flexible motif does not interact with the rest of the molecule and can form peptide and isopeptide bonds. The proteasome and the majority of ubiquitin-binding domains (UBDs) recognise ubiquitin through its exposed I44 hydrophobic patch centred on L8, I44, V70 [10, 11]. Another hydrophobic surface involves I36, L71, and L73 of the ubiquitin tail (Figure 1.1.1 A). The I36 patch mediates interactions between ubiquitin moieties in ubiquitin chains and provides a binding surface for ubiquitin ligases, UBDs, and deubiquitylating enzymes (DUBs). Ubiquitin contains several other important motifs and interaction surfaces, like the TEK-box that includes T12, T14, E34, K6, and K11 [2, 12, 3]. Other small proteins with folds similar to ubiquitin have also been identified, among which are NEDD8, SUMO1, SUMO2, SUMO3, ATG8, ISG15, and FAT10. These proteins are collectively called ubiquitin-like proteins (Ubls) [2].

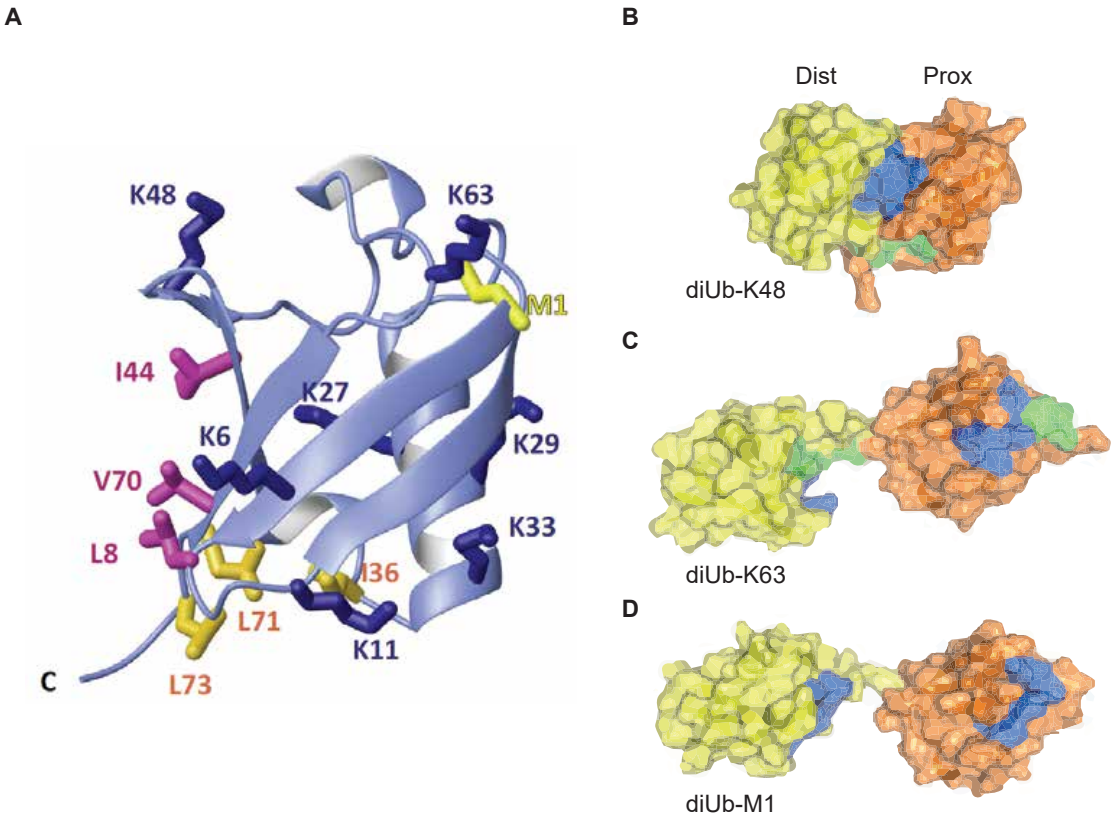

Figure 1.1.1: Ubiquitin structure and topologies. (A) Ribbon representation of monoubiquitin, protein data bank, PDB: 1ubq [2]. The I44 patch is highlighted in magenta, the I36 patch in orange, ubiquitin's seven acceptor lysine residues in blue, and the N-terminus in yellow. (B-D) Diubiquitin (diUb) molecules of different linkages are shown with the distal (dist) molecule in yellow and the proximal (prox) molecule in orange. I44 (blue) and I36 (green) patches are indicated. (B) K48-linked diUb, PDB: 1aar [13]. (C) K63-linked polyubiquitin, PDB: 2jf5 [14]. (D) M1-linked polyubiquitin, PDB: 2w9n [14]. The figure is modified from Komander *et al.*, 2012 and Alfano *et al.*, 2016 [3, 2].

1.1.2 The ubiquitylation cascade

Conjugation of ubiquitin to target proteins happens in a sequential enzymatic activity of ubiquitin-activating (E1), ubiquitin-conjugating (E2), and ubiquitin-ligating (E3) enzymes. An E1 initiates the ubiquitylation cascade by ATP consumption and activation of ubiquitin trough thioesterification. Subsequently, the activated ubiquitin is transferred to the active site cysteine of an E2. Finally, an E3 brings the E2-Ub complex in proximity to the substrate and catalyses a covalent transfer of the ubiquitin moiety either to the ε-amino group of a lysine residue or to the extreme amino terminus of a polypeptide. Ubiquitin itself carries seven lysine residues and a methionine on its N-terminus. Successive rounds of conjugation lead to the formation of polyubiquitin chains. DUBs cleave or trim ubiquitylated substrates and polyubiquitin chains to reverse or modulate the biological outcome (Figure 1.1.2) [15, 12, 16, 17]. The ability to form structurally distinct ubiquitin chains and the dynamic assembly and disassembly of the modification increase the complexity of the ubiquitin code. Similar to any conventional language or functional code, the ubiquitin code requires a specific assembly of factors and meaningful sequence of events that would set the command, decode the message, and terminate the signal promptly. Such

an ordered arrangement in ubiquitylation is brought by the ubiquitin code writers, readers, and erasers. In this section, I will shortly describe the function, diversity, and the importance of each player in the ubiquitin code.

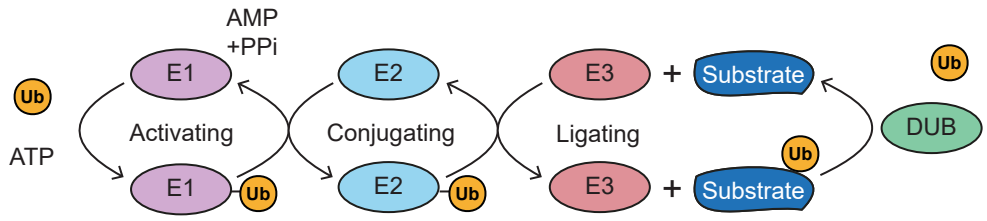

Figure 1.1.2: Enzymatic cascade of ubiquitylation. The activity of three enzymes is required for ubiquitylation: a ubiquitin-activating enzyme (E1), a ubiquitin-conjugating enzyme (E2) and a ubiquitin ligase (E3) that recognises the substrate. The completion of one ubiquitylation cycle results in a monoubiquitylated substrate. The action of a deubiquitylating enzyme (DUB) reveres the modification [16]. For more details, see the main text (1.1.2).

1.1.3 Ubiquitin chain topologies

Ubiquitylation of proteins happens in various modes and flavours. Monoubiquitylation is the attachment of a single ubiquitin molecule to a substrate, such as ubiquitylation of proliferating cell nuclear antigen (PCNA) on the conserved K164 [18]. In contrast, multiubiquitylation is the attachment of multiple single ubiquitin molecules to several acceptor lysines as for the epidermal growth factor receptor (EGFR) [19]. Mono- or multiubiquitylation often mediates functions such as protein binding, subcellular localisation, intracellular trafficking, and modulation of activity [20]. A substrate-attached ubiquitin can be itself a target for ubiquitylation, where modification of the N-terminal methionine or one of the seven lysine residues forms polymeric ubiquitin chains. These chains can be short with two ubiquitin molecules or long, carrying more than ten moieties [3]. During chain elongation, modification of similar residues results in homogenous ubiquitin chains, like in M1- (or linear), K11-, K48-, or K63-linked chains (Figures 1.1.1 and 1.1.3). Chains with mixed topologies arise when different linkages form between succeeding ubiquitin moieties (Figure 1.1.3), as seen in protein trafficking [21]. Modification of single ubiquitin with multiple molecules creates a unique coding signal of branched ubiquitin chains, for example, the role of K48-K63 branched chains in activation of NF-kB signalling [22] (Figure 1.1.3).

1.1.4 Biological functions of ubiquitin and its homogenous chains

Cells make use of ubiquitin chains with all possible linkages [23]. The role of ubiquitin chains in cellular physiology was established by fundamental and incentive studies of the canonical K48-, K63-linked, and linear chains, which function mainly in protein degradation, stress signalling, and immune response. Quantification of the different polyubiquitin chains in yeast revealed the abundance of noncanonical linkages as well (i.e. K6, K11, K27, K29, and K33) [24]. Continuous development of new methods to detect ubiquitin modifications is assigning specific functions to these noncanonical ubiquitin chains [25, 26].

1.1.4.1 Proteolytic functions of ubiquitin

Proteasomal degradation

A role for ubiquitin chains in targeting proteins for 26S proteasome was first assigned to K48-linked chains [27]. Several E3s, like Skp-Cullin-F-box containing complex (SCF) and E6-associated protein (E6AP), involve in substrate turnover by attaching K48-linked chains to their targets [28, 29], making these type of chains to be the most abundant in quantitative proteomic studies [24, 30, 26]. Inhibition of proteasome leads to a rapid increase not only in K48-linked chains but also other atypical linkages, suggesting that they contribute to protein degradation [24]. For example, proteasomal receptors recognise K11-linked chains on cell cycle regulators and trigger their degradation during mitosis. The anaphase-promoting complex/cyclosome (APC/C) is one of the main E3s to produce K11 linkages in mammalian cells. Inhibition of K11-linked chain formation stabilises APC/C substrates and causes cell cycle arrest [31, 32]. For efficient ubiquitylation coupled degradation, APC/C and SCF interact directly with the proteasome [33, 34].
Other types of ubiquitin chains involve in proteasomal degradation less frequently. The role of K29-linked chains in substrate turnover is evident in the ubiquitin-fusion-degradation (UFD) pathway [35]. K63-linked chains are also reported to trigger degradation, in which K63 polyubiquitylation of p120 by the E3 Rsp5 is sufficient for proteasome binding and subsequent processing [36]. The diversity in targeting signals reflects the plasticity in substrate recognition by proteasomal subunits [37].

Lysosomal degradation

Lysosomes are proteolytic compartments that degrade plasma membrane proteins and protein aggregates. Degradation of substrates happens through monoubiquitylation or K63-linked polyubiquitylation [38]. The E3 Rsp5 ubiquitylates its substrates at the cell membrane leading to endocytosis of yeast membrane receptors [39]. Ubiquitylation can also happen at the endosomal membrane after internalisation to control the localisation of substrates, as reported for EGFR [40].

1.1.4.2 Nonproteolytic functions of ubiquitin

Monoubiquitylation, linear, and K63-linked ubiquitin chains are the main contributors for nonproteolytic features of the ubiquitin code. These functions include regulation of a substrate's interactions, changes in its localisation, and modulation of its activity.

Manipulating protein interactions

Monoubiquitylation efficiently recruits binding partners. For example, attachment of a single ubiquitin to PCNA initiates ubiquitin-dependent polymerase switch that rescues stalled replication forks [18]. Similarly, monoubiquitylation of FANCD2 and FANCI, proteins involved in interstrand crosslink DNA repair, recruits the nuclease FAN1 for damage processing [41]. K63-linked chains also regulate protein interactions. For instance, K63 polyubiquitylation of a ribosomal protein stabilises polysomes and promotes translation [42]. Besides, K63-linked chains have an evident role in DNA damage signalling,

where the recruitment of the E3 (RNF168) and several repair factors (BRCA1 and RAP80), is dependent on such chain topologies. These factors, in turn, create a ubiquitin-rich environment to initiate repair of the damage and halt the cell cycle [43].

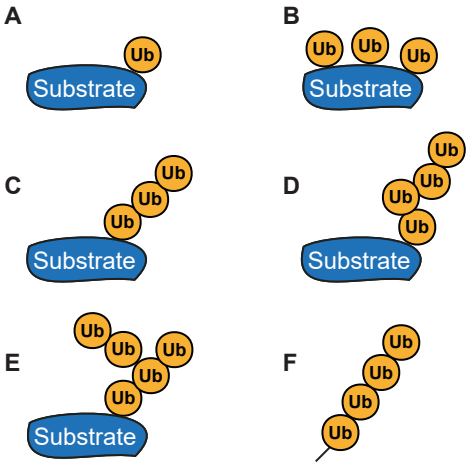

Figure 1.1.3: The different modes of ubiquitylation. (A) Monoubiquitylation. (B) Multimonoubiquitylation. (C) Homogenous ubiquitin chain. (D) Heterogenous ubiquitin chain. (E) Branched ubiquitin chain. (F) Unanchored ubiquitin chain [44].

Manipulating protein localisation

Ubiquitin-dependent changes in localisation were first described in yeast, where monoubiquitylation of plasma membrane proteins was reported to lead to their internalisation [39]. Multiubiquitylation of the transcription factor p53 results in its nuclear export, likely because of changes in the accessibility of the nuclear export sequence [45].

Manipulating protein activity

Distinct types of ubiquitin chain topologies regulate protein activity through inhibitor degradation, proteasomal processing, allosteric activation, or recruitment of an activator. For example, the NF-kB transcription factor is activated, once its inhibitor, IkBα, is degraded by modification with K48-linked chains [46]. In contrast, the proteasomal cleavage of inhibitory domains activates the NF-kB precursor [47]. NEMO is a subunit of the IkBα kinase (IKK) complex. Linear ubiquitin chains on NEMO are recognised by NEMO itself, causing an allosteric activation of IKK [48]. Besides, K63-linked chains promote binding of IKK to its upstream activator kinase TAK1 [49].

1.1.5 Writing the ubiquitin code

In *S. cerevisiae*, the ubiquitin conjugation machinery shows hierarchical organisation with one E1 (1-2 in humans), 11 E2s (~ 40 in humans), and 60-100 of E3s (more than 700 in humans). This section briefly describes the characteristics, functions, and diversity of each factor as well as the unidirectional manner of ubiquitin conjugation.

1.1.5.1 Ubiquitin-activating enzymes

The essential *UBA1* gene encodes the single E1 protein in yeast [50]. The temperature-sensitive *uba1* allele (*uba1-206*) shows rapid depletion of ubiquitin conjugates at the nonpermissive temperature [51]. Multiple E1s are found in higher eukaryotes, like UBA1 and UBA6 in humans [52, 53].

1.1.5.2 Ubiquitin-conjugating enzymes

The E2s lie at the centre of the ubiquitylation cascade. They interact both with an E1 and E3s, ensuring a unidirectional transfer of ubiquitin from an E1 to the substrate. E1 and E3s share a binding site on E2s, which prevents recharging of E2s bound to E3s and forces their disassembly before the next round of conjugation [54]. A total of 13 yeast *UBC* genes exist of which Ubc9 conjugates the ubiquitin-like protein Smt3 (mammalian SUMO), whereas Ubc12 conjugates Rub1 (mammalian NEDD8) [55, 56]. Among the 11 ubiquitin-specific E2, only Cdc34/Ubc3 is essential for viability [57]. Some E2 are highly similar and function redundantly in the conjugation of ubiquitin to a particular substrate, whereas many other substrates may rely on a single E2. E2s can also operate sequentially for efficient substrate polyubiquitylation in two distinct conjugation events. For example, the rate-limiting monoubiquitylation step of PCNA is catalysed by Rad6, followed by cycles of ubiquitin chain elongation by Ubc13/Mms2 [18]. Nevertheless, the same E2 can often catalyse both mono- and polyubiquitylation. Ubiquitin-conjugating enzymes are also important to define the polyubiquitin chain architecture. Principally, E2s dictate the linkage type when paired with really interesting new gene (RING) ubiquitin ligases, whereas homologous to E6AP C-terminus (HECT) E3s override any intrinsic chain topology preference of E2s [37].

1.1.5.3 Ubiquitin ligases

Ubiquitin ligases (E3s) are the largest group of proteins involved in ubiquitylation. They interact directly with E2s and substrates, mediating the exquisite selectivity of ubiquitylation [58, 37]. All E3s fall into two major classes: HECT and RING domain E3s. These two classes of E3s follow distinct mechanisms to catalyse ubiquitylation.

HECT ubiquitin ligases

The homologous to E6AP C-terminus (HECT) E3s are named after their founding member E6AP that ubiquitylates mammalian p53 in cells expressing the human papillomavirus protein E6. The HECT domain is a 350 amino acid stretch consisting of N- and C-terminal lobes. The N-terminal lobe binds an E2, whereas the C-terminal lobe contains the active site cysteine, which forms a thioester intermediate

with ubiquitin received from an E2 before its transfer to the substrate (Figure 1.1.4) [59, 60]. In HECT E3s, the E3-Ub thioester intermediate defines the linkage type during ubiquitin chain synthesis [29].

RING domain ubiquitin ligases

The really interesting new gene (RING) E3s are the biggest class of ubiquitin ligases. RING domains coordinate two Zn^{2+} ions in a cross-braced arrangement that facilitates interaction with E2s [61]. The two proteins of the U-box family (Ufd2 and Prp19) adopt a RING-like structure without employing metal ions [15, 62]. Unlike HECT E3s, RING E3s do not form thioester intermediates; instead, they directly transfer the ubiquitin from the charged E2-Ub to the acceptor lysine in the substrate (Figure 1.1.4). Substrate-binding domains either within the same RING protein (single subunit RING E3s) or specialised substrate receptors (multisubunit RING E3s) facilitate the binding of E3s with their cognate substrates [15]. Examples of the single subunit RING E3s are Rad18 and Rad5, which catalyse the sequential mono- and polyubiquitylation of PCNA [18]. One of the most sophisticated members of the multisubunit RING E3s is the APC/C consisting of 13 subunits. APC/C has an essential role in controlling the mitotic cell cycle progression [63, 64]. Cullin-RING ligases (CRLs) are another example of multisubunit RING E3s. A typical CRL contains four subunits: a cullin, the RING protein Hrt1, a linker protein, and an alternative substrate receptor. A cullin forms the central scaffold subunit that binds on its C-terminus with the RING subunit Hrt1, whereas the N-terminus of cullin interacts with the substrate receptor via a linker protein [28, 65].

RBR ubiquitin ligases

The RING-in-between-RING (RBR) proteins form a subclass of RING E3s and function as RING/HECT hybrids. One RING domain binds E2s and stimulates the transfer of ubiquitin onto an active site cysteine in the second RING domain, generating an E3-Ub thioester intermediate before conjugating the ubiquitin moiety onto the substrate. RBRs are conserved in all eukaryotes and play essential roles in biology [66, 67].

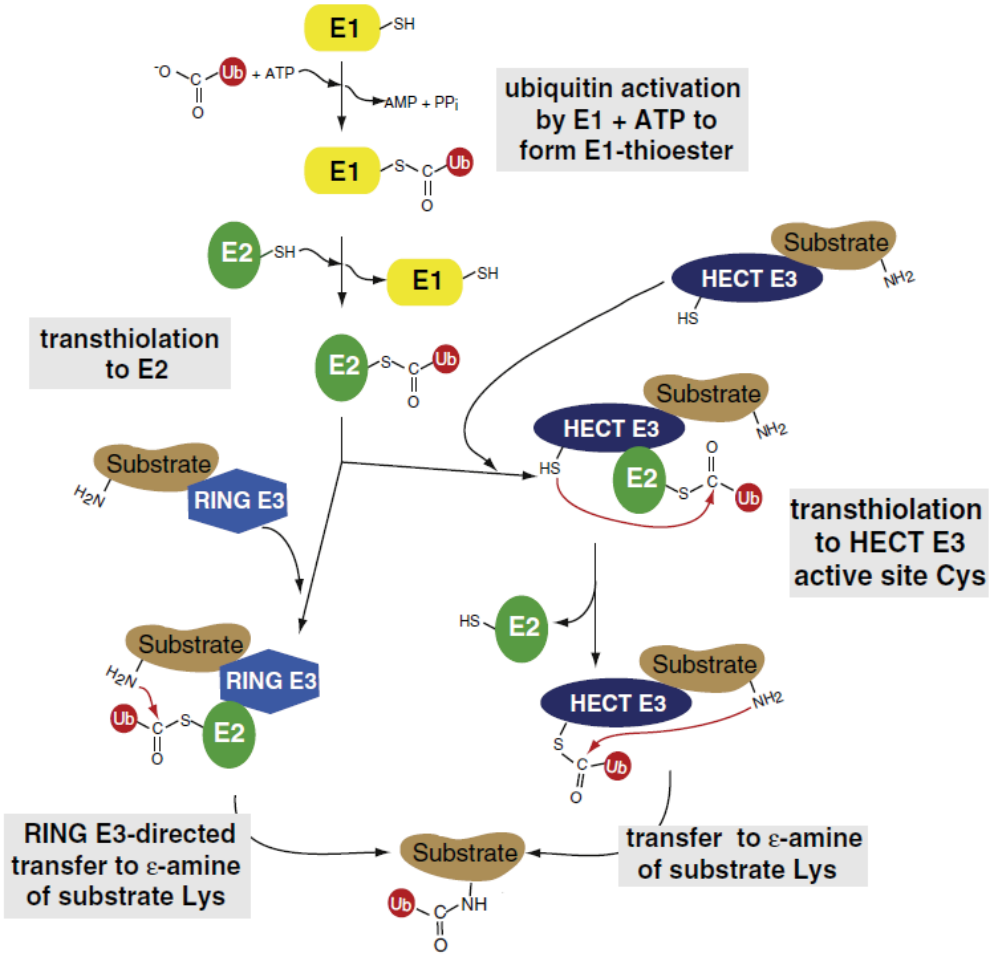

Figure 1.1.4: Ubiquitylation by HECT and RING E3s. For details, see the description in the main text (1.1.5.3). The figure is modified from Metzger *et al.*, 2014 [62].

1.1.6 Reading the ubiquitin code

Receptor proteins with ubiquitin-binding domains (UBDs) read and translate the ubiquitin code into specific outcomes [16]. UBDs are small (20-150 amino acid) independently folded domains that interact directly with monoubiquitin, polyubiquitin chains, or both [68]. UBDs are usually found in ubiquitin code writers (E1, E2s and E3s), readers, and erasers (DUBs). There are more than twenty different families of UBDs, and the number of newly identified UBDs is on the rise. UBDs diverge both in structure and in the type of ubiquitin recognition, allowing them to recognise and distinguish different types of ubiquitin modifications and contribute to diverse biological functions. The most common structures of UBDs are α-helixes, like ubiquitin-interacting motif (UIM) and ubiquitin-binding in ABIN and NEMO (UBAN); zinc fingers, like ubiquitin-binding ZnF (UBZ) and nuclear localisation-4 ZnF (NZF); ubiquitin-conjugating (UBC) domains present in E2 enzymes; or pleckstrin homology (PH) folds [16]. The widespread use of the I44-containing surface by UBDs makes the binding of UBDs to ubiquitin mutually exclusive. This exclusive binding mode may prevent each ubiquitin from stimulating multiple processes, leading to discordance within the cell. However, there are several exceptions to this rule. In the

following subsections, I describe the principles by which distinct classes of UBDs interact with ubiquitin modifications.

1.1.6.1 Recognising the distance between ubiquitin moieties

The distance between successive ubiquitin moieties differs broadly in different ubiquitin chain types. Ubiquitin receptors containing tandem repeats of UIMs exploit this property by variating the spacer between the UBDs [69, 70]. UIMs consist of an α-helix with a hydrophobic binding site for the I44 patch of ubiquitin [71]. In RAP80, a seven-residue linker separates two UIMs, positioning them to recognise extended K63-, but not compact K48-linked chains (Figure 1.1.5 A) [69, 70]. In contrast, a short linker of two residues sets apart the two UIMs of Ataxin-3, which results in preferential binding to the compact K48 linkages. Importantly, swapping the linkers between these two proteins switches their chain selectivity, which emphasises the effect of the linker length in conferring binding specificity [70].

1.1.6.2 Recognising the linkage environment

The isopeptide bond between two ubiquitin moieties provides another interaction surface for receptors containing UBDs. For instance, the K63-linkage specific antibody interacts with the C-terminus and the I36 patch of the distal ubiquitin (Figure 1.1.5 E). Besides, residues in the proximity of K63 on the proximal ubiquitin mediate antibody binding [72]. The UBAN domain of NEMO, a subunit of IkB kinase, also recognises the linkage environment of linear ubiquitin chains, resulting in 100-fold higher affinity to linear than to K63-linked chains [44, 48, 73]. The symmetrical dimer of NEMO with two adjacent UBDs interacts asymmetrically with linear chains. One UBD recognises the distal I44 patch and the second binds to the proximal F4 (Figure 1.1.5 D) [48]. Besides, the Q2 at the linkage environment of the proximal ubiquitin makes a fundamental interaction. When binding to K63-linked chains, NEMO recapitulates the interactions only with the distal patch, resulting in a weaker single site-binding mode [73].

1.1.6.3 Recognising ubiquitin chain flexibility

The UBA domains of proteasomal shuttling factors slot into a K48-linked ubiquitin dimer to interact with I44 patches of both ubiquitin molecules (Figure 1.1.5 C). This event requires a dynamic opening of the compact K48-linked chains [74, 75], referring to the importance of ubiquitin chain flexibility for recognition of a particular linkage. Similarly, the dynamic nature of K63-linked ubiquitin chains allows the NZF domain of TAB2, an adaptor of the TAK1 kinase complex, to distinguish between structurally similar K63-linked and linear chains. The conformational constraints imposed by TAB2 on K63-linked chains cannot be adopted by linear chains (Figure 1.1.5 B) [69, 76].

1.1.6.4 Utilising multiple binding surfaces

Recognising different surfaces in multiple ubiquitin moieties of a chain can also contribute to the specificity of a UBD. For example, the ubiquitin editing protein A20 binds preferentially K63-linked chains via distinct interactions with the I44 patch, the TEK-box, and a surface around D58 of different ubiquitin molecules (Figure 1.1.5 F) [77].

1.1.6.5 Capturing free C-termini

Cleavage of ubiquitin chains by deubiquitylating enzymes and production of unanchored chains by E3s create free ubiquitin C-termini. The zinc-finger UBD (ZnF-UBP) of the DUB Isopeptidase T (IsoT, or USP5) contains a deep binding pocket, where the C-terminal diglycine motif of ubiquitin is inserted. This binding is necessary for the catalytic activity of IsoT [78]. Such a domain is present in several other protein families. Similarly, the crystal structure of HDAC6 bound to ubiquitin shows that the ZnF-UBP of HDAC6 sequesters the free ubiquitin diglycine into a deep pocket (Figure 1.1.5 G) [79].

1.1.6.6 Simultaneous binding to substrate and chain

The ubiquitin recognition modes described above are mostly independent of the substrate carrying the ubiquitin chains. Nevertheless, several reader proteins can simultaneously bind to ubiquitin and the target molecule via multiple binding surfaces. For instance, a conserved UBZ and a PCNA-interacting peptide (PIP box) in the TLS polymerase η (Pol η) allow its selective binding to ubiquitylated PCNA [80], thereby activating the error-prone DNA damage bypass. Another example is the DNA helicase Zinc finger RANBP2-type containing 3 (ZRANB3). It interacts with PCNA via a PIP box and an AlkB homolog 2 PCNA-interaction motif (APIM). ZRANB3 also binds K63-linked ubiquitin chains via an NZF zinc finger. The combined effects of these motifs allow ZRANB3 to recognise preferentially K63-linked polyubiquitylated PCNA [81, 82, 83]. Similarly, with its UBZ domain, the FAN1 nuclease promotes ICL repair by specifically binding to ubiquitylated FANCD2–FANCI dimers [84]. In DSB repair signalling, 53BP1 reads the ubiquitin mark on histone H2A with its ubiquitylation-dependent recruitment (UDR) motif and simultaneously binds methylated K20 on histone H4 via a Tudor domain [85].

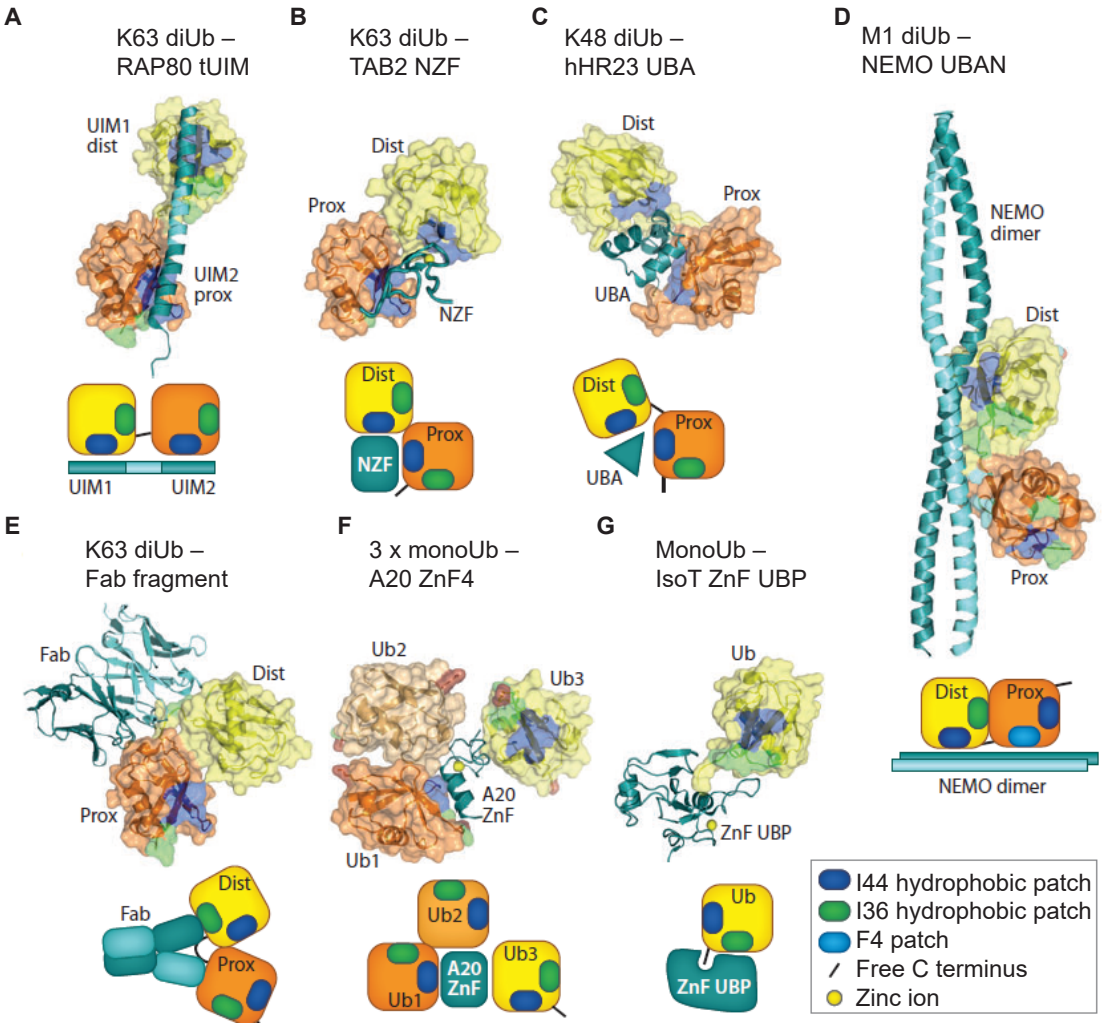

Figure 1.1.5: Principles of ubiquitin recognition. Ubiquitin binding domains are depicted in cyan. Diubiquitin (diUb) molecules are shown with the distal (dist) molecule in yellow and the proximal (prox) molecule in orange. Zinc ions are shown as yellow spheres. (A) Crystal structure of the RAP80 tandem ubiquitin-interacting motif (tUIM) bound to K63-linked diubiquitin, PDB: 3a1q [69]. (B) Crystal structure of the TAB2 NZF domain bound to K63-linked diubiquitin, PDB: 2wwz [76]. (C) NMR model of the hHR23 UBA domain and K48-linked diubiquitin, PDB: 1zo6 [74].(D) Crystal structure of the NEMO UBAN domain bound to linear diubiquitin, PDB: 2zvn [48]. (E) Crystal structure of the K63-specific antibody (Fab fragment) bound to K63-linked diubiquitin, PDB: 3dvg [72]. (F) Crystal structure of the A20 ZnF domain bound to three ubiquitin molecules, PDB: 3oj3 [77]. (G) Crystal structure of the Usp5/IsoT ZnF UBP domain bound to ubiquitin, PDB: 2g45 [78]. The figure is modified from Komander *et al.*, 2012 [3].

1.1.7 Erasing the ubiquitin code

A prompt termination of the ubiquitin code is achieved by deubiquitylating enzymes (DUBs) that cleave the isopeptide bond between ubiquitin and a substrate [78]. Mammalian cells carry around 100 DUBs, whereas yeast contains only 20. DUBs fall into two main classes, papain-like cysteine proteases and zinc metalloproteases [86, 87]. The cysteine proteases include four families: ubiquitin C-terminal hydrolases (UCHs), ubiquitin-specific protease (USP/UBP), ovarian tumour domain (OTU), and Machado-Josephin domain (MJD) DUBs. The only family of the metalloprotease DUBs is JAB1/MPN/Mov34 metalloenzyme (JAMM). The DUBs are functionally diverse both in their subcellular localisation and substrate specificity. They can involve in chromatin remodelling [88] and gene silencing, function in endocytosis [89] and multivesicular bodies [90], and assist in the proper functioning of mitochondria [91].

The two essential functions of DUBs that contribute to cellular homeostasis are ubiquitin recycling and biosynthesis. Ubp6 and Rpn11 (POH1/Rpn11, USP14, and UCH37 in humans) recover ubiquitin from ubiquitin-protein conjugates before their degradation by the proteasome [86, 87, 92, 93]. Defects in this process reduce ubiquitin levels and lead to pleiotropic stress sensitivities. In yeast, the ubiquitin-ribosomal fusion genes (*UBI1*, *UBI2*, and *UBI3*), as well as the stress-induced *UBI4*, are the only source of ubiquitin in the cell. Processing of these ubiquitin precursors is necessary to release the blocked C-termini of ubiquitin [5, 94, 95]. Similar processing by DUBs is also required for the human ubiquitin precursors; UBA52 and UBA80, ubiquitin-ribosomal fusions [96]; UBB and UBC, head-to-tail ubiquitin fusions [97]. Redundancy in DUB activities and the co-translational cleavage of ubiquitin gene products make it challenging to identify the corresponding DUBs [98].

DUBs are often activated by incorporation into a protein complex. For example, Ubp6 and Rpn11 are reported to be active only when associated with the proteasome [99, 86]. Interestingly, Ubp2 forms a complex with the ligase Rsp5 and antagonises its action [100]. Several DUBs display linkage specificity such as JAMM family DUBs that are often K63 specific [69]. OTU family of DUBs also show preference to some linkages, such as OTUB1 for K48 [101] and Cezanne for K11 linkages [102]. DUBs are abundant in yeast cells. Hence, it is necessary to avoid deubiquitylation when assessing the role of ubiquitin. The alkylating agent N-ethylmaleimide (NEM) inactivates DUBs that are cysteine proteases, and the zinc chelating agent O-phenanthroline (OPA) neutralises the metalloprotease Rpn11 [86].

1.1.8 Tools and Methods to study ubiquitylation

Diverse quantitative and qualitative approaches allow detailed analysis of ubiquitin modifications. *In vitro*, using ubiquitin mutants in reconstitution studies discovered the role of K63-linked chains in kinase activation [103] and involvement of K11-linked chains in controlling the mitotic exit [31]. Besides, structural analysis of linear chains revealed their contribution in NF-kB signalling [48]. Fusions between ubiquitin and a candidate substrate allow studying monoubiquitylation *in vivo* [39, 104]. Moreover, the functions of different ubiquitin chinas can be dissected by injection or overexpression of ubiquitin mutants [31]. A better-controlled and physiologically relevant approach is the replacement of endogenous ubiquitin and ubiquitin-ribosome fusions with exogenous ubiquitin mutants [105]. The abundance of a distinct type of ubiquitin modification is studied by chain-specific antibodies, UBDs and DUBs, and quantitative proteomics. A brief description of these approaches is indicated in the following subsections.

1.1.8.1 Chain-specific antibodies, UBDs, and DUBs

Development of linkage-specific antibodies against linear (M1-), K11-, K48- and K63-linked chains provided powerful reagents to characterise the physiological function of a particular chain type. Experiments using these antibodies revealed that K11-linked chains are highly enriched in human mitotic cells and that APC/C is the major source of K11-linked chains in cells [32]. Similarly, antibodies specific for linear and K63-linked chains provided and insight into the structural nature of these chains and their essential role in activating the NF-kB signalling [72, 106].

Majority of UBDs recognise a small set of residues on ubiquitin, usually the I44 patch [16, 3]. This binding feature can be exploited to interfere with ubiquitin signalling because simultaneous binding of several ubiquitin readers to the same surface is typically rare. Indeed, expression of K63-specific UBD (Rx3(A7)) in mammalian cells leads to accumulation of K63-conjugates as measured by quantitative methods. Besides, wild type yeast cells get sensitive to DNA damage when they overexpress the K63-specific UBD (Vx3) fused to a nuclear localisation signal (NLS) [107]. Another example is the Tandem-repeated ubiquitin-binding entities (TUBEs) that are based on ubiquitin-associated (UBA) domains. Exogenous expression of TUBEs in mammalian cells or adding them to cell lysates stabilises K63 polyubiquitylated proteins by effectively masking their recognition by DUBs [108, 109]. UBDs have also been exploited in establishing microscopy-based sensors to study ubiquitin dynamics. In mammalian cells, linear and K63-specific sensors were used to detect mitophagy, DNA double-strand breaks, and NF-kB signalling. However, these sensors interfere with the endogenous pathways, such as delaying the resolution of DSBs [110, 107].

Ubiquitin chain restriction (UbiCRest) provides a qualitative method to gain insights into the ubiquitin chain type. In UbiCRest, ubiquitylated substrates are treated in parallel with a panel of linkage-specific DUBs and the chain architecture is determined by gel-based analysis [111].

1.1.8.2 Affimers

Affimer technology is an alternative to antibodies to generate specific and high-affinity binding reagents. Affimers are 12-kDa non-antibody scaffolds that are thermally stable and highly expressed in *E.coli*. They fold into a cystatin-like structure, in which randomisation of two surface loops enables the generation of large (10^{10}) libraries of scaffolds. These libraries can be screened against any desired epitope to select for specific binders [112, 113]. An affimer screen using diubiqitin chains with K6 and K33 linkers identified selective binders for these non-canonical chain types. These reagents were shown to be very useful in a broad range of applications from structural studies to pull-downs, western blotting, and microscopy. The combined outcome of these experiments revealed HUWE1 to be a major K6 ligase in cells and mitofusin-2 being one of its substrates. These affimers also identified RNF144A and RNF144B as E3s that build K6-, K11, and K48-linked chains [113].

1.1.8.3 Quantitative methods

The ubiquitin code was most profoundly studied by mass spectrometry for the identification of chain types and ubiquitin modifications [114]. Relative quantitative techniques include tandem mass tag (TMT) labelling [115] and stable isotope labelling by amino acids in cell culture (SILAC) [116]. At the same time, absolute quantification (AQUA) method employs labelled ubiquitin peptide standards to determine the exact quantities of each ubiquitin chain type [117]. In combination with antibody- or UBD-based enrichment, these quantitative methods uncovered valuable insights into the singularities of the distinct ubiquitin chain types. Interestingly, the discovery that tryptic digestion leaves a diglycine remnant on ubiquitylated substrates and the development of an antibody that interacts specifically with diglycine remnants have revolutionised the field's ability to identify endogenously ubiquitylated proteins [30, 26, 118]. Because the mass spectrometry-based methods depend on tryptic digestion of ubiquitin, it prevents an in-depth understanding of the interplay between modifications, like in the case of branched ubiquitin chains.

1.2 Genome stability

The genetic material of a cell, the genome, constitutes the blueprint of life. Preserving the integrity of genetic information, therefore, is one of the fundamental evolutionary goals of organisms. A multifold of environmental stress and metabolic by-products can inflict damage and severely compromise the genome integrity of an organism during its lifetime. Consequently, cells have developed evolutionarily conserved defence mechanisms to counteract the harmful effects of such events and safeguard genetic information, ensuring a precise transition of information to their descendants, meanwhile inhibiting tumorigenic transformations and ageing [119, 120, 121].

1.2.1 DNA damage and repair

Depending on its origin DNA damage can be classified into either endogenous or exogenous damage. On the one hand, the endogenous DNA damage arises from interactions between DNA and chemically active metabolites, like reactive oxygen species (ROS). On the other hand, exogenous DNA damage is caused by environmental, physical, and chemical agents. For example, ultra-violet light (UV) and ionising radiation (IR), alkylating agents, and crosslinking agents. The defence mechanisms against DNA damage are collectively known as the DNA damage response (DDR), consisting of complex signalling pathways that include sensing the damaged DNA, amplifying and transducing the signal to effector proteins, and repairing the damage [119, 122, 120]. A plethora of DNA repair pathways cooperates throughout different cell cycle stages, allowing cells to repair DNA damage. The major DNA repair pathways include base excision repair (BER), nucleotide excision repair (NER), mismatch repair (MMR), homologous recombination (HR), and non-homologous end-joining (NHEJ). Besides, some specific types of DNA lesions are targets of direct enzymatic reversal, interstrand crosslink (ICL) repair, and DNA damage tolerance (DTT) pathways (Figure 1.2.1) [122].

1.2.1.1 Exogenous DNA-damaging agents

Some of the widely used DNA damaging drugs to study DNA damage response are briefly described here. Methyl methanesulfonate (MMS) is an alkylating agent that transfers methyl groups to oxygen or nitrogen atoms of DNA bases, creating highly mutagenic base lesions, like N^3-methyladenine and O^6-methylguanine [123, 124]. In contrast, UV-C radiation exerts its genotoxic effects by producing cyclobutane–pyrimidine dimers (CPDs) and 6–4 photoproducts (6–4 PPs) that are pyrimidine adducts (Figure 1.2.1) [125]. The DNA damaging agent 4-nitroquinoline oxide (4-NQO) is a UV-mimicking drug that puts bulky adducts on DNA. Hydroxyurea (HU) treatment prevents DNA synthesis by inhibiting ribonucleotide reductase, thereby depleting the dNTP pool and depriving the replicative polymerases [126]. Furthermore, the continuous action of replicative DNA helicases leads to the accumulation of single-stranded DNA (ssDNA) gaps [127, 128]. Camptothecin (CPT) is a topoisomerase I inhibitor that covalently locks the enzyme to DNA. During DNA replication, CPT-induced protein DNA adducts are converted to DSBs upon collisions with replicative polymerases [129]. Another widely used DSB-inducing agent is zeocin. It is a radiomimetic chemical that belongs to the bleomycin family of antibiotics. Zeocin intercalates into the DNA and generates DSBs (Figure 1.2.1) [130, 131].

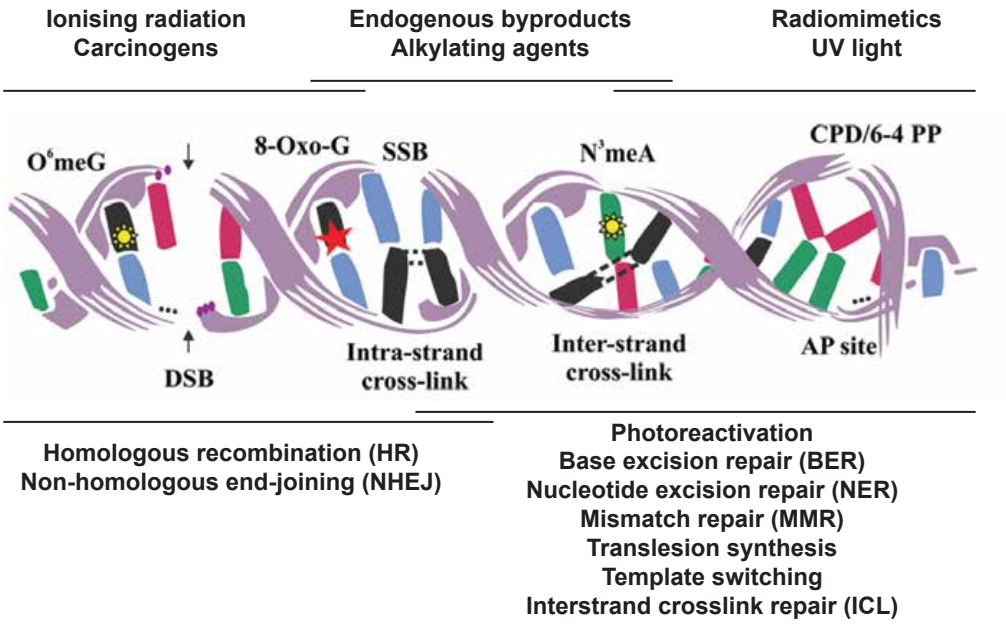

Figure 1.2.1: Types of DNA damage and repair. Schematic representation of the major DNA lesions induced by various external and endogenous factors. The corresponding DNA repair mechanisms to remove a particular lesion are indicated. In some circumstances, crosstalk between different repair pathways is possible. AP: abasic site, DSB: double-strand break, SSB: single-strand break, O6-meG: O6-methylguanine, 8-Oxo-G: 8-oxoguanine, N6-MeA: N6-methyladenine, CPD: cyclobutane-pyrimidine dimer, 4-6 PP: 4-6 photoproducts. The figure is modified from Manova *et al*., 2015 [132].

1.2.1.2 Replication and replication stress

In eukaryotes, DNA replication initiates at thousands of replication origins forming bidirectional replication forks. During G1 phase, a complex of replication initiation proteins license origins for replication. In S phase, the firing of replication origins follows a sequential order, starting with early- and finishing with late-replicating origins [133]. Majority of the licensed origins do not fire during an unperturbed replication. Instead, these dormant origins provide a backup plan to complete replication of stalled replication forks [134, 135]. Replication stress is defined as the slowing or stalling of replication fork progression and DNA synthesis. A wide variety of physical obstacles can generate replication stress, which usually results in the accumulation of ssDNA gaps. The continuous action of the replicative helicase in unwinding DNA in front of a stalled polymerase contributes to the formation of ssDNA gaps [136]. Replication protein A (RPA) coated ssDNA and the primer-template junctions serve as signals to activate the replication stress response [137].

1.2.1.3 Sources of replication stress

One of the most common sources of replication stress is unrepaired DNA lesions caused by endogenous and exogenous factors mentioned above (Subsection 1.2.1.1). Nicks and ssDNA gaps are considered as sources and consequences of replication stress. They arise as natural intermediates of many DNA repair mechanisms and as products of DNA manipulations, like the release of torsional stress by topoisomerases. A shortage in some replication factors, such as nucleotides and components of the replication machinery can slow replication fork speed and induce replication stress (Figure 1.2.2) [138].

The replicative polymerases Pol δ and Pol ε have a high rate of ribonucleotide (rNTP) misincorporation [139]. Nevertheless, the specialised enzyme RNase H2 removes misincorporated rNTPs through ribonucleotide excision repair (RNR) [140]. If kept unrepaired, rNTPs may stall the replicative polymerases in the next round of replication (Figure 1.2.2).

Some DNA sequences are intrinsically challenging for the replication machinery, like trinucleotide repeats that form secondary DNA structures (hairpins) and block replication fork progression [141]. G-quadruplexes are also DNA secondary structures that form in GC-rich regions. Their chemical stabilisation or the loss of helicases that resolve these secondary structures, such as Pif1 lead to a reduction in replication speed (Figure 1.2.2) [142].

Last but not least, collisions between replication and transcription machineries are unavoidable because the two processes operate on DNA and create topological stress. Moreover, nascent transcripts may hybridise with the template DNA, forming an R-loop (an RNA-DNA hybrid with a displaced ssDNA strand), which may hamper the progression of replication forks (Figure 1.2.2) [143, 144].

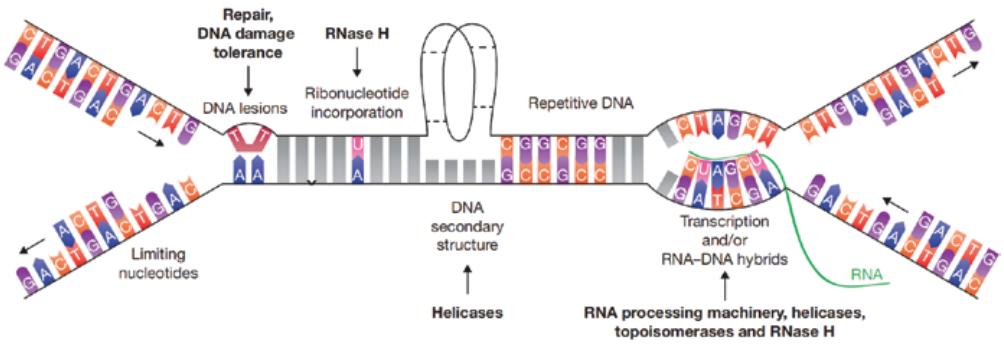

Figure 1.2.2: Sources of replication stress. Some of the obstacles that can slow or stall DNA replication include limiting nucleotides, DNA lesions, ribonucleotide incorporation, repetitive DNA elements, transcription complexes (R-loops), DNA secondary structures (hairpins and G-quadruplexes). The repair pathways of some replication obstacles are indicated in bold. The figure is modified from Zeman *et al.*, 2014 [137].

1.2.1.4 Ubiquitylation and genome maintenance

Ubiquitylation has emerged as an essential regulatory mechanism in DNA damage response and repair pathways [145, 146, 147]. Numerous large-scale proteomic approaches and systematic studies of chromatin-associated factors have revealed the dynamics of ubiquitylation under unperturbed and replication stress conditions [148, 149, 150]. Unlike the well-characterised function of ubiquitylation in protein degradation and homeostasis, ubiquitylation of multifold proteins after DNA damage activates a bundle of repair mechanisms or protects the damaged DNA from additional harm [147]. In addition to PCNA, many other factors at the replication fork are modified by ubiquitin in response to genotoxic stress. RPA complex is one of the most abundant proteins at stressed replication forks and undergoes several post-translational modifications like phosphorylation and ubiquitylation. The ubiquitin ligases PRP19 and RFWD3 have been reported to ubiquitylate subunits of the RPA complex upon UV irradiation or treatment with genotoxic agents, like 4-NQO or HU. RFWD3 constitutively associates with the replication fork, whereas PRP19 binds to RPA only after DNA damage [151, 152, 153, 154, 155, 156]. Ubiquitylation and stabilisation of polymerase η (Pol η), a translesion synthesis polymerase, after UV irradiation are also reported; however, the mechanistic function of Pol η modification is still controversial [157, 158]. A proper formation of the pre-replication complex, the association of the replisome and RPA with replication origins, and progression of replication forks after replication stress require ubiquitylation of histone (H2B) [159]. Moreover, replication stress induces ubiquitylation of a plethora of other repair factors, for example, MSH2, TOP1, XPC, DDB2, and FANCD2/I [160, 148, 145, 146, 147].

1.2.2 DNA damage bypass and postreplicative repair

Excision repair pathways remove DNA lesions by generating a single-stranded gap then filling it using the complementary, undamaged strand as a template. Such repair operates only in the context of damage within double-stranded DNA. When a lesion escapes repair and is encountered by the replication machinery, it can block DNA synthesis and casue stalling of the replication fork, which in turn result in a single-stranded gap opposite the lesion and cell-cycle arrest. DNA damage tolerance (DDT) or bypass pathways allow completion of replication in the presence of DNA lesions. Hence, these pathways are crucial during S and G2 phases. Once replication is completed, the damage lies again in duplex DNA and can be resolved by excision repair [161, 162].

1.2.2.1 Post-translational modification of PCNA

In eukaryotes, the DNA damage bypass pathways are regulated by ubiquitylation of an essential replication factor, PCNA. Upon replication stress, stretches of ssDNA accumulate at and behind the replication fork [128, 163]. RPA coats ssDNA gaps and recruits the ubiquitin ligase complex Rad6/Rad18, which then monoubiquitylate PCNA on a highly conserved lysine residue (K164) (Figures 1.2.3 and 1.2.4) [18]. Via conserved UBDs and a PIP box, a set of damage-tolerant DNA polymerases (i.e. Pol η and Rev1) recognise the modified PCNA preferentially [80]. These polymerases can replicate across DNA lesions through a mechanism known as translesion synthesis (TLS) [164]. Yet, this bypass pathway is considered error-prone because of the mutagenic nature of TLS polymerases [165].

Alternatively, the heterodimeric Ubc13-Mms2 (E2) and Rad5 (E3) further modify monoubiquitylated PCNA with K63-linked polyubiquitin chains [166]. This modification activates an error-free mode of damage bypass involving template switching (TS), in which the newly synthesised sister chromatid is used as a template to replicate over lesions (Figure 1.2.3). Contribution of replication fork reversal to the error-free bypass is also reported [167, 168]. Although template switching is generally error-free, recombination events may occur within incorrect genomic regions, leading to gross genetic rearrangements (Figure 1.2.4). Moreover, the factors that recognise K63-linked polyubiquitylated PCNA and act in the downstream error-free damage bypass are unknown [169, 162].

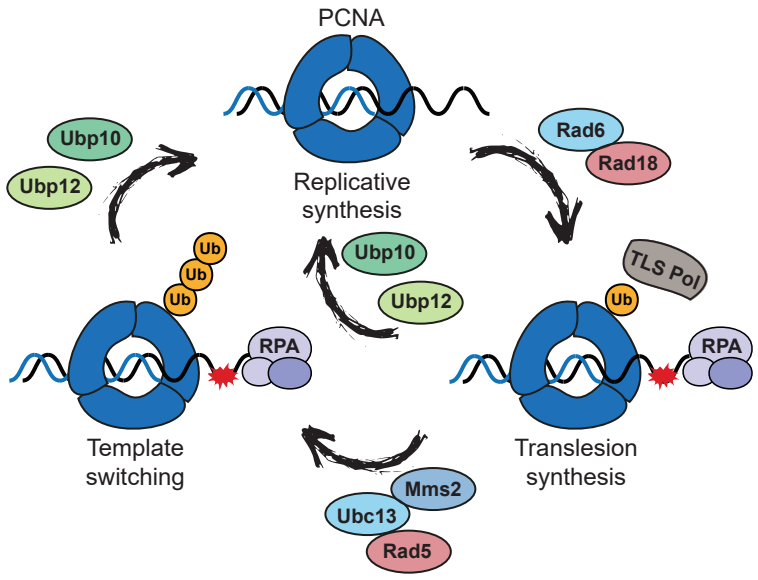

Figure 1.2.3: PCNA ubiquitylation and activation of DNA damage bypass. PCNA ubiquitylation cycle. The corresponding E2/E3 pairs for mono- and polyubiquitylation are indicated. The ssDNA gaps are coated by RPA, and the signal is terminated by the action of DUBs (Ubp10 and Ubp12). Monoubiquitylation triggers TLS, whereas polyubiquitylation of PCNA initiates template switching. For more details, see the main text (1.2.2.1).

The two DUBs, Ubp10 and Ubp12, counteract PCNA ubiquitylation, thereby terminating the damage bypass events in *S.cerevisiae*. Ubp10 efficiently deubiquitylates both mono- and polyubiquitylated PCNA, whereas Ubp12 cleaves only polyubiquitin chains from PCNA. A genome-wide localisation study

showed that Ubp10 and Ubp12 divide the workload of PCNA deubiquitylation between them in a strand-specific manner at stalled replication forks (Figure 1.2.3) [170]. In humans, UPS1 is responsible for PCNA deubiquitylation [171].

In budding yeast, PCNA is also SUMOylated during unperturbed replication at the highly conserved lysine, K164, and to a lesser degree at K127 [18]. The SUMO E2/E3 complex Ubc9/Siz1 mediates the transfer of SUMO to the K164 residue of PCNA, which is triggered by the loading of PCNA onto DNA. In contrast, Ubc9/Siz2 is responsible for SUMOylation of PCNA at K127 [172]. SUMO modification of PCNA is recognised by the helicase suppressor of rad six 2 (Srs2) that prevents unscheduled recombination events by disrupting Rad51 filaments [173, 174, 175, 176]. Srs2 interacts with SUMOylated PCNA through its C-terminus that contains a PIP-like interaction motif next to a SUMO-interaction motif (SIM) [174, 177]. Similarly, a SIM-mediated interaction of Rad18 with SUMOylated PCNA enhances Rad18's E3 activity, making Rad18 a necessary switch between replication-associated SUMOylation and damage-induced ubiquitylation [178].

1.2.2.2 Translesion synthesis and TLS polymerases

Translesion synthesis is performed by conserved and specialised TLS polymerases, which can replicate past DNA lesions with a lower fidelity than replicative DNA polymerases [179]. On the one hand, the low fidelity of TLS polymerases contributes to tumorigenesis and disease. On the other hand, it supports the overall fitness and evolution of organisms. There are four families of TLS polymerases (Y, B, X, and A) and PrimPol. In eukaryotes, a total of eleven TLS polymerases are known of which, Rev1, Pol η (Rad30), and Pol ζ with its two subunits Rev3/Rev7 exist in *S.cerevisiae*. Some TLS polymerases can replicate accurately over specific cognate lesions, such as Pol η over CPDs [180, 181]. In humans, xeroderma pigmentosum variant (XPV) patients lack POL η. They exhibit photosensitivity and predisposition to skin cancer because other TLS polymerases bypass the UV-induced CPDs in an error-prone manner [182, 183].
Distinct structural and biochemical features of TLS polymerases distinguish them from the replicative polymerases. TLS polymerases lack a 3'-5' exonuclease proofreading domain, contain a relatively larger and open active site, and carry other features such as the polymerase-associated domain (PAD) that facilitate additional DNA binding [181, 179].

There are two proposed models for damage bypass by TLS.

Polymerase switch model

It is a two-step process in which TLS polymerases act sequentially to replicate the damaged DNA. First, an inserter TLS polymerase, usually Pol η and less often Rev1, incorporates a nucleotide opposite the DNA lesion. Then, an extender polymerase, usually Pol ζ replaces the inserter polymerase and extends the primer-template termini [184, 185, 186].

Gap-filling model

This model suggests a role for TLS polymerases in filling the ssDNA gaps left behind by replicative polymerases or incomplete repair processes [179]. However, we lack a specific sequence of events in such gap-filling TLS. In mouse cells, Rev1 gets recruited to the gaps by 5'-termini and involves in synthesis across postreplicative gaps [187, 179]. Similarly, Rev3 engages in TLS of gaps opposite 6-4 photoproducts [188].
Addition roles of TLS polymerases are assigned in other repair pathways, such as in ICL repair, BER and NER to synthesise new DNA after the excision step.

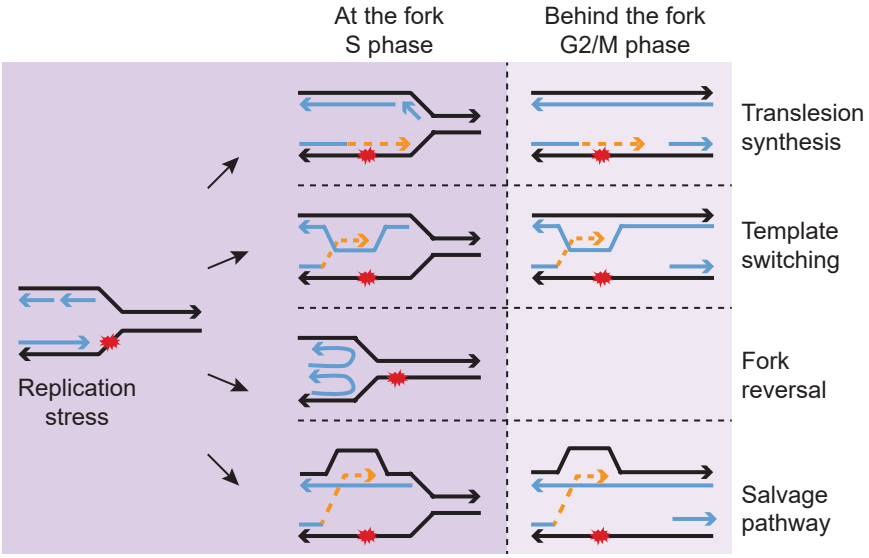

Figure 1.2.4: Multiple flavours of DNA damage bypass. Apart from fork reversal, all the DNA damages bypass modes can operate on-the-fly during replication or in a postreplicative manner behind the replication fork. Fork reversal is possible only during S phase. Black and blue lines correspond to template and nascent DNA strands during replication, dotted orange lines represent DNA synthesised during damage bypass, and the DNA lesion is indicated in red. For more details, see the main text (1.2.2).

1.2.2.3 Template switching

Unlike the well-characterised role and mechanisms of the error-prone TLS in damage bypass, very little is known about the molecular details of template switching and downstream effector proteins.

Structural nature and mediators of template switching

Template switching is a recombination-based process but genetically distinct from HR. This conclusion was based on classical epistasis studies and 2D gel analysis of DNA replication intermediates that revealed a population of recombination-like structures consisting of sister chromatid junctions (SCJs) in mutants of template switching [189]. SCJs usually form at stalled replication forks, and their resolution depends on the conserved helicase slow growth suppressor (Sgs1, BML in mammals) that works hand-in-hand with the topoisomerase Top3 [190, 191, 189]. Mutants of *sgs1Δ* accumulate

SCJs and are epistatic with template switching factors, indicating that Sgs1 functions downstream of polyubiquitylated PCNA [189, 192]. In mutants defective in PCNA modification, recombination structures resembling SCJs mediate DNA damage tolerance that requires Sgs1 for their resolution. This PCNA ubiquitylation-independent and recombination-based repair is known as the "salvage pathway" (Figure 1.2.4) [189, 193, 194, 195]. Several other factors are implicated in the promotion and resolution of template switching intermediates. These factors include the 9-1-1 checkpoint clamp; the PCNA unloader Elg1 and RFC complex; the replicative polymerase δ; strand invasion and homologous recombination proteins Rad51, Rad52, Rad55, Rad57, and the Shu complex; helicases Sgs1 and Mph1; resolvases Esc2 and Smc5/6 complex [196, 197, 198, 193]; and the DNA bending factor Hmo1[194].

Location and timing of template switching

Template switching can operate in two possible locations. Either it associates on-the-fly with the replication fork or works on ssDNA gaps left behind the replication fork (Figure 1.2.4). There is multifold evidence supporting both scenarios.

Postreplicative template switching: Since the 1970s, several indirect evidence suggested a post-replicate function of template switching. In alkaline sucrose sedimentation experiments, pulse labelling of DNA at various times after UV irradiation revealed a gradual conversion of low to high molecular weight fragments, consistent with the filling of daughter-strand gaps [199]. In the presence of RPA at ssDNA gaps, loading of the 9-1-1 clamp (a heterotrimer of Rad9, Rad1, and Hus1) is directed to the 5'-junctions of the single- and double-stranded DNA. Such structures are not expected at replication forks, rather present at daughter-strand gaps arising from either unfinished Okazaki fragments or repriming events on the leading strand [200]. Analysis of replication intermediates with electron microscopy (EM) brought some direct evidence of gap formation on leading and lagging strands as well as for the intermediates implicated in gap-filling [201, 202]. Besides, several independent studies concluded that template switching could operate independently of replication forks. Placing the bypass factors under the control of regulatable promoters and restricting their expression to the G2/M phase until the bulk genome replication is completed, do not affect the survival of cells after UV irradiation [192, 203]. Such an experimental setup also allowed a direct detection of gap-filling events. Labelling of newly synthesised DNA in G2/M by the nucleotide analogue 5-bromo-2-deoxyuridine (BrdU) followed by DNA fibres analysis revealed that Rad18-dependent bypass tracts are distinct from the replication tracts [203]. More recently, by tracing fluorescent RPA and gap-filling our lab demonstrated that template switching operates predominantly in a postreplicative manner and is not restricted to stalled replication forks [204, 163]. Both in yeast and higher eukaryotes, the postreplicative action of damage bypass requires repriming downstream of the damage site, which serves as an initiation point for template switching [205, 201, 206, 202]. Indeed, studies in budding yeast indicate a crucial role for the Pol α/Primase in template switching. Failure in such repriming events leads to an increase in the number of reversed forks [207]. For an efficient repriming, expansion of daughter-strand gaps is necessary, which speculates the involvement of DNA processing enzymes in some steps of template switching. Indeed, our lab showed that deletion of the nuclease Exo1 and the helicase Pif1 sharply reduce the damage-dependent accumulation of single-stranded regions in newly replicated DNA (Figure 1.2.5) [208, 204].

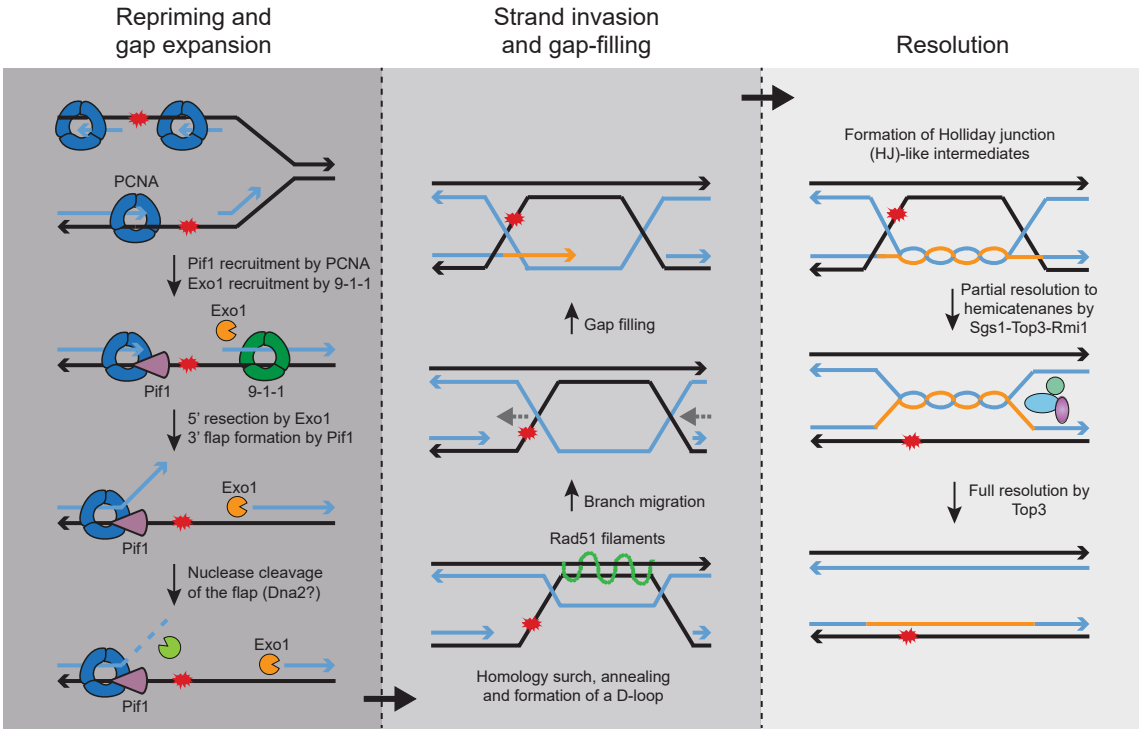

Figure 1.2.5: A proposed model for template switching. Schematic representation of postreplicative gap-filling by template switching. The DNA lesion is shown in red. Black and blue lines correspond to template and nascent DNA strands during replication, and orange lines represent DNA synthesised during template switching. The green circle is a nuclease (Dna2?). For more details, see the main text (1.2.2.3). The figure was modified from Branzei *et al*., 2016, Garcia-Rodriguez *et al*., 2018, and Dr Sabrina Wegmann's thesis [208, 209].

Fork-associated template switching: The evidence discussed above mainly supports the action of template switching behind the replication fork. Nevertheless, several observations also support a replication-associated action of the error-free bypass. *In vitro*, fork reversal so-called "chicken-foot" can be catalysed by many enzymes such as Rad5, Rad51, Rad54, and Mph1/FANCM [210, 211, 212, 213]. During fork reversal, the two complementary nascent DNA strands anneal, providing a template for synthesis past a blockage on the other strand. Besides, higher eukaryotes utilise replication fork reversal during stress to slow DNA replication [214]. Rad5 is the E3 responsible for PCNA polyubiquitylation. In addition to a RING finger motif, Rad5 contains an ATPase domain [215, 216]. This domain shows fork-specific helicase and branch migration activities and promotes fork reversal to initiate template switching. However, controversial studies about different Rad5 helicase mutants make it challenging to assign a fork reversal activity to the error-free damage bypass [217, 218, 219, 195]. Besides, reversed replication forks are challenging to detect in yeast and accumulate only in checkpoint-deficient cells [220]. Fork reversal in mammalian cells has rather a fork stabilising function [214]. For example, an interesting finding indicates that the translocase ZRANB3 interacts with polyubiquitylated PCNA and its fork reversal activity promotes damage tolerance by stabilising the replication fork and slowing the replication speed [221].

Envisioned mechanisms of template switching

Recently our lab proposed a model for initiation of template switching, which depends on the combined action of the 3'- 5' helicase Pif1 and the nuclease Exo1. ssDNA gaps accumulate behind stalled replication forks most probably due to repriming events. The 5'- 3' exonucleolytic activity of Exo1 expands the gaps at their 5'-junction with the help of 9-1-1 checkpoint clamp. Via a PIP box interaction, PCNA recruits Pif1, which contributes to gap expansion by generating ssDNA 3'-flaps that are subsequently cleaved possibly by the nuclease Dna2. This gap expansion facilitates invasion of the damaged strand into the newly synthesized sister chromatid, thereby initiating template switching (Figure 1.2.5) [208]. Visualising template switching intermediates by electron microscopy brought mechanistic evidence for the later steps of template switching. With the assistance of Rad51 filaments, the ssDNA gap anneals to the homologous duplex, forming a D-loop structure. Then, the newly synthesised sister-strand is used as a template for replication, resulting in a double Holliday junction (HJ)-like intermediate, in which the parental and the newly synthesised strands pair in a conservative manner. In the final step, the Sgs1-Top3-Rmi1 complex partly resolves the HJ-like intermediates to hemicatenanes, followed by full resolution via the activity of Top3 (Figure 1.2.5) [202].

1.2.2.4 Factors influencing the bypass choice

Several physiological and experimental factors can channel the bypass pathway to one of its branches. Some of these factors and the underlying challenges to build a decisive conclusion are described in the next paragraphs.

Species under study: Based on solid *in vivo* and *in vitro* reconstitution studies in *S. cerevisiae*, the main biological switch between TLS and template switching is the mono- and polyubiquitylation state of PCNA [18, 165, 222]. Interestingly, in *S.pombe*, PCNA polyubiquitylation activates TLS to a greater degree than PCNA monoubiquitylation [223]. In higher eukaryotes, like in chicken DT40 cells and mammalian cultures, regulation of the bypass choice by PCNA ubiquitylation is more puzzling. On the one hand, a panel of reports indicates that PCNA monoubiquitylation is not essential for TLS activation [224, 225, 226, 227, 228]. On the other hand, detection of polyubiquitylated PCNA in vertebrates is challenging because of its low abundance. Moreover, E3s other than Rad5 homologs (HLTF and SHPRH) are involved in PCNA polyubiquitylation [229, 230]. Since the bypass factors and modification sites on PCNA are highly conserved from yeast to the higher eukaryote, the contradictions in the literature could be assigned to the incomparable methodologies and experimental conditions of the studies.

Type of DNA lesions: Many DNA-damaging agents, such as UV irradiation, HU, MMS, and 4-NQO induce PCNA ubiquitylation to different degrees in the various tested model organisms [18, 231, 223, 128], whereas exposure to DNA DSB-inducing drugs does not lead to PCNA ubiquitylation [231, 232, 219, 128]. Moreover, PCNA ubiquitylation accumulates with different kinetics after exposure to these damaging agents [231, 233, 234, 235]. It is still obscure why some DNA-damaging agents induce PCNA ubiquitylation and others not, and why PCNA ubiquitylation shows varying kinetics to the different drugs.

Load of DNA damage: Recently, several genetic studies revealed that cellular responses to chronic low-dose UV damage differ from those observed after exposure to an acute dose of UV [236]. The DNA damage caused by acute UV exposure is mainly repaired by the NER pathway, whereas Rad6/Rad18-dependent damage bypass is more important to survive chronic low-doses of UV [236]. Such dose-dependent differences were also described in case of damage caused by MMS, where the a dose of 0.001% defines the border between chronic and acute exposures [237].

Availability of different repair factors: Accumulation of RPA at ssDNA gaps behind stressed replication forks stimulates PCNA ubiquitylation [128]. The stimulating role of RPA was confirmed by the decline in PCNA ubiquitylation following RPA depletion in yeast and mammalian cells [238, 128, 235]. These observations built the model that RPA-coated ssDNA gaps serve as a recruitment signal for Rad18 via a direct physical interaction [128]. In the absence of the rate-limiting factor Rad18, PCNA ubiquitylation is compromised whereas overproduction of Rad18 induces PCNA ubiquitylation even in unchallenged *S. cerevisiae* and mammalian cells [238, 128]. Interestingly, in *Xenop*us embryos, Rad18 is a maternally-loaded and abundant factor. At early cell division cycles until the mid-blastula transition (MBT), Rad18 constitutively ubiquitylates PCNA thereby inhibits checkpoint activation and confers resistance to DNA damage [239]. Rad5, with its ubiquitin ligase and ATPase/helicase domains, is necessary to complete replication under DNA damage conditions. Moreover, expression of Rad5 peaks in S phase and accumulates in nuclear foci when replication forks progress in the presence of MMS [195]. Rad5 also engages in spontaneous mutagenesis in a Rad6/Rad18-independent manner [240, 241]. A recent study showed that Rad5 is enriched at replication stress sites in the absence of base lesions. At these sites, Rad5 recruits TLS polymerases and promotes mutagenic TLS, thereby prevents more dangerous chromosomal aberrations [**?**]. The subunits of the E2 complex, Ubc13 and Mms2, are mainly cytosolic but translocate to the nucleus upon DNA damage [216]. The TLS polymerase Rev1 is cell cycle controlled, where its expression peaks during G2/M phase [181]. In contrast, the levels of Pol η stay constant during the cell cycle [181].

Cell cycle phase: Constitutive and damage-induced PCNA ubiquitylation happens mainly during S phase, whereas exposure to damage in G1 or G2 does not generally induce PCNA modification [128], which correlates well with the replicative function of PCNA. Nevertheless, several studies showed that cells could complete the bulk genome replication in the presence of damage when DNA damage bypass is restricted to G2 phase [236, 237, 203, 192, 161]. These findings indicate that the gaps accumulated behind stressed replication forks and not replication forks themselves trigger PCNA ubiquitylation. The direct visualisation of ssDNA gaps left behind replication forks confirmed the postreplicative action of damage bypass [201, 242, 192, 163]. However, these observations do not exclude that in wild-type cells, bypass events may as well happen in S phase in a postreplicative manner [163, 203, 192]. The requirement for Rad5's ligase and helicase function for replication fork progression through MMS-damaged DNA supports the role of damage bypass in S phase [195]. Both in yeast and mammalian cells, genome-wide analyses of spontaneous mutation rates showed that early-replicating regions accumulate more deletions and duplications. In contrast, late-replicating regions have higher mutation rates suggesting a defined time-window of action for the error-free and error-prone damage bypass [243, 244, 245].

1.2.2.5 Rad5: its domains and homologues

Central to the two branches of DNA damage bypass is the ubiquitin ligase/DNA helicase Rad5 and its two mammalian homologues, helicase-like transcription factor (HLTF) and SNF2 histone linker PHD RING helicase (SHPRH). Rad5 is a large multi-functional protein containing an N-terminal Rev1 interaction domain, a HIRAN domain, an SNF2 ATPase/helicase domain, and a RING finger ubiquitin ligase domain (Figure 1.2.6). The structure and function of the yeast Rad5 are conserved with its human homologues, HLTF and SHPRH [246].

Interactions and recruitment of Rad5/HLTF/SHPRH

Protein-protein and protein-DNA interactions recruit Rad5 and HLTF to stressed replication forks. Via its N-terminus Rad5 physically interacts with PCNA and Rad18 [216, 18, 219, 247]. RPA coated ssDNA recruits Rad18 [128] and most likely Rad5. Monoubiquitylation of PCNA is also necessary for the engagement of Rad5 with HU-stressed replication forks [**?**]. The region of Rad5 that interacts with ubiquitylated PCNA is not yet identified but most probably lie within the HIRAN domain (Figure 1.2.6) [248]. HLTF also physically interacts with PCNA, Rad18 [229], and RPA [249]. Similarly, SHPRH physically interacts with PCNA and Rad18 [229].

E3 function of Rad5/HLTF/SHPRH

The ubiquitin ligase function of Rad5 [250, 216] together with the E2 complex Ubc13-Mms2 [251] build K63-linked polyubiquitin chains on PCNA to initiate template switching, allowing to complete replication in the presence of DNA lesions [18]. Ubc13-Uev1 are the human homologs of Ubc13-Mms2 [252]. The two homologs of Rad5, HLTF and SHPRH both function redundantly in PCNA polyubiquitylation [253, 229, 246]. HLTF and SHPRH double knockout mouse cells have residual PCNA polyubiquitylation after replication stress [230]. Involvement of HLTF and SHPRH in TLS is also described. MMS treatment leads to degradation of HLTF, which promotes interaction of SHPRH with Rad18 and Pol κ. In contrast, after UV-treatment, HLTF antagonises SHPRH-Rad18 interaction by binding to SHPRH, thereby promoting PCNA monoubiquitylation and recruitment of Pol η [254]. In budding yeast, polyubiquitylation of PCNA by Rad5 activates error-free template switching, but the details of the downstream signalling have remained enigmatic.

The HIRAN domain

The N-terminal HIRAN domain of Rad5 and HLTF is highly conserved from bacteria to humans [255] (Figure 1.2.6). The crystal and NMR structures of HIRAN domain in higher eukaryote revealed that it physically interacts with the free 3'OH of an ssDNA overhang in duplex DNA [256, 217, 186]. This interaction protects the 3' end of daughter strands at stalled replication forks [257]. HIRAN domain has no catalytic activity, but its deletion in HLTF impairs the repair of ssDNA gaps and reduces cell survival after UV damage [258]. Besides, mutants of HIRAN domain show a reduction in PCNA ubiquitylation and disrupted helicase activity [259], suggesting an essential structural role of this domain.

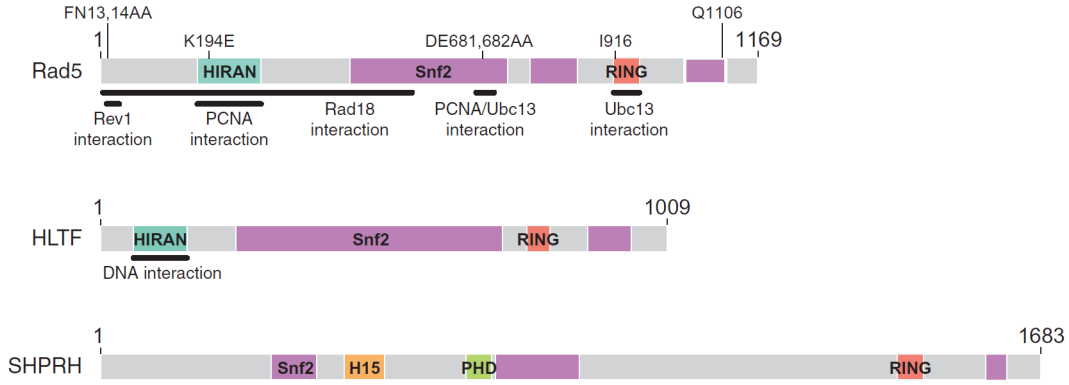

Figure 1.2.6: Domain structure of Rad5 and its homologues. Rad5, HLTF, and SHPRH have conserved RING finger E3 ubiquitin ligase and Snf2 helicase domains. Both Rad5 and HLTF contain an N-terminal HIRAN domain, whereas SHPRH has an H15 linker histone H1 and H5 family and PHD-finger domains. Regions required for physical interactions with Rev1, Rad18, PCNA, Ubc13, and DNA are indicated in black bars. Mutations that disrupt Rad5's physical interaction with Rev1 (FN13, 14AA), 3'OH binding (K194E), the Walker B motif (DE681, 682AA), physical interaction with Ubc13 (I916A) and DNA helicase activity (Q1106D) are shown as well. The figure is modified from Gallo *et al.*, 2019 [260].

The ATPase/Helicase domain

Rad5, HLTF, and SHPRH have a conserved SNF2 DNA-dependent ATPase/helicase activity (Figure 1.2.6) [215]. Rad5 preferentially binds dsDNA and can reverse model DNA replication forks [210]. Similarly, HLTF shows replication fork reversal activity *in vitro* [261]. The ligase domain of Rad5 is embedded in the helicase domain containing seven consensus motifs. Thus, assigning a function to Rad5's helicase domain was challenging. Using various helicase-dead mutants of Rad5 several studies concluded controversial outcomes, like the involvement of the helicase domain in replication fork reversal, slowing, and restart of stalled replication forks [210, 256, 218, 195]. Nevertheless, a true separation-of-function allele of Rad5 (*rad5-Q1106D*) was created. This allele only disrupts ATPase/helicase activity while leaving PCNA ubiquitylation intact. Using this Rad5 mutant in genetic and biochemical experiments, Choi *et al.*, 2015 unravelled a role of the helicase domain in promoting PCNA ubiquitylation and its contribution to recombination-dependent and independent damage bypass [247].

Interaction with TLS polymerases

Contribution of Rad5 to template switching was studied intensively. However, recent molecular evidence indicates that Rad5 binds to and recruits TLS polymerases to stressed replication forks and promotes TLS. Genetic analysis of bypass mutants discovered a positive effect of Rad5 in spontaneous mutagenesis at the *CAN1* locus when PCNA polyubiquitylation was impaired [240, 262]. The mutagenic bypass or gap-filling by Rad5 is also required for specific types of DNA lesions. In plasmid-based assays, synthesis by Pol ζ past an apurinic/apyrimidinic sites and (6-4)-photoproducts requires Rad5 [263]. Co-immunoprecipitation experiments confirmed a direct physical interaction between the N-terminus of Rad5 and Rev1 [263] mediated by the F13-N14 residues of Rad5 [264, 265]. In cells, Rad5 recruits Rev1

to HU-stressed replication forks [**?**]. Compared to *RAD5* deletion, the ligase-dead (*rad5-I916A*) mutant has higher spontaneous, UV, or HU-induced mutation rates of *trp1-289* and *CAN1* markers [218, 265**?**], whereas the double mutant *rad5-FN13-14AA-I916A* has comparable MMS and HU sensitivity as of Rad5 deletion. Fission yeast's Rad5 homologue, Rad8, is required for TLS-dependent replication of plasmids containing CPDs and (6-4)-photoproducts [223]. The extreme N-terminus of Rad5 that is required for Rev1 interaction is not present in HLTF, making the interaction between HLTF and REV1 less likely in humans. SHPRH has better sequence conservation with the N-terminus of Rad5 but lacks the essential phenylalanine residue. Moreover, after MMS damage SHPRH physically interacts with Pol κ and to a lesser degree with Pol η [254].

1.2.3 Tools and methods to study DNA damage bypass

1.2.3.1 Capturing postreplicative DNA synthesis

One of the classical methods to catch evidence of postreplicative DNA synthesis is alkaline sucrose sedimentation. Briefly, DNA is pulse labelled with radioactive nucleotide analogues at various times after UV irradiation. Filling of daughter-strand gaps leads to a gradual conversion of low to high molecular weight fragments [199]. Although this approach gives a qualitative view of damage bypass, it is difficult to gain information about the number and the size of DNA fragments. Direct visualisation of DNA gap-filling events is possible in experimental conditions, in which the expression of the bypass factors is restricted to the G2/M phase, and the gap-filling happens once the bulk genome replication is completed [192, 203]. Labelling of the newly synthesised DNA in G2/M by the nucleotide analogue BrdU followed by microscopy analysis of DNA fibres allow the detection of postreplicative DNA tracts [203]. An alternative approach to analyse active DNA synthesis is to use another thymidine analogue 5-ethynyl-2-deoxyuridine (EdU). EdU is detected by Click reaction, which is a copper-catalysed reaction between an azide and an alkyne. The advantage of EdU labelling over BdU is the mild treatment conditions for EdU detection. In contrast, DNA denaturation (typically by HCl or heat) is required to expose BrdU for detection with an anti-BrdU antibody [266].

1.2.3.2 Visualising postreplicative gaps by microscopy

Analysis of replication intermediates with electron microscopy brought some direct evidence of gap formation on leading and lagging strands as well as for the intermediates implicated in gap-filling [201, 202]. Alternatively, tracing DNA repair factors by fluorescence microscopy allows the detection of DNA repair dynamics. Recently, our lab developed a new *in vivo* system to visualise the appearance and resolution of ssDNA gaps during replication stress by tracing RPA, an ssDNA binding protein complex [163]. These analyses revealed that RPA foci form predominantly away from active replication sites and do not coexist with known DNA repair centres. Instead, they represent sites of postreplicative DNA damage bypass involving TLS and template switching [163]. The proposed model for the genesis of these postreplicative repair territories (PORTs) is the generation and expansion of ssSDNA gaps. Presence of DNA lesions during replication causes the appearance of small daughter-strand gaps via repriming while Exo1 and Pif1 contribute to their expansion. In turn, visible RPA foci arise by the expansion of gaps emerging from a replication centre [133]. Consequently, TLS polymerases and recombination factors resolve the RPA foci by gap-filling [163].

1.3 Aims and goals of this thesis

DNA damage bypass pathways safeguard cells from replication problems, genomic instability, and malignant transformation. These pathways are regulated by post-translational modifications of PCNA. Monoubiquitylation of PCNA recruits damage-tolerant DNA polymerases to activate error-prone TLS, whereas K63-linked polyubiquitylation of PCNA initiates error-free template switching. However, how these two bypass pathways cooperate is not well understood. The aim of this study was to gain a detailed insight into the choice between the two branches of DNA damage bypass and understand the mechanism and regulation of polyubiquitin-dependent template switching. A better understanding of the bypass choice requires a delicate and careful analysis of the emergence of ubiquitylated PCNA, accumulation of ssDNA gaps, checkpoint activation, and resolution of the damage in timecourse experiments with synchronised cultures. Besides, using genome-wide approaches may ease finding factors that engage in template switching.

In the first two parts of the thesis, I intended to develop and optimise fluorescent microscopy and genomics systems to study the dynamics of DNA damage bypass in live cells of *S.cerevisiae*. These systems were based on specialised probes that exclusively recognise mono- and polyubiquitylated PCNA. On the one hand, the microscopy-based approach allowed dissecting the regulation of DNA damage bypass in time and space. On the other hand, the genomics method aimed to gain a genome-wide view of PCNA mono- and polyubiquitylation.

There is a lack of evidence about the molecular details of error-free template switching and the factors that bind preferentially to polyubiquitylated PCNA. Hence, the identification of such effector proteins would be a significant milestone in the fields of post-translational modification and DNA repair. The last part of this work aspired toward identifying, validating, and characterising effector receptors of polyubiquitylated PCNA by using the specialised PCNA probes in novel genetic screening approaches.

Chapter 2

Material and methods

2.1 Reagents

2.1.1 Chemicals and reaction buffers

Unless stated differently, chemicals were purchased from Sigma-Aldrich (Merck) or Thermo Fisher Scientific. The table below lists the most frequently used chemicals or the ones purchased from other companies.

Chemical	Source
4x NuPAGE LDS buffer	Thermo Fisher Scientific
5x Herculase reaction buffer	Agilent
10x Pfu reaction buffer,	Agilent
10x Restriction enzymes reaction buffer	New England Biolabs
10x Antarctic phosphatase reaction buffer	New England Biolabs
10x T4 DNA ligase buffer	New England Biolabs
Concanavalin A	Sigma-Aldrich L7647
Doxycycline hydrochloride	Sigma-Aldrich - D3447
DNA Clean & Concentrator	Zymo Research
FACSFlow, FACSRinse, and FACSClean	BD Biosciences
InstantBlue Ultrafast Protein Stain	Biozol Diagnostica
MasterPure^{TM} Yeast DNA Purification Kit	Biozym - MPY80200
Methyl methanesulfonate	Sigma-Aldrich - 129925
Ni-NTA Agarose	Qiagen
QIAquick Gel Extraction Kit	Qiagen
5-Flouroorotic acid monohydrate	TCR/ Biozol - F595000

Table 2.1.1: A list of chemicals and reagents

2.1.2 Proteins

Protein	Source
α-factor	Eurogentec Germany - AS602215
Antarctic phosphatase	New England Biolabs - M0289S
Bovine serum albumin (BSA)	Sigma-Aldrich - A7906
Fast alkaline phosphatase	Thermo Fisher Scientific - EF0651
^{GFP}Ubi	A kind gift from Dr Sabrina Wegmann (Ulrich lab alumnus)
Herculase II DNA polymerase	Agilent - 600679
Pfu Turbo DNA polymerase	Agilent -600250-100U
Pfu Ultra DNA polymerase	Agilent - 600380
Phusion HF DNA polymerase	New England Biolabs - M530L
Proteinase K	Sigma-Aldrich - P4850
Q5 DNA polymerase	New England Biolabs - M0491S
Restriction enzymes	New England Biolabs
RNase A	Sigma-Aldrich - 10109169001
T4 DNA ligase	New England Biolabs - M0202L
Taq DNA polymerase	IMB's Protein production facility
USP2	IMB's Protein production facility
Zymolyase 20T	AMS Biotechnology- 120491-1
Zymolyase 100T	AMS Biotechnology- 120493-1

Table 2.1.2: A list of proteins used in this study

2.1.3 Antibodies

Clonal type	ID	Specificity	Host	Clone	Dilution	Source (catalog #)
Monoclonal	24	mCherry	Mouse	1C51	1:2000	Abcam ab125096
	42	FLAG	Mouse	M2	1:2000	Sigma-Aldrich F1804
	45	GAL4-TA	Mouse IgG2b	C10	1:1000	Santa Cruz SC1663
	46	GAL4 (DBD)	Mouse IgG2a kappa	RK5C1	1:1000	Santa Cruz SC-510
	49	GFP	Mouse IgG1 kappa	7.1/13.1	1:5000	Roche via Sigma-Aldrich 11814460001
	100	c-Myc	Mouse IgG1	9E10	1:2000	Invitrogen 13-2500
	137	Phosphoglycerate kinase	Mouse IgG1 kappa	22C5D8	1:10.000	Invitrogen 459250
	250	Tubulin alpha Yeast	Rabbit IgG	EPR13799	1:10.000	Abcam ab184970
	280	VSV Glycoprotein	Mouse	P5D4	1:1000	Sigma-Aldrich SAB4200695
	297	Rad53	Mouse	N/A	1:200	Susan Gasser
	315	Sic1	Rabbit IgG	FL-284	1:1000	Santa Cruz SC50441 discontinued
Polyclonal	150	PCNA/Pol 30 Yeast	Rabbit Serum	Bleed 37/38	1:1000	In-house
	350	tRFP	Rabbit	N/A	1:2500	BioCat - AB233

Table 2.1.3: A list of primary antibodies used in this study

ID	Specificity	Host	Dilution	Source (catalog #)
91	Mouse - 680LT	Donkey	1:10.000	Licor - 926-68022
92	Mouse - 800CW	Donkey	1:10.000	Licor - 926-32212
93	Polyclonal anti-mouse HRP	Goat	1:10.000	Dako - P044701-2
154	Rabbit - 680LT	Donkey	1:10.000	Licor- -926-68023
155	Rabbit - 800CW	Goat	1:10.000	Licor - 926-32211
156	Polyclonal anti-rabbit HRP	Goat	1:10.000	Dako - P044801-2
159	Monoclonal anti-rabbit IgG light chain HRP	Mouse	1:10.000	Jackson IR - 211-002-171

Table 2.1.4: A list of secondary antibodies used in this study

2.2 Media

2.2.1 Bacterial growth media

Luria Broth (LB) liquid medium and LB agar plates were prepared by the Institute of Molecular Biology's media laboratory. For the selection of transformed bacterial cells, desired antibiotics were supplemented to the LB media from 1000x stock solutions stored at -20^{o} C to a final 1x concentration.

Antibiotic	1000x stock solutions (mg/mL)	Solvent
Ampicillin	100	Water
Chloramphenicol	34	Ethanol
Geniticin (G418)	200	Water
Hygromycin B	400	Invivogen buffer
Kanamycin	30	Water
Nourseothricin	100	Water

Table 2.2.1: A list of antibiotics used in this thesis

2.2.2 Yeast growth media

Yeast Peptone (YP) medium, Yeast Peptone Glucose/Dextrose (YPD) medium, 2% YPD agar, 4% (w/v) water-agar, and 20% (w/v) glucose were prepared by Institute of Molecular Biology's media laboratory.

Dropout powder: 2 g of p-aminobenzoic acid and 20 g of each of alanine, arginine, asparagine, aspartic acid, cysteine, glutamine, glutamic acid, glycine, inositol, isoleucine, lysine, methionine, phenylalanine, proline, serine, threonine, tyrosine, and valine were mixed overnight on a roller mixer

in room temperature.

Synthetic Complete (SC) powder: 36.7 g of dropout powder, 0.5 g adenine, 2 g histidine, 4 g leucine, 2 g tryptophan, and 2 g uracil were mixed overnight on a roller mixer in room temperature. Specific SC powder stocks were prepared by excluding the desired amino acid.

2.5x SC medium: 12.5 g of ammonium sulfate, 4.25 g of yeast nitrogen base (without amino acids and ammonium sulfate), and 5 g of the desired SC powder were mixed in 1 L of water, stirred for 30 min, and autoclaved.

Liquid SC medium: 200 mL of 2.5x SC medium, 250 mL of distilled water, and 50 mL of 20% (w/v) glucose, raffinose, or galactose were mixed and filter-sterilised.

SC-agar: 200 mL of 2.5x SC medium, 250 mL of 4% melted water-agar, and 50 mL of 20% (w/v) glucose, raffinose, or galactose were mixed. Petri dishes with 20 mL of media and Singer PlusPlates with 50 mL media were prepared under a fume hood on an even surface.

YPD-agar with antibiotics: 2% YPD agar was melted, cooled to 50° C, and supplemented with either geneticin (G418), hygromycin B, or nourseothricin.

5-FOA SC-agar: 200 mL of 2.5x SC complete medium, 250 mL of melted 4% w/v water-agar, 50 mL of 20% w/v glucose, 8 mL of (2 mg/mL) uracil , 8 mL of (2 mg/mL) adenine, and 500 mg 5-fluoroorotic acid.

20% w/v galactose: 200 g of galactose and warm water up to 1 L were mixed and autoclaved.

20% w/v raffinose: 200 g of raffinose and warm water up to 1 L were mixed and autoclaved.

100 mM $CuSO_4$: 24.97 g of copper sulphate pentahydrate was mixed with water up to 100 mL and filter-sterilised.

1% w/v KOAc: 1 g of potassium acetate was mixed with water up to 100 mL and filter-sterilised.

2.3 Solutions and buffers

2.3.1 General solutions and buffers

The media laboratory of Institute of Molecular Biology has prepared according to general recipes the following buffers: 0.5 M EDTA pH 8.0, 5 M NaCl, 5x PBS, 10x SDS running buffer, 10x transfer buffer, 10x Tris-HCl pH 7.5, 10x TBE.

2.3.2 Buffers for DNA and proteins

6x DNA loading buffer: 50% (w/v) sucrose, 0.1% (w/v) bromophenol blue, and 0.1% (w/v) xylene cyanol F in TE

Annealing buffer: 10 mM Tris-HCl pH 7.5, 50 mM NaCl, and 1 mM EDTA

Blocking solution: 5% (w/v) skimmed milk powder (Sigma-Aldrich) in PBS-T

Blotting buffer (Turbo transfer): 3.9 mM glycine, 4.8 mM Tris, 0.13 mM SDS, and 20% (v/v) ethanol

Blotting buffer (wet transfer): 192 mM glycine, 25 mM Tris, and 15% (v/v) methanol

HU buffer: 8 M urea, 5% (w/v) SDS, 200 mM Tris-HCl pH 6.8, 1 mM EDTA, 0.1% (w/v) bromophenol blue, and 50 mM DTT

NuPAGE MES SDS-running buffer: 50 mM MES hydrate, 50 mM Tris-HCl pH 7.3, 0.1 % (v/v) SDS, and 1 mM ETDA

NuPAGE MOPS SDS-running buffer: 50 mM MOPS, 50 mM Tris-HCl pH 7.7, 0.1 % (v/v) SDS, and 1 mM ETDA

PBS-T: 1x PBS and 0.1% (v/v) Tween 20

Ponceau S solution: 0.1 % (w/v) Ponceau S in 5 % acetic acid (v/v)

Stripping buffer: 200 mM glycine, 0.1% SDS, 1% Tween 20, at pH 2.2

2.3.3 Buffers for protein purification

IMAC buffer A: 50 mM Tris, 300 mM NaCl, 15 mM imidazol, pH 8.0, freshly added 1 mM DTT

IMAC buffer B: 50 mM Tris, 300 mM NaCl, 500 mM imidazol, pH 8.0, freshly added 1 mM DTT

Protein storage buffer: 50 mM HEPES, 50 mM NaCl, 1 mM DTT, 10 % glycerol, at pH 7.4

2.3.4 Buffers for chromatin immunoprecipitaion

Quenching solution: 2.5 M (w/v) glycine (Sigma-Aldrich) in PBS

Lysis buffer: 50 mM HEPES pH 7.4-7.5, 1 mM EDTA, 140 mM NaCl, 1% Triton X-100, and 0.1% (w/v) sodium deoxycholate. Before each use, the buffer was freshly supplemented with 1x Protease Inhibitor Cocktail (EDTA-free, Sigma-Aldrich), 10 mM N-ethylmaleimide, and 10 mM O-phenanthroline

Washing buffer I: 50 mM HEPES pH 7.4-7.5, 1 mM EDTA, 500 mM NaCl, 1% Triton X-100, and 0.1% (w/v) sodium deoxycholate

Washing buffer II: 10 mM Tris-HCl pH 8.0, 1 mM EDTA, 250 mM LiCl, 0.5% IGEPAL CA-630, and 0.5% (w/v) sodium deoxycholate

Elution buffer: 50 mM Tris-HCl pH 8.0, 10 mM EDTA, and 1% (w/v) SDS

10x TE buffer: 100 mM Tris-Cl pH 8.0 and 10 mM EDTA pH 8.0

2.3.5 Buffers for yeast cells

50 mM citrate buffer: 2.94 g of trisodium citrate dissolved in distilled water, pH adjusted the to 7.0 with 1 N citric acid

HT DNA solution: Herring testes DNA Type XIV (Sigma-Aldrich) was dissolved and vigorously sonicated in TE buffer (10 mg/mL), phenol/chloroform extracted, precipitated with ethanol, and resuspended in TE buffer before boiling at 95^{o} C for 5 min. Afterwards the solution was quickly incubated on ice for 5 min and stored at 4^{o} C.

10x LiAc buffer: 1 M lithium acetate, autoclaved

PEG buffer: 50% (w/v) PEG 3350 in sterile water, autoclaved

NaOH/β-mercaptoethanol: 925 μL of 2 M NaOH and 75 μL of β-mercaptoethanol

Propidium iodide stock solution: 160 μg/mL propidium iodide in 50 mM citrate buffer

Sporulation solution: 1% (w/v) potassium acetate, filter-sterilised

STE buffer: 1.2 M sorbitol, 25 mM Tris-HCl pH 8.0, 25 mM EDTA pH 8.0, filter-sterilised

STE-Zymolyase solution: 37 μL of STE buffer, 2 μL of 1 M DTT, and 1 μL of a 20 mg/mL Zymolyase (20 T) solution

2.4 DNA oligonucleotides

DNA oligonucleotides for the experiments of this study were purchased either from Sigma-Aldrich or Integrated DNA Technologies (IDT).

Table 2.4.1: A list of the DNA oligonucleotides used in this study

ID	Name	Sequence
527	9Myc-For	TCTCTAAATGATTGGCGTACGTTGCAGGTCGAC
665	ARS501-For	AAGCAAATTGCAGAAGGTTATGAA
666	ARS501-Rev	TTCAAGGCTCTAGCATATGAAACG
2745	KpnI-yeGFP-For-overlap-mUBD	CCGAAGGTACCGGATCCGGAGCAGGTGCTGGTG
2746	KpnI-yeGFP-overlap-polUBD-For	CTCTGCTGGTACCGGATCCGGAGCGGTGCTGGTG
2748	BglII-SmaI-NLS-PIP-UBD-For	GGAAGATCTCCCGGGATGCCCAAGAAAAAGCGTAAGGTCCATAATCCGGATGACACTAC
2749	PIP-polUBD-KpnI-overlap-yeGFP-Rev	GGATCCGGTACCAGCAGAGTTACGGCACTCC
2750	PIP-polUBD-KpnI-VSV-SalI-Rev	AAAAGTCGACCTACTTTCCCAATCTGTTCATTTCTATGTCAGTATAGGTACCAGCAGAGTTACGGCACTCC
2751	PIP-mUBD-KpnI-Overlap-yeGFP-Rev	CCGGATCCGGTACCTTCGGCAGCTGCACGTTCTGC
2752	PIP-mUBD-KpnI-VSV-SalI-Rev	AAAAGTCGACCTACTTTCCCAATCTGTTCATTTCTATGTCAGTATAGGTACCTTCGGCAGCTGCACGTTC
2754	M13-For	TGTAAAACGACGGCCAGT
2755	M13-Rev	CAGGAAACAGCTATGAC
2757	yeGFP-SalI-NotI-Rev	AAATATGGCGGCCGCGGTCGACTTATTTGTACAATTCATCCAT
2758	KpnI-yeGFP-overlap-PIP-For	AAACAACGGTACCGGATCCGGAGCAGGTGCTGGTG

Table 2.4.1: A list of the DNA oligonucleotides used in this study

ID	Name	Sequence
2759	BglII-SmaI-NLS-mUBD-For	ATAGGAAGATCTCCCGGGATGCCCAAGAAAAAGCGTAAGGTCACTGAAGAGGAGCAGATTGC
2760	BglII-SmaI-NLS-polyUBD-For	ATAGGAAGATCTCCCGGGATGCCCAAGAAAAAGCGTAAGGTCGCAGCTGCTGCAGCTGCTGCTGAAAAAGC
2761	PIP-KpnI-overlap-yeGFP-Rev	CCGGATCCGGTACCGTTGTTTAATTTTG
2763	CYC1-TATA-For	TATACTTCTATAGACACGC
2766	CYC1TT-BglII	AGCCTAGATCTTCGACGGCCGCAAATTAAAGCCTTC
2767	VP16-(tTA)-EcoRI-Rev	AACCGGAATTCCTACCCACCGTACTCGTCAATTCC
3143	ARS607-For	CGGCTCGTGCATTAAGCTTG
3144	ARS607-Rev	TGCCGCACGCCAAACATTGC
3649	mCherry-NotI-Rev	AAGCTGCGGCCGCTTATTTGTACAGCTCGTCCATGCCGC
3829	HTA2-tag-For	CCAAAGAAGTCTGCCAAGACTGCCAAAGCTTCTCAAGAACTGCGTACGCTGCAGGTCGAC
3830	HTA2-tag-Rev	CCCCAAATGACAAGAATGTTTGATTTGCTTTGTTTCTTTTCAACTCCATCGATGAATTCGAGCTCG
3831	NIC96-tag-For	AGGGAAACGTACAGCACTTTAATTAATATAGACGTCTCTCTACGTACGCTGCAGGTCGAC
3832	NIC96-tag-Rev	CGCATACTGATATATAGATATAAACAAAAATATACAATATTTAAAACATCGATGAATTCGAGCTCG
3877	RAD5-C914S-For	TCGTTTCAGTCCTTAGAGAGTTCCATCTGCACAACGGAA
3878	RAD5-C914S-Rev	TTCCGTTGTGCAGATGGAACTCTCTAAGGACTGAAACGA

Table 2.4.1: A list of the DNA oligonucleotides used in this study

ID	Name	Sequence
3881	9Myc-NotI-Rev	AAATATGGCGGCCGCGGAATGATCG TTCCACTTTTTAGCTAGTGGA
3901	monoUBD-K26R-K27R-For	GGTTCCGATCTCCTGTGCAGAAGAG GATGTGGTTACTACGGC
3902	monoUBD-K26R-K27R-Rev	GCCGTAGTAACCACATCCTCTTCTG CACAGGAGATCGGAACC
3975	BglII-3xNLS-For	GGAAGATCTATGCCTAAGAAGAAGA GAAAGGTCGATCCTAAAAAGAAAC GCAAAGTGGACCCCAAGAAAAAAC GAAAAGTC
3976	3xNLS-EcoRI-Rev	CCGAGAATTCGACTTTTCGTTTTTTC TTGGGGTCCACTTTGCGTTTCTTTTT AGGATCGACCTTTCTCTTCTTCTTAG G
3977	EcoRI-PIP-For	GGAAGAATTCCATAATCCGGATGAC ACTACAG
4099	ECM32-KO-For	ATAAGGAGTTCCGCAGACTAAGAAG TACTACACGCGTACGCTGCAGGTCG ACGG
4100	ECM32-KO-Rev	AAACAGTGGATTTTCTTGCCGCCGC CTAGCCGGATCGATGAATTCGAGCT CG
4101	YBL036C-KO-For	CTTTTTGACTAAGATTCCAGCATCAC ATTGCAATCGTACGCTGCAGGTCGA CGG
4102	YBL036C-KO-Rev	GATCTTCGTATAAAATCTCAGTTCAT TCAACCTAATCGATGAATTCGAGCT CG
4116	monoUBD-Overlap-HpaI-linker-yomRuby2-For	GCTGCCGAAGTTAACTCGTACGCTG CAGGTCG
4117	polyUBD-Overlap-BamHI-linker-yomRuby2-For	AACTCTGCTGGATCCTCGTACGCTG CAGGTCG
4118	NotI-yomRuby2-Rev	AAGCTGCGGCCGCTTACTTATACAA TTCATCCATACCACC

Table 2.4.1: A list of the DNA oligonucleotides used in this study

ID	Name	Sequence
4119	yomRuby2-Overlap-HpaI-monoUBD-Rev	AGCGTACGAGTTAACTTCGGCAGCT GCACGTTCTGC
4120	yomRuby2-Overlap-BamHI-polyUBD-Rev	AGCGTACGAGGATCCAGCAGAGTTA CGGCACTCC
4121	BamHI-yomRuby2-For	GCATGGATCCATGGTGTCCAAAGGA GAGGAG
4132	HTA2-pFA6a-tag-For	CCAAAGAAGTCTGCCAAGACTGCC AAAGCTTCTCAAGAACTGCCAGCT GAAGCTTCGTAC
4144	ADH1-terminator-NotI-Rev	AAGCTGCGGCCGCCCGGTAGAGGT GTGGTCAAT
4287	BglII-1xNLS-GFP-For	GGAAGATCTCCCGGGATGCCCAAG AAAAAGCGTAAGGTCTCTAAAGGTG AAGAATTATTC
4345	NOP1-tag-For	TGTATCGTCGTTGGTAGATACATGAG AAGCGGTTTGAAGAAACGTACGCT GCAGGTCGAC
4346	NOP1-tag-Rev	ATAATTGAGCAAGCTACCAGAAACT TTTGACTAATTTCCTTTATTCCATCGA TGAATTCGAGCTCG
4413	ECM32-tag-For	CTCGAGGAACAAGAGGTCATATTCA CTGATCTCACAGCTTACCGTACGCT GCAGGTCGAC
4414	ECM32-tag-Rev	GCAATCAATACATAAACAGTGGATTT TCTTGCCGCCGCCTAGCCGGCATCG ATGAATTCGAGCTCG
4415	YBL036C-tag-For	ATTTTTGGTGCTAGACCTCCAAAAA ATGAAGCTAGAATCATTCGTACGCT GCAGGTCGAC
4416	YBL036C-tag-Rev	TATAAAAAAAAAGATCTTCGTATAAA ATCTCAGTTCATTCAACCTACATCGA TGAATTCGAGCTCG

Table 2.4.1: A list of the DNA oligonucleotides used in this study

ID	Name	Sequence
4417	UPF3-tag-For	GTACCACGGGTAAAAATTTTGCATC GTGATGATACCAAGAAGCGTACGCT GCAGGTCGAC
4418	UPF3-tag-Rev	TATAAATGTATTCCATATATAATATATA AGAAGCCATGAGCTTTTACATCGAT GAATTCGAGCTCG
4468	monoUBD-K43R-For	TGGCAGGGTTTCTGCTCCAGATGCT GGAGGGAAGAGGCC
4469	monoUBD-K43R-Rev	GGCCTCTTCCCTCCAGCATCTGGAG CAGAAACCCTGCCA
4470	monoUBD-K51R-For	TGGAGGGAAGAGGCCTGCAGGGCA GCTGCAGAACGTGCA
4471	monoUBD-K51R-Rev	TGCACGTTCTGCAGCTGCCCTGCAG GCCTCTTCCCTCCA
4550	RNH1-KO-For	CCTTGCTTATCGAAGGAACTATCGAT TCCTAATTTCGTACGCTGCAGGTCG ACGG
4551	RNH1-KO-Rev	ACAGGTCCAGTAAGAAGCCAAGCA AAAAACAGCAATCGATGAATTCGAG CTCG
4552	RNH201-KO-For	AAACAACTACTGCACACCAAATTGA TACGATTAATCGTACGCTGCAGGTC GACGG
4553	RNH201-KO-Rev	ATGAAGATATATAGTATGTGCAAACT GGAGGTGAATCGATGAATTCGAGCT CG
4554	RNH1-D193N-For	TCTATGAACGTTTACTGTAACGGTTC AAGTTTTGGAAAC
4555	RNH1-D193N-Rev	GTTTCCAAAACTTGAACCGTTACAG TAAACGTTCATAGA
4556	EcoRI-linker-yomRuby2-Rev	GGTTGAATTCAGGCAGAATTGCTCC AGCACCAGCACCAGCACCTGCTCC GGACCCGTCCTTATACAATTCATCCA TACC

Table 2.4.1: A list of the DNA oligonucleotides used in this study

ID	Name	Sequence
4564	NdeI-Flag-NdeI -For	TATGGATTATAAAGATGATGACGATA AGGGCGGCCA
4565	NdeI-Flag-NdeI-Rev	TATGGCCGCCCTTATCGTCATCATCT TTATAATCCA
4566	RAP1-tag-For	GGTAGAATGGAAATGAGGAAAAGAT TTTTTGAGAAGGACCTGTTATCGTAC GCTGCAGGTCGA
4567	RAP1-tag-Rev	AAGGAGTAAAATAAGTTAAACAATG ATGTTACTTAATTCAATTACATCGATG AATTCGAGCTCG
4569	CBF1-tag-For	GAGAACGAAAGAAAAAGCACTAGG AGCGATAATCCACATGAGGCTTCGT ACGCTGCAGGTCGA
4570	CBF1-tag-Rev	TACATAGGGAGACTCGAAATACATTT AGCTATCTATTTTTAACTCCATCGAT GAATTCGAGCTCG
4574	ECM32-ORF-For	CGCGGATCCATGGATTTTCAGTGCA GAACGTGTAG
4575	ECM32-ORF-Rev	ACGCGTCGACCTAGTAAGCTGTGAG ATCAGTGAAT
4576	YBL036C-ORF-For	CGCGGATCCATGTCCACTGGTATTAC TTATGATGA
4577	YBL036C-ORF-Rev	ACGCGTCGACCTAAATGATTCTAGC TTCATTTTTT
4578	UPF3-ORF-For	CGCGGATCCATGAGCAATGTGGCTG GGGAATTGAA
4579	UPF3-ORF-Rev	ACGCGTCGACCTACTTCTTGGTATCA TCACGATGC
4580	NAM7/UPF1-ORF-For	CGCGGATCCATGGTCGGTTCCGGTT CTCACACTCC
4581	NAM7/UPF1-ORF-Rev	ACGCGTCGACTTATATTCCCAAATTG CTGAAGTCT

Table 2.4.1: A list of the DNA oligonucleotides used in this study

ID	Name	Sequence
4623	EcoRI-GFP/mCherry-For	CCGGAATTCGGATCCGGAGCAGGTG CTGGTG
4624	CYC1TT-NsiI-Rev	AGCCTATGCATTCGACGGCCGCAAA TTAAAGCCTTC
4636	RNH1-NotI-Rev	AAGCTGCGGCCGCCTATCGTCTAGA TGCTCCTTTCT
4637	NAM7/UPF1-KO-For	CTTTTTATATTACATCAATCATTGTCA TTATCAACGTACGCTGCAGGTCGACGG
4638	NAM7/UPF1-KO-Rev	AGTTTAACATTTTATTTTAACAGGGTT CACCGAAATCGATGAATTCGAGCTCG
4639	UPF3-KO-For	TACATTTCTGCTGAAATATATAGTAAT CTATCCGTACGCTGCAGGTCGACGG
4705	RAP1-GFP-tag-For	GGTAGAATGGAAATGAGGAAAAGAT TTTTTGAGAAGGACCTGTTACGTAC GCTGCAGGTCGA
5083	CFP-BamHI -For	GCATGGATCCATGAGCAAGGGCGAG GAGCT
5084	CFP-NotI-Rev	AAGCTGCGGCCGCTTACTTGTACAG CTCGTCC
5228	RAD5-FN13-14AA-For	GGAAGAAAGGAAGAGGTTTGCAGC AGATGACCTTGACACTTCAGA
5229	RAD5-FN13-14AA-Rev	TCTGAAGTGTCAAGGTCATCTGCTG CAAACCTCTTCCTTTCTTCC

2.5 Plasmids

Table 2.5.1: A list of plasmids used in this study

ID	Name	Use	Source
66	YIp128	Yeast integrative plasmid, *LEU2* auxotrophic marker	Helle Ulrich
67	YIp204	Yeast integrative plasmid, *TRP1* auxotrophic marker	Helle Ulrich
73	YEp195-pGAL1	Gal-inducible overexpression in yeast, *URA3* auxotrophic marker	Helle Ulrich
191	pGAD-C1	Yeast two-hybrid expression vector, *LEU2* auxotrophic marker	Philip James
194	pGBD-C1	Yeast two-hybrid expression vector, *TRP1* auxotrophic marker	Philip James
233	pFA6a-HIS3MX	HIS3MX disruption cassette for gene deletion	Helle Ulrich
309	pFA6a-KanMX	KanMX disruption cassette for gene deletion	Michael Knop [267]
386	YEp112	Overexpression in yeast, *TRP1* auxotrophic marker	Helle Ulrich
654	YEp181-pADH1	Overexpression in yeast, *LEU2* auxotrophic marker	Helle Ulrich
1633	pFA6a-NatNT2	Nourseothricin disruption cassette for gene deletion	John Diffley, Euroscarf: P30346
1633	pFA6a-hphNT1	Hygromycin B disruption cassette for gene deletion	John Diffley, Euroscarf: P30347
1656	pYES2-RAD5	Gal-inducible overexpression of *RAD5*, *URA3* auxotrophic marker	Helle Ulrich
2123	pYM-GFP-HIS3MX6 (pYM44)	Yeast enhanced GFP C-terminal tagging cassette, HIS3MX6 auxotrophic marker	Michael Knop [267] Euroscarf: P30256

Table 2.5.1: A list of plasmids used in this study

ID	Name	Use	Source
2167	YEp195-pADH1	Overexpression in yeast, *URA3* auxotrophic marker	Helle Ulrich
2230	pYM-YFP-hphNT1 (pYM40)	Yeast enhanced YFP C-terminal tagging cassette, Hygromycin B selection marker	Michael Knop [267] Euroscarf: P30252
2398	pYM-9Myc-NatNT2	9Myc C-terminal tagging cassette, Nourseothricin selection marker	Helle Ulrich
2401	pFA6a-link-yomRuby2-SpHIS5	Yeast optimised mRuby2 C-terminal tagging cassette, *SpHIS5* auxotrophic marker	[268] Addgene: 44858
2413	pYM26-GFP-KlTRP1	Yeast enhanced GFP C-terminal tagging cassette, *KlTRP1* auxotrophic marker	Michael Knop [267] Euroscarf: P30238
2453	pYES2-RAD5-Q1106D	Gal-inducible overexpression of *RAD5* mutant, *URA3* auxotrophic marker	Helle Ulrich
2556	pYM-CFP-KlTRP1 (pYM32)	Enhanced CFP tagging C-terminal cassette, *KlTRP1* auxotrophic marker	Michael Knop [267] Euroscarf: P30244
2586	pYM-mCherry-HIS3MX6	mCherry C-terminal tagging cassette, HIS3MX6 auxotrophic marker	Helle Ulrich
2623	pYM-mCherry-hphNT1	mCherry C-terminal tagging cassette, Hygromycin B selection marker	Helle Ulrich
2636	YIp211-pCUP1	Cu^{2+}–inducible expression of any gene of interest, *URA3* auxotrophic marker	This study
2637	YIp211-pCUP1-1xNLS-PIP-monoUBD-yeGFP	Cu^{2+}–inducible expression of the probe for microscopy, *URA3* auxotrophic marker	This study

Table 2.5.1: A list of plasmids used in this study

ID	Name	Use	Source
2638	YIp211-pCUP1-1xNLS-PIP-polyUBD1-yeGFP	Cu^{2+}–inducible expression of the probe for microscopy, *URA3* auxotrophic marker	This study
2639	YEp181-pADH1-1xNLS-PIP-monoUBD-VSV	Overexpression of the probe for spot assay, *LEU2* auxotrophic marker	This study
2640	YEp181-pADH1-1xNLS-PIP-polyUBD1-VSV	Overexpression of the probe for spot assay, *LEU2* auxotrophic marker	This study
2641	YEp181-pADH1-1xNLS-PIP-polyUBD2-VSV	Overexpression of the probe for spot assay, *LEU2* auxotrophic marker	This study
2642	YEp181-pADH1-1xNLS-PIP-polyUBD3-VSV	Overexpression of the probe for spot assay, *LEU2* auxotrophic marker	This study
2717	YEp181-pADH1-1xNLS-PIP-VSV	Overexpression of the single-domain control for spot assay, *LEU2* auxotrophic marker	This study
2718	YEp181-pADH1-1xNLS-monoUBD-VSV	Overexpression of the single-domain control for spot assay, *LEU2* auxotrophic marker	This study
2719	YEp181-pADH1-1xNLS-polyUBD1-VSV	Overexpression of the single-domain control for spot assay, *LEU2* auxotrophic marker	This study
2725	YIp211-Tet-ON-1xNLS-PIP-GFP	Dox-inducible expression of the single-domain control for microscopy, *URA3* auxotrophic marker	This study
2726	YIp211-Tet-ON-1xNLS-monoUBD-GFP	Dox-inducible expression of the single-domain control for microscopy, *URA3* auxotrophic marker	This study

Table 2.5.1: A list of plasmids used in this study

ID	Name	Use	Source
2727	YIp211-Tet-ON-1xNLS-polyUBD1-GFP	Dox-inducible expression of the single-domain control for microscopy, *URA3* auxotrophic marker	This study
2728	YIp211-Tet-ON-1xNLS-PIP-mUBD-GFP	Dox-inducible expression of the probe for microscopy, *URA3* auxotrophic marker	This study
2729	YIp211-Tet-ON-1xNLS-PIP-polyUBD1-GFP	Doxinducible expression of the probe for microscopy, *URA3* auxotrophic marker	This study
2998	YIp128-Tet-ON-lambda linker	Dox-inducible expression of any gene of interest, *LEU2* auxotrophic marker	This study
2999	YIp128-Tet-ON-1xNLS-PIP-monoUBD-GFP	Dox-inducible expression of the probe for microscopy, *LEU2* auxotrophic marker	This study
3000	YIp128-Tet-ON-1xNLS-PIP-polyUBD2-GFP	Dox-inducible expression of the probe for microscopy, *LEU2* auxotrophic marker	This study
3001	YIp128-Tet-ON-1xNLS-PIP-monoUBD-mCherry	Dox-inducible expression of the probe for microscopy, *LEU2* auxotrophic marker	This study
3002	YIp128-Tet-ON-1xNLS-PIP-polyUBD1-mCherry	Dox-inducible expression of the probe for microscopy, *LEU2* auxotrophic marker	This study
3003	YIp204-Tet-ON-3xNLS-PIP-monoUBD-9xMyc	Dox-inducible expression of the probe for chromatin spreads/ microscopy, *TRP1* auxotrophic marker	This study
3004	YIp204-Tet-ON-3xNLS-PIP-polyUBD1-9xMyc	Dox-inducible expression of the probe for chromatin spreads/ microscopy, *TRP1* auxotrophic marker	This study

Table 2.5.1: A list of plasmids used in this study

ID	Name	Use	Source
3178	pUN100-nup133DN	Overexpression of a trancated protein that collapses the nuclear pore into a one focus	Susan Gasser
3288	YIp211-Tet-ON-1xNLS-PIP-polyUBD2-GFP	Dox-inducible expression of the probe for microscopy, *URA3* auxotrophic marker	This study
3289	YIp211-Tet-ON-1xNLS-PIP-polyUBD3-GFP	Dox-inducible expression of the probe for microscopy, *URA3* auxotrophic marker	This study
3290	YIp128-Tet-ON-1xNLS-PIP-polyUBD2-mCherry	Dox-inducible expression of the probe for microscopy, *LEU2* auxotrophic marker	This study
3291	YIp128-Tet-ON-1xNLS-PIP-polyUBD3-mCherry	Dox-inducible expression of the probe for microscopy, *LEU2* auxotrophic marker	This study
3292	pYES2-His preSc-RAD5-I916A	Gal-inducible overexpression of *RAD5* mutant, *URA3* auxotrophic marker	This study
3293	pYES2-His preSc-RAD5-I916A-Q1106D	Gal-inducible overexpression of *RAD5* mutant, *URA3* auxotrophic marker	This study
3295	YIp211-Tet-ON-3xNLS-PIP-monoUBD-GFP	Dox-inducible expression of the probe for microscopy, *URA3* auxotrophic marker	This study
3296	YIp211-Tet-ON-3xNLS-PIP-polyUBD1-GFP	Dox-inducible expression of the probe for microscopy, *URA3* auxotrophic marker	This study
3297	YIp211-Tet-ON-3xNLS-PIP-polyUBD2-GFP	Dox-inducible expression of the probe for microscopy, *URA3* auxotrophic marker	This study
3298	YIp211-Tet-ON-3xNLS-PIP-polyUBD3-GFP	Dox-inducible expression of the probe for microscopy, *URA3* auxotrophic marker	This study

Table 2.5.1: A list of plasmids used in this study

ID	Name	Use	Source
3300	YIp128-Tet-ON-1xNLS-PIP-monoUBD-mRuby2	Dox-inducible expression of the probe for microscopy, *LEU2* auxotrophic marker	This study
3301	YIp128-Tet-ON-1xNLS-PIP-polyUBD1-mRuby2	Dox-inducible expression of the probe for microscopy, *LEU2* auxotrophic marker	This study
3302	YIp128-Tet-ON-1xNLS-PIP-polyUBD2-mRuby2	Dox-inducible expression of the probe for microscopy, *LEU2* auxotrophic marker	This study
3303	YIp128-Tet-ON-1xNLS-PIP-polyUBD3-mRuby2	Dox-inducible expression of the probe for microscopy, *LEU2* auxotrophic marker	This study
3395	pET28b-PIP-monoUBD	Overproduction of the probe in *E.coli*	Robert Cohen
3396	pET28b-PIP-polyUBD1	Overproduction of the probe in *E.coli*	Robert Cohen
3397	pET28b-PIP-polyUBD2	Overproduction of the probe in *E.coli*	Robert Cohen
3398	pET28b-PIP-polyUBD3	Overproduction of the probe in *E.coli*	Robert Cohen
3586	YEp181-pADH1-1xNLS-PIP-monoUBD-K26R-K27R-VSV	Overexpression of the mutant probe for spot assay, *LEU2* auxotrophic marker	This study
3587	YEp181-pADH1-1xNLS-monoUBD-K26R-K27R-VSV	Overexpression of the mutant probe for spot assay, *LEU2* auxotrophic marker	This study
3617	pRS423-GPD-RNH1-HA	Overxpression of Rnh1, *HIS3* auxotrophic marker	Brian Luke
3618	YEp181-pADH1-1xNLS-PIP-monoUBD-K43R-VSV	Overexpression of the mutant probe for spot assay, *LEU2* auxotrophic marker	This study
3619	YEp181-pADH1-1xNLS-PIP-monoUBD-K26-K27R-K43R-VSV	Overexpression of the mutant probe for spot assay, *LEU2* auxotrophic marker	This study

Table 2.5.1: A list of plasmids used in this study

ID	Name	Use	Source
3620	YEp181-pADH1-1xNLS-PIP-monoUBD-K51R-VSV	Overexpression of the mutant probe for spot assay, *LEU2* auxotrophic marker	This study
3621	YEp181-pADH1-1xNLS-PIP-monoUBD_K26R-K27R-K51R-VSV	Overexpression of the mutant probe for spot assay, *LEU2* auxotrophic marker	This study
3622	YEp181-pADH1-1xNLS-PIP-monoUBD-K43R-K51R-VSV	Overexpression of the mutant probe for spot assay, *LEU2* auxotrophic marker	This study
3623	YEp181-pADH1-1xNLS-PIP-monoUBD-K26R-K27R-K43R-K51R-VSV	Overexpression of the mutant probe for spot assay, *LEU2* auxotrophic marker	This study
3626	YEp112-pADH1-1xNLS-PIP-monoUBD-VSV	Overexpression of the probe for spot assay, *TRP1* auxotrophic marker	This study
3627	YEp112-pADH1-1xNLS-PIP-polyUBD1-VSV	Overexpression of the probe for spot assay, *TRP1* auxotrophic marker	This study
3635	pGAP1-mRuby2-RNH1-HA	Overxpression of mRuby2-Rnh1, *HIS3* auxotrophic marker	This study
3636	pGAP1-mRuby2-RNH1-D193N-HA	Overxpression of mutant mRuby2-Rnh1, *HIS3* auxotrophic marker	This study
3661	pGAD-C1-ECM32	Yeast two-hybrid assay, *LEU2* auxotrophic marker	This study
3662	pGAD-C1-YBL036C	Yeast two-hybrid assay, *LEU2* uxotrophic marker	This study
3663	pGAD-C1-UPF3	Yeast two-hybrid assay, *LEU2* auxotrophic marker	This study
3664	pGAD-C-NAM7/UPF1	Yeast two-hybrid assay, *LEU2* auxotrophic marker	This study
3665	pGBD-C1-ECM32	Yeast two-hybrid assay, *TRP1* auxotrophic marker	This study

Table 2.5.1: A list of plasmids used in this study

ID	Name	Use	Source
3666	pGBD-C1-YBL036C	Yeast two-hybrid assay, *TRP1* auxotrophic marker	This study
3667	pGBD-C1-UPF3	Yeast two-hybrid assay, *TRP1* auxotrophic marker	This study
3668	pGBD-C1-NAM7/UPF1	Yeast two-hybrid assay, *TRP1* auxotrophic marker	This study
3717	pET28b-His-3xFlag-PIP-monoUBD	Overproduction of the probe in *E.coli*	This study
3719	pET28b-His-4xFlag-PIP-polyUBD1	Overproduction of the probe in *E.coli*	This study
3732	YIp128-Tet-ON-mRuby2-RNH1-D193N	Dox-inducible expression of mutant mRuby2-Rnh1 for microscopy, *LEU2* auxotrophic marker	This study
3776	YIp128-Tet-ON-3xNLS-PIP-monoUBD-mRuby2	Dox-inducible expression of the probe for microscopy, *LEU2* auxotrophic marker	This study
3890	YIp128-Tet-ON-3xNLS-PIP-polyUBD1-mRuby2	Dox-inducible expression of the probe for microscopy, *LEU2* auxotrophic marker	This study
3891	YIp128-Tet-ON-3xNLS-PIP-polyUBD2-mRuby2	Dox-inducible expression of the probe for microscopy, *LEU2* auxotrophic marker	This study
3892	YIp128-Tet-ON-3xNLS-PIP-polyUBD3-mRuby2	Dox-inducible expression of the probe for microscopy, *LEU2* auxotrophic marker	This study
3939	YEplac195-pGal-VSV-PIP-E3(63)	Gal-inducible overexpression, *URA3* auxotrophic marker	This study
4038	YIp211-Tet-ON-1xNLS PIP-monoUBD-VSV	Dox-inducible expression of the probe for ChIP, *URA3* auxotrophic marker	This study
4039	YIp211-Tet-ON-1xNLS-PIP-polyUBD1-VSV	Dox-inducible expression of the probe for ChIP, *URA3* auxotrophic marker	This study

Table 2.5.1: A list of plasmids used in this study

ID	Name	Use	Source
4061	YIp211-Tet-ON-1xNLS-PIP-polyUBD3-VSV	Dox-inducible expression of the probe for ChIP, *URA3* auxotrophic marker	This study
4353	YIp204-Tet-ON-lambda linker	Dox-inducible expression of any gene of interest, *TRP1* auxotrophic marker	This study
4354	YIp204-Tet-ON-1xNLS-PIP-monoUBD-GFP	Dox-inducible expression of the probe for microscopy, *TRP1* auxotrophic marker	This study
4355	YIp204-Tet-ON-1xNLS-PIP-polyUBD2-GFP	Dox-inducible expression of the probe for microscopy, *TRP1* auxotrophic marker	This study
4399	YIp211-Tet-ON-1xNLS-PIP-monoUBD-YFP	Dox-inducible expression of the probe for microscopy, *URA3* auxotrophic marker	This study
4400	YIp211-Tet-ON-1xNLS-PIP-polyUBD2-YFP	Dox-inducible expression of the probe for microscopy, *URA3* auxotrophic marker	This study
4611	pYES2-RAD5-FN13-14AA	Gal-inducible overexpression of *RAD5* mutant, *URA3* auxotrophic marker	This study
4612	pYES2-RAD5-FN13-14AA-I916A	Gal-inducible overexpression of *RAD5* mutant, *U*RA3 auxotrophic marker	This study
4614	pYES2-RAD5-FN13-14AA-I916A-Q1106D	Gal-inducible overexpression of *RAD5* mutant, *URA3* auxotrophic marker	This study

2.6 Strains

2.6.1 *Escherichia coli* strains

ID	Name	Genotype	Use	Source
5	BL21-Codonplus DE3 RIL-(Codon +)	BF-ompT hsdSB(rB-mB-) dcm+ Tetr gal l(DE3) endA Hte [argU ileY leuW Camr]	Expression of proteins with rare codons: AGA, AGG, AUA, CUA	Stratagene
14	Top Ten (Top10)	F-mcrAΔ(mrr-hsdRMS-mcrBC) φ80lacZΔ M15 ΔlacX74 recA1 araD139Δ(ara-leu)7697 galU galK λ-rpsL(StrR) endA1 nupG	Blue white screening, standard cloning	Invitrogen

Table 2.6.1: A list of *E.coli* strains used in this study

2.6.2 *Saccharomyces cerevisiae* strains

Derivatives of haploid and diploid *Saccharomyces cerevisiae* strains and arrayed libraries with different genetic backgrounds were used in this study as indicated in table (2.6.2).

Strain background	Use	Source
BY4741	Spot assay, genetic screen	Euroscarf [269]
DF5	Microscopy, spot assay	Helle Ulrich [216]
PJ69-4A	Yeast two-hybrid assay	Philip James [270]
UDS (W4730-257)	Plasmid delivery, genetic screen	Rodney Rothstein [271]
W303 RAD5+	Spot assay	Rodney Rothstein [272]
Y258	Genetic screen	Dharmacon [273]

Table 2.6.2: Backgrounds of *S. cerevisiae* strains used in this study

Library	Background and genotype	Source
Yeast ORF collection	Y258 *(MAT-a, pep4-3, his4-580, ura3-52, leu2-3,112)*	Dharmacon #YSC3870 [273]
Yeast knockout collection	BY4741 *(MAT-a, leu2Δ0, met15Δ0, ura3Δ0, his3Δ0, xyz::KanMX)*	Euroscarf [269]

Table 2.6.3: Arrayed *S. cerevisiae* libraries used in this study

Table 2.6.4: A list of *S. cerevisiae* strains received from external sources or used for expression of episomal plasmids

ID	Name	Genotype	Scource
2	DF5 WT	*MAT-alpha, his3-Δ200, leu2-3,2-112, lys2-801, trp1-1(am), ura3-52*	Helle Ulrich [216]
3	DF5 WT	*MAT-a, his3-Δ200, leu2-3,2-112, lys2-801, trp1-1(am), ura3-52*	Helle Ulrich [216]
29	*mms2Δ*	*MAT-a, his3-Δ200, leu2-3,2-112, lys2-801, trp1-1(am), ura3-52 mms2::HIS3*	Helle Ulrich
50	*rad18Δ*	*MAT-a, his3-Δ200, leu2-3,2-112, lys2-801, trp1-1(am), ura3-52 rad18::LEU2*	Helle Ulrich
150	PJ69-4A	*trp1-901, leu2-3,112, ura3-52, his3-Δ200, gal4Δ, gal80Δ, LYS2::GAL1-HIS3, GAL2-ADE2, met2::GAL7-lacZ*	Philip James [270]
162	*rad18Δ*	*MAT-a, his3-Δ200, leu2-3,2-112, lys2-801, trp1-1(am), ura3-52, rad18::TRP1*	Helle Ulrich
170	*rad5Δ*	*MAT-a, his3-Δ200, leu2-3,2-112, lys2-801, trp1-1(am), ura3-52, rad5::HIS3*	Helle Ulrich
345	*ubc13Δ*	*MAT-a, his3-Δ200, leu2-3,2-112, lys2-801, trp1-1(am), ura3-52, ubc13::HIS3*	Helle Ulrich
349	*ubc13Δ rad18Δ*	*MAT-a, his3-Δ200, leu2-3,2-112, lys2-801, trp1-1(am), ura3-52, ubc13::HIS3, rad18::TRP1*	Helle Ulrich
351	*rad5Δ ubc13Δ*	*MAT-a, his3-Δ200, leu2-3,2-112, lys2-801, trp1-1(am), ura3-52, ubc13::HIS3, rad5::HIS3*	Helle Ulrich
790	BY4741 WT	*MAT-a, leu2Δ0, met15Δ0, ura3Δ0, his3Δ0*	Euroscarf [269]
989	POL30 *siz1Δ*	*MAT-a, his3-Δ200, lys2-801, trp1-1(am), ura3-52, pol30::HisG-URA3, siz1::KanMX, leu2-3,2-112::YIp128P30-POL30-LEU3*	Helle Ulrich

Table 2.6.4: A list of *S. cerevisiae* strains received from external sources or used for expression of episomal plasmids

ID	Name	Genotype	Scource
1001	POL30 *ubc13Δ siz1Δ*	*MAT-a, his3-Δ200, lys2-801, trp1-1(am), ura3-52, ubc13::HIS3, pol30::HisG-URA3, siz1::KanMX, leu2-3,2-112::YIp128-P30-POL30-LEU3*	Helle Ulrich
1002	*pol30-K164R ubc13Δ*	*MAT-a, his3-Δ200, lys2-801, trp1-1(am), ura3-52, ubc13::HIS3, pol30::HisG-URA3, leu2-3,2-112::YIp128-P30-pol30(K164R)-LEU2*	Helle Ulrich
1245	*pol30-K164R*	*MAT-a, his3-Δ200, leu2-3,2-112, lys2-801, trp1-1(am), ura3-52, pol30(K164R)*	Helle Ulrich
1320	*rad18Δ siz1Δ*	*MAT-a, his3-Δ200, leu2-3,2-112, lys2-801, trp1-1(am), ura3-52, rad18::TRP1, siz1::KanMX*	Helle Ulrich
1560	*pol30-K127-164R*	*MAT-a, his3-Δ200, lys2-801, trp1-1(am), ura3-52, pol30::URA3, leu2-3,2-112::YIp128-P30-6His-pol30(K127/164R)-LEU2*	Helle Ulrich
1561	*pol30-K127-164R siz1Δ*	*MAT-a, his3-Δ200, lys2-801, trp1-1(am), ura3-52, siz1::KanMX, pol30::URA3, leu2-3,2-112::YIp128-P30-6His-pol30(K127/164R)-LEU2*	Helle Ulrich
2034	*pol32Δ*	*MAT-a, his3-Δ200, leu2-3,2-112, lys2-801, trp1-1(am), ura3-52, pol32::KanMX*	Helle Ulrich
2214	*pol30-K164R*	*MAT-alpha, his3-Δ200, lys2-801, trp1-1(am), ura3-52, pol30::HisG-URA3, leu2-3,2-112::YIp128-P30-pol30(K164R)-LEU2*	Helle Ulrich
2440	*tlsΔ*	*MAT-a, his3-Δ200, leu2-3,2-112, lys2-801, trp1-1(am), ura3-52, rev1::URA3, rev3::KanMX, rad30::HIS3*	Helle Ulrich

Table 2.6.4: A list of *S. cerevisiae* strains received from external sources or used for expression of episomal plasmids

ID	Name	Genotype	Scource
2820	W303 RAD5+ WT	*MAT-alpha, leu2-3,112 trp1-1 can1-100 ura3-1 ade2-1 his3-11,15, RAD5+*	Rodney Rothstein [274, 272]
2821	W303 RAD5+ WT	*MAT-a, leu2-3,112, trp1-1, can1-100, ura3-1, ade2-1, his3-11,15, RAD5+*	Rodney Rothstein [274, 272]
3753	*smc6-56-13Myc*	*MAT-a, ade2-1, can1-100, ura3-1, his3-11,15, leu2-3,112 trp1-1 rad5-535, smc6-56-13MYC::KanMX, RAD5+*	Xiaolan Zhao [198]
3838	Y258 a	*MAT-a, pep4-3, his4-580, ura3-52, leu2-3,112*	Dharmacon [273]
3839	Y258 alpha	*MAT-alpha, pep4-3, his4-580, ura3-52, leu2-3,112*	This study
3886	Universal Donor Strain-2B	*MAT-alpha, trp1-1, his3-11.15, leu2-3.112, ura3-1, RAD5, MET17, ADE2, LYS2, CEN1-16::Gal-Kl-URA3*	Rodney Rothstein [271]

Table 2.6.5: A list of *S. cerevisiae* strains created for this study

ID	Name	Genotype
3826	pCUP1-1xNLS-PIP-monoUBD-GFP	*MAT-a, his3-Δ200, leu2-3,2-112, lys2-801, trp1-1(am), ura3-52::YIp211-CUP1-1xNLS-PIP-monoUBD-GFP-URA3*
3827	pCUP1-1xNLS-PIP-polyUBD1-GFP	*MAT-a, his3-Δ200, leu2-3,2-112, lys2-801, trp1-1(am), ura3-52::YIp211-CUP1-1xNLS-PIP-polyUBD1-GFP-URA3*
4156	HTA2-mCherry	*MAT-alpha, his3-Δ200, leu2-3,2-112, lys2-801, trp1-1(am), ura3-52, HTA2-mCherry::HIS3*
4473	Tet-ON-3xNLS-PIP-monoUBD-mRuby2 MCM4-4GFP	*MAT-a, his3-Δ200, lys2-801, trp1-1(am), ura3-52, leu2-3,2-112::YIp211-Tet-ON-3xNLS-PIP-monoUBD-mRuby2-LEU2, MCM4-4GFP::KanMX*
4523	Tet-ON-1xNLS-PIP-polyUBD1-GFP	*MAT-a, his3-Δ200, leu2-3,2-112, lys2-801, trp1-1(am), ura3-52::YIp211-Tet-ON-1xNLS-PIP-polyUBD1-GFP-URA3*
4524	Tet-ON-1xNLS-PIP-polyUBD1-GFP *mms2Δ*	*MAT-a, his3-Δ200, leu2-3,2-112, lys2-801, trp1-1(am), mms2::HIS3, ura3-5::YIp211-Tet-ON-1xNLS-PIP-polyUBD1-GFP-URA3*
4525	Tet-ON-1xNLS-PIP-polyUBD1-GFP *ubc13Δ*	*MAT-a, his3-Δ200, leu2-3,2-112, lys2-801, trp1-1(am), ubc13::HIS3, ura3-52::YIp211-Tet-ON-1xNLS-PIP-polyUBD1-GFP-URA3*
4526	Tet-ON-1xNLS-PIP-monoUBD-GFP	*MAT-a, his3-Δ200, leu2-3,2-112, lys2-801, trp1-1(am), ura3-52::YIp211-Tet-ON-1xNLS-PIP-monoUBD-GFP-URA3*
4531	Tet-ON-1xNLS-PIP-monoUBD-mCherry	*MAT-alpha, his3-Δ200, lys2-801, trp1-1(am), ura3-52, leu2-3,2-112::YIp128-Tet-ON-1xNLS-PIP-monoUBD-mCherry-LEU2*
4532	Tet-ON-1xNLS-PIP-polyUBD3-GFP	*MAT-a, his3-Δ200, leu2-3,2-112, lys2-801, trp1-1(am), ura3-52::YIp211-Tet-ON-1xNLS-PIP-polyUBD3-GFP-URA3*
4535	Tet-ON-3xNLS-PIP-monoUBD-GFP	*MAT-a, his3-Δ200, leu2-3,2-112, lys2-801, trp1-1(am), ura3-52::YIp211-Tet-ON-3xNLS-PIP-monoUBD-GFP-URA3*
4536	Tet-ON-3xNLS-PIP-polyUBD2-GFP	*MAT-a, his3-Δ200, leu2-3,2-112, lys2-801, trp1-1(am), ura3-52::YIp211-Tet-ON-3xNLS-PIP-polyUBD2-GFP-URA3*

Table 2.6.5: A list of *S. cerevisiae* strains created for this study

ID	Name	Genotype
4537	Tet-ON-3xNLS-PIP-polyUBD3-GFP	*MAT-a, his3-Δ200, leu2-3,2-112, lys2-801, trp1-1(am), ura3-52::YIp211-Tet-ON-3xNLS-PIP-polyUBD3-GFP-URA3*
4538	Tet-ON-1xNLS-PIP-GFP	*MAT-a, his3-Δ200, leu2-3,2-112, lys2-801, trp1-1(am), ura3-52::YIp211-Tet-ON-1xNLS-PIP-GFP-URA3*
4539	Tet-ON-1xNLS-monoUBD-GFP	*MAT-a, his3-Δ200, leu2-3,2-112, lys2-801, trp1-1(am), ura3-52::YIp211-Tet-ON-1xNLS-monoUBD-GFP-URA3*
4540	Tet-ON-1xNLS-polyUBD-GFP	*MAT-a, his3-Δ200, leu2-3,2-112, lys2-801, trp1-1(am), ura3-52::YIp211-Tet-ON-1xNLS-polyUBD-GFP-URA3*
4541	Tet-ON-1xNLS-PIP-polyUBD2-GFP *ubc13Δ*	*MAT-a, his3-Δ200, leu2-3,2-112, lys2-801, trp1-1(am), ubc13::HIS3, ura3-52::YIp211-Tet-ON-1xNLS-PIP-polyUBD2-GFP-URA3*
4542	Tet-ON-1xNLS-PIP-polyUBD2-GFP *mms2Δ*	*MAT-a, his3-Δ200, leu2-3,2-112, lys2-801, trp1-1(am), mms2::HIS3, ura3-52::YIp211-Tet-ON-1xNLS-PIP-polyUBD2-GFP-URA3*
4543	Tet-ON-1xNLS-PIP-monoUBD-GFP High Expression	*MAT-a, his3-Δ200, leu2-3,2-112, lys2-801, trp1-1(am), ura3-52::YIp211-Tet-ON-1xNLS-PIP-monoUBD-GFP-URA3*
4544	Tet-ON-1xNLS-PIP-monoUBD-GFP *ubc13Δ*	*MAT-a, his3-Δ200, leu2-3,2-112, lys2-801, trp1-1(am), ubc13::HIS3, ura3-52::YIp211-Tet-ON-1xNLS-PIP-monoUBD-GFP-URA3*
4545	Tet-ON-1xNLS-PIP-monoUBD-GFP *mms2Δ*	*MAT-a, his3-Δ200, leu2-3,2-112, lys2-801, trp1-1(am), mms2::HIS3, ura3-52::YIp211-Tet-ON-1xNLS-PIP-monoUBD-GFP-URA3*
4546	GFP-POL30 POL30 a	*MAT-a, his3-Δ200, lys2-801, trp1-1(am), ura3-52, leu2-3,2-112::GFP-POL30-LEU2*
4547	GFP-POL30 POL30 alpha	*MAT-alpha, his3-Δ200, lys2-801, trp1-1(am), ura3-52, leu2-3,2-112::GFP-POL30-LEU2*
4548	Tet-ON-3xNLS-PIP-polyUBD1-GFP	*MAT-a, his3-Δ200, leu2-3,2-112, lys2-801, trp1-1(am), ura3-52::YIp211-Tet-ON-3xNLS-PIP-polyUBD1-GFP-URA3*
4551	Tet-ON-1xNLS-PIP-polyUBD2-mCherry	*MAT-a, his3-Δ200, lys2-801, trp1-1(am), ura3-52, leu2-3,2-112::YIp128-Tet-ON-1xNLS-PIP-polyUBD2-mCherry-LEU2*

Table 2.6.5: A list of *S. cerevisiae* strains created for this study

ID	Name	Genotype
4552	Tet-ON-1xNLS-PIP-polyUBD3-mCherry	*MAT-a, his3-Δ200, lys2-801, trp1-1(am), ura3-52, leu2-3,2-112::YIp128-Tet-ON-1xNLS-PIP-polyUBD3-mCherry-LEU2*
4553	*ecm32Δ* DF5	*MAT-a, his3-Δ200, leu2-3,2-112, lys2-801, trp1-1(am), ura3-52, ecm32::HIS3*
4554	*ybl036cΔ* DF5	*MAT-a, his3-Δ200, leu2-3,2-112, lys2-801, trp1-1(am), ura3-52, ybl036c::HIS3*
4555	*pol32Δ ecm32Δ* DF5	*MAT-a, his3-Δ200, leu2-3,2-112, lys2-801, trp1-1(am), ura3-52, pol32::KanMX, ecm32::HIS3*
4556	*pol32Δ ybl036cΔ* DF5	*MAT-a, his3-Δ200, leu2-3,2-112, lys2-801, trp1-1(am), ura3-52, pol32::KanMX, ybl036c::HIS3*
4557	*ecm32Δ* W303 RAD5+	*MAT-a, leu2-3,2-112, trp1-1, can1-100, ura3-1, ade2-1, his3-11,15, ecm32::HIS3, RAD5+*
4558	*ybl036cΔ* W303 RAD5+	*MAT-a, leu2-3,2-112, trp1-1, can1-100, ura3-1, ade2-1, his3-11,15, ybl036c::HIS3, RAD5+*
4559	*smc6-56 ecm32Δ* W303 RAD5+	*MAT-a, ade2-1, can1-100, ura3-1, his3–11,15, leu2-3,2-112, trp1-1 rad5-535, smc6-56-13Myc::KanMX, ecm32::HIS, RAD5+*
4560	*smc6-56 ybl036cΔ* W303 RAD5+	*MAT-a, ade2-1, can1-100, ura3-1, his3–11,15, leu2-3,2-112, trp1-1 rad5-535, smc6-56-13Myc::KanMX, ybl036c::HIS, RAD5+*
4561	Tet-ON-1xNLS-PIP-polyUBD1-mRuby2	*MAT-a, his3-Δ200, lys2-801, trp1-1(am), ura3-52, leu2-3,2-112::YIp128-Tet-ON-1xNLS-PIP-polyUBD1-mRuby2-LEU2*
4562	Tet-ON-1xNLS-PIP-polyUBD3-mRuby2	*MAT-a, his3-Δ200, lys2-801, trp1-1(am), ura3-52, leu2-3,2-112::YIp128-Tet-ON-1xNLS-PIP-polyUBD3-mRuby2-LEU2*
4563	Tet-ON-1xNLS-PIP-polyUBD2-GFP HTA2-mCherry	*MAT-a/alpha, his3-Δ200, leu2-3,2-112, lys2-801, trp1-1(am), ura3-52::YIp211-Tet-ON-1xNLS-PIP-polyUBD2-GFP-URA3, HTA2-mCherry::HIS3*
4565	Tet-ON-1xNLS-PIP-monoUBD-GFP High Expression HTA2-mCherry	*MAT-a/alpha, his3-Δ200, leu2-3,2-112, lys2-801, trp1-1(am), ura3-52::YIp211-Tet-ON-1xNLS-PIP-monoUBD-GFP-URA3, HTA2-mCherry::HIS3*

Table 2.6.5: A list of *S. cerevisiae* strains created for this study

ID	Name	Genotype
4567	NOP1-mCherry	*MAT-alpha, his3-Δ200, leu2-3,2-112, lys2-801, trp1-1(am), ura3-52, NOP1-mCherry::hphNT1*
4569	Tet-ON-1xNLS-PIP-monoUBD-mRuby2	*MAT-alpha, his3-Δ200, lys2-801, trp1-1(am), ura3-52, leu2-3,2-112::YIp211-Tet-ON-1xNLS-PIP-monoUBD-mRuby2-LEU2*
4570	Tet-ON-1xNLS-PIP-polyUBD1-mRuby2	*MAT-alpha, his3-Δ200, lys2-801, trp1-1(am), ura3-52, leu2-3,2-112::YIp211-Tet-ON-1xNLS-PIP-polyUBD1-mRuby2-LEU2*
4571	Tet-ON-1xNLS-PIP-polyUBD2-mRuby2	*MAT-alpha, his3-Δ200, lys2-801, trp1-1(am), ura3-52, leu2-3,2-112::YIp211-Tet-ON-1xNLS-PIP-polyUBD2-mRuby2-LEU2*
4572	Tet-ON-1xNLS-PIP-polyUBD2-GFP HTA2-mCherry	*MAT-a, his3-Δ200, leu2-3,2-112, lys2-801, trp1-1(am), ura3-52::YIp211-Tet-ON-1xNLS-PIP-polyUBD2-GFP-URA3, HTA2-mCherry::HIS3*
4573	Tet-ON-1xNLS-PIP-polyUBD2-GFP	*MAT-a, his3-Δ200, leu2-3,2-112, lys2-801, trp1-1(am), ura3-52::YIp211-Tet-ON-1xNLS-PIP-polyUBD2-GFP-URA3*
4574	Tet-ON-1xNLS-PIP-monoUBD-GFP *pol30(K164R)*	*MAT-a, his3-Δ200, lys2-801, trp1-1(am), pol30::HisG, leu2-3,2-112::YIp128-P30-pol30(K164R)-LEU2, ura3-52::YIp211-Tet-ON-1xNLS-PIP-monoUBD-GFP-URA3*
4575	Tet-ON-1xNLS-PIP-polyUBD2-GFP *pol30(K164R)*	*MAT-a, his3-Δ200, lys2-801, trp1-1(am), pol30::HisG, leu2-3,2-112::YIp128-P30-pol30(K164R)-LEU2, ura3-52::YIp211-Tet-ON-1xNLS-PIP-polyUBD2-GFP-URA3*
4577	ECM32-GFP	*MAT-a, his3-Δ200, leu2-3,2-112, lys2-801, trp1-1(am), ura3-52, ECM32-GFP::TRP1*
4578	YBL036C-GFP	*MAT-a, his3-Δ200, leu2-3,2-112, lys2-801, trp1-1(am), ura3-52, YBL036C-GFP::TRP1*
4579	UPF3-GFP	*MAT-a, his3-Δ200, leu2-3,2-112, lys2-801, trp1-1(am), ura3-52, UPF3-GFP::TRP1*
4582	Tet-ON-1xNLS-PIP-monoUBD-GFP HTA2-mCherry	*MAT-a, his3-Δ200, leu2-3,2-112, lys2-801, trp1-1(am), ura3-52::YIp211-Tet-ON-1xNLS-PIP-monoUBD-GFP-URA3, HTA2-mCherry::HIS3*

Table 2.6.5: A list of *S. cerevisiae* strains created for this study

ID	Name	Genotype
4583	*rnh1Δ* DF5	*MAT-alpha, his3-Δ200, leu2-3,2-112, lys2-801, trp1-1(am), ura3-52, rnh1::KanMX*
4586	*ecm32Δ ubc13Δ* BY	*MAT-a, leu2Δ0, met15Δ0, ura3Δ0, his3Δ0, ecm32::KanMX, ubc13::HIS3*
4587	*ybl036cΔ ubc13Δ* BY	*MAT-alpha, leu2Δ0, lys2Δ0, ura3Δ0, his3Δ0, ybl036c::KanMX, ubc13::HIS3*
4588	*upf3Δ ubc13Δ* BY	*MAT-a, leu2Δ0, met15Δ0, ura3Δ0, his3Δ0, upf3::KanMX, ubc13::HIS3*
4589	*upf1/nam7Δ ubc13Δ* BY	*MAT-alpha, leu2Δ0, lys2Δ0, ura3Δ0, his3Δ0, upf1/nam7::KanMX ubc13::HIS3*
4590	RAP1-mRuby2	*MAT-alpha, his3-Δ200, leu2-3,2-112, lys2-801, trp1-1(am), ura3-52, RAP1-mRuby2::HIS3*
4591	CBF1-mRuby2	*MAT-alpha, his3-Δ200, leu2-3,2-112, lys2-801, trp1-1(am), ura3-52, CBF1-mRuby2::HIS3*
4598	*rnh201Δ* DF5	*MAT-alpha, his3-Δ200, leu2-3,2-112, lys2-801, trp1-1(am), ura3-52, rnh201::hphNT1*
4599	*rnh1Δ rnh201Δ* DF5	*MAT-alpha, his3-Δ200, leu2-3,2-112, lys2-801, trp1-1(am), ura3-52, rnh1::KanMX, rnh201::hphNT1*
4606	Tet-ON-mRuby2-RNH1-D193N *rnh1Δ rnh201Δ*	*MAT-alpha, his3-Δ200, lys2-801, trp1-1(am), ura3-52, rnh1::KanMX, rnh201::hphNT1, leu2-3,2-112::YIp128-Tet-ON-mRuby2-RNH1-D193N-LEU2*
4607	Tet-ON-mRuby2-RNH1-D193N	*MAT-alpha, his3-Δ200, lys2-801, trp1-1(am), ura3-52, leu2-3,2-112::YIp128-Tet-ON-mRuby2-RNH1-D193N-LEU2*
4613	Tet-ON-1xNLS-PIP-monoUBD-GFP CBF1-mRuby2	*MAT-a/alpha, his3-Δ200, leu2-3,2-112, lys2-801, trp1-1(am), ura3-52::YIp211-Tet-ON-1xNLS-PIP-monoUBD-GFP-URA3, CBF1-mRuby2::HIS3*
4617	Tet-ON-mRuby2-RNH1-D193N rnh1*Δ rnh201Δ* RAP1-GFP	*MAT-alpha, his3-Δ200, lys2-801, trp1-1(am), ura3-52, rnh1::KanMX, rnh201::hphNT1, leu2-3,2-112::YIp128-Tet-ON-mRuby2-RNH1-D193N-LEU2, RAP1-GFP::HIS3*

Table 2.6.5: A list of *S. cerevisiae* strains created for this study

ID	Name	Genotype
4618	Tet-ON-3xNLS-PIP-monoUBD-mRuby2	*MAT-alpha, his3-Δ200, lys2-801, trp1-1(am), ura3-52, leu2-3,2-112::YIp128-Tet-ON-3xNLS-PIP-monoUBD-mRuby2-LEU2*
4623	*ecm32Δ* W303 RAD5+	*MAT-alpha, leu2-3,112, trp1-1, can1-100, ura3-1, ade2-1, his3-11,15, ecm32::HIS3, RAD5+*
4624	*ybl036cΔ* W303 RAD5+	*MAT-alpha, leu2-3,112, trp1-1, can1-100, ura3-1, ade2-1, his3-11,15, ybl036c::HIS3, RAD5+*
4625	*upf3Δ* W303 RAD5+	*MAT-alpha, leu2-3,112, trp1-1, can1-100, ura3-1, ade2-1, his3-11,15, upf3::HIS3, RAD5+*
4626	*upf1/nam7Δ* W303 RAD5+	*MAT-alpha, leu2-3,112, trp1-1, can1-100, ura3-1, ade2-1, his3-11,15, upf1/nam7::HIS3, RAD5+*
4627	*mms2Δ* W303 RAD5+	*MAT-a, leu2-3,112, trp1-1, can1-100, ura3-1, ade2-1, his3-11,15, mms2::hphNT2, RAD5+*
4628	*ecm32Δ* W303 RAD5+	*MAT-a, leu2-3,112, trp1-1, can1-100, ura3-1, ade2-1, his3-11,15, ecm32::hphNT2, RAD5+*
4635	Tet-ON-1xNLS-PIP-monoUBD-GFP RAP1-mRuby2	*MAT-a, his3-Δ200, leu2-3,2-112, lys2-801, trp1-1(am), ura3-52::YIp211-Tet-ON-1xNLS-PIP-monoUBD-GFP-URA3, RAP1-mRuby2::HIS3*
4636	Tet-ON-1xNLS-PIP-polyUBD2-GFP RAP1-mRuby2	*MAT-a, his3-Δ200, leu2-3,2-112, lys2-801, trp1-1(am), ura3-52::YIp211-Tet-ON-1xNLS-PIP-polyUBD2-GFP-URA3, RAP1-mRuby2::HIS3*
4639	*ecm32Δ ubc13Δ* W303 RAD5+	*MAT-a, leu2-3,112, trp1-1, can1-100, ura3-1, ade2-1, his3-11,15, ecm32::HIS3, ubc13::natNT2, RAD5+*
4640	*ecm32Δ mms2Δ* W303 RAD5+	*MAT-a, leu2-3,112, trp1-1, can1-100, ura3-1, ade2-1, his3-11,15, ecm32::HIS3, mms2::hphNT2, RAD5+*
4642	*ybl036cΔ ubc13Δ* W303 RAD5+	*MAT-a, leu2-3,112, trp1-1, can1-100, ura3-1, ade2-1, his3-11,15, ybl036c::HIS3, ubc13::natNT2, RAD5+*
4644	*upf1/nam7Δ ubc13Δ* W303 RAD5+	*MAT-a, leu2-3,112, trp1-1, can1-100, ura3-1, ade2-1, his3-11,15, upf1/nam7::HIS3, ubc13::natNT2, RAD5+*
4646	*upf1/nam7Δ mms2Δ* W303 RAD5+	*MAT-a, leu2-3,112, trp1-1, can1-100, ura3-1, ade2-1, his3-11,15, upf1/nam7::HIS3, mms2::hphNT2, RAD5+*

Table 2.6.5: A list of *S. cerevisiae* strains created for this study

ID	Name	Genotype
4652	Tet-ON-3xNLS-PIP-polyUBD1-mRuby2	*MAT-alpha, his3-Δ200, lys2-801, trp1-1(am), ura3-52, leu2-3,2-112::YIp128-Tet-ON-3xNLS-PIP-polyUBD1-mRuby2-LEU2*
4653	Tet-ON-3xNLS-PIP-polyUBD2-mRuby2	*MAT-alpha, his3-Δ200, lys2-801, trp1-1(am), ura3-52, leu2-3,2-112::YIp128-Tet-ON-3xNLS-PIP-polyUBD2-mRuby2-LEU2*
4654	Tet-ON-3xNLS-PIP-polyUBD3-mRuby2	*MAT-alpha, his3-Δ200, lys2-801, trp1-1(am), ura3-52, leu2-3,2-112::YIp128-Tet-ON-3xNLS-PIP-polyUBD3-mRuby2-LEU2*
4657	Tet-ON-3xNLS-PIP-monoUBD-mRuby2 GFP-POL30 POL30	*MAT-a/alpha, his3-Δ200, lys2-801, trp1-1(am), ura3-52, leu2-3,2-112::YIp128-Tet-ON-3xNLS-PIP-monoUBD-mRuby2-LEU2, leu2-3,2-112::YIp128-GFP-POL30-LEU2*
4658	Tet-ON-3xNLS-PIP-polyUBD1-mRuby2 GFP-POL30 POL30	*MAT-a/alpha, his3-Δ200, lys2-801, trp1-1(am), ura3-52, leu2-3,2-112::YIp128-Tet-ON-3xNLS-PIP-polyUBD1-mRuby2-LEU2, leu2-3,2-112::YIp128-GFP-POL30-LEU2*
4679	Tet-ON-3xNLS-PIP-monoUBD-mRuby2 Tet-ON-3xNLS-PIP-polyUBD2-GFP	*MAT-a, his3-Δ200, lys2-801, trp1-1(am), leu2-3,2-112::YIp128-Tet-ON-3xNLS-PIP-monoUBD-mRuby2-LEU2, ura3-52::YIp211-Tet-ON-3xNLS-PIP-polyUBD2-GFP-URA3*
4692	Tet-ON-mRuby2-RNH1-D193N *rnh1Δ rnh201Δ* Tet-ON-PIP-polyUBD2-GFP	*MAT-a, his3-Δ200, lys2-801, trp1-1(am), rnh1::KanMX, rnh201::hphNT1, leu2-3,2-112::YIp128-Tet-ON-mRuby2-RNH1-D193N-LEU2, ura3-52::YIp211-Tet-ON-1xNLS-PIP-polyUBD2-GFP-URA3*
4703	Tet-ON-mRuby2-RNH1-D193N *rnh1Δ rnh201Δ* Tet-ON-PIP-monoUBD-GFP	*MAT-a, his3-Δ200, lys2-801, trp1-1(am), rnh1::KanMX, rnh201::hphNT1, leu2-3,2-112::YIp128-Tet-ON-mRuby2-RNH1-D193N-LEU2, ura3-52::YIp211-Tet-ON-1xNLS-PIP-monoUBD-GFP-URA3*
4715	Tet-ON-1xNLS-PIP-monoUBD-VSV	*MAT-a, his3-Δ200, leu2-3,2-112, lys2-801, trp1-1(am), ura3-52::YIp211-Tet-ON-1xNLS-PIP-monoUBD-VSV-URA3*

Table 2.6.5: A list of *S. cerevisiae* strains created for this study

ID	Name	Genotype
4716	Tet-ON-1xNLS-PIP-polyUBD1-VSV	*MAT-a, his3-Δ200, leu2-3,2-112, lys2-801, trp1-1(am), ura3-52::YIp211-Tet-ON-1xNLS-PIP-polyUBD1-VSV-URA3*
4717	Tet-ON-1xNLS-PIP-monoUBD-VSV *rad18Δ*	*MAT-a, his3-Δ200, leu2-3,2-112, lys2-801, trp1-1(am), rad18::LEU2, ura3-52::YIp211-Tet-ON-1xNLS-PIP-monoUBD-VSV-URA3*
4718	Tet-ON-1xNLS-PIP-polyUBD1-VSV *rad18Δ*	*MAT-a, his3-Δ200, leu2-3,2-112, lys2-801, trp1-1(am), rad18::LEU2, ura3-52::YIp211-Tet-ON-1xNLS-PIP-polyUBD1-VSV-URA3*
4722	Tet-ON-1xNLS-PIP-monoUBD-VSV *ubc13Δ*	*MAT-a, his3-Δ200, leu2-3,2-112, lys2-801, trp1-1(am), ubc13::HIS3, ura3-52::YIp211-Tet-ON-1xNLS-PIP-monoUBD-VSV-URA3*
4723	Tet-ON-1xNLS-PIP-polyUBD1-VSV *ubc13Δ*	*MAT-a, his3-Δ200, leu2-3,2-112, lys2-801, trp1-1(am), ubc13::HIS3, ura3-52::YIp211-Tet-ON-1xNLS-PIP-polyUBD1-VSV-URA3*
4754	Tet-ON-1xNLS-PIP-polyUBD3-VSV	*MAT-a, his3-Δ200, leu2-3,2-112, lys2-801, trp1-1(am), ura3-52::YIp211-Tet-ON-1xNLS-PIP-polyUBD3-VSV-URA3*
4755	Tet-ON-1xNLS-PIP-polyUBD3-VSV *ubc13Δ*	*MAT-a, his3-Δ200, leu2-3,2-112, lys2-801, trp1-1(am), ubc13::HIS3, ura3-52::YIp211-Tet-ON-1xNLS-PIP-polyUBD3-VSV-URA3*
4780	Tet-ON-1xNLS-PIP-monoUBD-GFP RFA1-mRuby2	*MAT-a, his3-Δ200, leu2-3,2-112, lys2-801, trp1-1(am), ura3-52::YIp211-Tet-ON-1xNLS-PIP-monoUBD-GFP-URA3, RFA1-mRuby2::HIS3*
4782	Tet-ON-1xNLS-PIP-polyUBD2-GFP RFA1-mRuby2	*MAT-a, his3-Δ200, leu2-3,2-112, lys2-801, trp1-1(am), ura3-52::YIp211-Tet-ON-1xNLS-PIP-polyUBD2-GFP-URA3, RFA1-mRuby2::HIS3*
4788	*nup133ΔN nup133* NIC96-CFP	*MAT-alpha, his3-Δ200, leu2-3,2-112, lys2-801, trp1-1(am), ura3-52, pUN100-nup133ΔN-LEU2, nup133::natNT2, NIC96-CFP::KlTRP1*
4811	*nup133ΔN nup133* NIC96-CFP HTA2-mCherry	*MAT-alpha, his3-Δ200, leu2-3,2-112, lys2-801, trp1-1(am), ura3-52, pUN100-nup133ΔN-LEU2, nup133::natNT2, NIC96-CFP::KlTRP1, HTA2-mCherry::HIS3*

Table 2.6.5: A list of *S. cerevisiae* strains created for this study

ID	Name	Genotype
4821	NOP1-mCherry HTA2-CFP	*MAT-a, his3-Δ200, leu2-3,2-112, lys2-801, trp1-1(am), ura3-52, NOP1-mCherry::hphNT1, HTA2-CFP::KlTRP*
4825	*nup133ΔN nup133* NIC96-CFP HTA2-mCherry Tet-ON-1xNLS-PIP-monoUBD-YFP	*MAT-a, his3-Δ200, leu2-3,2-112, lys2-801, trp1-1(am), pUN100-nup133ΔN-LEU2, nup133::natNT2, NIC96-CFP::KlTRP1, HTA2-mCherry::HIS3, ura3-52::YIp211-Tet-ON-1xNLS-PIP-monoUBD-YFP-URA3*
4826	*nup133ΔN nup133* NIC96-CFP HTA2-mCherry Tet-ON-1xNLS-PIP-polyUBD2-YFP	*MAT-a, his3-Δ200, leu2-3,2-112, lys2-801, trp1-1(am), pUN100-nup133ΔN-LEU2, nup133::natNT2, NIC96-CFP::KlTRP1, HTA2-mCherry::HIS3, ura3-52::YIp211-Tet-ON-1xNLS-PIP-polyUBD2-YFP-URA3*
4951	Tet-ON-3xNLS-PIP-monoUBD-GFP HTA2-mCherry	*MAT-a, his3-Δ200, leu2-3,2-112, lys2-801, trp1-1(am), ura3-52::YIp211-Tet-ON-3xNLS-PIP-monoUBD-GFP-URA3, HTA2-mCherry::HIS3MX6*
4952	Tet-ON-3xNLS-PIP-polyUBD2-GFP HTA2-mCherry	*MAT-a, his3-Δ200, leu2-3,2-112, lys2-801, trp1-1(am), ura3-52::YIp211-Tet-ON-3xNLS-PIP-polyUBD2-GFP-URA3, HTA2-mCherry::HIS3MX6*
4982	NOP1-mCherry HTA2-CFP Tet-ON-1xNLS-PIP-monoUBD-YFP	*MAT-a, his3-Δ200, leu2-3,2-112, lys2-801, trp1-1(am), NOP1-mCherry-::hphNT1, HTA2-CFP::KlTRP, ura3-52::YIp211-Tet-ON-1xNLS-PIP-monoUBD-YFP-URA3*
4983	NOP1-mCherry HTA2-CFP Tet-ON-1xNLS-PIP-polyUBD2-YFP	*MAT-a, his3-Δ200, leu2-3,2-112, lys2-801, trp1-1(am), NOP1-mCherry::hphNT1, HTA2-CFP::KlTRP, ura3-52::YIp211-Tet-ON-1xNLS-PIP-polyUBD2-YFP-URA3*
5043	Tet-ON-1xNLS-PIP-GFP HTA2-mCherry	*MAT-a/alpha, his3-Δ200, leu2-3,2-112, lys2-801, trp1-1(am), ura3-52::YIp211-Tet-ON-1xNLS-PIP-GFP-URA3, HTA2-mCherry::HIS3MX6*
5044	Tet-ON-1xNLS-monoUBD-GFP HTA2-mCherry	*MAT-a/alpha, his3-Δ200, leu2-3,2-112, lys2-801, trp1-1(am), ura3-52::YIp211-Tet-ON-1xNLS-monoUBD-GFP-URA3, HTA2-mCherry::HIS3MX6*

Table 2.6.5: A list of *S. cerevisiae* strains created for this study

ID	Name	Genotype
5045	Tet-ON-1xNLS-polyUBD-GFP HTA2-mCherry	*MAT-a/alpha, his3-Δ200, leu2-3,2-112, lys2-801, trp1-1(am), ura3-52::YIp211-Tet-ON-1xNLS-polyUBD-GFP-URA3, HTA2-mCherry::HIS3MX6*

2.7 Software and algorithms

Unless stated differently, the following software and algorithms were used to design, acquire, process images, assemble graphs, and write the thesis.

Software	Use	Source
Adobe illustrator	Assembly and editing of figures	https://www.adobe.com/
FlowJo - V10	Plotting cell cycle profiles	FlowJo, LLC
ImageJ - Fiji	Analysis and editing of microscopy images	https://fiji.sc/
Image Studio™	Analysis and editing of western blots	LI-COR
Image Lab	Image acquisition and editing of western blots and agarose gels	Bio-Rad
LYX	Processing of thesis documents	https://www.lyx.org/
SGAtools	Image analysis and scoring of the high-throughput genetic screens	http://sgatools.ccbr.utoronto.ca/
SnapGene	Designing oligonucleotides, creating plasmid maps, and simulating tagging PCRs	https://www.snapgene.com/
SoftWoRx	Acquisition and deconvolution of microscopy images	GE Healthcare

Table 2.7.1: A list of software and algorithms used in this study

2.8 General methods for DNA manipulation and molecular cloning

2.8.1 Determination of DNA concentration

The absorbance of DNA samples at 260 nm was measured on Multiskan GO Microplate spectrophotometer (Thermo Scientific) or NanoDrop2000 (Thermo Scientific). Then, DNA concentration was calculated according to the formula that 50 μg/mL pure dsDNA equals to an absorbance of 1 at 260 nm. DNA concentration of ChIP samples was accurately measured on a Qubit fluorometer 2.0 using the Qubit dsDNA HS (high sensitivity) assay and following the manufacturer's protocol.

2.8.2 Native agarose gel electrophoresis

1% (w/v) agarose gels were prepared by dissolving agarose (Sigma-Aldrich) in 1xTBE buffer. For detection of nucleic acids, 1x SYBR Safe DNA Stain (Invitrogen) was added to the melted agarose freshly

before solidification. DNA samples were mixed 5:1 with 6x DNA loading buffer, loaded on a solidified gel in 1xTBE buffer, and run at 80 V for 20-30 min in a Bio-Rad's horizontal gel electrophoresis tank. 100 bp, 1 kbp, or 2 log DNA ladders (New England Biolabs) were used as size standards. Nucleic acids were visualised at 460 nm either on Chemidoc XRS Imager (Bio-Rad) or Fusion FX7 (Vilber Lourmat S.A).

2.8.3 Polymerase chain reaction (PCR)

DNA products were amplified using either the high fidelity Phusion or Q5 DNA polymerases (New England Biolabs) on a Professional TRIO 48 cycler (Biometra). According to the manufacture's manual, 10 ng of DNA template was added to a 50 μL PCR reaction mix containing 10 μL 5x HF reaction buffer, 1 μL dNTPs (10 mM each), 1.5 μL DMSO, 2.5 μL of each forward and reverse oligonucleotides (10 μM), and 0.5 μL of DNA polymerase. The mix was brought to a volume of 50 μL using sterile water. A typical thermal cycling protocol contained the following steps: initial denaturing step at 98^{o} C for 30 sec, followed by 30 cycles of 98^{o} C for 10 sec, 50-72^{o} C (depending on the T_m of used oligonucleotides) for 30 sec, then 72^{o} C for 30 sec per kb. To complete the extension of the amplicons, a final 5 min incubation at 72^{o} C was included.

2.8.4 Overlap extension PCR

The probes were tagged with fluorescent proteins using an overlap extension PCR method. In the first step, a 18-20 bp homology sequence (linker) on the 3'-end of the probe and the 5'-end of the fluorescent protein was inserted by a regular PCR reaction using the Phusion HF DNA polymerase (see 2.8.3). The PCR amplicons were purified with the DNA Clean and Concentrator Kit (Zymo Research). In the next step, a PCR mix without any oligonucleotides was prepared, in which the PCR products from the first step were used as templates in a molar ratio of 1:1. Then the thermal cycles were run as follow: initial denaturing step at 98^{o} C for 30 sec, followed by 15 cycles of 98^{o} C for 10 seconds, 55-65^{o} C (depending on the Tm of the homology region) for 30 seconds, then 72^{o} C for 30 seconds per kb, and a final extension step at 72^{o} C for 5 min. In these PCR cycles, the homology sequence between the two fragments served as a primer for DNA synthesis. In the final step, oligonucleotides that anneal at the distal ends of the merged fragments were added to the PCR mix (final 0.5 μM of each). Then the reaction was continued for another 15 cycles with the following settings: initial denaturing step at 98^{o} C for 30 sec, followed by 15 cycles of 98^{o} C for 10 seconds, then 72^{o} C for 30 seconds per kb, and a final extension step at 72^{o} C for 5 min. The resulting merged PCR product was purified and used subsequently in cut-and-paste cloning (see 2.8.7).

2.8.5 Site-directed mutagenesis

The site-directed mutagenesis was performed using intergenic primers carrying desired point mutations. The reaction was carried out following the protocol described for the QuickChange II site-directed mutagenesis kit (Agilent) utilising either PfuUltra or Herculase DNA polymerases. The PCR conditions were as follow: 95^{o} C for 1 min, then 18 cycles of 95^{o} C for 30 sec, 60^{o} C for 30 sec, and 68^{o} C for 60 sec per kb. A final 10 min extension step at 68^{o} C was also included. To inhibit amplification of

the parental template plasmid in bacterial cells, the PCR reactions were incubated with 10 Units of DpnI (New England Biolabs) for 1 h at 37° C before being transformed in Top10 competent cells (see 2.10.2).

2.8.6 Annealing of oligonucleotides

Double-stranded 3xNLS fragments were prepared by mixing equal amounts of sense and antisense ssDNA oligonucleotides in annealing buffer with a final concentration of 50 μM. The mixture was heated at 98° C for 3 min in a heat block then left to cool down to room temperature slowly. The resulting dsDNA was used in cut-and-paste cloning.

2.8.7 Cut-and-paste cloning

In typical cut-and-paste cloning, 1-2 μg of plasmid or PCR product (see 2.8.3) was digested for 3 h at 37° C in a 30 μL reaction containing 20 Units of the relevant restriction endonuclease and the corresponding 1x reaction buffer. To dephosphorylate DNA ends, digested backbone vectors were usually treated with 1 Unit of Fast alkaline phosphatase (Thermo Scientific) for 10 min at 37° C. The products were separated by agarose gel electrophoresis (see 2.8.2). Then, the desired DNA fragments were excised and extracted with a Gel Extraction Kit (Qiagen) following the manufacturer's instructions. Ligation reactions were performed using 50 ng of digested vector DNA and a 3-5 fold excess molar ratio of the insert. 1 μL of T4 DNA ligase (New England Biolabs) was added to the ligation reaction in a total volume of 20 μL in sterile water. The reactions were incubated either at 25° C for 15 min or at 16° C overnight. Finally, 10 μL of the ligation product was used to transform Top10 competent cells (see 2.10.2).

2.8.8 DNA sequencing

For DNA sequencing, 250-500 ng of DNA was mixed with 1 μL of sequencing oligonucleotide (10 μM) in a total volume of 7-10 μL with sterile water. Then, samples were sent either to GATC or StarSEQ GmbH (Mainz) for sequencing. The sequencing results were viewed, and the accuracy of cloning was checked by SnapGene.

2.8.9 DNA purification by phenol-chloroform

DNA from the ChIP samples were purified using 2 mL 5Prime Phase Lock Gel Heavy tubes (QuantaBio). The tubes were briefly spun (14000 rpm for 1 min) before use. The volume of ChIP DNA samples was brought to 200 μL with TE buffer. Then, 300 μL of phenol: chloroform: isoamylalcohol (25:24:1) was added to each sample. The mixture was transferred to a Phase Lock tube, mixed by inverting several times without vortexing, and centrifuged at 14000 rpm for 5 min. Next, 300 μL of chloroform was added to each sample, mixed by inverting several times without vortexing, and centrifuged at 14000 rpm for 5 min. Then, the upper phase was transferred to fresh Eppendorf tubes (~ 200 μL) containing 10 μL glycogen (5 μg/μL). Next, 20 μL of 3 M NaOAc pH 5.3 and 550 μL of 100% ice-chilled ethanol were added and the samples were placed at –80° C for at least 1 h . Then, the samples were spun at 14000 rpm for 30 min at 4° C, washed with 500 μL of 70% ethanol, and spun at 14000 rpm for 10 min at 4° C. Finally, DNA pellets were air-dried for 10 min at room temperature, resuspended in 30 μL TE buffer, quantified (see 2.8.1), and used in downstream applications or stored at –20° C.

2.8.10 Quantitative PCR (qPCR)

Enrichment of a genomic locus of interest in ChIP samples was analysed by qPCR. 10 μL reactions were prepared by adding 5 μL 2x SYBR Green PCR Master Mix (Applied Biosystems), 1 μL each of forward and reveres oligonucleotides (10 μM), and 3 μL of input or ChIP samples diluted in TE buffer. Each sample was loaded in 10 μL quadruplicates into 384-well MicroAmp optical reaction plates (Applied Biosystems). The plates were sealed with a transparent PCR plate seals, vortexed to mix, and briefly centrifuged at 1000 g. The qPCR reactions were run on a Viia7 system cycler with a QuantStudio™ Real-Time PCR software (Life Technologies) using the following programme: 95° C for 15 min, 40 cycles of 95° C for 15 sec, 55° C for 30 sec, 72° C for 30 sec, followed by a melting curve measurement: 95° C for 15 sec, 60° C for 1 min, 0.05° C/sec to 95° C for 15 sec. Fold enrichment was analysed using the percent input (% Input) method. Primers that used to amplify regions in *Saccharomyces cerevisiae* genome corresponded to the early replicating origin ARS607, the late replicating origin ARS501, and an origin-independent *ACT1* locus.

2.9 General methods for protein manipulation and purification

2.9.1 Measurement of protein concentration

The OD_{280} of purified proteins was measured with a Nanodrop2000 spectrophotometer (Thermo Scientific), and their extinction coefficients (ε) were calculated using the ExPASy online tool. Having these values, the concentration of proteins were calculated according to Beer-Lamberts low (Concentration = OD_{280}/Path length $* \varepsilon$) [275]. Bio-Rad's Protein Assay was used to measure the protein concentration of cell extracts by Bradford's method [276], following the manufacturer's protocol. The OD_{595} was measured with an Eppendorf Biophotometer and plotted against OD_{595} values of known BSA concentrations.

2.9.2 Polyacrylamide gel electrophoresis (SDS-PAGE)

SDS-PAGE was performed using either 4-15% Mini-PROTEAN™ TGX Stain-free™ protein gels (10- or 15-wells, Bio-Rad) or 4-15% Criterion™ TGX Stain-Free™ (26-wells, Bio-Rad) protein gels. To separate proteins, 1x SDS running buffer was used in the respective electrophoresis chamber (Mini-PROTEAN™ system or Criterion™ vertical electrophoresis cell, Bio-Rad). For some experiments, the NuPAGE 4-12% Bis-Tris precast gels (Life Technologies) and homemade NuPAGE MOPS buffer were utilised in X-Cell SureLock mini-cells (Invitrogen). Precast gels from Expedeon were run in RunBlue Rapid SDS buffer (Expedeon) using a Mini-PROTEAN™ electrophoresis system (Bio-Rad). In all cases, protein samples were mixed with sample buffer (NuPAGE 4x LDS buffer) and freshly supplemented with 100 mM DTT. Then, the samples were heated for 10 min at 65° C and loaded onto the gels. The prestained PageRuler (Thermo Fisher Scientific) was used as a size ladder.

2.9.3 Coomassie blue staining

The proteins on electrophoresed gels were visualised by Coomassie Blue-based stain InstantBlue (Expedeon) after incubation and vertical agitation for 30-60 min. Then washed several times with water.

2.9.4 Western blotting

2.9.4.1 Western blotting by wet transfer

The transfer/western blotting sandwich was assembled on a gel holder cassette from bottom to top as follow: 3 layers of 1 mm Whatman papers (Thermo Fisher Scientific), a nitrocellulose membrane (Bio-Rad, pore size 0.2 μm), the electrophoresed gel, and another 3 layers of 1 mm Whatman papers. The papers and the membrane were presoaked in the transfer buffer. The cassette was placed vertically in a Mini Trans-Blot cell (Bio-Rad) containing transfer buffer with the membrane side of the sandwich facing the anode. Transfer of the proteins onto the membrane was done by applying a constant voltage of 100 V for 1 h. Afterwards, the membrane was rinsed with PBS-T and blocked in 5% milk in PBS-T on a horizontal shaker for 30 min followed by incubation with a primary antibody (Table 2.1.3) in blocking solution either overnight at 4^{o} C or for 2-3 h at room temperature on a horizontal shaker. To remove the unbound antibody, the membrane was washed three times with PBS-T each for 5 min then incubated with the respective secondary antibody (Table 2.1.4) in blocking solution for 1 h at room temperature on a horizontal shaker. Similarly, the unbound secondary antibody was removed by three constitutive washes with PBS-T each for 5 min. Finally, if a secondary antibody with fluorescent label was used, the blot was imaged on an Odyssey CLx Imaging System (LI-COR). Membranes incubated with HRP fused secondary antibodies were developed by Amersham ECL Select or Prime Western Blotting Detection Reagents (GE Healthcare) following the manufacture's instructions and imaged on a Chemidoc XRS (Bio-Rad) or Fusion FX (Vilber Lourmat S.A). Whenever needed, the membrane was stripped of bound antibodies by washing three times with the stripping buffer each for 10 min at room temperature. Next, the membrane was washed several times with PBS-T then blocked and probed again as described above.

2.9.4.2 Western blotting by Trans-Blot Turbo system

Alternatively, electrophoresed gels were blotted on nitrocellulose membranes (Bio-Rad) using the Trans-Blot Turbo System (Bio-Rad) following the manufacturer's protocol. Trans-Blot Turbo RTA Mini Nitrocellulose Transfer Kit (Bio-Rad) was utilised for electroblotting of 4-15% Mini-PROTEAN TGX Stain-free protein gels. The electroblotting stack of 4-15% Criterion TGX Stain-free protein gels was prepared as follow: Six layers of Wypall X60 cloths (Kimberly-Clark) soaked in Turbo Blot Transfer buffer (Bio-Rad) were laid on the anode of the transfer cassette, then a nitrocellulose membrane (Bio-Rad, pore size 0.2 μm) pre-equilibrated in Turbo Blot Transfer buffer, the electrophoresed gel, another six layers of presoaked Wypall X60 cloths, and finally the cathode of the transfer cassette. The electroblotting of Mini gels was performed using Bio-Rad's High MW blotting programme (10 min at 1.3 A and up to 25 V), whereas the Midi (Criterion) gels were blotted by applying a constant current of 2.5 A and a maximum voltage of 25 V for 15 min. After a brief rinse with PBS-T, the membranes were blocked and probed as described for the wet transfer (2.9.4.1).

2.9.5 Protein production in *E.coli*

2.9.5.1 Protein expression and lysate preparation

Chemically-competent BL21-CodonPlus (DE3)-RIL *E. coli* cells (Stratagene) (Table 2.6.1) were transformed with the desired expression plasmids (Table 2.4.1). Single clones were inoculated in liquid

LB medium containing the relevant antibiotic. The cultures were grown overnight at 37° C with agitation. On the next day, saturated cultures were diluted to 100-fold in 100 mL of antibiotic-containing liquid LB medium and incubated at 37°C to reach an OD_{600} of 0.6-0.7. Before inducing the expression of the transgenes, cells were shifted to 4° C for 30 min. Then, the expression of His-tagged proteins was induced by adding 0.2 mM IPTG (MP Biomedicals) to the cultures and incubating at 18° C for 16 h. Protein samples were taken before and after the addition of IPTG to test for the induction efficiency. Cells were harvested by centrifugation at 4000 g for 15 min at 4° C and resuspended in 3 mL of IMAC buffer A supplemented with protease inhibitors and 0.1% Triton X-100. Next, cells were lysed by sonication on a Branson sonifier using a tip with 3 mm diameter. Five cycles of lysis were performed using the following settings: 50% output, 30 s of sonication pulses, and 2 min rest on ice. Finally, lysates were cleared by centrifugation at 40000 g for 20 min at 4° C. The solubility of the proteins was checked by collecting pellet and supernatant fractions. Rest of the supernatants were processed further to purify the expressed proteins by IMAC method.

2.9.5.2 Protein purification

The cleared lysates were incubated with 500 μL (per L of expression culture) of equilibrated Ni^{2+}NTA beads for 90 min at 4° C with rotation. Samples of non-bound proteins were collected as flow-through (FT) fractions. The bound proteins were washed five times with IMAC buffer A (in a five-time excess volume of Ni^{2+}NTA beads). Then, the bound proteins were eluted with 500 mM imidazole containing IMAC B elution buffer (in an equal volume of Ni^{2+}NTA beads) in five elution rounds. A portion of the collected samples was analysed by SDS-PAGE, followed by Coomassie staining. Fractions containing the expressed proteins were pooled and rebuffered into the storage buffer using PD10 columns (GE Healthcare). The protein samples were concentrated into 500 μL using Vivaspin columns with a suitable MWCO (Thermo Fisher Scientific). Finally, the concentration of protein samples was determined by Nanodrop2000 (Thermo Scientific) (see 2.9.1).

2.9.6 Flag-tag pull-down assay

In vitro pull-down of PCNA, Ub-PCNA, or K63-Ub-PCNA was carried on by adding 20 fold molar excess of purified Flag-tagged probes to the reaction mix in HEPES-based lysis buffer. The samples were incubated on a rotating wheel overnight at 4° C. Equiliberated 10 μL of M2-Flag magnetic beads slurry was added to the samples and incubated for another 2 h at 4° C. The bound protein complexes were separated using a magnetic rack (The DynaMagt^{TM}-2 magnet, Thermo Fischer Scientific), washed with lysis buffer, wash buffer I, wash buffer II, and TE buffer each for 10 min on a rotating wheel at 4° C. Finally, the protein complexes were eluted by adding 50 μL 1x NuPAGE LDS Sample Buffer supplemented with 100 mM DTT and boiled for 10 min at 95° C. Alongside the pull-down samples, 1.5 % of the input samples were analysed by SDS-PAGE and western blotting for PCNA and Flag-tag to check for pull-down efficiency (see 2.9.4.1).

2.9.7 Deubiquitylation assay

Deubiquitylation assays were performed by adding the deubiquitylating enzyme USP2 and 1 mM DTT to yeast cell lysates in the absence of protease inhibitors. Ubiquitin-GFP fusion was used as a positive

control. The samples were incubated at 15° C for 150 min. Then, NuPAGE LDS Sample Buffer supplemented with 100 mM DTT was added to a final 1x concentration and samples were boiled for 10 min at 95° C. Finally, the reactions were analysed by SDS-PAGE and western blotting (see 2.9.4.1).

2.10 Molecular biology methods for *E.coli*

2.10.1 Preparation of chemically competent cells

A fresh overnight culture of *E.coli* was diluted 1:100 fold in LB medium and incubated with agitation at 25° C to reach an OD_{600} of 0.4-0.6. Then, cells were harvested by centrifugation for 10 minutes at 1000 g and 4° C. After washing steps, chemically competent cells were prepared using the Mix & Go! *E. coli* Transformation Kit (Zymo Research) following the manufacturer's procedure. Next, aliquots of cells were snap-frozen in liquid nitrogen and saved at –80° C. Preparation of chemically-competent cells was usually done by our lab technicians Sonja Braun and Laura Tomini.

2.10.2 Transformation of chemically competent cells

An aliquot of chemically competent cells was thawed on ice and mixed with 50-200 ng of plasmid DNA. After a 30 min incubation on ice, cells were heat-shocked for 45 sec at 42° C and placed on ice for another 5 min. In the case of ampicillin-dependent selection, cells were directly spread on LB^{Amp+} agar plates. Otherwise, the heat-shocked cells were recovered for 1-2 h at 37° C in 1 mL LB media. Then, cells were centrifuged, resuspended in 100 μL of distilled water, and spread on LB agar plates containing the respective antibiotic for selection (Table 2.2.1).

2.10.3 Growth conditions of *E.coli*

For amplification of plasmid DNA using *E. coli* cells, the cultures were grown at 37° C in LB medium supplemented with the respective antibiotic for selection (Table 2.2.1).

2.10.4 Isolation of plasmid DNA

For extraction of plasmid DNA, single colonies of *E.coli* were inoculated in 3 mL of LB medium supplemented with the respective antibiotic for selection (Table 2.2.1). Then, cultures were grown overnight at 37° C with agitation at 200 rpm. Finally, plasmid DNA was extracted using the GeneJET Plasmid Miniprep Kit (Thermo Scientific) following the manufacturer's protocol.

2.11 Molecular biology and genetic methods for yeast

2.11.1 PCR-based gene tagging or disruption

Strains carrying gene deletions or tags were generated with standard one-step PCR-based methods [267, 268]. For gene deletions, PCR cassettes were amplified using oligonucleotides that carry around 40 bp homologies at the 5'- and 3'-ends of the desired gene. In contrast, for tagging proteins on their C-termini, an oligonucleotide pair that shares a homology sequence only with the 3'-end of the desired

gene was utilised to amplify the tagging cassette. 7-10 μL of knockout or tagging PCR cassette was used to transform yeast strains with the lithium acetate transformation protocol (see 2.11.2). Positive clones were identified by colony PCR (see 2.11.4) and antibiotic or auxotrophic selection.

2.11.2 Chemical transformation of yeast cells

A volume of exponentially growing yeast cells equivalent to 2-3 OD_{600} was harvested by centrifugation at 1500 g for 2 min and washed once with 1 mL sterile water. A second wash was performed with 500 μL of 100 mM lithium acetate buffer. After centrifugation, the cells were resuspended in 240 μL of 50% PEG-3350. Then, the other reagents were added in the following order: 36 μL 1 M lithium acetate, 15 μL single-stranded Herring testis DNA solution, and the desired DNA fragment (100-500 ng uncut plasmid, ~1 μg linearised plasmid, or 10 μL PCR cassette). The mixture was vortexed well and incubated on a rotating wheel for 30 min at room temperature. Next, the cells were heat-shocked for 15 min at 42^{o} C. Cells were spun and washes once with sterile water. After resuspension, the cells were directly spread on the respective auxotrophic selection agar plates. In case of the antibiotic selection markers, cells were recovered in 1 mL YPD for 2-3 h at 30^{o} C, centrifuged briefly, and plated on antibiotic-containing agar plates. Colonies were visible after 3-4 days and were checked for correct integration by colony PCR (see 2.11.4).

2.11.3 Strain construction by mating and tetrad dissection

Overnight grown cultures of freshly streaked haploid mutant or tagged strains with opposite mating types were mixed on YPD agar plates and incubated for 3-5 h at 30^{o} C. Then, zygotes were picked up using the MSM micromanipulator (Singer) on YPD plates and incubated for 2-3 days at 30^{o} C. The resulting a/α cells were streaked on selective agar plates to ensure proper isolation of diploids. Next, the diploids were grown overnight in a liquid YPD media. On the next day, 500 μL of the cultures were washed five times with sterile water and once with the sporulation media (1% w/v KOAc). Cells were resuspended in 2 mL of sporulation media and incubated for 3 days at 25^{o} C. To destroy the ascus wall and separate the tetrads, 20 μL of the sporulated cultures were mixed with 20 μL STE-Zymolyase solution and incubated for 15 min at room temperature. Then, 10 μL of the mixture was dropped gently on one side of a YPD plate. The drop was left to move smoothly along the surface and air-dry by tilting the plate gradually. Tetrads were dissected using the MSM micromanipulator (Singer) on YPD plates. Finally, tetrads containing the desired mutations or tags were identified by testing the ability of the germinated spores to grow on certain selective media by replica plating using sterile velvet and a replica-plating tool. The mating type of the haploids was determined by complementation of a rare auxotrophic marker with tester strains.

2.11.4 Colony PCR

A small portion of cells from single colonies was scraped with a 200 μL tip and transferred into a PCR tube. Cells then were microwaved for 1 min at 600 W power. Per reaction, a PCR mix was prepared as follow: 5 μL 5x Green GoTaq Reaction Buffer (Promega), 0.3125 μL 10 mM dNTP mix, 0.5 μL of each forward and reverse oligonucleotide (10 μM), and 0.25 μL homemade Taq DNA polymerase. Next, 25 μL of the PCR mix was added to the tubes. The reactions were run on a Professional TRIO 48 cycler

(Biometra) with the following thermal cycles: an initial denaturation step of 95° C for 2 min, 30 cycles of 95° C for 30 sec, 53° C for 30 sec, and 72° C for 1 min, followed by a final extension step at 72° C for 5 min. The PCR products were directly loaded on a 1% agarose gel and analysed by electrophoresis (see 2.8.2).

2.11.5 Growth conditions of yeast cultures

Yeast strains used in this thesis with their respective genotype are listed in (Table 2.6.4). Gene deletions or tags were introduced by PCR-based methods (see 2.11.1) or by mating relevant strains and tetrad dissection (see 2.11.3). All strains were cultured in YPD or synthetic complete (SC) media supplemented with appropriate amino acids at 30° C. Unless otherwise stated, 2% (w/v) glucose was used as the carbon source. For induction of *GAL1* promoter, yeast strains were grown in media containing 2% (w/v) galactose as the carbon source. Expression by the *CUP1* promoter was induced by adding 100 μM of $CuSO_4$. For the induction of the TET-ON expression, doxycycline was used at concentrations indicated in relevant sections. For harvesting small volumes of culture, tabletop centrifuges (Thermo Scientific) were used, whereas large volumes of cells were collected with SORVALL RC 6+ (Thermo Scientific) at 4000 rpm.

2.11.6 Determination of cell density

Cell number and density of yeast cultures were determined by measuring OD_{600} of 1:10 dilutions of cells on an Eppendorf Biophotometer, assuming that 0.25 OD_{600} of exponential YPD culture equals to ~3 x 10^6 cells/mL.

2.11.7 Analysis of DNA damage sensitivity by spotting assay

The sensitivity of yeast strains to different DNA damaging conditions was determined by spotting 5-fold serial dilutions of exponentially growing cultures onto SC or SC-selective agar plates containing the indicated concentrations of damaging agents. The starting dilution was 0.16 OD_{600}. Cells were spotted on agar plates using a Replica Plater for 96-Well Plate (Sigma-Aldrich). Then, the plates were incubated at 30° C and images were taken after 2-3 days. For cold sensitivity assays, plates were incubated at 19° C, 17° C, or 15° C for 5-6 days before imaging.

2.11.8 Cell cycle synchronisation and release

Exponentially growing *MATa* cells (OD_{600} ~ 0.7) were synchronised at the G1 phase by incubating them for 2 h at 30° C with 5 μg/mL of α-factor. Then, cells were treated with or without 0.02% MMS for 30 min or 20 J/m^2 UV. Next, the cultures were spun and washed twice in prewarmed sterile water. Finally, the cells were released from the G1 arrest into the S phase either in the absence of any damaging agent or in the presence of 100 mM HU or 0.05% MMS. Samples were collected at the indicated time points, immediately killed in 1% sodium azide or fixed in 1% formaldehyde then harvested by centrifugation.

2.11.9 Cell cycle analysis by flow cytometry

1 mL of yeast cultures were taken at the indicated times and killed with 1% of sodium azide. Then, cells were once washed with water and fixed in 70% ethanol for 15 min at room temperature. Cells were washed twice with 1 mL of 50 mM sodium citrate buffer pH 7.0. Then, the samples were resuspended in 1 mL of the same buffer containing 800 μg of RNase A and incubated at 50^{o} C for 1 h. Next, Proteinase K was added to the samples to a concentration of 80 μg/μL and incubated at 50^{o} C for another 1 h. Cells were then stained with 32 μg/μL propidium iodide and sonicated on a Branson sonifier for 1-2 s at 10% power. Finally, the DNA content was analysed by flow cytometry on a FACSVerse cytometer (BD Biosciences), and data were visualised with FlowJo v10 software (FlowJo, LLC).

2.11.10 Yeast two-hybrid assay

The reporter yeast strain PJ69-4A (*MATa*) (Table 2.6.2) was chemically transformed with plasmids carrying the *GAL4* activation (AD) and DNA-binding (BD) domain fused to relevant genes and spread on SC agar plates lacking leucine and tryptophan. The plates were incubated for 2-3 days at 30^{o} C. Next, 4-5 colonies of the resulting strains were resuspended in 500 μL of sterile water and vortexed. Then, 5 μL of each strain was spotted on SC agar plates lacking specific amino acids and grown at 30^{o} C for 4-5 days. The presence of both yeast two-hybrid plasmids was confirmed by growth on plates lacking leucine and tryptophan. Positive interactions between the candidate proteins were determined by growth on plates lacking leucine, tryptophan and histidine.

2.11.11 Preparation of yeast whole-cell lysates

2.11.11.1 Mechanical lysis

Equivalents of 75-100 OD_{600} of exponentially growing yeast cultures were harvested by centrifugation at 1500 g for 2 min at 4^{o} C and washed twice in ice-cold PBS. Then, cells were resuspended in 750 μL of lysis buffer in 1.5 mL screw-cap tubes (VWR International) containing 250 μL of 0.5 mm zirconia beads (Carl Roth). Cryolysis was performed in a Precellys 24/ Evolution tissue homogenizer (Bertin Instruments) using 12 cycles of a built-in lysis setting (Hard: lysis for 20 sec, pause for 30 sec, 6800 rpm). Alternatively, cells were lysed by bead-beating in Lysing Matrix C tubes (MP Biomedicals) containing 1 mm silica spheres on a FastPrep-24 instrument (MP Biomedicals) with 15-17 cycles of beating for 40 sec at 5.5 m/sec and 2 min pause on ice. Next, the bottom of lysis tubes was punctured with a hot needle (G25 5/8”). The crude lysates were separated from the beads into 2 mL collection tubes by spinning at 1000 g for 2 min at 4^{o} C. Then, the cleared cell lysates were transferred to 15 mL Bioruptor sonication tubes containing 200 μL of beads (> 1mm) and sonicated at 4^{o} C in a Bioruptor Pico sonication device for 2 x 10 cycles of (30 sec ON, 30 Sec OFF) with 15 min pause on ice after the first 10 cycles. Finally, the sonication tube was punctured as mentioned above, and the lysates were cleared of the beads and collected by centrifugation at 1000 g for 2 min at 4^{o} C into 50 mL tubes using home-made adapters. The resulting extracts were used in downstream applications.

2.11.11.2 Alkaline lysis

Equivalents of 1.5 OD_{600} of exponentially growing yeast strains were washed once in water and resuspended in 500 μL of ice-cold water. Then, 75 μL of NaOH/β-mercaptoethanol solution was added to the samples, vortexed, and incubated on ice for 15 min. Next, the lysates were mixed with 75 μL of 55% w/v trichloroacetic acid (TCA) and placed on ice for an additional 10 min. Then, the extracts were centrifuged at 21000 g for 10 min at 4° C, and the supernatants were removed by aspiration using a vacuum pump. Samples were briefly centrifuged again for 2 min to eliminate any remaining traces of lysis buffer. Pellets were resuspended in 55 μL of 1x NuPage LDS Sample Buffer supplemented with fresh 100 mM DTT then incubated at 65° C for 15 min in a thermomixer (Eppendorf) with gentle shaking [277]. The resulting extracts were used in downstream analysis by SDS-PAGE (see 2.9.2).

2.11.12 Switching the mating type of yeast strains

MATa yeast cells were switched into *MAT*α by transforming the cells with an episomal plasmid carrying the homothallic switching (HO) endonuclease and *URA3* auxotrophic marker. Expression of the HO endonuclease was transiently induced by incubating the cells in 2% w/v galactose containing media [278]. Next, the episomal plasmid was eliminated by *URA3* counter-selection with a toxic uracil analogue 5-fluoroorotic acid (5-FOA). Finally, the mating type of the resulting colonies was determined by crossing them with the parental *MATa* strain.

2.11.13 High-throughput genetic screens

2.11.13.1 Genetic screen using the arrayed ORF collection

The high-throughput genetic screen in the array format was performed using a galactose-inducible (*GAL1*) overexpression library that consists of around 5000 yeast open reading frames (ORFs). First, using the ROTOR HDA benchtop robot (Singer) the arrayed ORF library (*MATa*, *URA3*) was crossed to a query strain overexpressing PIP-polyUBD1 (*MAT*α, *LEU2*) on YPD PlusPlates (Singer) in a 384-format and grown at 30° C for 1 day. Then, the diploids were pinned in quadruples on SC-LEU-URA plates containing 2% w/v glucose as the carbon source and incubated at 30° C for 2 days. This step eliminated any remaining haploid cells and increased the library format from 384 to 1536. In the following steps, the diploids were always kept under auxotrophic (-LEU-URA) selection to prevent losing the episomal plasmids carrying PIP-polyUBD1 and ORFs. Next, the library was re-pinned on media with 2% w/v raffinose as the carbon source. After 3 days, the colonies were re-pinned on selective plates containing 2% w/v galactose to induce the expression of the library and incubated for another 3 days. Then, the library was pinned on 2% w/v galactose plate with or without 0.01% MMS and grown for 3 days. Finally, the library was pinned for a second time on MMS containing plates to increase the growth contrast between MMS sensitive and resistant colonies. Fitness of the colonies was analysed after three days of incubation. All the incubation steps were done at 30° C, and the plates were placed in plastic bags to prevent dehydration of the agar plates. Colourimetric images of the library plates were taken in each step using a Chemidoc XRS (Bio-Rad) imaging system.

2.11.13.2 Genetic screens using the yeast knockout library

A universal donor strain (UDS) was used to deliver either an empty plasmid or a plasmid carrying PIP-polyUBD1 into the yeast knockout library by mating and selective ploidy ablation. The UDS strain contains conditionally stable centromeres due to insertion of a galactose-inducible promoter and a *URA3* counter-selectable marker adjacent to the centromere (CEN) of every yeast chromosome. The plasmid-containing donor strains were mated with the yeast knockout library on YPD plates using the ROTOR HDA (Singer). On the next day, the diploids were pinned on SC-LEU-URA media with 2% w/v glucose to eliminate the haploids. CEN destabilisation was carried out by sequentially shifting the diploids from 2% w/v glucose to 2 % w/v raffinose, then to 2% w/v galactose on SC-LEU and uracil rich media. Next, libraries were grown on a similar media containing a toxic uracil analogue 5-FOA to eliminate any remaining *URA3* positive cells. These steps ensured a selective loss of heterozygosity (LOH) for each conditional chromosome producing haploid strains carrying the transferred plasmid. Then, the haploid libraries carrying the plasmids were pinned on SC-LEU agar plates with or without 0.01% MMS. Finally, the libraries were pinned for a second time on MMS containing plates to increase the growth contrast between MMS sensitive and resistant colonies. Fitness of the colonies was analysed after three days. All the incubation steps were done at 30^{o} C, and the plates were placed in plastic bags to prevent dehydration of the agar plates. Colourimetric images of the libraries were taken in each step using a Chemidoc XRS (Bio-Rad) imaging system.

2.12 Chromatin immunoprecipitation

Relevant yeast strains were cultured, synchronised, and released as described in sections (2.11.5 and 2.11.8). Equivalents of 35-50 OD_{600} of yeast cells (per ChIP and per time point) were collected in 50 mL Falcon tubes. Cells were immediately cross-linked with 1% formaldehyde for 10 min by rolling at room temperature. Then, the cross-linking agent was quenched with 125 mM of glycine by rolling for 5 min at room temperature. Next, cells were harvested by centrifugation at 2000 g for 2 min at 4^{o} C, resuspended in ice-cold PBS and kept on ice until all the time points were collected. For cell cycle analysis, 1 mL of the cultures was collected at each time point and immediately killed in 1% sodium azide (see 2.11.9). After harvesting all the time points, cells were washed twice with ice-cold PBS, resuspended in 750 μL of lysis buffer supplemented with EDTA-free Protease Inhibitor Cocktail (Sigma-Aldrich), 10 mM NEM, and 10 mM O-PA. Next, the cells were transferred into screw-cap tubes containing 250 μL of zirconia/glass beads. The samples were either snap-frozen on dry ice and saved at –80^{o} C or processed for mechanical cell lysis and DNA shearing by sonication as described in section (2.11.11.1). Before proceeding with the ChIP protocol, sonication/ DNA shearing efficiency was tested by taking a 50 μL fraction of each sample, adding SDS to 0.5%, and reversing the cross-link (for reversal of cross-links, see the end of this section). Then, DNA was purified using the ChIP DNA purification kit (Zymo Research), eluted in 10 μL elution buffer, mixed with 6x DNA samples buffer, and the samples were run on a 1% agarose gel (see 2.8.2). The optimal DNA fragment size should be between 200-500 bp. Another 20 μL of each sample was taken as whole-cell extract fraction (WCE) to test the ChIP efficiency at the end of the ChIP procedure. All the following steps were performed at 4^{o} C either on ice or in the cold room. The ChIP samples were pre-incubated with 75 μL of 50% Protein A agarose beads slurry (washed 3

times with lysis buffer) to eliminate any background biding to the beads. Samples then were incubated on a rotating wheel for 20 min, centrifuged at 1500 g for 2 min, and the supernatants were transferred to fresh Eppendorf tubes. 20 μL of each sample was removed as input, supplemented with 0.1 SDS %, and kept at 4^{o} C. For the remaining of the samples, 2-5 μg of the desired antibody was added per sample and incubated on a rotating wheel for 90 min in the cold room. Next, 50 μL of pre-washed 50% Protein A agarose beads slurry was added to each sample and kept rotating overnight in the cold room. On the next day, beads were precipitated at 1500 g for 5 min, 20 μL of the supernatants were collected as non-bound (NB) fractions, and saved at 4^{o} C. ChIP samples were then washed sequentially with lysis buffer, washing buffer I, washing buffer II, and TE buffer each with 750 μL and for 10 min on a rotating wheel in the cold room. After the washes, samples were eluted off the beads by adding 100 μL 1x Elution Buffer and boiling the beads at 95^{o} C for 10 min. Samples were then spun at 1500 g for 2 min, and the supernatants were transferred into fresh Eppendorf tubes. The elution step was repeated with another 100 μL 1x Elution Buffer and boiling for 10 min. In this stage, 20 μL of each sample was collected as bound (B) fraction. Next, 4 μL of RNase A (10 mg/mL, Sigma-Aldrich) was added to the input, ChIP, and sonication test samples and incubated at 50^{o} C oven for 1 h. Then, 4 μL of Proteinase K (Sigma-Aldrich) was added to the samples and incubated at 50^{o} C for another 1 h. For reversing the cross-link, samples were incubated overnight at 65^{o} C. On the next day, the samples were brought to the room temperature, spun at 1500 g for 2 min, and DNA was purified with the phenol-chloroform extraction method using phase-lock tubes (see 2.8.9). The concentration of DNA samples was measured by Qubit dsDNA HS kit (see 2.8.1), and the samples were diluted to threefold in TE buffer. Finally, 3 μL of each DNA sample was used for amplification by qPCR (see 2.8.10). To check for ChIP efficiency, all the collected test fractions (WCE, NB, B, and beads) were analysed by SDS-PAGE and western blotting after addition of NuPAGE LDS Sample Buffer containing 10 mM DTT (see 2.9.2 and 2.9.4).

2.13 Fluorescence microscopy and live-cell imaging

For live-cell imaging, relevant yeast strains were cultured, synchronised, and released as described in sections (2.11.5 and 2.11.8). Because of technical reasons, images of yeast strains expressing Cu^{2+}-inducible sensors were acquired on a wide-field fluorescence microscope (AF7000, Leica) using 63x objective, an ORCA-Flash 4.0 V2 digital CMOS camera (Hamamatsu), and LAS AF software (Leica). For rest of the yeast strains, equivalents of 0.7-1.0 OD_{600} cells were immediately plated on concanavalin A coated chambered coverslip with a glass-bottom (Ibidi), washed twice with media, and released into fresh prewarmed SC medium with or without 2 μg/mL doxycycline (30^{o} C) in an environmental control chamber at 30^{o} C. Images of cells were taken at the indicated time points. Corresponding FACS samples of each time point were collected from a liquid culture incubated in the same environmental control chamber at 30^{o} C. The imaging was done using a wide-field DeltaVision Elite system (GE Healthcare) equipped with a 60x oil immersion objective (NA = 1.42), InsightSSITM solid-state illumination, Scientific CMOS camera, SoftWoRxTM software, and a built-in deconvolution algorithm. Z stacks with 20-30 planes (step size = 0.2 μm) were acquired for each image. Fluorescent proteins CFP, YFP, GFP, and mCherry were imaged with their optimised filters, mRuby2 with a TRITC filter, and DIC was used for whole-cell images. The built-in deconvolution algorithm from SoftWoRxTM was used to reconstruct images.

2.14 Quantification and statistical analysis

2.14.1 Image processing and analysis

For foci counting of deconvolved live-cell images, two different image analyses were utilised; 2D manual foci counting and 3D automated colocalisation and foci counting. For 2D analysis, 20 Z-planes were projected with maximum intensity using ImageJ FIJI software. The Hta2^{mCherry} signal was used to create nuclear masks, and nuclei with at least one focus were manually counted using the Cell Counter plugin of ImageJ. Automated 3D foci counting was carried out using unbiased and customised scripts written in ImageJ macro and Jython languages with ImageJ FIJI software (developed in-house by Dr Ronald P. Wong and Dr Maria Hanulova). Nuclear masks were created from Hta2^{mCherry} or the background signal of Rfa1 or the sensors using filtering and auto-thresholding. The number of foci per cell was determined from each nuclear mask using an absolute threshold for foci segmentation in 3D. For colocalisation analysis, nuclear masks were generated from the background signal of nuclear proteins (Rfa1 or the sensors). An absolute threshold was applied on deconvolved live-cell images to segment objects from each channel. Colocalisation was quantified from the volume percentage of each object covered by the other object in 3D. The size of objects was calculated from the volumes of object masks. The zoning assay was performed by creating 3D nuclear masks from the nuclear Hta2^{mCherry} signal using a Laplacian of Gaussian filter and auto-thresholding. The circularity of the resulting 3D objects was tested, and objects that did not pass a threshold value were excluded. Then ellipsoids were fitted onto the objects and eroded into three 3D zones of equal volume. Finally, an absolute threshold was used to segment the foci, and their localisation in the nuclear zones was quantified. The original analysis scripts are available at https://github.com/helle-ulrich-lab/image-analysis-PORTs, whereas the modified ones for the purpose of this study are included in the supplementary data on a DVD.

2.14.2 Analysis of qPCR data

ChIP-qPCR data were analysed by percent input (% Input) method, which served to normalise both for background levels and input chromatin used for ChIP. First, the inputs were adjusted to 100% by subtracting the log2 of the initial input percentage used in qPCR from the threshold cycle (Ct) of the respective input (i.e. if 1% of input was used in qPCR, log2 of 100 = 6.644 was subtracted). Then, the Ct values obtained from the ChIP samples were divided by the adjusted Ct value of the corresponding input sample. The following formulas were used to calculate % Input:

$$Adjusted\ Input\ =\ Ct\,(Input) - log2\,(percentage\ of\ used\ input)$$

$$\%\ Input\ =\ 100\ *\ 2^{(Ct\,(ChIP)\ -\ Adjusted\ Input)}$$

ChIP data were averaged over two or three independent experiments with qPCR performed in quadruples. Microsoft Excel was used to calculate the % Input, standard deviation (STDEV), and standard error of the mean (SEM). The data were represented in a heatmap format using plotting script created in our lab by Dr Nicola Zilio and available on GitHub

https://github.com/helle-ulrich-lab/plot-heatmap-chip. The SEMs are not shown on the heatmaps.

2.14.3 Statistical analysis

All statistical tests and numbers of replicates are indicated in the respective figure legends. The Z score method was used to compare the statistical significance between additivity/sensitivity screens and previously published data. The statistical tests were performed with Microsoft Excel.

Chapter 3

Strategy and experimental approach

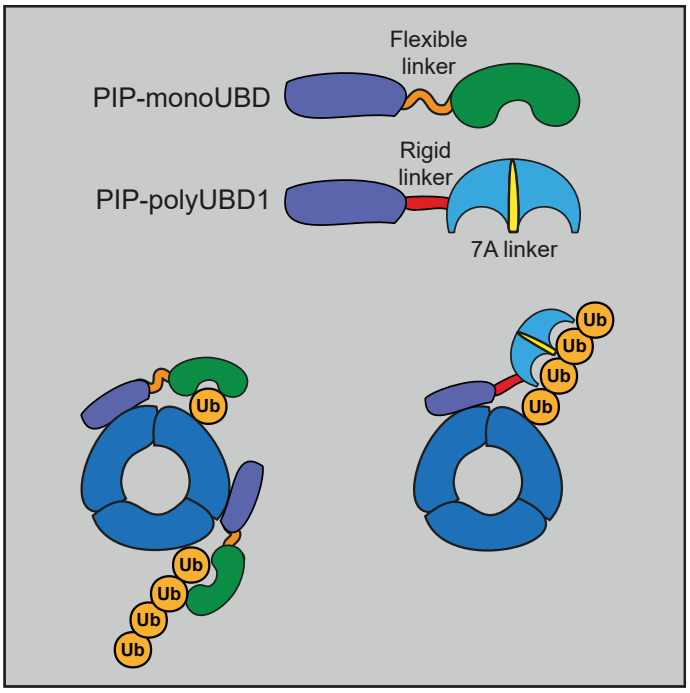

In a nutshell

This chapter briefly describes the main tools of this study, which are new and novel affinity probes for ubiquitylated PCNA developed by the laboratory of Prof. Dr Robert Cohen.

Highlights

- Unique affinity probes recognise ubiquitylated PCNA
- The combined affinity of a PIP box and a UBD defines the specificity of the probes
- The affinity probes distinguish between mono- and polyubiquitylated PCNA

3.1 Basis of the study

The doughnut-shaped PCNA lies at the centre of the eukaryotic replication machinery. The molecular functions and structural details of this essential replication factor were intensively analysed in pioneering studies, which defined the fundamental role of PCNA in stimulating DNA polymerases. With the development of technical methods and availability of genetic manipulation tools, more and more features and functions of PCNA was discovered. PCNA became the textbook model for the post-translational modification with ubiquitin. Moreover, PCNA has been set not only in the core of faithful replication but also as the leading player in DNA damage tolerance mechanisms. Although the far-reaching impacts of PCNA on a myriad of cellular functions has been primarily deciphered, the role of PCNA ubiquitylation is still puzzling [279].
In this chapter, I briefly describe the functional features of new and novel affinity probes to study PCNA modification with ubiquitin. These probes are the building blocks of the current work.

3.2 Design and affinities of Ub-PCNA probes

The DNA sliding clamp, PCNA, is an essential factor that orchestrates in DNA synthesis. It acts as a tethering platform for replicative polymerases and several other factors required for precise replication of the genome. Majority of the PCNA-interacting partners bind to the C-side of PCNA via a conserved motif known as PCNA interacting protein box (PIP box) [280]. A PIP box has the consensus QxxΨ (Ψ represents the hydrophobic residues L, M, or I). This core element is usually flanked by the sequence xxϑϑ on its C-terminus (ϑ represents the aromatic residues Y or F) and sometimes by the sequence KAx on its N-terminus [281, 282]. By fusing such a PIP box to different ubiquitin-binding domains (UBD), the laboratory of Prof. Dr Robert E Cohen (University of Colorado, USA) has created specific probes that bind to ubiquitylated PCNA. These probes are known as PIP-monoUBD and PIP-polyUBD (Figure 3.2.1). As a source for the PIP box, a 56 amino acid sequence (1107-1162) from the yeast protein Srs2 has been used [176, 174, 177]. The ubiquitin-binding domain of PIP-monoUBD is derived from the ubiquitin interacting motif (UIM2) of the S5a (a subunit of the 26S proteasome) [283, 284]. A flexible linker connects the monoUBD to the PIP box allowing PIP-monoUBD to recognise both mono- and polyubiquitylated PCNA. The polyUBD consists of two tandem UIM2s of vacuolar protein sorting 27 (Vps27) separated by seven alanine residues (7A). This 7A linker between the two UIM2s increases the avidity of polyUBD towards K63 polyubiquitin chains (more details in 1.1.6) [71, 107]. In PIP-polyUBD, the two domains (i.e. PIP and polyUBD) are connected via a rigid linker. This rigid linker spans the distance occupied by the proximal ubiquitin moiety on PCNA. Therefore, PIP-polyUBD binds exclusively to K63-polyubiquitylated PCNA.

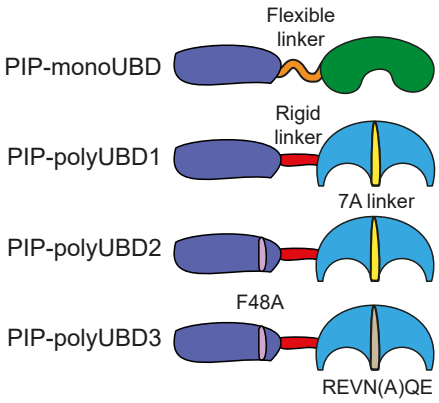

Figure 3.2.1: Domain structure of Ub-PCNA probes. A schematic representation of PIP-monoUBD and the three different versions of PIP-polyUBD, where the PIP box from Srs2 is indicated in magenta, the monoUBD from S5a in green, and the polyUBD from Vps27 in blue. The linkers that connect the PIP box to the respective UBD are indicated either in orange (flexible inker) or in red (rigid linker). The pink stripe in the PIP box refers to the point mutation F48A. The yellow stripe in the polyUBD refers to the 7A linker, whereas the grey stripe refers to the RAP80 S107A linker.

K_d or K_i (nM)	PCNA	Ub_1-PCNA
PIP-monoUBD	13,311 ± 3,034	54 ± 14
K_d or K_i (nM)	**Ub_1-PCNA**	**Ub_3-PCNA**
PIP-polyUBD1	7,291 ± 1,565	7 ± 1
PIP-polyUBD2	14,833 ± 2,405	22 ± 4
PIP-polyUBD3	23,047 ± 2,495	67 ± 20

Table 3.2.1: Affinity constants of the Ub-PCNA probes. The dissociation constant K_d or inhibitor constant K_i of the Ub-PCNA probes were measured by fluorescence anisotropy. PCNA, Ub_1-PCNA, and Ub_3-PCNA were used as substrates for the affinity measurements.These data were collected and analysed by the lab of Prof. Dr Robert Cohen, Colorado state university, USA (unpublished data).

Biochemical properties of the probes were characterised and analysed in a pure *in vitro* manner by the lab of prof. Dr Robert Cohen. Affinities of the probes (either K_d or K_i) were measured by fluorescence anisotropy [285, 286]. In the affinity measurements, PCNA, monoubiquitylated (Ub_1-PCNA), and polyubiquitylated PCNA (Ub_3-PCNA) were used as binding substrates for the probes (Table 3.2.1). PIP-monoUBD binds preferentially (K_d: 54 nM) to Ub_1-PCNA over unmodified PCNA, whereas PIP-polyUBD1 has 1000 fold higher affinity to Ub_3-PCNA over Ub_1-PCNA. Cohen's lab has further modified the PIP-polyUBD1 probe to create additional ones with a bit lower affinities that are closer to dissociation constants of typical biological interactions. Compared to PIP-polyUBD1, a point mutation in the PIP box of PIP-polyUBD2 (F48A) reduces its affinity to Ub_3-PCNA about three folds. In PIP-polyUBD3 the 7A linker between the UIMs is replaced with a linker (REVNSQE) derived from the mammalian receptor-associated protein (RAP80) in which the serine is substituted with an alanine residue (REVNAQE) [287, 288, 289, 290, 69, 70]. This linker in combination with the PIP box mutation gives PIP-polyUBD3 a ten-fold lower affinity than PIP-polyUBD1 to the substrate Ub_3-PCNA (Table 3.2.1). The amino acid

sequences of all the probes and a comparison between their unique linkers and mutations are shown in (Figure 3.2.2).

PIP-monoUBD

```
  1 - M  H  N  P  D  D  T  T  V  D  N  R  P  I  I  S  N  A  K  F - 20
 21 - L  A  D  A  A  M  K  K  T  Q  K  F  S  K  K  V  K  N  E  P - 40
 41 - A  S  S  Q  M  D  I  F  S  Q  L  S  R  A  K  K  K  S  K  L - 60
 61 - N  N  G  S  T  E  E  E  Q  I  A  Y  A  M  Q  M  S  L  R  E - 80
 81 - A  G  G  G  S  D  L  L  C  K  K  G  C  G  Y  Y  G  N  P  A - 100
101 - W  Q  G  F  C  S  K  C  W  R  E  E  A  C  K  A  A  A  E  R - 120
121 - A  A  A  E  *
```

PIP-polyUBD1

```
  1 - M  H  N  P  D  D  T  T  V  D  N  R  P  I  I  S  N  A  K  F - 20
 21 - L  A  D  A  A  M  K  K  T  Q  K  F  S  K  K  V  K  N  E  P - 40
 41 - A  S  S  Q  M  D  I  F  S  Q  L  S  R  A  K  K  K  A  A  A - 60
 61 - A  A  A  A  E  K  A  E  I  Q  E  E  L  R  E  A  A  A  A  A - 80
 81 - A  A  A  E  D  E  E  E  L  I  R  K  A  I  E  L  S  L  K  E - 100
101 - S  A  A  A  A  A  A  A  E  D  E  E  E  L  I  R  K  A  I  E - 120
121 - L  S  L  K  E  C  R  N  S  A  *
```

PIP-polyUBD2

```
  1 - M  H  N  P  D  D  T  T  V  D  N  R  P  I  I  S  N  A  K  F - 20
 21 - L  A  D  A  A  M  K  K  T  Q  K  F  S  K  K  V  K  N  E  P - 40
 41 - A  S  S  Q  M  D  I  A  S  Q  L  S  R  A  K  K  K  A  A  A - 60
 61 - A  A  A  A  E  K  A  E  I  Q  E  E  L  R  E  A  A  A  A  A - 80
 81 - A  A  A  E  D  E  E  E  L  I  R  K  A  I  E  L  S  L  K  E - 100
101 - S  A  A  A  A  A  A  A  E  D  E  E  E  L  I  R  K  A  I  E - 120
121 - L  S  L  K  E  C  R  N  S  A  *
```

PIP-polyUBD3

```
  1 - M  H  N  P  D  D  T  T  V  D  N  R  P  I  I  S  N  A  K  F - 20
 21 - L  A  D  A  A  M  K  K  T  Q  K  F  S  K  K  V  K  N  E  P - 40
 41 - A  S  S  Q  M  D  I  A  S  Q  L  S  R  A  K  K  K  A  A  A - 60
 61 - A  A  A  A  E  K  A  E  I  Q  E  E  L  R  E  A  A  A  A  A - 80
 81 - A  A  A  E  D  E  E  E  L  I  R  K  A  I  E  L  S  L  K  E - 100
101 - S  R  E  V  N  A  Q  E  E  D  E  E  E  L  I  R  K  A  I  E - 120
121 - L  S  L  K  E  C  R  N  S  A  *
```

Orange: Flexible linker Red: Rigid linker Green: PIP box mutation F48A

Blue: 7A linker Gray: RAP80 linker S107A

Figure 3.2.2: Unique sequences in each Ub-PCNA probe define their specificity and affinity. A comparison between the amino acid (aa) sequences of the different Ub-PCNA probes. The aa differences between the probes are highlighted in different colours.

Chapter 4

In vivo optimisation and applications of the Ub-PCNA probes

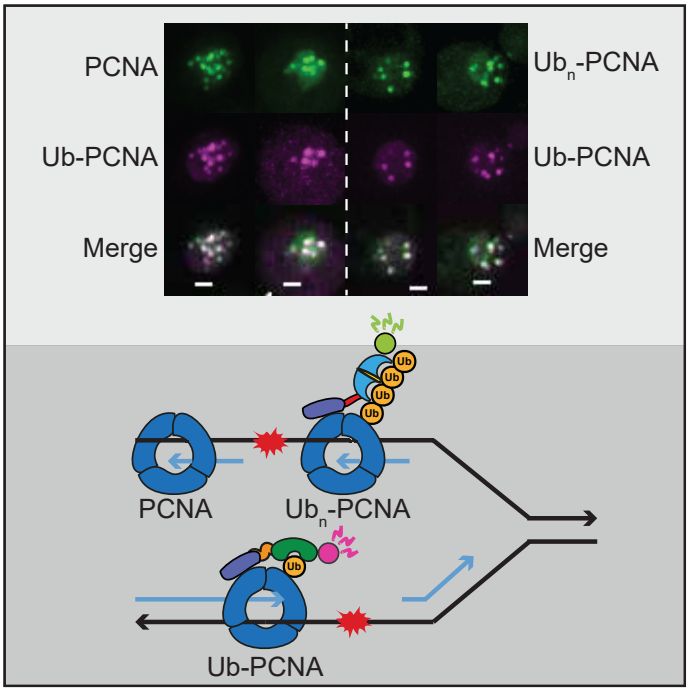

In a nutshell

This chapter unravels the *in vivo* potentials of the PCNA affinity probes trough the establishment and optimisation of genetics and microscopy approaches. Moreover, it describes the application of such approaches in addressing some aspects of DNA damage bypass.

Highlights

- Overexpressed Ub-PCNA probes act as inhibitors of DNA damage bypass
- Inducible Ub-PCNA sensors form nuclear foci after replication stress
- The Ub-PCNA sensors mark and colocalise with ubiquitylated PCNA
- PCNA mono- and polyubiquitylation partially overlap during replication stress

4.1 Prologue I

In eukaryotes, the DNA damage bypass pathways are regulated by ubiquitylation of PCNA [165]. Monoubiquitylation of PCNA activates error-prone translesion synthesis, which relies on damage-tolerant DNA polymerases [167, 164]. Alternatively, modification of PCNA with K63-linked polyubiquitin chains promotes error-free template switching that uses information provided by the sister chromatid [203] (more details in section 1.2.2). It is poorly understood how cells choose one pathway over the other in response to genotoxic stress. Several physiological and experimental factors can channel the bypass pathway to one of its branches. Some of these factors include, for example, the tested species. In budding yeast, the main biological switch between TLS and template switching is the mono- and polyubiquitylation state of PCNA [18, 165, 222]. However, the picture gets more complicated in higher eukaryotes because of an overlap between the two bypass modes and availability of additional regulatory factors [223, 229, 230]. Type and nature of DNA lesions, as well as the amount of damage (i.e. acute vs chronic), can influence the pathway choice [232, 236, 237, 128]. Availability of different repair factors in a particular cell cycle [201, 161, 203, 245], and the fine-tuning of their levels play critical roles in the preference of bypass mode [216, 181, 235**?**]. Moreover, chromatin arrangement and cellular compartmentalisation are decisive for the pathway choice [291, 292, 293, 294]. These points are discussed in more details in the introduction (1.2.2.4).

Despite all the intensive research and findings of DNA damage bypass, a better understanding of the relationship between the error-free and error-prone damage bypass requires a delicate and careful analysis of the emergence of ubiquitylated PCNA, accumulation of ssDNA gaps, checkpoint activation, and resolution of the damage in a synchronised time-dependent manner. This chapter aimed to establish, optimise, and validate a set of tools to investigate and dissect the DNA damage bypass in minute details *in vivo*. Key players of the *in vivo* experiments of this study were the PCNA-specific affinity probes (described in chapter 3). These probes selectively recognise and distinguish between different species of ubiquitylated PCNA. In the first part, I aimed to put forward the best technical parameters to use the probes in live cells, like the expression levels and affinities of the probes, their localisation within cells, their pathway specificity *in vivo*, and type of fluorophore to use. Such parameters were very critical in defining the function and the purpose of the probes in cells. In the second part, using the optimised probes, I revisited and reevaluated some previous findings about damage bypass, and intended to address some of its undiscovered aspects.

4.2 Results I

4.2.1 The Ub-PCNA probes are suitable for *in vitro* pull-downs

As a kind gift from the Cohen lab, our lab has received a copy of plasmids carrying the Ub-PCNA probes. Although the *in vitro* properties of the probes were analysed in detail by the Cohen lab, we wanted to confirm the functionality of the probes in pull-down assays. To this end, I cloned the probes into bacterial expression vectors to tag them with Flag tags on their N-termini and a small 6xHIS tag for purification. The accuracy of the constructs was confirmed by Sanger sequencing. The Flag-tagged PIP-monoUBD and PIP-polyUBD1 were purified by affinity purification, immobilised metal ion affinity chromatography (IMAC) [295, 296, 297], using Ni^{2+}NTA-agarose beads (Figure 4.2.1 A). For *in vitro* pull-down assays, $\sim$ 200 µM purified probes were incubated either with 10 µM PCNA, 10 µM Ub-PCNA, or 10 µM of K63-Ub-PCNA reaction (prepared by Dr Sabrina Wegmann). The probe-substrate complexes were precipitated by M2-Flag magnetic beads. PIP-monoUBD interacted both with Ub-PCNA and K63-Ub-PCNA; however, some binding was also detected with unmodified PCNA. This background binding to PCNA could be explained by the affinity of the PIP box itself to PCNA (Figure 4.2.1 B). The pull-down pattern of PIP-polyUBD1 looked different from that of PIP-monoUBD, where a minimal binding to PCNA and Ub-PCNA was detected compared to the strong interaction with K63-Ub-PCNA. It is worth to notice the difference in the binding pattern of K63-Ub-PCNA. PIP-monoUBD binds to PCNA with short K63-Ub chains, whereas PIP-polyUBD1 binds preferentially to PCNA with long K63-Ub chains. This pull-down assay showed that tagging the probes with Flag tags did not change their behaviour and that these probes could be used in other *in vitro* experiments as well.

4.2.2 Manipulation of DNA damage bypass by the Ub-PCNA probes

Simultaneous binding of different ubiquitin readers or deubiquitylating enzymes to a particular type of ubiquitin chain is typically rare. Therefore, it is expected that the expression of a K63-specific UBD may inhibit K63-dependent signalling and prevent the deconjugation of such chains. Indeed, Sims *et al.*, 2012 [107] showed that expression of K63-specific UBDs leads to accumulation of K63-conjugates in mammalian cells and make yeast cells sensitive to the DNA-damaging agent MMS most probably by inhibiting K63-polyubiquitylation required for DNA damage resistance. Similarly, exogenous expression of TUBEs in mammalian cells or adding them to cell lysates stabilises K63-polyubiquitylated proteins through effectively masking their recognition by DUBs [108, 109].

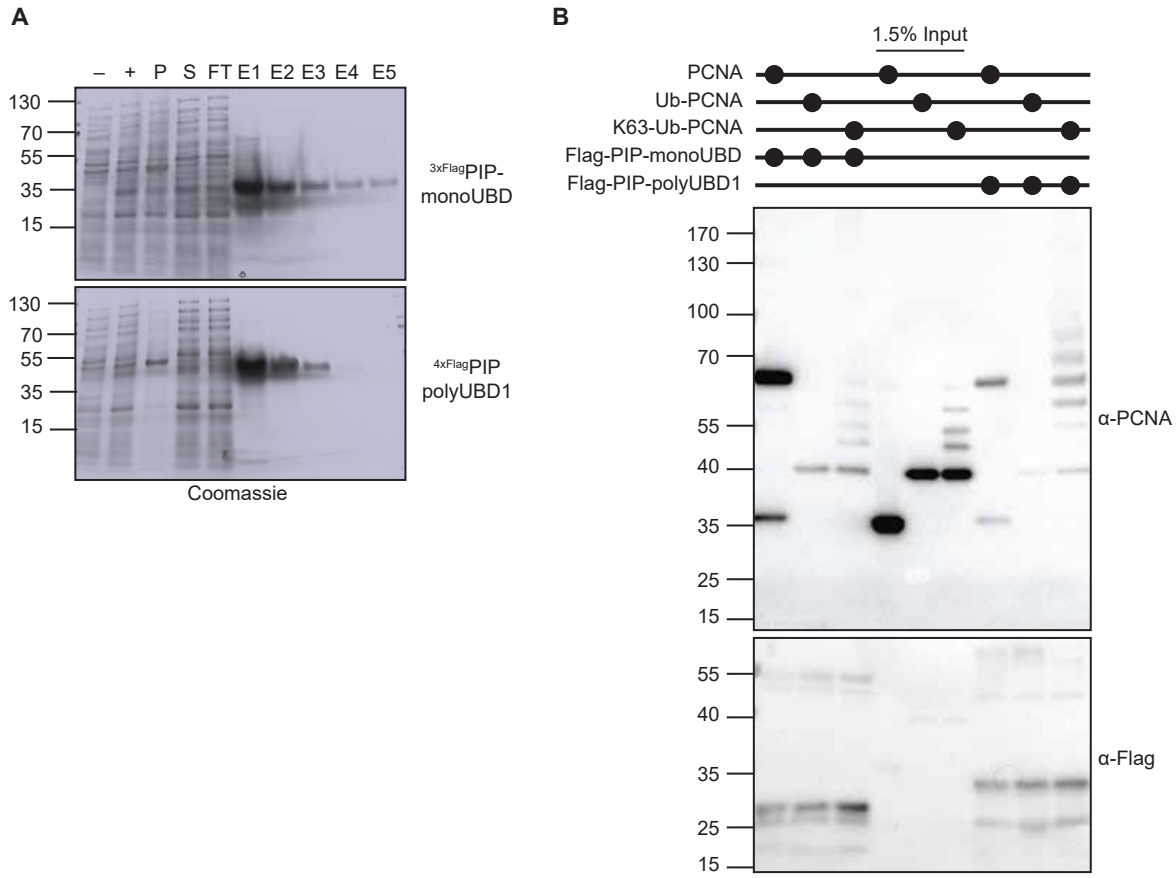

Figure 4.2.1: Validation of the Ub-PCNA probes for *in vitro* experiments. (A) Expression and purification of the Ub-PCNA probes. Plasmids carrying either $^{6xHIS\text{-}3xFlag}$PIP-monoUBD or $^{6xHIS\text{-}4xFlag}$PIP-polyUBD1 were expressed in *E.coli* cells. The solubility of the proteins was checked by collecting pellet (P) and supernatant (S) samples. The expressed proteins were purified with equilibrated Ni^{2+}NTA beads. Samples of non-bound proteins were collected as flow-through (FT) fractions. The bound proteins were eluted with imidazole containing elution buffer in five elution rounds (E1-E5). All the collected samples were analysed by SDS-PAGE, followed by Coomassie staining. (B) Pull-down of PCNA, Ub-PCNA, or K63-Ub-PCNA was done by adding 20 fold molar excess of the purified Flag-tagged probes to the reaction mix. Alongside the pull-down samples, 1.5 % of the input samples were analysed by SDS-PAGE and western blotting for PCNA and Flag-tag to check for pull-down efficiency.

4.2.2.1 The PIP-monoUBD probe is ubiquitylated in cells

Because the PCNA affinity probes contain UBDs, it is expected that the Ub-PCNA probes may also act as *in vivo* signal modulators and interfere with DNA damage bypass by competing with factors that would otherwise bind to mono- or polyubiquitylated PCNA. Generally, the expression level of an exogenous gene can be controlled by the strength of its promoter and the plasmid copy number [298]. To analyse the inhibitory effects of Ub-PCNA probes on DNA damage bypass, I overexpressed PIP-monoUBD and the three versions of PIP-polyUBD in wild type cells of the budding yeast *Saccharomyces cerevisiae*. I also expressed each domain of the probes (i.e. PIP, monoUBD, and polyUBD1) separately to use them as non-binding controls. These constructs were fused to a single nuclear localisation signal (NLS) on their N-termini and tagged with a vesicular stomatitis virus (VSV) tag on their C-termini. The expression of the constructs was under the control of constitutively active *ADH1* promoter in a multicopy yeast

expression plasmid [299]. Under these conditions, the probes and the single-domains were expressed to a similar level indicated by the western bolt (Figure 4.2.2 A).

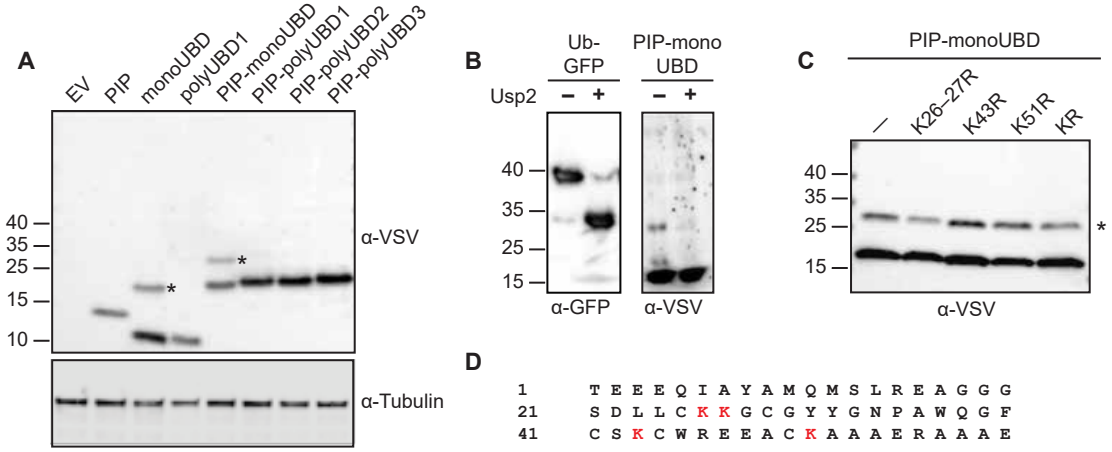

Figure 4.2.2: PIP-monoUBD is ubiquitylated *in vivo*. (A) Expression levels of the probes and the single-domains were detected by western blot. Whole cell lysates were collected from yeast strains overexpressing VSV-tagged probes or the single-domains under control of a constitutively active *ADH1* promoter. The probes and the single-domains are expressed to a similar level indicated by the VSV blot. The higher bands in monoUBD and PIP-monoUBD samples, indicated by asterisks, are ubiquitylated forms of these probes. Tubulin was used as a loading control. EV; empty vector. (B) Deubiquitylation of PIP-monoUBD was performed by adding the deubiquitylase (USP2) to the yeast cell lysates in the absence of protease inhibitors. Ubiquitin-GFP fusion served as a positive control for the deubiquitylation assay. The samples were analysed by SDS-PAGE and western blotting for VSV and GFP. (C) Point mutations in PIP-monoUBD on K26 and K27, K43, K51, or all four lysines (KR) did not abolish its ubiquitylation. (D) The amino acid sequence of monoUBD, in which all the possible ubiquitylation sites are indicated in red.

To our surprise, we detected additional bands running around 8-10 kDa higher than the expected sizes of monoUBD and PIP-monoUBD (indicated by asterisks) (Figure 4.2.2 A). These bands most probably were ubiquitylated forms of the probes. The phenomenon of ubiquitylation coupled to ubiquitin binding was reported as soon as UBDs were discovered [68]. Several studies showed that many ubiquitin readers are themselves ubiquitylated, and the ubiquitylation of the readers requires their UBDs [300, 301, 302]. UIM-containing proteins are the best-characterized examples of this phenomenon [68]. Fusing a UIM to glutathione-S-transferase (GST) or another protein leads to the ubiquitylation of the chimeric protein [303]. In particular, the UIM of S5a, which is the ubiquitin-binding domain in monoUBD and PIP-monoUBD, is ubiquitylated by several RING and HECT E3s [304]. To prove that the higher bands detected in monoUBD and PIP-monoUBD samples (Figure 4.2.2 A) are indeed their ubiquitylated forms, I performed a deubiquitylation assay. Lysates from yeast cells expressing PIP-monoUBD were incubated with the ubiquitin-specific protease 2 (USP2) in the absence of protease inhibitors. Ubiquitin fused to green fluorescent protein (GFP) served as a positive control (Figure 4.2.2 B). Disappearance of the higher bands in the USP2-treated samples confirmed that monoUBD and PIP-monoUBD were themselves ubiquitylated upon their *in vivo* expression (Figure 4.2.2 B). Thinking that the ubiquitin acceptor site lies most probably within the monoUBD, I mutated the four lysine residues in PIP-monoUBD either individually or collectively. Substituting the lysine residues in monoUBD did not eliminate the ubiquitylation of PIP-monoUBD (Figure 4.2.2 C-D). Oldham *et al.*, 2002 [303] and others, reported that

ubiquitylation of a UIM happens at a site on its N-terminus, not in the UIM itself [303, 68]. In agreement with these findings, the ubiquitin acceptor site on PIP-monoUBD may lie outside of monoUBD, either in the NLS, PIP, or the VSV-tag.

4.2.2.2 The Ub-PCNA probes act as *in vivo* inhibitors upon their overexpression

To analyse the overexpression effects of Ub-PCNA probes on DNA damage bypass and cell growth, I performed a spot assay of the same strains mentioned above in section (4.2.2.1). Compared to the empty vector (EV) control, yeast strains overexpressing PIP-monoUBD were sensitive to genotoxic stress indicated by their slow growth on MMS containing plates. PIP-polyUBD probes also rendered cells sensitive to MMS (Figure 4.2.3). Interestingly, PIP-polyUBD1 showed stronger inhibition than PIP-polyUBD2, whereas PIP-polyUBD3 had the weakest inhibitory effects (Figure 4.2.3). This gradient inhibition by the PIP-polyUBD probes correlates well with their *in vitro* affinities to polyubiquitylated PCNA (Table 3.2.1).

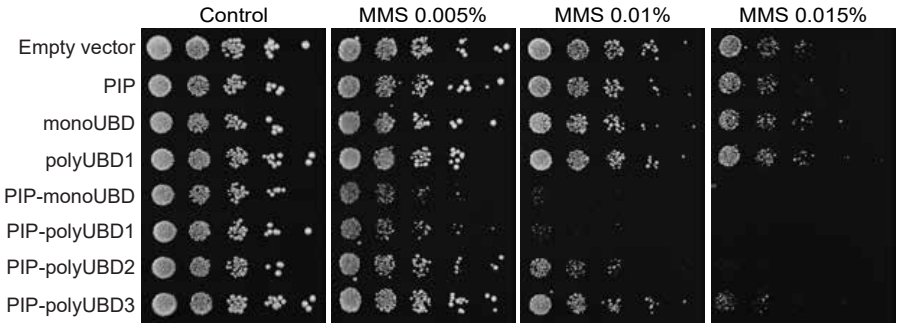

Figure 4.2.3: Overexpression of the Ub-PCNA probes interferes with DNA damage bypass. Spot assay of yeast strains overexpressing VSV-tagged probes or the single-domains under control of a constitutively active *ADH1* promoter. The strains were spotted on SC-LEU agar plates containing increasing doses of MMS.

4.2.2.3 Ub-PCNA probes inhibit the subpathways of DNA damage bypass to different degrees

In section 4.2.2.2, I showed that overexpression of PIP-monoUBD and PIP-polyUBD1 increase the sensitivity of WT yeast cells to replication stress caused by MMS. This MMS sensitivity could arise from two possible scenarios. On the one hand, the probes might recognise ubiquitylated PCNA exclusively and inhibit DNA damage bypass by competing with endogenous factors like TLS polymerases. On the other hand, the probes might bind to other ubiquitylated repair factors present at stressed replication forks. In budding yeast, ubiquitylation dynamics of such factors after replication stress is not yet well characterised. Nevertheless, budding yeast offers a grate genetic stage to play all the possible scenarios and test if the Ub-PCNA probes bind specifically to ubiquitylated PCNA *in vivo* and interfere only with DNA damage bypass or one of its sub-pathways.

To study the scenarios mentioned above, I analysed the inhibitory effects of the probes in yeast mutants that are deficient in one of the sub-branches of DNA damage bypass. Deletion of one subunit of the E2 heterodimer Ubc13/Mms2 abolishes the formation of K63-Ub chains on PCNA [250, 305, 216, 306]. Nevertheless, Rad6/Rad18 complex would still be able to monoubiquitylate PCNA.

Because *mms2Δ* or *ubc13Δ* mutants lack PCNA polyubiquitylation, I expected that PIP-polyUBD1 would no longer cause sensitivity to MMS or it would only have negligible effects. Indeed, unlike PIP-monoUBD overexpression of PIP-polyUBD1 in *mms2Δ* or *ubc13Δ* upon replication stress had marginal consequences on cell fitness, which was less drastic in comparison to the WT cells (Figure 4.2.4). Next I used a TLS deficient yeast mutant (*tlsΔ*), which lacks all the three TLS polymerases (*rev1Δ*, *rev3Δ*, *rad30Δ*) [307, 308, 309, 310, 311, 312, 313, 314], to confirm that PIP-polyUBD1 inhibits template switching. In *tlsΔ* mutant, the cells rely entirely on the error-free bypass to replicate over MMS induced lesions. Therefore, the inhibition caused by PIP-polyUBD1 overexpression was a bit stronger than that of PIP-monoUBD (Figure 4.2.4). These observations further supported the scenario, in which PIP-polyUBD1 binds only to K63-polyubiquitylated PCNA and interferes with template switching but not TLS.

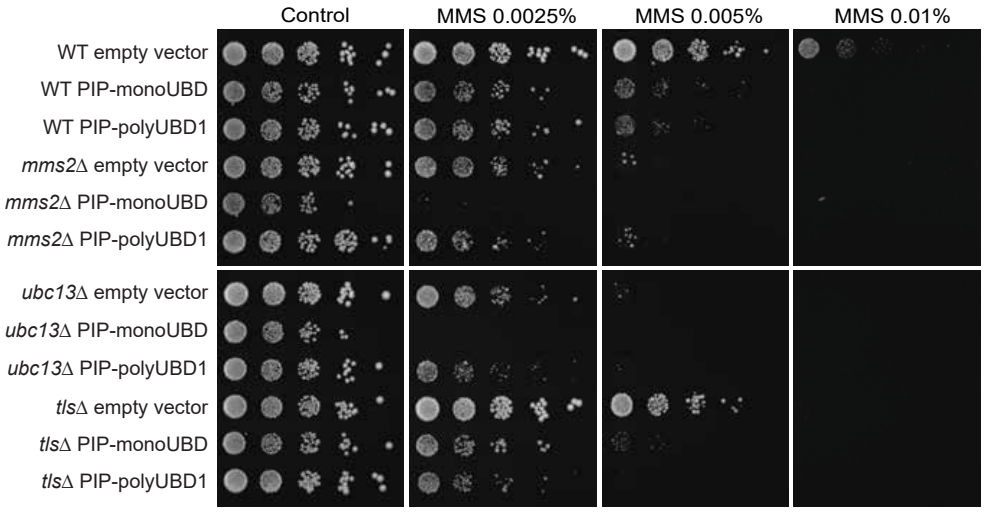

Figure 4.2.4: Overexpression of Ub-PCNA probes in PCNA polyubiquitylation or translesion synthesis mutants. Spot assay of wild-type (WT), *mms2Δ*, *ubc13Δ*, and *tlsΔ* mutant yeast strains overexpressing VSV-tagged Ub-PCNA probes under control of a constitutively active *ADH1* promoter. The strains were spotted on SC-LEU agar plates containing increasing doses of MMS.

Considering that Rad5 is the E3 that builds ubiquitin chains on PCNA, the yeast mutant *rad5Δ* is also deficient in PCNA polyubiquitylation. In addition to its E3 function, Rad5 is an ATP-dependent helicase and involves in TLS via its interaction with Rev1. Therefore, *rad5Δ* cells are more sensitive to replication stress in comparison to *mms2Δ* and *ubc13Δ* [307, 216, 315, 210, 247, 166]. In the experimental setups, *rad5Δ* cells were challenged with lower doses of MMS compared to WT or other bypass mutants. As in *mms2Δ* and *ubc13Δ*, overexpression of PIP-polyUBD1 in *rad5Δ* did not cause sensitivity to low doses of MMS. However, at higher MMS doses, *rad5Δ* cells showed some sensitivity, which was independent of the E2 subunit Ubc13 (Figure 4.2.5). These results indicate that PIP-polyUBD1 may cause some off-target effects most probably by hampering the replicative function of PCNA. In fact, in the absence of PCNA polyubiquitylation, PIP-polyUBD1 might also bind to other polyubiquitylated proteins at the replication fork. As shown earlier for the WT and mutants of template switching, *rad5Δ* cells overexpressing PIP-monoUBD were damage sensitive (Figure 4.2.5).

In addition to *rad5Δ*, all the tested strains so far (WT, *mms2Δ*, *ubc13Δ*, and *tlsΔ*) helped me to investigate the *in vivo* specificity of PIP-polyUBD1 only. Because PIP-monoUBD binds both to mono- and polyubiquitylated PCNA, it was better to test its *in vivo* specificity in mutants, which are entirely defective in PCNA ubiquitylation. One such mutant is *pol30-K164R*, in which the ubiquitin acceptor lysine on PCNA is substituted with arginine. Similarly, the *rad18Δ* mutant lacks the reaction limiting E3 enzyme, Rad18; thus, it is incapable of PCNA ubiquitylation [18, 166]. In these mutants, it was expected that overexpression of Ub-PCNA probes would be epistatic with loss of PCNA ubiquitylation and the cells would not show additional sensitivity to replication stress. Interestingly, overexpression of PIP-monoUBD or PIP-polyUBD1 rendered *pol30-K164R* cells sensitive to MMS. Moreover, deletion of Ubc13 rescued the sensitivity caused by PIP-polyUBD1 overexpression (Figure 4.2.6). These results suggest that in the absence of PCNA ubiquitylation, PIP-polyUBD1 may bind to other substrates that are K63 polyubiquitylated by Ubc13. However, such substrates and the E3s that cooperate with Ubc13 are not yet described.

In the budding yeast, PCNA is also SUMOylated on the conserved K164 by the E2/E3 pair Ubc9/Siz1 and K127 by Ubc9/Siz2 [18, 174, 172, 316]. To check for any possible cross-reaction of the probes with SUMOylated PCNA, I overexpressed the probes in the mutant (*pol30-K127-164R*) deficient in PCNA ubiquitylation and SUMOylation. The *pol30-K127-164R* mutant did not suppress the damage sensitivity caused by PIP-monoUBD overexpression. However, unlike in *pol30-K164R*, overexpression of PIP-polyUBD1 in *pol30-K127-164R* had very little to no effect on DNA damage resistance, and deletion of Siz1 did not cause additional effects (Figure 4.2.6).

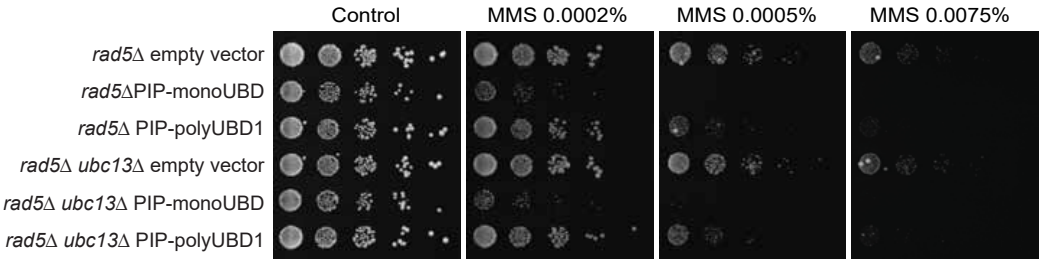

Figure 4.2.5: Overexpression of Ub-PCNA probes in *rad5Δ* mutant. Spot assay of *rad5Δ* mutant yeast strains overexpressing VSV-tagged Ub-PCNA probes under control of a constitutively active *ADH1* promoter. The strains were spotted on SC-LEU agar plates containing increasing doses of MMS, which were lower than the treatments used for the WT yeast strains.

In *rad18Δ*, the picture of overexpressing the probes looked much different. *rad18Δ* was the only damage bypass mutant tested, in which overexpression of PIP-monoUBD and PIP-polyUBD1 made the cells resistant to MMS. Moreover, this resistance was dependent on Ubc13 (Figure 4.2.7). Such a rescue of *rad18Δ* damage sensitivity is reported in cases where the signalling by PCNA SUMOylation is defective, like in *siz1Δ*, *srs2Δ*, and their combination *siz1Δ srs2Δ* [317, 18, 174, 176]. Interestingly, overexpression of PIP-polyUBD1 in *rad18Δ siz1Δ* background did not cause MMS sensitivity. Moreover, the suppression caused by PIP-monoUBD and PIP-polyUBD1 seen in *rad18Δ* was not evident in *rad18Δ siz1Δ* (Figure 4.2.7). All these results suggest the existence of a salvage DNA repair pathway, which depends on both SUMO-PCNA and Ubc13. Possible scenarios of such pathways are discussed in (Section 4.3).

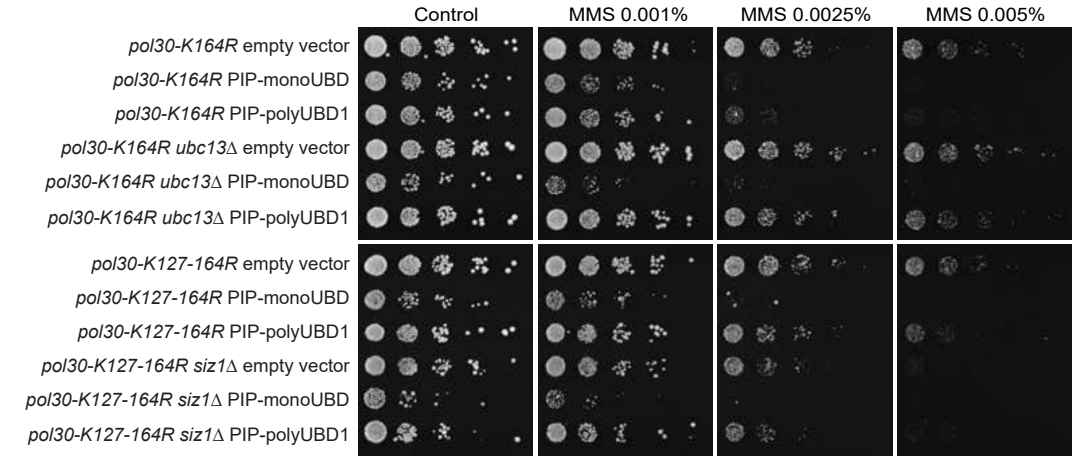

Figure 4.2.6: Overexpression of Ub-PCNA probes in PCNA point mutants. Spot assay of *pol30-K164R* and *pol30-K127-164R* mutant yeast strains in combination with either *ubc13Δ or siz1Δ* overexpressing VSV-tagged Ub-PCNA probes under control of a constitutively active *ADH1* promoter. The strains were spotted on SC-LEU agar plates containing increasing doses of MMS, which were lower than the treatments used for the WT yeast strains.

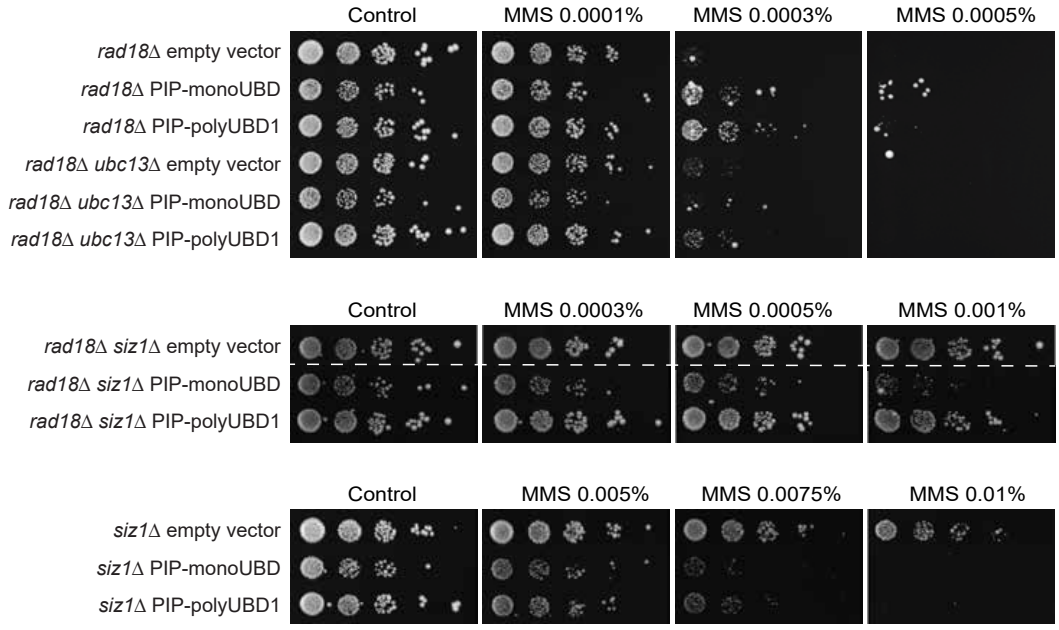

Figure 4.2.7: Overexpression of Ub-PCNA probes in *rad18Δ* and PCNA SUMOylation deficient mutants. Spot assay of *rad18Δ*, *rad18Δ ubc13Δ*, *rad18Δ siz1Δ*, and *siz1Δ* mutant yeast strains overexpressing VSV-tagged Ub-PCNA probes under control of a constitutively active *ADH1* promoter. The strains were spotted on SC-LEU agar plates containing increasing doses of MMS, which were lower than the treatments used for the WT yeast strains. The dashed line indicates cropped out strains between the EV and PIP-monoUBD.

4.2.3 Detection of ubiquitylated PCNA *in vivo* with the Ub-PCNA probes

Because of their dynamic nature, decoding the physiological significance of different ubiquitin modifications is challenging, despite of the recent methodological advances in genetic approaches [105], mass spectrometry [149, 318, 26], and development of chain-specific antibodies [32, 106, 72]. Fluorescent microscopy provides an alternative method to monitor the *in vivo* localisation and function of a specific ubiquitin modification. Indeed, few labs established UBD-based microscopy sensors and showed their convenient use in studying ubiquitin dynamics. In mammalian cells, linear and K63-specific sensors were used to detect mitophagy, DNA DSBs, and NF-κB signalling. However, it is also reported that these sensors interfere with the endogenous pathways, like delaying the resolution of DSBs [107, 110]. Similarly, fluorescently tagged forms of the Ub-PCNA probes may allow monitoring the spatial distribution of PCNA mono- and polyubiquitylation in real-time throughout a cell cycle. Moreover, the different probes could be expressed either analogously or simultaneously when they are tagged with two different fluorophores. However, to use the Ub-PCNA probes in live-cell imaging, they need to be present at sufficiently minute levels to avoid interference with ongoing damage bypass.

4.2.3.1 Inducible Ub-PCNA probes as sensors in fluorescence microscopy

In section 4.2.2.2, I mentioned that the expression level of a heterologous factor is defined by the promoter in use and the copy number of the plasmid carrying the heterologous factor. In *S.cerevicaie*, several well-characterised inducible promoters allow controlling the gene expression tightly. Examples of such promoters are the copper-induced *CUP1* promoter [319, 320], tetracycline-regulatable expression system (tetracycline operator *TetO*) [321], galactose-inducible promoter *GAL1* [322, 323, 324], and *MET3* promoter that is controlled by the presence of the amino acid methionine [325, 326]. However, these promoters differ significantly in their induction kinetics and genetic requirements. For example, the *GAL1* promoter is massively induced when cells are grown in medium containing galactose, and a proper induction by *MET3* promoter requires a methionine-sensitive yeast background [326]. As a pilot trial in turning the Ub-PCNA probes into fluorescent sensors of ubiquitylated PCNA, I fused the Ub-PCNA probes with 1xNLS on their N-termini, tagged them with yeast enhanced green fluorescent protein (yeGFP) on their C-termini, and control their expression by the *CUP1* promoter, which can be induced by the addition of the trace element copper (Cu^{2+}) to the growth media. A single copy of these constructs was inserted into the genome of budding yeast by using integrative plasmids (for more details see 2.11.2). The discovery that many DNA damage repair and signalling factors accumulate in distinct sub-nuclear foci at the damage sites assisted the rapid understanding of several repair mechanisms [327]. We predicted that the fluorescent Ub-PCNA sensors might also form such nuclear foci, thereby reflecting the accumulation of ubiquitylated PCNA. Indeed, both PIP-monoUBD^{GFP} and PIP-polyUBD1^{GFP} accumulated in nuclear foci upon replication stress induced by MMS but not under unchallenged conditions (Figure 4.2.8 A-B). It is worth to mention that some cytoplasmic background signal accompanied the nuclear signal of 1xNLS-PIP-polyUBD1^{GFP}. Expression of the sensors was not controlled tightly with the *CUP1* promoter because even a minute amount of copper activated the promoter to its maximum levels (Figure 4.2.8 C). These high expression levels of the Ub-PCNA sensors by *CUP1* promoter might interfere with the downstream bypass signalling and sensitise the cells to replication stress.

To avoid such a situation, I replaced the induction system with a tetracycline-inducible promoter/operator (TetO) [321]. This expression system is based on the tTA transactivator (VP16 activator domain of herpes simplex virus) attached via a spacer from the lambda bacteriophage cI gene to a mutant tetracycline-inducible repressor (TetR) in which the tetracycline analogue, doxycycline (Dox), induces TetO driven gene expression [328, 321]. To be concise and avoid any future confusions between the doxycycline-inducible and repressible systems, I will refer to the doxycycline-activated expression system used in this study as TET-ON system. By changing the doxycycline concentration in the growth medium, the TET-ON system allowed a titratable expression of the sensors, which was more tunable than the *CUP1* promoter (Figure 4.2.8 C-D).

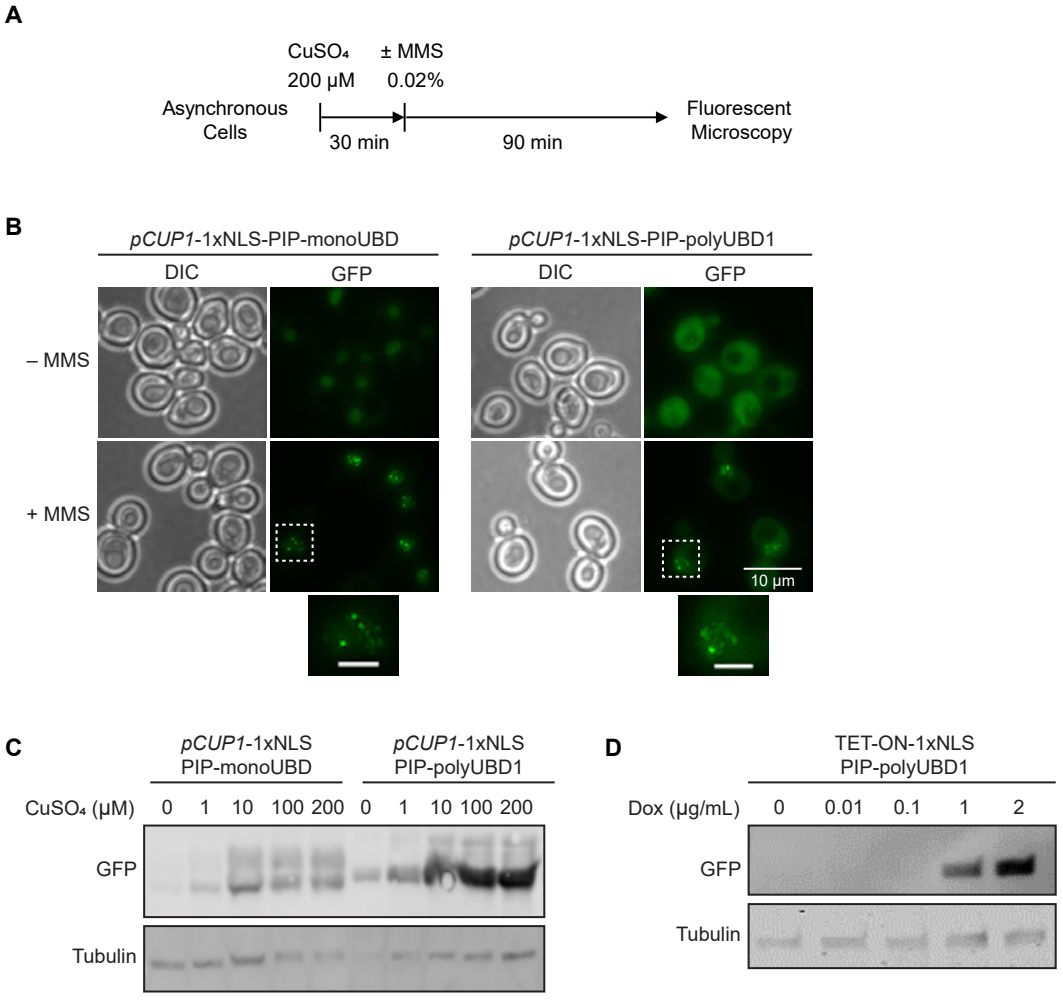

Figure 4.2.8: A pilot trial to detect ubiquitylated PCNA in *S.cerevicaie*. (A) Scheme of the experimental settings. (B) Microscopic images of wild-type yeast strains expressing the GFP-tagged Ub-PCNA sensors under the control of the inducible *CUP1* promoter. Expression of the sensors was induced by adding 200 μM of $CuSO_4$ to the growth media. The cells were either control-treated or damaged with 0.02% MMS for 90 min. The magnified images are the areas marked by white boxes. The scale bars in the magnified pictures equal to 1 μm. (C-D) Western blot depicting the expression levels of the sensors at different copper or Dox concentrations. Tubulin was used as a loading control. DIC; differential interference contrast.

4.2.3.2 Fine-tuning of the Ub-PCNA sensors for live-cell imaging

Having seen that both 1xNLS-PIP-monoUBD^{GFP} and 1xNLS-PIP-polyUBD1^{GFP} were highly suitable as sensors to detect PCNA ubiquitylation *in vivo* (Figure 4.2.8), we were trigged to check if the other two versions of PIP-polyUBD (2 and 3) with weaker affinities (Table 3.2.1) are also capable in forming nuclear foci under replication stress conditions. Since we aimed to make the Ub-PCNA sensors as delicate as possible to live cells, whereby we could detect the sensors by microscopy without interfering with damage bypass, we set to find the optimal doxycycline concentration and treatment conditions to fulfil these criteria. The constitutive nuclear residences of a cohort of replication and repair factors, like MCM10, BRCA1, and BRCA2, are achieved by the presence of bipartite or multiple NLSs [329, 330, 331]. Attaching three nuclear localisation signals (3xNLS) to the Ub-PCNA sensors instead of one (1xNLS) might reduce the cytoplasmic background signal detected in PIP-polyUBD1^{GFP}. Therefore, all four Ub-PCNA probes were cloned into the TET-ON expression system containing either 1x or 3xNLS on their N-termini and tagged with GFP on their C-termini. The fluorescent signal and foci count of all the sensors were systematically checked at different doxycycline concentrations, the damage sensitivity of the cells was evaluated by spot assays, and the expression of the sensors was verified by western blots. I saw that PIP-polyUBD2^{GFP} and PIP-polyUBD3^{GFP} were also able to form nuclear foci after MMS damage. However, their fluorescence was accompanied by some cytoplasmic background signal, as in PIP-polyUBD1^{GFP} (Figures 4.2.11 A and 4.2.12 A). Containing 1x or 3xNLS did not make any significant difference in the fluorescence and the foci count of PIP-monoUBD^{GFP} and PIP-polyUBD2^{GFP} sensors, where the foci were detectable at doxycycline concentrations as little as 0.1 μg/mL (Figures 4.2.9 A-B and 4.2.11 A-B). In the case of PIP-polyUBD1^{GFP} and PIP-polyUBD3^{GFP}, having 3xNLS enhanced the brightness of the nuclear foci and their count (Figures 4.2.10 A-B and 4.2.12 A-B). However, cells expressing 3xNLS versions of the sensors were more sensitive to DNA damage than the ones with 1xNLS (Figures 4.2.9 C, 4.2.10 C, 4.2.11 C, and 4.2.12 C). It is also noteworthy that the expression levels of the 3xNLS sensors were much higher than the 1xNLS versions (Figure 4.2.13 E). It could be that sequestering the sensors in the nucleus protects them from degradation. Because fusing the sensors with 1x or 3xNLS affected their fluorescence behaviour differently, we decided to carry on our experiments with sensors that have weaker toxicity and brighter nuclear foci, namely, 1xNLS-PIP-monoUBD^{GFP} and 1xNLS-PIP-polyUBD2^{GFP}.

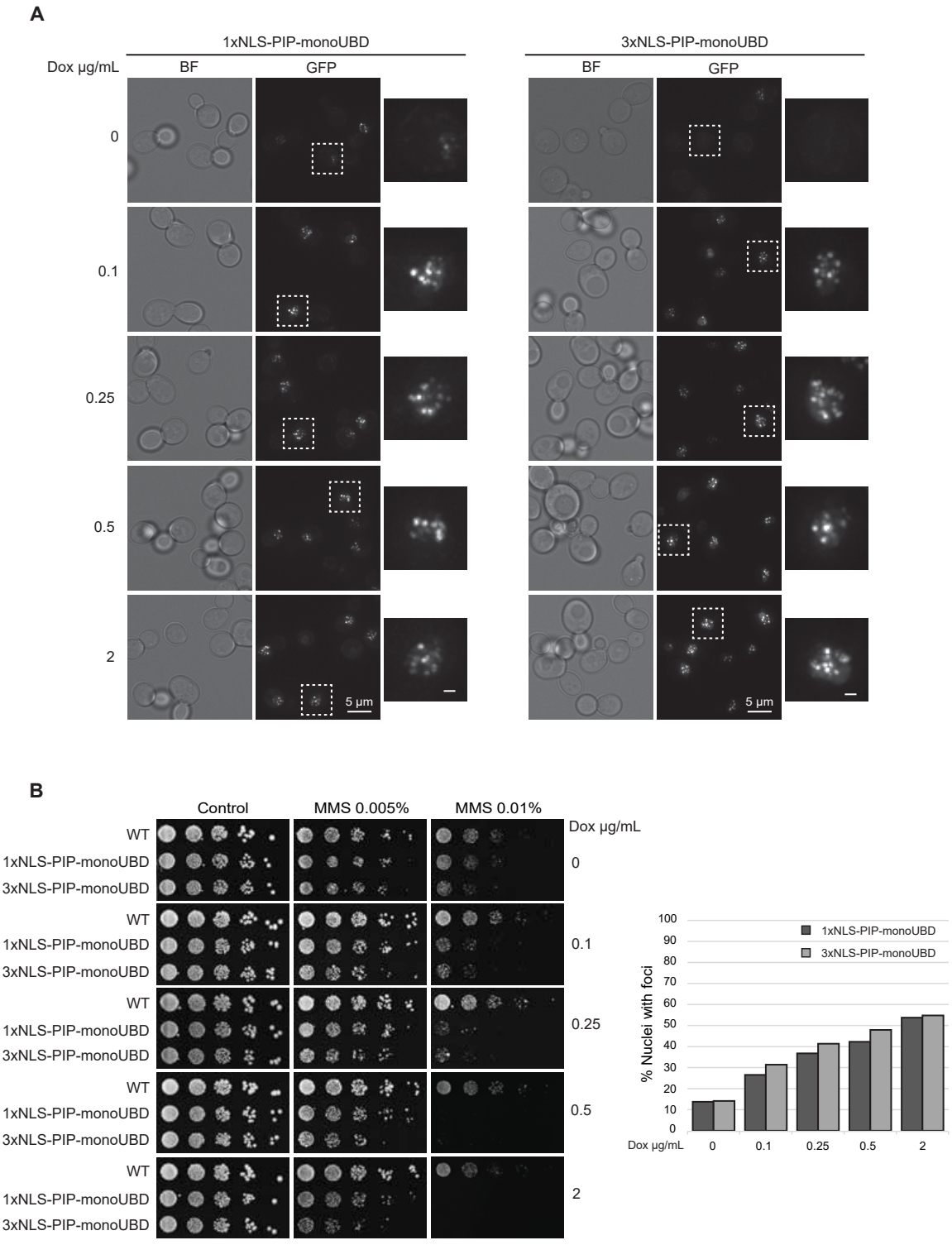

Figure 4.2.9: Fine-tuning of PIP-monoUBD for live-cell imaging. (A) Microscopic images of yeast cells expressing either TET-ON-1xNLS- or TET-ON-3xNLS-PIP-monoUBD^{GFP}. Images were taken after 90 min of incubation with the indicated doses of doxycycline and 0.02% MMS. The scale bar in the magnified picture equals to 1 μm. BF; bright field. (B) Left: Spot assay of the indicated strains on synthetic complete agar plates containing increasing doses of doxycycline and MMS. Right: quantification of TET-ON-1xNLS- and TET-ON-3xNLS-PIP-monoUBD^{GFP} foci under different doxycycline concentration, 400 – 600 cells were quantified per condition.

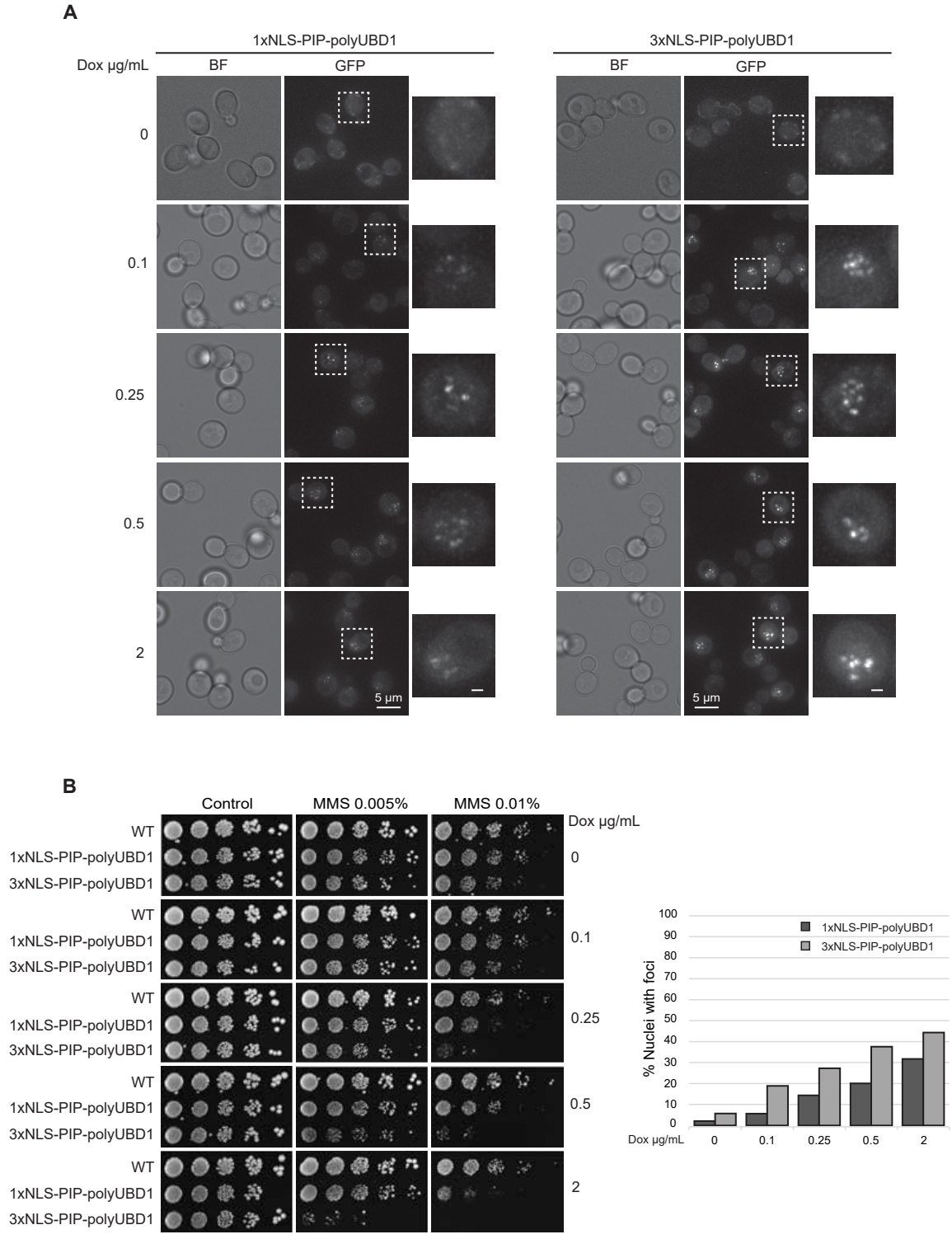

Figure 4.2.10: Fine-tuning of PIP-polyUBD1 for live-cell imaging. (A) Microscopic images of yeast cells expressing either TET-ON-1xNLS- or TET-ON-3xNLS-PIP-polyUBD1^{GFP}. Images were taken after 90 min of incubation with the indicated doses of doxycycline and 0.02% MMS. The scale bar in the magnified picture equals to 1 μm. BF; bright field. (B) Left: Spot assay of the indicated strains on synthetic complete agar plates containing increasing doses of doxycycline and MMS. Right: quantification of TET-ON-1xNLS- and TET-ON-3xNLS-PIP-polyUBD1^{GFP} foci under different doxycycline concentration, 400 – 600 cells were quantified per condition.

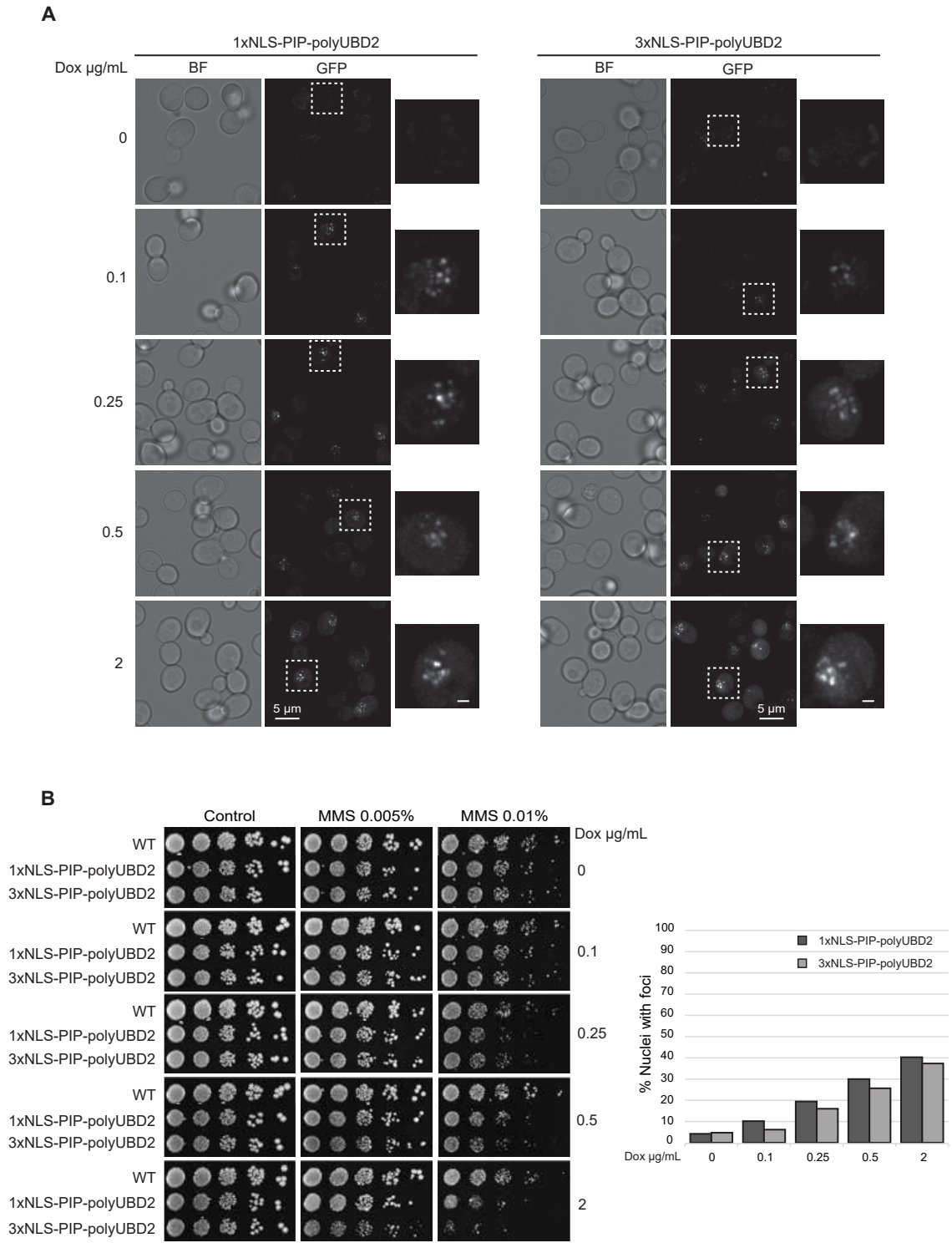

Figure 4.2.11: Fine-tuning of PIP-polyUBD2 for live-cell imaging. (A) Microscopic images of yeast cells expressing either TET-ON-1xNLS- or TET-ON-3xNLS-PIP-polyUBD2^{GFP}. Images were taken after 90 min of incubation with the indicated doses of doxycycline and 0.02% MMS. The scale bar in the magnified picture equals to 1 μm. BF; bright field. (B) Left: Spot assay of the indicated strains on synthetic complete agar plates containing increasing doses of doxycycline and MMS. Right: quantification of TET-ON-1xNLS- and TET-ON-3xNLS-PIP-polyUBD2^{GFP} foci under different doxycycline concentration, 400 – 600 cells were quantified per condition.

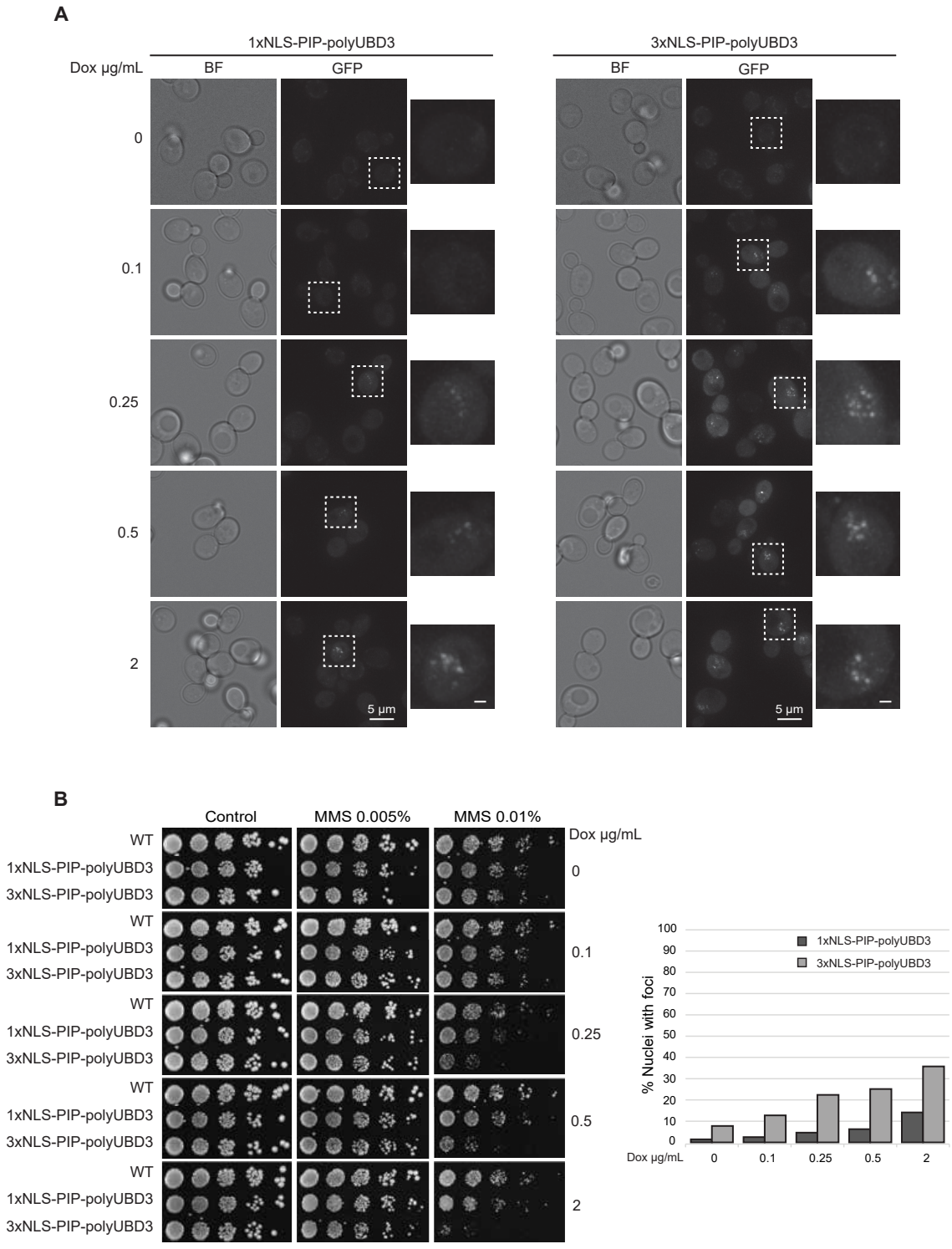

Figure 4.2.12: Fine-tuning of PIP-polyUBD3 for live-cell imaging. (A) Microscopic images of yeast cells expressing either TET-ON-1xNLS- or TET-ON-3xNLS-PIP-polyUBD3^{GFP}. Images were taken after 90 min of incubation with the indicated doses of doxycycline and 0.02% MMS. The scale bar in the magnified picture equals to 1 μm. BF; bright field. (B) Left: Spot assay of the indicated strains on synthetic complete agar plates containing increasing doses of doxycycline and MMS. Right: quantification of TET-ON-1xNLS- and TET-ON-3xNLS-PIP-polyUBD3^{GFP} foci under different doxycycline concentration, 400 – 600 cells were quantified per condition.

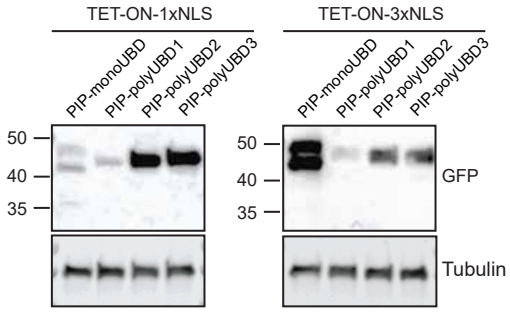

Figure 4.2.13: Comparing the expression levels of the inducible Ub-PCNA sensors. Expression levels of the 1xNLS and 3xNLS GFP-tagged Ub-PCNA sensors at 2 μg/mL of doxycycline concentration after 2 hours of induction. Tubulin was used as a loading control. Part of the membrane containing the TET-ON-1xNLS sensors was exposed longer.

4.2.3.3 The Ub-PCNA sensors colocalise with PCNA

Many *in vitro* studies suggested different models of PCNA mono- and polyubiquitylation. One of the favourite models is the stepwise ubiquitylation, where Rad6/Rad18 hands over monoubiquitylated PCNA to Mms2-Ubc13/Rad5 for the polyubiquitylation reaction to take place [18]. Another model suggests an *en block* transfer of ubiquitin chains onto PCNA [332, 259]. However, how dynamic are these models in living cells is not well defined. Besides, PCNA is a homotrimer in which each subunit carries a ubiquitin acceptor lysine. This means that at any given time, DNA-loaded PCNA subunits can be either unmodified, all carry similar post-translational modification, or each subunit is modified differently. Therefore, it would be exciting to know how long would it take for PCNA monoubiquitin signal to turn into polyubiquitin signal and the crosstalk between them. To tackle some of these aspects, I aimed to express the two different sensors simultaneously and measure their colocalisation. The most technically feasible fluorescent protein pair to study colocalisation is GFP and mCherry. Having seen that GFP-tagged Ub-PCNA sensors worked very well in fluorescent microscopy, I developed mCherry versions of the sensors. Although the mCherry-tagged sensors localised to the nucleus, they were unable to form foci under damage conditions. In addition, carrying 1x or 3xNLS did not make any significant difference (data are not shown). mRuby2 is an improved variant of the red fluorescent protein (RFP) with better photokinetics. mRuby2 is brighter, more photostable, and has a higher quantum yield than mCherry making it a better fluorophore for live-cell imaging [333, 334]. Like in the case of mCherry, mRuby2-tagged Ub-PCNA sensors with 1xNLS did not form foci. However, adding 3xNLS instead of 1xNLS improved the brightness and foci formation of PIP-monoUBD^{mRuby2} and PIP-polyUBD1^{mRuby2} (Figure 4.2.14 A). Although, 3xNLS-PIP-polyUBD2 and 3xNLS-PIP-polyUBD3 tagged with mRuby2 had comparable expressions levels to 3xNLS-PIP-polyUBD1^{mRuby2} and cells expressing them were sensitive to MMS, these sensors were incapable of forming damage-dependent foci (Figure 4.2.14).

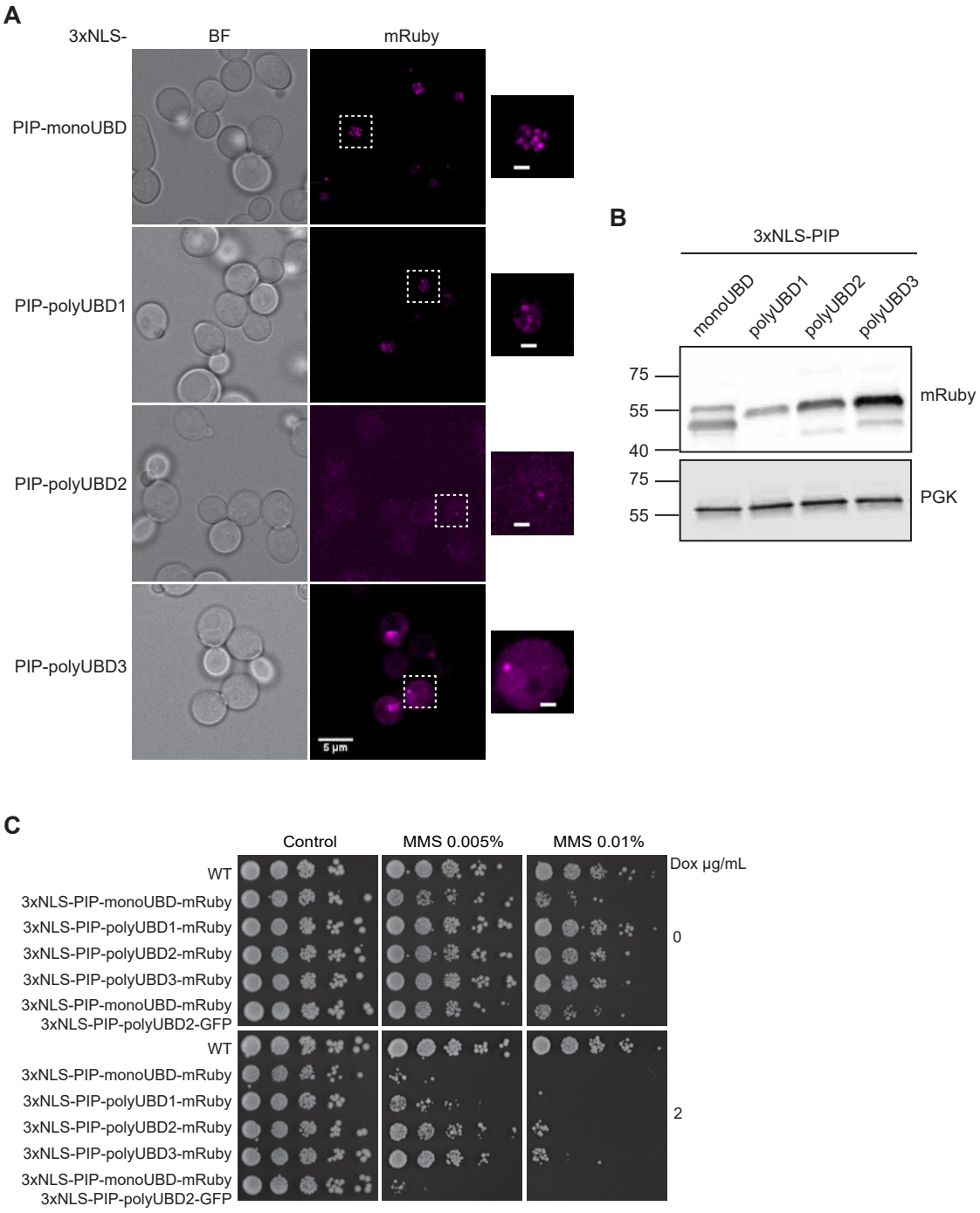

Figure 4.2.14: Optimisation of red fluorescent Ub-PCNA sensors. (A) Microscopic images of wild-type yeast cells expressing mRuby-tagged Ub-PCNA sensors with 3xNLS and under the control of TET-ON promoter. Images were taken after 90 min of incubation with 2 μg/mL of doxycycline and 0.02% MMS. The scale bars in the magnified images equal to 1 μm. BF; bright field. (B) Expression levels of the different sensors at 2 μg/mL of doxycycline concentration after 2 hours of induction. (C) Spot assay to check the damage sensitivity of the strains expressing mRuby-tagged Ub-PCNA sensors on synthetic complete agar plates with or without doxycycline and increasing doses of MMS.

In general, the doxycycline-inducible mRuby2-tagged versions of the Ub-PCNA sensors were not as good as the GFP-tagged ones indicated by foci formation after MMS damage (Figure 4.2.14 A, 4.2.9 A, and 4.2.10 A), though, the detected signal was enough to perform some colocalisation analysis. To confirm that the sensors mark ubiquitylated PCNA *in vivo*, I analysed their colocalisation with PCNA itself. N- or C-terminal tagging of PCNA with GFP in its endogenous locus renders cells sensitive to DNA damage. Thus, I introduced an additional copy of ^{GFP}PCNA heterologously in yeast strains that express either TET-ON-3xNLS-PIP-monoUBD^{mRuby2} or TET-ON-3xNLS-PIP-polyUBD1^{mRuby2}. The foci of both sensors showed around 85% colocalisation with PCNA (Figure 4.2.15 A-B and C). The 15% no overlap seen between the sensors' foci and ^{GFP}PCNA could be explained by the threshold used for the automated image analysis. Moreover, fewer ^{GFP}PCNA foci overlapped with the sensors indicating that only a subset of PCNA molecules, mostly those at stressed replication forks, were modified by ubiquitin (Figure 4.2.15 A-B and D).

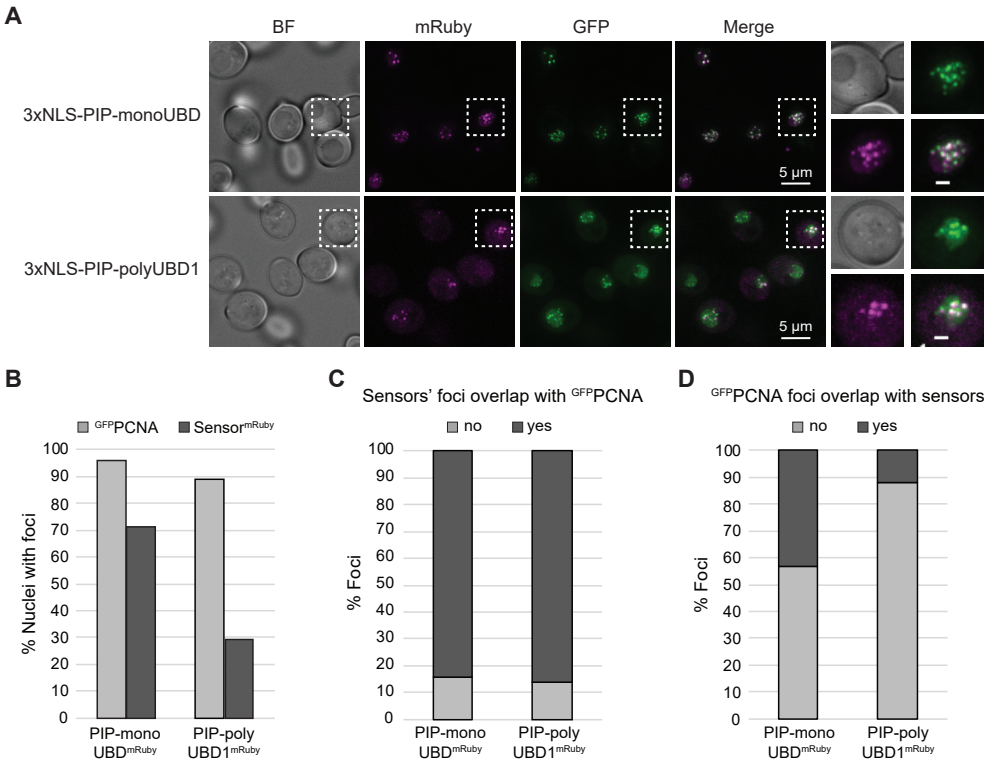

Figure 4.2.15: The Ub-PCNA sensors colocalise with PCNA. (A) Microscopic images of yeast cells containing ^{GFP}PCNA and expressing mRuby-tagged Ub-PCNA sensors with 3xNLS under the control of TET-ON promoter. Images were taken after 90 min of incubation with 2 μg/mL of doxycycline and 0.02% MMS. The scale bars in the magnified images equal to 1 μm. BF; bright field. (B) Quantification of sensor^{mRuby} and ^{GFP}PCNA foci, 200 – 500 cells were quantified per condition. (C) Percentage of sensor^{mRuby} foci covered by ^{GFP}PCNA in the same cells as in B. (D) Percentage of ^{GFP}PCNA foci covered by sensor^{mRuby} in the same cells as in B.

4.2.3.4 Simultaneous visualisation of PCNA mono- and polyubiquitylation

An intriguing aspect of DNA damage bypass that I wanted to address using the Ub-PCNA sensors was the ability to analyse the overlap between PCNA mono- and polyubiquitin signals, and their dynamics during the cell cycle. I expected that coexpression of PIP-monoUBD in the same strain as PIP-polyUBD might lead to some competitive effects where PIP-monoUBD might interfere with the foci formation of PIP-polyUBD. Interference between the sensors may happen when their expression is turned on before DNA damage induction. However, providing the substrates of the different sensors by damage induction ahead of their expression may not cause any cross-interference between the sensors. To check these assumptions, I analysed the ability of the sensors to form foci under a panel of different expression and damage conditions. For these experiments, I used a yeast strain that expressed TET-ON-3xNLS-PIP-monoUBD^{mRuby} and TET-ON-3xNLS-PIP-polyUBD2^{GFP}, and their parental strains that expressed only one of the sensors. Load of the DNA damage was fixed to a two-hour exposure to 0.02% MMS and the expression of the probes was turned on before, together, or after MMS exposure (Figure 4.2.16 and 4.2.17 A). In all the tested damage conditions, more than 65% of cells expressing only one of the sensors contained at least one focus. Interestingly, in the strain that coexpresses the sensors for shorter periods, the percentage of the population with foci dropped to around 25-40% (Figure 4.2.17 A). The drop in the foci count upon coexpression of the sensors could have raised from interference between the sensors, indicating that not only PIP-monoUBD but also PIP-polyUBD can exert some competitive effects. However, having both sensors under TET-ON expression system might titrate away the doxycycline concentration leading to a reduction in their expression. Therefore, it is worth to compare the protein levels of the sensors under each condition by a western bolt. To our surprise, a four-hour expression of the 3xNLS-PIP-monoUBD^{mRuby} without any MMS damage led to an accumulation of foci in the majority of the cells. More interestingly, the accumulated 3xNLS-PIP-monoUBD^{mRuby} foci induced the formation of 3xNLS-PIP-polyUBD2^{GFP} foci as well, and most of these foci overlapped nicely with each other. These observations indicate that expressing the sensors for extended periods may interfere with ongoing unperturbed replication, creating replication stress and causing a PCNA ubiquitylation feedback loop. The sensitivity of this strain on MMS plates in the absence of doxycycline showed that the TET-ON promoter was not controlled tightly (Figure 4.2.14 C). The TET-ON expression system could be further optimised by using the repressor/activator dual system or reducing the expression periods and doxycycline concentrations. Analysing the overlap between the two sensors, showed that around 30-50% of PIP-monoUBD^{mRuby} foci colocalise with PIP-polyUBD2^{GFP} in all the different expression conditions (Figure 4.2.17 B). In the case of PIP-polyUBD2^{GFP} foci, the degree of overlap differed significantly from one condition to another where more overlap was detected in the prolonged-expression conditions. Owing to its high affinity to polyubiquitylated PCNA, PIP-polyUBD2 sensor might dislocate PIP-monoUBD from polyubiquitylated PCNA. It is also foreseen that in prolonged-expression conditions, more monoubiquitylated PCNA convert into polyubiquitylated PCNA, thereby providing more binding substrate for PIP-polyUBD2. Because of the obscure effects of the sensors upon their coexpression, performing experiments with such a strain would not correctly reflect the biological dynamics of PCNA ubiquitylation. Hence, we decided to continue our studies always in parallel experiments using strains that express the sensors separately. Nevertheless, it would be interesting to analyse the foci dynamics of the sensors in synchronised time-course experiments once the expression of 3xNLS-PIP-monoUBD^{mRuby} is optimised.

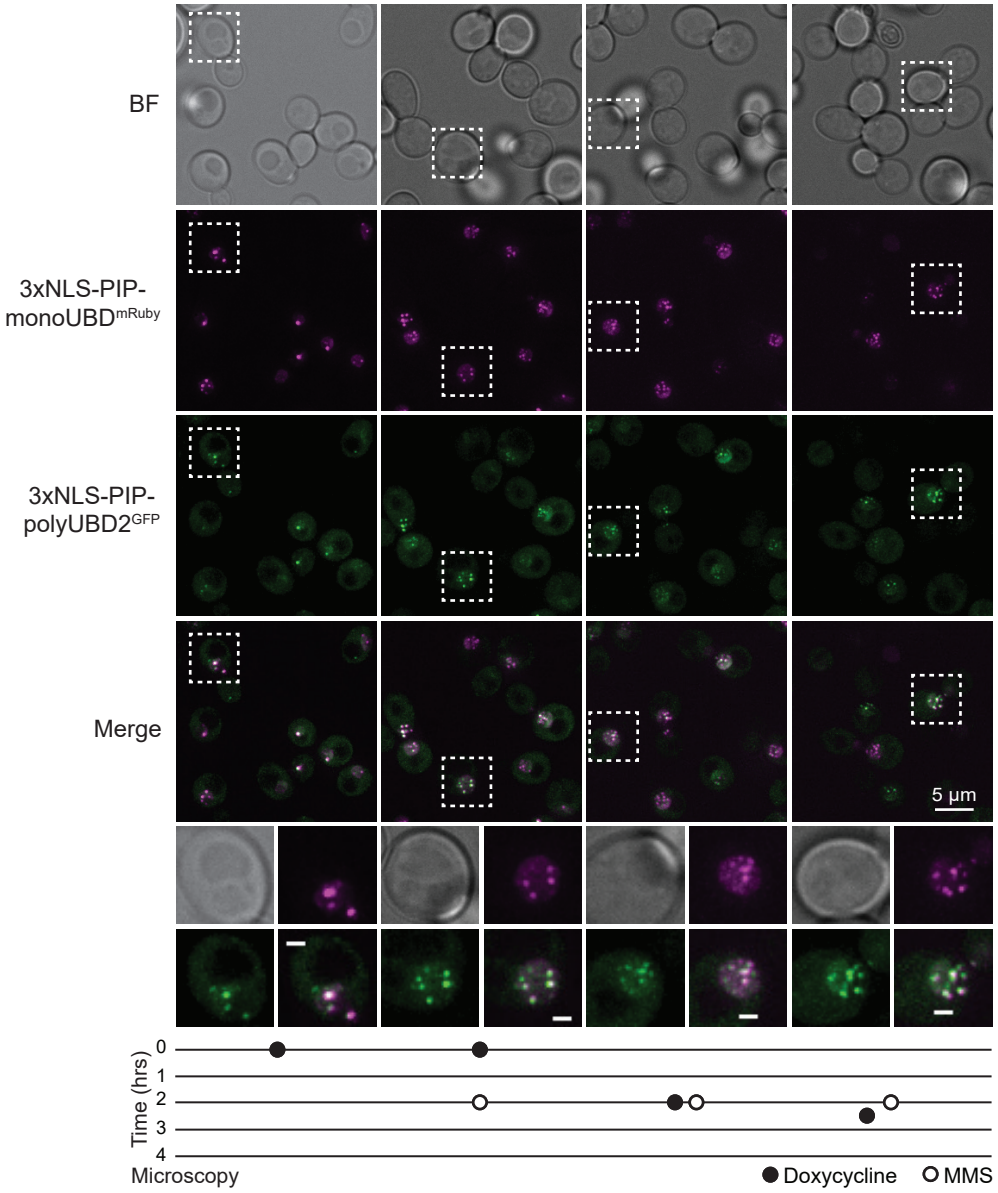

Figure 4.2.16: Simultaneous visualisation of PCNA mono- and polyubiquitylation. Representative microscopy images of the sensors and their colocalisation. Asynchronously growing yeast strains that contain either TET-ON-3xNLS-PIP-monoUBD^{mRuby}, TET-ON-3xNLS-PIP-polyUBD2^{GFP}, or both were incubated in four different conditions; four hours of doxycycline, two hours of doxycycline then two hours of MMS, two hours of doxycycline and MMS, 30 minutes of MMS then 90 minutes of doxycycline. In all the four conditions, 2 μg/mL of doxycycline and 0.02% MMS were used. Images of live cells were taken after the indicated incubation periods. The scale bars in the magnified images equal to 1 μm. BF; bright field.

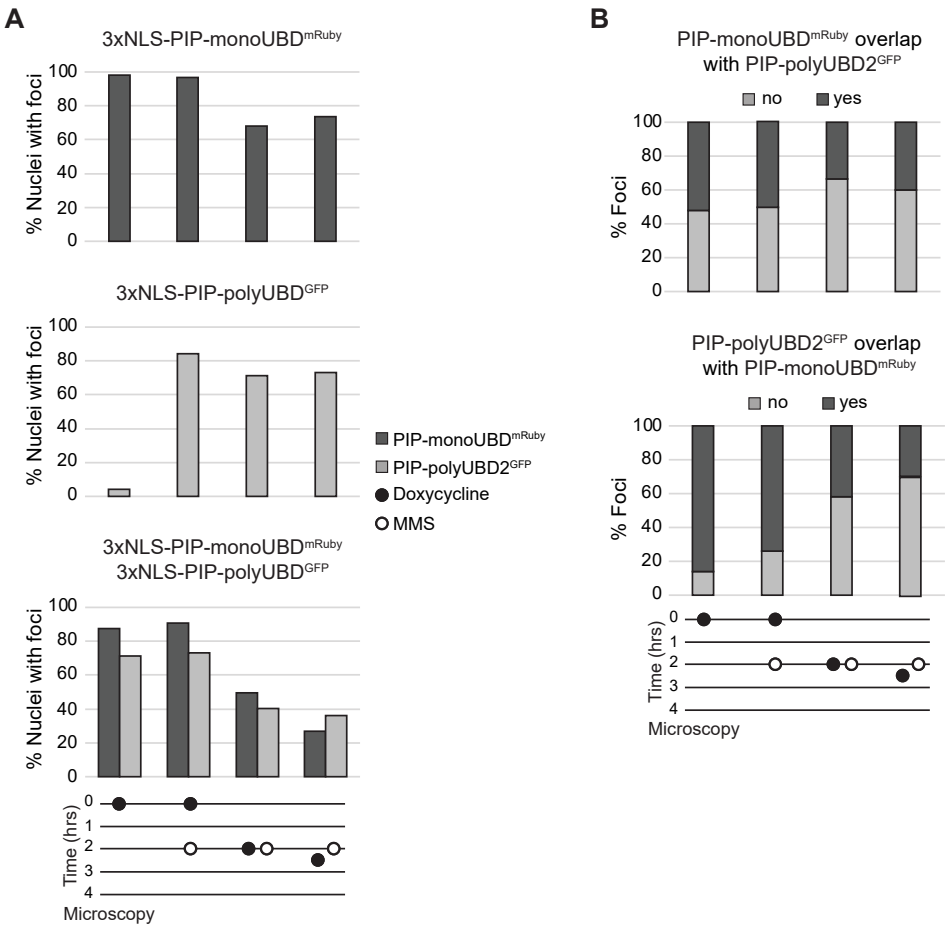

Figure 4.2.17: Mono- and polyubiquitylated PCNA partially colocalise. (A) Asynchronously growing yeast strains that contain either TET-ON-3xNLS-PIP-monoUBD^{mRuby}, TET-ON-3xNLS-PIP-polyUBD2^{GFP}, or both were incubated in four different conditions; four hours of doxycycline, two hours of doxycycline then two hours of MMS, two hours of doxycycline and MMS, 30 minutes of MMS then 90 minutes of doxycycline. In all the four conditions, 2 μg/mL of doxycycline and 0.02% MMS were used. Images of live cells were taken after the indicated incubation periods followed by analyses of foci count and colocalisation. Between 200 – 400 cells were quantified per condition. (B) Degree of overlap between the two sensors under the different expression conditions in the strain that coexpresses the sensors.

4.2.3.5 Doxycycline-inducible and damage-dependent detection of ubiquitylated PCNA

Post-translational modifications of PCNA is restricted to the nucleus; however, PCNA is assigned to cytosolic functions as well [335, 336]. Thus, in the microscopic analysis of this study, the nuclear pool of PCNA was monitored by tagging a subunit of the histone core complex, Hta2 (H2A2), with the red fluorescent protein (mCherry) [337]. PCNA ubiquitylation is reported to appear also during the bulk replication of the genome in a damage-independent manner [176, 128]. Besides, the TET-ON system may have some basal expression activity even in the absence of doxycycline [338]. Therefore, the doxycycline-inducibility and damage-dependency of the Ub-PCNA sensors were further confirmed in experiments with different incubation conditions. Undamaged cultures incubated without Dox (–Dox –MMS) barely had any cells with Ub-PCNA foci (Figure 4.2.18). A small percentage of unperturbed cells formed some PIP-monoUBD^{GFP} foci upon addition of Dox (+Dox –MMS) (Figure 4.2.18 A-B). These results correlate well with previous findings that indicate the requirement of PCNA ubiquitylation for efficient replication in the absence of exogenous DNA damage [128, 339]. In contrast to the undamaged conditions, replication stress caused by MMS treatment led to a significant increase in the percentage of cells with Ub-PCNA foci (+Dox +MMS) (Figure 4.2.18). Some PIP-monoUBD^{GFP} foci were also detected in MMS damaged cultures in the absence of Dox (–Dox +MMS) (Figure 4.2.18 A-B), which reflects the background activity of the TET-ON system. These experiments concluded that the expression of the fluorescent Ub-PCNA sensors could be controlled relatively well with the TET-ON system and that the Ub-PCNA foci appear mainly after MMS induced replication stress. Furthermore, the absence of any foci outside of the nuclear mask, defined by Hta2^{mCherry}, confirmed that the Ub-PCNA sensors did not cross-react with cytosolic PCNA. The so-far analysed features of the Ub-PCNA sensors and their inducible expression system encouraged me to further validate their specificity to ubiquitylated PCNA.

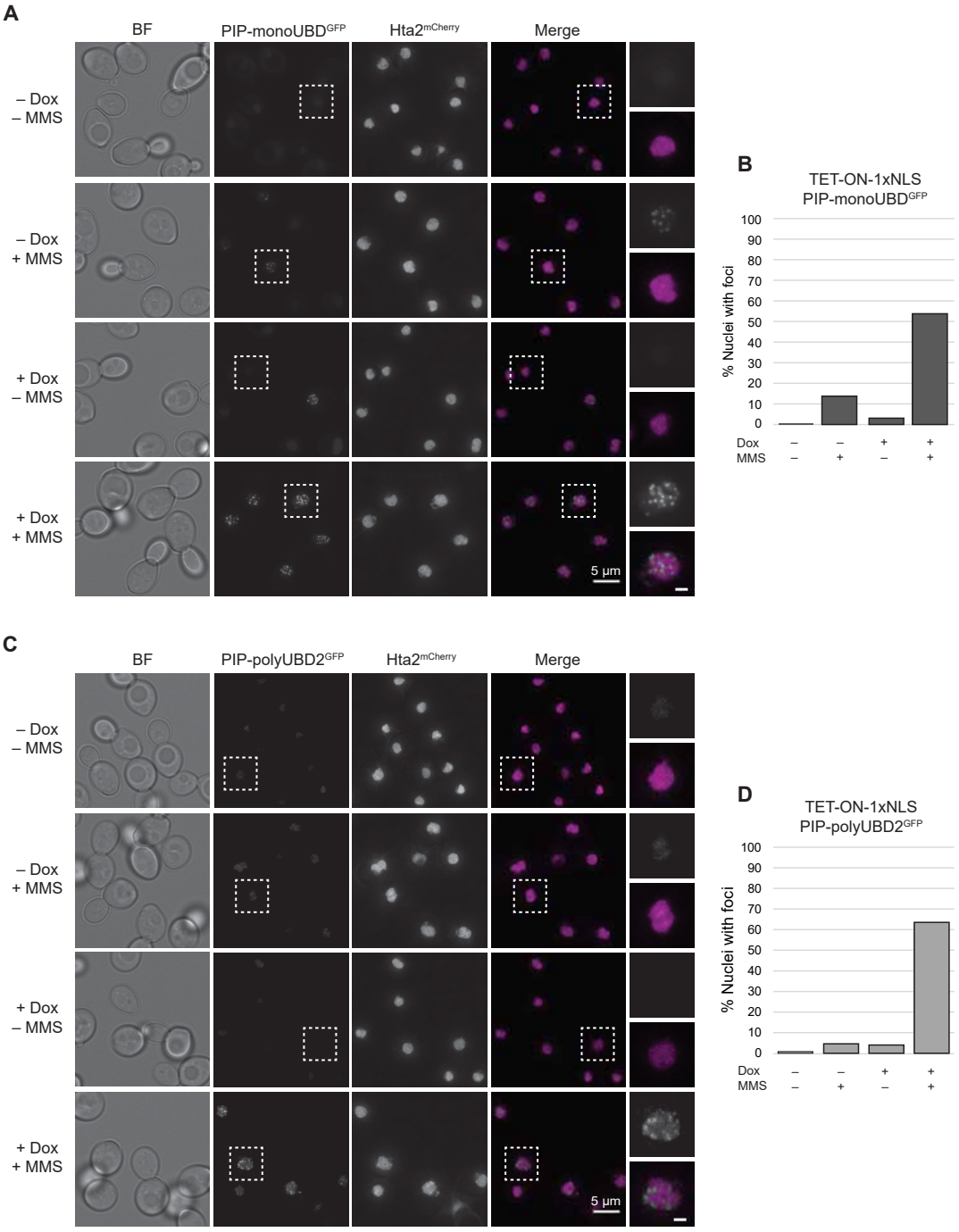

Figure 4.2.18: Foci of Ub-PCNA sensors are doxycycline-inducible and damage-dependent. (A) Microscopic images of wild-type yeast cells expressing TET-ON-1xNLS-PIP-monoUBD^{GFP} by adding 2 μg/mL of doxycycline to the growth media. Images were taken after 90 min of incubation with or without 0.02% MMS. To mark the nuclei, histone (Hta2) was tagged endogenously with mCherry. In the merged images, PIP-monoUBD^{GFP} is shown in green and Hta2^{mCherry} in magenta.The scale bar in the magnified picture equals to 1 μm. BF; bright field. (B) Quantification of TET-ON-1xNLS-PIP-monoUBD^{GFP} foci shown in A, 200 – 400 cells were quantified per condition. (C-D) Examples of TET-ON-1xNLS-PIP-polyUBD2^{GFP} foci. Cells were imaged and quantified as in A and B.

4.2.3.6 The Ub-PCNA sensors detect ubiquitylated PCNA exclusively

I successfully showed that the GFP-tagged Ub-PCNA sensors accumulate in foci after treating a wild-type yeast strain with MMS (Figure 4.2.18). However, as mentioned earlier 4.2.2.3, ubiquitylated proteins are abundant at stressed replication forks. Thus, the Ub-PCNA sensors might accumulate in foci by binding to ubiquitylated proteins other than PCNA. First, I checked if the single domains of the sensors (i.e. PIP, monoUBD, and polyUBD1) were by themselves able to form foci under replication stress conditions. Like the full-length sensors, the single domains were fused with 1xNSL, GFP, and their expression was induced by doxycycline. Yeast strains expressing either TET-ON-1xNLS-PIP^{GFP}, TET-ON-1xNLS-monoUBD^{GFP} or TET-ON-1xNLS-polyUBD1^{GFP} did not form any visible foci in the nucleus upon damage induction (Figure 4.2.19 A-B), even though the expression levels of the single-domains were around five-fold higher than the full-length Ub-PCNA sensors (Figure 4.2.19 C). This observation supports the finding that the combined affinity of the PIP box and the UBD confers Ub-PCNA sensors their specificity.

To further confirm that the detected signal corresponded to ubiquitylated PCNA, I expressed the TET-ON-1xNLS-PIP-monoUBD^{GFP} and TET-ON-1xNLS-PIP-polyUBD2^{GFP} in the mutant yeast strains, *mms2Δ* and *ubc13Δ*, which are defective in PCNA polyubiquitylation [250, 305, 216, 306]. As I predicted, in these strains, only PIP-monoUBD^{GFP} formed foci after MMS damage but not PIP-polyUBD2^{GFP} (Figure 4.2.20 A-C). Besides, the yeast strain that carries a point mutation on the ubiquitin-acceptor lysine (*pol30-K164R*) [216, 18, 166] accumulated neither PIP-monoUBD^{GFP} nor PIP-polyUBD2^{GFP} foci (Figure 4.2.20 A-C). In addition to the single-domain controls analysing the foci formation in the bypass mutants further confirmed the specificity of the sensors. In contrast to the overexpression conditions, the TET-ON sensors did not have any off-target effects. These results were encouraging enough to continue using these Ub-PCNA sensors in analysing the damage bypass pathways and addressing some of the open and mostly contradicting aspects of DNA damage bypass.

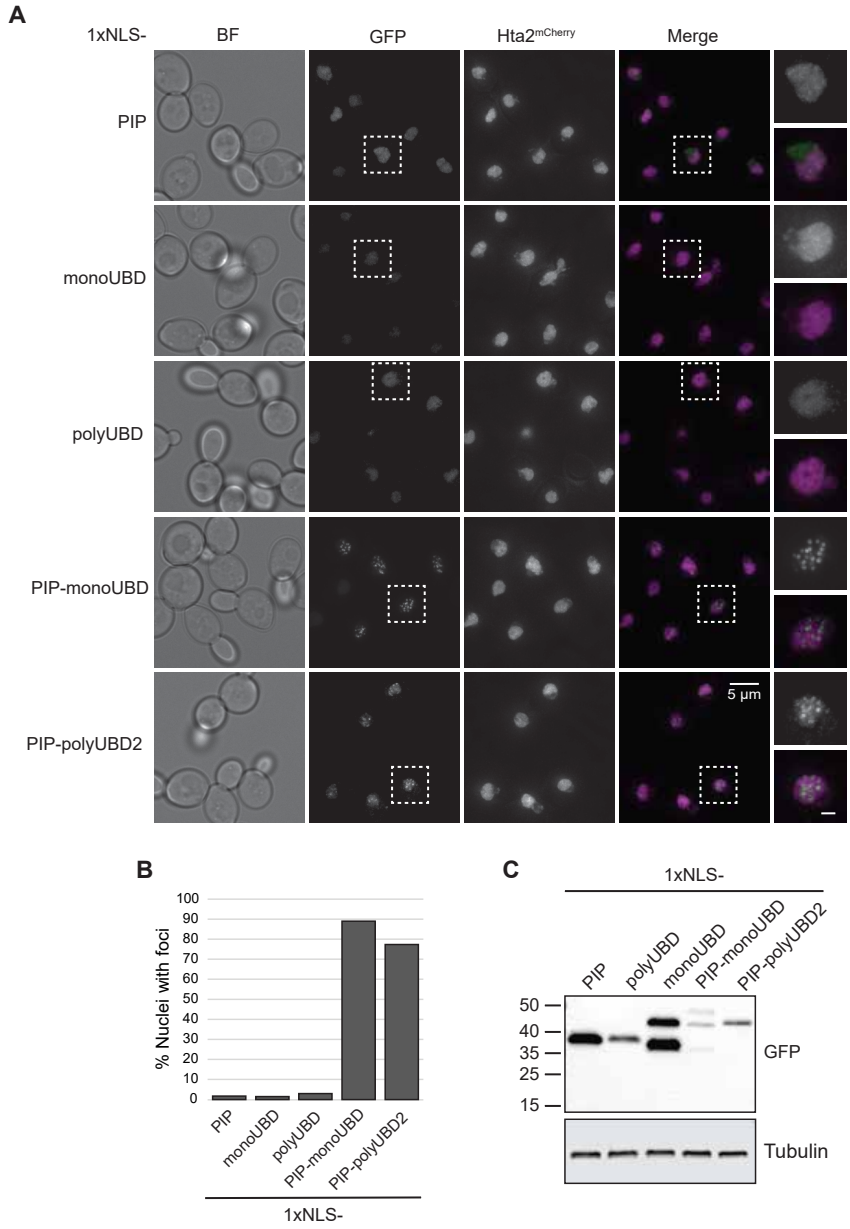

Figure 4.2.19: The single domains of the sensors do not form foci. (A) Microscopic images of wild-type yeast cells expressing GFP-tagged 1xNLS-single-domain controls, 1xNLS-PIP-monoUBD or 1xNLS-PIP-polyUBD2 under the control of TET-ON promoter. Images were taken after 90 min of incubation with 2 μg/mL of doxycycline and 0.02% MMS. To mark the nuclei, histone (Hta2) was tagged endogenously with mCherry. In the merged images, the controls and the sensors are shown in green and Hta2^{mCherry} in magenta. The scale bars in the magnified pictures equal to 1 μm. BF; bright field. (B) Quantification of the foci in A, 200 – 300 cells were quantified per condition. (C) Expression levels of the single-domain controls and the full-length sensors detected by GFP antibody. Tubulin was used as a loading control.

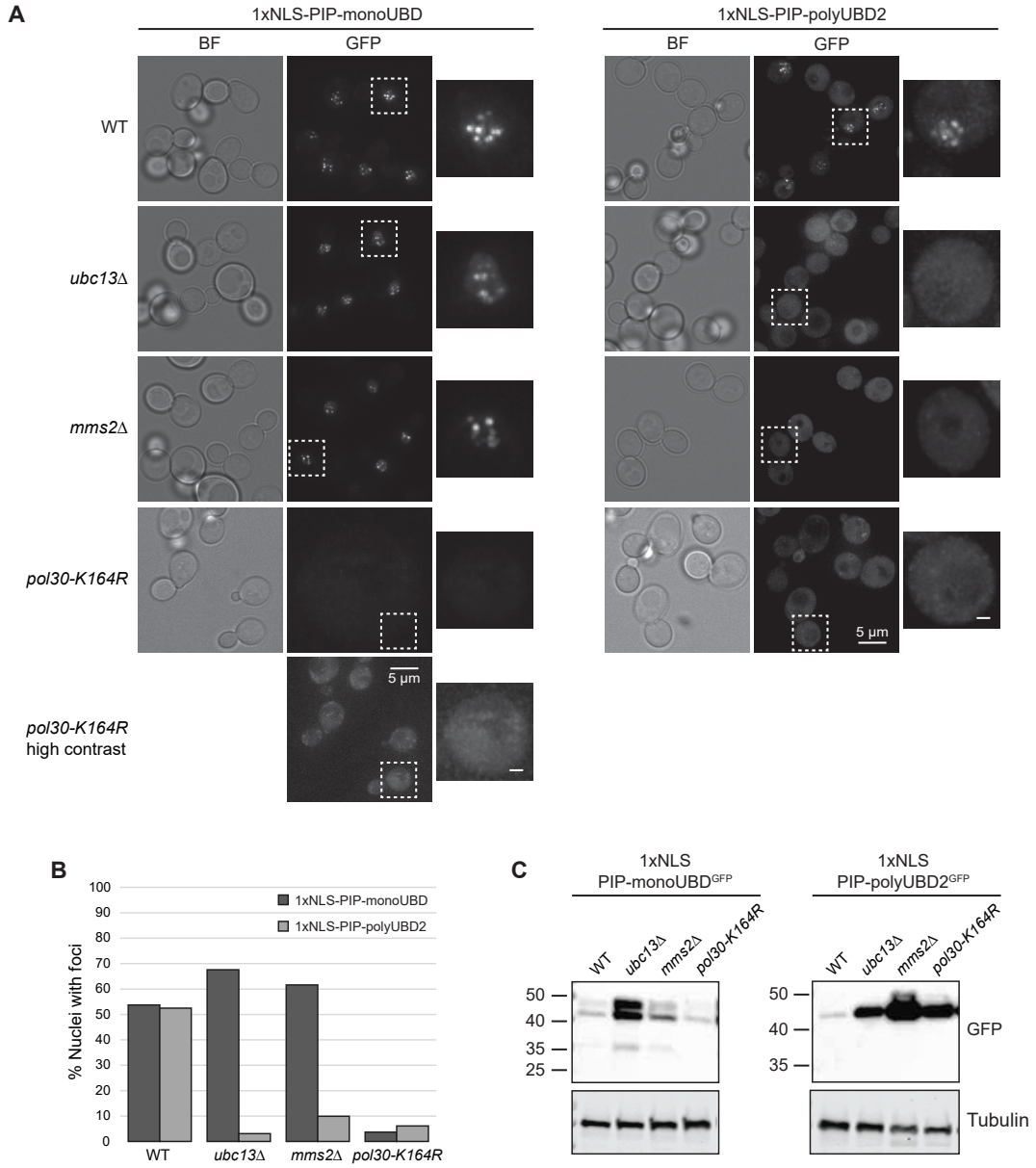

Figure 4.2.20: The Ub-PCNA sensors highlight ubiquitylated PCNA exclusively. (A) Microscopic images of wild-type and mutant yeast strains (*mms2Δ*, *ubc13Δ*, and *pol30-K164R*) expressing GFP-tagged 1xNLS-PIP-monoUBD (left) or 1xNLS-PIP-olyUBD2 (right) under the control of TET-ON promoter. Images were taken after 90 min of incubation with 2 μg/mL of doxycycline and 0.02% MMS. The scale bars in the magnified pictures equal to 1 μm. BF; bright field. (B) Quantification of the foci in A, 300 – 400 cells were quantified per condition. (C) Expression levels of the probes in the different mutants detected by GFP antibody. Tubulin was used as a loading control.

4.2.3.7 Ubiquitylated PCNA forms nuclear foci mainly after replication stress

PCNA ubiquitylation is known to be induced by specific types of DNA lesions primarily by base modifications and stretches of ssDNA gaps [18, 128]. MMS and UV radiation are the best-known agents to induce PCNA ubiquitylation. To support these findings, I asked if Ub-PCNA sensors accumulate in foci at sites of replication stress but not DSBs. Thus, I analysed the capability of a panel of DNA damaging agents to induce the formation of Ub-PCNA foci. Replication stress-inducing treatments, such as MMS, UV, 4-NQO, and HU resulted in foci accumulation to different degrees (Figure 4.2.21 and 4.2.22 A). DSB-inducing agents, such as CPT and zeocin, did not casue foci formation like MMS or UV (Figure 4.2.22 A-B). It is worth to mention that the doses of CPT and zeocin used in these experiments were enough to generate DSBs, as indicated by the growth defects of *mre11Δ* strain in the spot assays and checkpoint activation indicated by Rad53 phosphorylation (Figure 4.2.22 B-D). Therefore, accumulation of Ub-PCNA foci after replication stress but not DSBs correlates well with elevated levels of ssDNA at stressed replication forks.

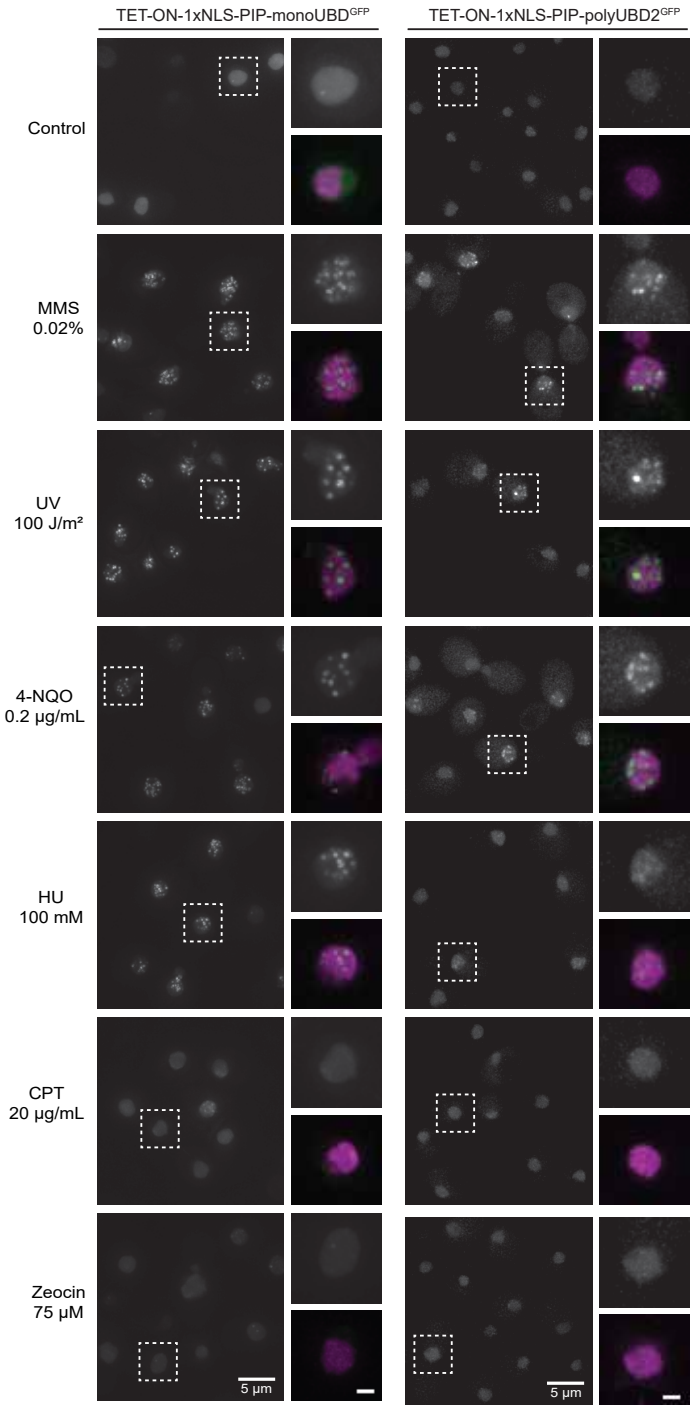

Figure 4.2.21: Ub-PCNA sensors form foci after replication stress. Microscopic images of wild-type yeast strains expressing 1xNLS-GFP-tagged sensors under the control of TET-ON promoter by adding 2 μg/mL of doxycycline to the growth media. Images were taken after 90 min exposure to the indicated doses of the damaging agents or after 40 min for the UV treated samples. Histone (Hta2) was tagged endogenously with mCherry to mark the nuclei. The signal of the sensors is indicated in gray. In the merged images, the sensors are shown in green and $Hta2^{mCherry}$ in magenta. The scale bar in the magnified picture equals to 1 μm. 4-NQO: 4-nitroquinoline oxide, HU: hydroxyurea, CPT: camptothecin, Zeo: zeocin.

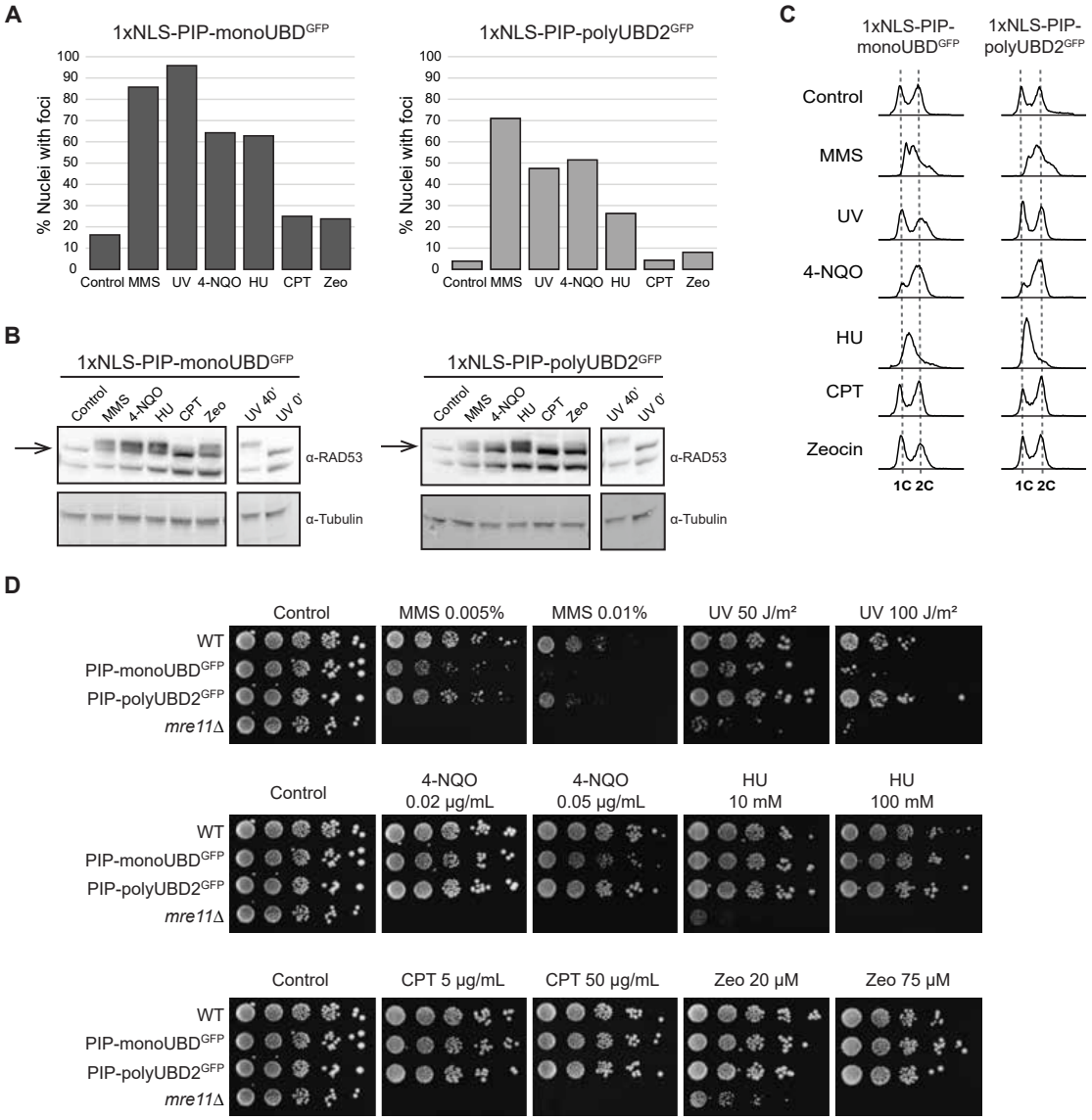

Figure 4.2.22: Not all types of DNA damage induce PCNA ubiquitylation. (A) Quantification of the sensor^{GFP} foci after 90 min exposure to the indicated doses of the damaging agents or after 40 min for the UV treated samples. 200 – 600 cells were quantified per condition. (B) Activation of the DNA damage checkpoint after the different DNA damaging treatments is indicted by Rad53 phosphorylation. Arrows point to the Rad53 specific band. (C) Cell cycle profile of cells in A-B. (D) Sensitivity of the cells to different DNA damaging agents. The strains were spotted on synthetic complete agar plates containing 2 μg/mL of doxycycline and different DNA damaging agents at the indicated doses. The mutant *mre11Δ* was used as a damage sensitivity control for DSBs. 4-NQO: 4-nitroquinoline oxide, HU: hydroxyurea, CPT: camptothecin, Zeo: zeocin.

4.2.3.8 Cell cycle phase, damage load, and lesion type may influence the choice of bypass pathways

It was interesting to see that the percentage of cells with PIP-monoUBD^{GFP} or PIP-polyUBD2^{GFP} foci differed to a higher degree in UV treated cells compared to a very little difference in MMS treated cells (Figure 4.2.22 A). The reason for this difference could be biological or technical. Either the cells activate the bypass pathways differently after MMS and UV damage or the doses used in these experiments create different loads of DNA damage. To check for the dose-dependent effect, I analysed the foci count of Ub-PCNA sensors after exposing cells to increasing doses of MMS or UV. In the case of PIP-monoUBD^{GFP} foci, cells reacted similarly to MMS and UV damage. The percentage of cells with foci increased gradually at low doses until it reached a plateau at medium doses then decreased at high doses, which could be explained by a rapid checkpoint activation (Figure 4.2.23 A-B). The foci count of PIP-polyUBD2^{GFP} after MMS damage followed a similar pattern to the foci count of PIP-monoUBD^{GFP} (Figure 4.2.23 A). In contrast, the percentage of cells with PIP-polyUBD2^{GFP} foci was fairly steady-state and did not increase with increasing doses of UV damage (Figure 4.2.23 B). The elevated accumulation of PIP-monoUBD^{GFP} foci after UV and high doses of MMS correlates well and supports previous findings from our lab, which indicates that cells depend mainly on TLS under similar damage conditions [163]. According to the literature, MMS and UV doses used in these experiments are considered as acute treatments [236, 237, 161]. Under chronic low-dose UV conditions (0.18 J/m^2 min), error-free damage bypass plays a significant role in cell survival and growth. In contrast, the repair of acute high-dose UV damage depends on NER pathway [236]. There is also evidence that both error-prone and error-free bypass pathways are required for cell viability under chronic low-dose UV or MMS (0.0001%) treatments [161]. Yet another study indicated the role of cell cycle in bypass preference of chronic low-dose MMS, where the error-free bypass occurs in S phase and the error-prone in G2 [237]. It would be exciting to see if the foci count of Ub-PCNA sensors would also show differences when chronic low-dose MMS or UV exposures are applied.

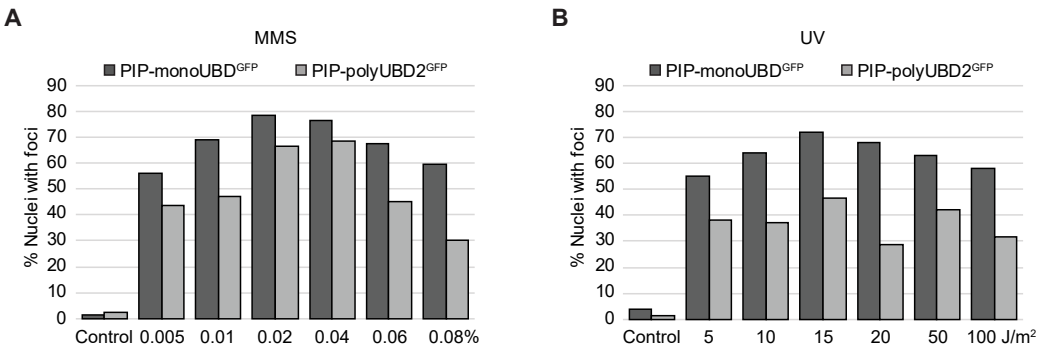

Figure 4.2.23: Effects of DNA damage load on the bypass choice. (A) Quantification of 1xNLS-PIP-monoUBD^{GFP} and 1xNLS-PIP-polyUBD2^{GFP} foci after incubation with 2 μg/mL of doxycycline and increasing doses of MMS for 90 min. At least 100 cells were quantified per condition. (B) Cells were incubation with 2 μg/mL of doxycycline for 90 min, exposed to the indicated doses of UV. Images were taken after 40 min, and the foci were analysed as in A.

It is worth to mention that in the experiments of this subsection, cells were asynchronous at the time of DNA damage induction. Therefore, we cannot exclude that the cells react differently to UV and MMS treatment at different cell cycle stages. To analyse the effect of cell cycle on the bypass choice, I performed a time-course experiment where cells expressing the sensors were synchronised in G1 by α-factor, damaged with an acute dose of MMS or UV, and the foci were analysed after releasing the cells into the cell cycle. Both PIP-monoUBD^{GFP} and PIP-polyUBD2^{GFP} foci started to accumulate at early S phase, reached the maximum at late S/early G2, and resolved during G2. The only difference was that the PIP-monoUBD^{GFP} foci resolved a bit slower than PIP-polyUBD2^{GFP} after UV damage (Figure 4.2.24 B-C). This observation supports the findings in mammalian cultures, indicating that the signal of monoubiquitylated PCNA stays a bit longer even after the repair is completed [235].

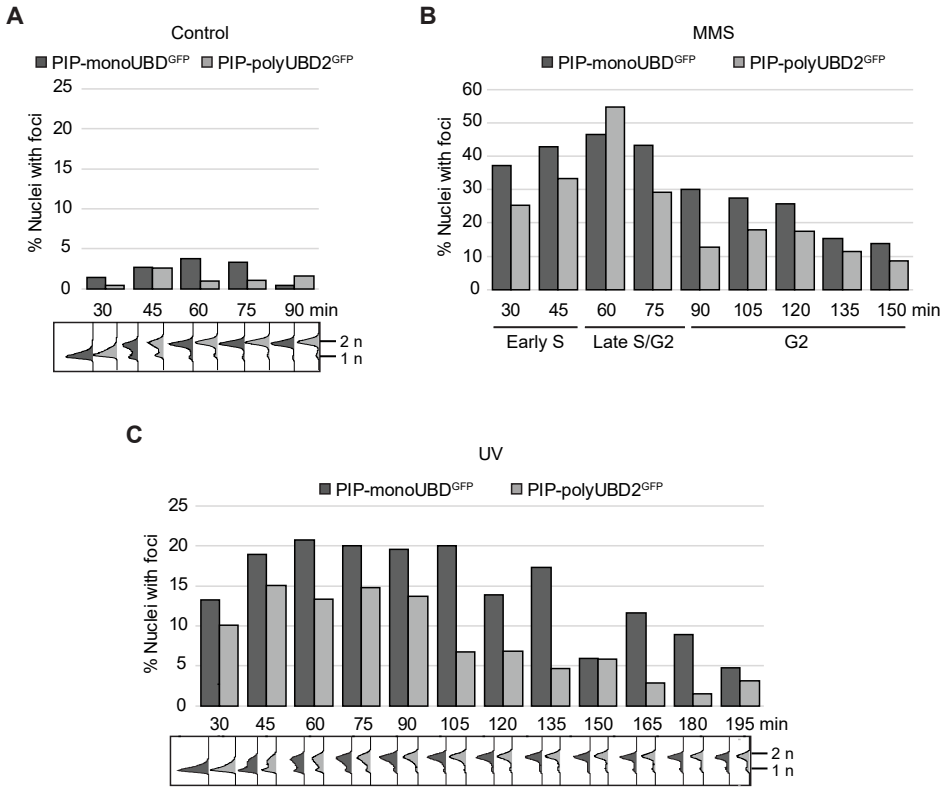

Figure 4.2.24: Effects of cell cycle on the bypass choice. Accumulation and resolution of 1xNLS-PIP-monoUBD^{GFP} and 1xNLS-PIP-polyUBD2^{GFP} foci. Cells were incubated with 2 μg/mL of doxycycline and α-factor for 90 minutes. Then the cultures were kept either unperturbed (A), damaged with an acute dose of MMS (0.02% for 30 min, B), or UV (20 J/m^2, C). Cells were released from G1 arrest and images of live cells were taken each 15 minutes. The percentage of cells with foci in each time point was quantified at least from 150 cells. The cell cycle phase was determined either by FACS (A and C) or by the budding ratio of yeast cells (B).

In the case of the undamaged condition, only few cells formed foci during the S phase. Compared to asynchronous cultures (Figure 4.2.22 and 4.2.23), a lower percentage of cells formed foci when cultures were damaged in G1 phase (Figure 4.2.24). This lower foci count could be explained by the shorter exposure periods to the damaging agents (30 vs 90 min of 0.02% MMS) and repair of the damage by excision repair before a replication fork encounters the damage. In future time-course experiments, it

might be better to use the sensors with 3xNLS to capture more of PCNA ubiquitylation events. All the facts mentioned above and the results of this subsection suggest that the balance between error-prone TLS and error-free template switching might be influenced by a combination of the cell cycle phase, the damage load, and the type of lesion.

4.3 Epilogue and discussion I

The two sub pathways of DNA damage bypass, translesion synthesis and template switching, provide a fast and efficient way to replicate over a damaged DNA template. As mentioned in section (1.2.2), TLS and template switching differ in their manners of damage resolution and thus in their fidelity. However, it is poorly understood how cells choose one bypass pathway over the other in response to genotoxic stress. Several factors can channel the bypass pathway to one of its branches, for example, type of the lesion and load of the damage, cell cycle phase, competition between TLS polymerases and Rad5 in binding monoubiquitylated PCNA, chromatin organisation and compartmentalisation, species under study and more (Section 1.2.2.4). To gain a detailed insight into the choice between the error-free and error-prone damage bypass, I developed, optimised, and validated a set of tools that allow performing well-controlled analysis of PCNA ubiquitylation in the model organism *Saccharomyces cerevisiae*. These tools were PCNA-specific probes that selectively recognised and distinguished between different species of ubiquitylated PCNA. I showed that the fluorescent forms of the probes were suitable for live-cell imaging and used them to explore some of the undiscovered corners of DNA damage bypass.

4.3.1 Novel affinity reagents for ubiquitylated PCNA

Ub-PCNA probes, PIP-monoUBD and PIP-polyUBD, are specific probes that bind to ubiquitylated PCNA. They were created by the laboratory of Prof. Dr Robert Cohen. The probes consist of two domains, a PIP box and a UBD, which binds either to a single ubiquitin moiety or to K63-linked polyubiquitin chains [71, 107, 70]. The simple yet elegant design of the probes allows them to recognise ubiquitylated species of PCNA exclusively (Figure 3.2.1) with excellent biochemical properties and affinities in the nanomolar range (Table 3.2.1). By using Flag-tagged versions of these probes in pull-down assays, I confirmed that PIP-monoUBD binds to mono- and polyubiquitylated PCNA whereas PIP-polyUBD binds preferentially to PCNA with long K63-Ub chains. It is worth to mention that the probes have some background binding to unmodified PCNA, which could be explained by the affinity of the PIP box itself to PCNA (Figure 4.2.1). These observations confirmed that tagging the probes does not change their behaviour, and they could be used in further analyses.

4.3.2 Ub-PCNA probes: Multi-tool gadgets with several *in vivo* functions

Because of a similar binding surface, many UBDs do not bind to a particular type of ubiquitin chain at once. This limited interaction zone creates a competitive environment where the most abundant ubiquitin reader or the one with a stronger affinity would have an advantage in reading or modifying the ubiquitin code. It is expected, therefore, that expression of exogenous UBDs would interfere with the endogenous ubiquitin signalling [108, 107, 109]. Intrigued by this idea, I showed that constitutive expression of the Ub-PCNA probes rendered the budding yeast sensitive to MMS damage and the

degree of sensitivity relatively correlated with the affinity of each probe (Figure 4.2.3 and table 3.2.1). Interestingly, overexpression of the PIP box or UBD alone did not have any effect on cell survival under damage conditions. These observations let us to conclude that upon constitutive expression, the Ub-PCNA probes act as *in vivo* inhibitors and interfere with DNA damage bypass pathways by competing with factors that bind to mono- or polyubiquitylated PCNA. Despite their function as inhibitors, Ub-PCNA probes may allow visualising PCNA mono- and polyubiquitylation by fluorescent microscopy. Indeed, some labs established UBD-based microscopy sensors to study ubiquitin dynamics [110, 107]. However, to use the Ub-PCNA probes in live-cell imaging, they need to be present at minimal levels to avoid interference with ongoing damage bypass (Subsections 4.2.3.1 and 4.2.3.2). To overcome such shortcomings, I made use of an inducible expression system controlled by doxycycline (TET-ON system) and showed that the fluorescent Ub-PCNA probes accumulate in nuclear foci after MMS-induced replication stress (Figure 4.2.8). With this, I concluded that the inducible Ub-PCNA probes are highly suitable as sensors to detect PCNA ubiquitylation in live cells, which added another function to these multi-tools.

4.3.3 Possible off-target effects of the Ub-PCNA probes as inhibitors

In addition to PCNA, a bundle of factors at replication forks are modified by ubiquitin in response to genotoxic stress [147]. The Ub-PCNA probes could cause MMS sensitivity in two possible ways. Either they interfere with ubiquitylated PCNA directly or bind to other ubiquitylated repair factors present at stressed replication forks. By analysing the inhibitory effects of the probes in mutant yeast strains that are deficient in PCNA polyubiquitylation or TLS (*mms2Δ*, *ubc13Δ*, and *tlsΔ*), I demonstrated that PIP-polyUBD1 binds predominantly to K63-polyubiquitylated PCNA and interferes mainly with template switching and not TLS (Figure 4.2.4). Nevertheless, *rad5Δ* cells expressing PIP-polyUBD1 are sensitive to high doses of MMS in Ubc13-independent manner, suggesting that in the absence of PCNA polyubiquitylation PIP-polyUBD1 hampers the replicative function of PCNA via its PIP domain (Figure 4.2.5). Overexpression of the Ub-PCNA probes in a mutant that lacks PCNA ubiquitylation entirely, *pol30-K164R* [18, 166], caused unexpected MMS sensitivity indicating that the probes had off-target effects in the absence of PCNA ubiquitylation. Interestingly, the sensitivity caused by PIP-polyUBD1 was dependent on Ubc13 (Figure 4.2.6) hinting that PIP-polyUBD1 may bind to other K63 polyubiquitylated substrates. However, such substrates and E3s that cooperate with Ubc13 are not yet described. Surprisingly, constitutive expression of the inhibitors rescued the damage sensitivity of *rad18Δ* cells in a Ubc13-dependent way. Such a rescue happens when the signalling by PCNA SUMOylation is compromised, like in *siz1Δ*, *srs2Δ* [317, 18, 174, 176]. Besides, the rescue of *rad18Δ* damage sensitivity by Ub-PCNA probes was not evident in *rad18Δ siz1Δ*. All these results suggest the existence of yet another DNA repair pathway, which depends both on SUMO-PCNA and Ubc13. Possible scenarios of such a pathway could be as follow:

Scenario 1: Ubc13-Mms2/Rad5 complex has other substrates. In the absence of the ubiquitin acceptor lysine on PCNA (*pol30-K164R*) the E2/E3 complex may build K63-linked ubiquitin chains on another protein at stalled replication forks. However, this situation can be counter-argued by the requirement of Rad6/Rad18 to provide Ubc13-Mms2/Rad5 with the first ubiquitin for chain elongation [18] unless there is another E2/E3 pair that monoubiquitylates the unknown factor. It is also possible that in *pol30-K164R*,

Rad18 recognises the RPA coated ssDNA gaps, recruits Rad5, and the Ubc13-Mms2/Rad5 complex builds some K63-linked ubiquitin chains; however, these chains stay attached to the E2/E3 complex.

Scenario 2: Readers of SUMO-PCNA. Several factors bind to SUMO-PCNA (Srs2, Rad18, and Elg1) and channel the repair of damaged DNA into one of the genome maintenance pathways [340]. Srs2 is a helicase that interacts preferentially with SUMOylated PCNA and inhibits unscheduled recombination events by displacing the Rad51 nucleoprotein filaments. Besides, Srs2 deletion suppresses the damage sensitivity of yeast mutants deficient in damage bypass [317, 18, 174, 176]. A recent study proposed a new role of Srs2 that is independent of Rad51 and Srs2's helicase function but dependent on SUMO-PCNA. Srs2 binding to SUMO-PCNA dislocates Pol δ and Pol η, thereby blocks the extension of repair synthesis during template switching or homologous recombination [341]. Elg1 binds to SUMO-PCNA and initiates its unloading from the chromatin. Similar to Srs2, deletion of Elg1 suppresses *rad18Δ* damage sensitivity [342, 343]. In addition to Srs2 and Elg1, Rad18 itself reads SUMO-PCNA modification via its SUMO-interacting motif (SIM). Binding to SUMOylatied PCNA enhances the ubiquitin ligase activity of Rad18, making Rad18 a necessary switch between replication-associated SUMOylation and damage-induced ubiquitylation [178]. Apart from Rad18, there is no evidence of Ubc13 collaboration with Srs2 or Elg1 in a repair pathway signalling. Therefore, it would be very interesting to investigate if Ubc13 collaborates with Siz1/Srs2 and involves in the salvage repair pathway.

Scenario 3: SUMO-targeted ubiquitin ligases (STUbLs). The off-target inhibitory effects of PIP-polyUBD1, which depend on SUMO-PCNA and Ubc13, raise the possibility of STUbLs involvement. In budding yeast, there are only two well characterised STUbLs so far, the heterodimer Slx5-Slx8 and Uls1. The Slx5-Slx8 STUbL accumulate at replication stress sites [344] and DSBs [345], where it mediates relocation of irreparable damaged DNA to the nuclear pore [292]. Uls1 is a member of the SWI2/SNF2 ATPase family and a STUbL that physically interacts with PCNA and Srs2. Uls1 regulates Srs2-SUMO levels at replication forks, thereby promotes binding of Srs2 to PCNA [346, 347, 348]. Both of these STUbLs cooperate with Ubc4 to build K48-linked ubiquitin chains on their substrates; hence, controlling their substrate abundance and stability [344, 347, 348]. Nevertheless, there is growing evidence in higher eukaryotes that STUbLs can also promote nonproteolytic, K63-linked ubiquitylation of SUMOylated substrates. For example, the STUbL, Arkadia/RNF111, cooperates with Ubc13-Mms2 in the ubiquitylation of SUMOylated XPC, thereby regulates the repair of UV lesions by the NER [349].

All the factors and scenarios mentioned above could somehow be involved in the SUMO-PCNA and Ubc13 dependent off-target inhibitory effects of the Ub-PCNA probes. However, with the limited genetic data in this study, it is challenging to draw a concise conclusion. It would be exciting to investigate these assumptions by additional genetic and biochemical approaches.

4.3.4 Seeing is believing: Ubiquitylated PCNA under the microscope

The inducible Ub-PCNA probes seemed to be highly suitable as sensors to detect PCNA ubiquitylation in live cells (Figure 4.2.18). These novel fluorescent sensors formed foci mainly after MMS-induced replication stress where the foci were restricted to the nucleus, confirming that the sensors did not cross-react with cytosolic PCNA [335, 336]. Interestingly all three versions of PIP-polyUBD (1, 2, and 3)

could form nuclear foci after MMS damage (Subsection 4.2.3.2). A small percentage of unperturbed cells also accumulated foci (Figure 4.2.18), confirming the requirement of PCNA ubiquitylation for efficient replication in the absence of exogenous DNA damage [176, 128, 339]. The TET-ON system worked relatively well in controlling the expression of the sensors. Fusing the sensors with 3xNLS instead of 1xNLS improved the detection of the foci by microscopy (Subsection 4.2.3.2). Moreover, titrating the doxycycline concentration allowed making the sensors as delicate as possible to live cells without interfering with damage bypass.

Having the ambition to study the simultaneous action of the sensors and the signal switch from mono- to polyubiquitylated PCNA in living cells, I developed red fluorescent versions of the sensors. In general, the TET-ON mRuby-tagged sensors were not as good as the GFP-tagged ones in forming foci after MMS damage (Figure 4.2.14 and 4.2.15). Nevertheless, they were useful enough to show some colocalisation with ^{GFP}PCNA. It is worth to mention that not all ^{GFP}PCNA foci overlapped with the sensors indicating that only a subset of PCNA molecules, mostly those at stressed replication forks, were modified by ubiquitin.
Because PCNA monoubiquitylation is a requirement for its polyubiquitylation, we expected that co-expression of PIP-monoUBD might competitively interfere with PIP-polyUBD. But to our surprise, both sensors had a cross-competitive action and interfered with the foci formation of the other (Figure 4.2.16). This observation hints that TLS and template switching might not act randomly at a given damage site; instead, the action of TLS and template switching might be restricted to assigned genomic territories. It is therefore interesting to further investigate this aspect with various genetics, genomics, and microscopy experiments. However, caution should be taken when working with such a strain because the interference between the sensors might not correctly reflect the biological dynamics of PCNA ubiquitylation.

4.3.5 Ub-PCNA sensors highlight the sites of ubiquitylated PCNA specifically

Because ubiquitylated proteins are abundant at stressed replication forks, the Ub-PCNA sensors might accumulate in foci by binding to proteins other than PCNA. Nevertheless, the single domains of the sensors (i.e. PIP, monoUBD, and polyUBD1) did not form foci by themselves under replication stress conditions (Figure 4.2.20), supporting the finding that the combined affinity of the PIP and the UBD confers the Ub-PCNA sensors their specificity. In the absence of PCNA polyubiquitylation in *ubc13Δ* and *mms2Δ*, PIP-polyUBD2 foci were not detected. Besides, neither of the Ub-PCNA sensors formed foci in the *pol30-K164R* mutant, in which the PCNA ubiquitylation is abolished entirely (Figure 4.2.20). These observations, further confirmed the specificity of the sensors and the absence of any off-targets, unlike in the case of the overexpression (Subsection 4.2.2).

4.3.6 PCNA ubiquitylation accumulates in the wake of replication and after replication stress

The Ub-PCNA sensors formed foci after exposure to replication stress-inducing agents, such as MMS, UV, 4-NQO, and HU, whereas these foci were not evident by DSB-inducing drugs, like CPT and zeocin. These results strongly support previous findings that inducers of PCNA ubiquitylation are specific types

of DNA lesions, mainly base modifications and stretches of ssDNA gaps [18, 128]. In response to UV irradiation and exposure to high doses of MMS, cells depend mainly on TLS [163]. This observation was reflected in the foci formation pattern of the sensors. The percentage of cells with PIP-monoUBD increased relatively with increasing doses of UV damage, whereas PIP-polyUBD2 foci count stayed fairly steady-state (Figure 4.2.23). However, the dependency on TLS after UV damage was described mainly for acute UV treatments. It would be exciting to see if the foci count of the sensors would also show some differences after chronic low-dose UV or MMS exposures. I addressed the cell cycle dependency of the bypass choice in time-course experiments of synchronised cultures. PCNA ubiquitylation detected by the sensors started to accumulate at the onset of replication reaching the maximum at late S/early G2 followed by a resolution in the G2 phase. It is worth to mention that the signal of monoubiquitylated PCNA took longer to resolve after UV damage (Figure 4.2.23), supporting the findings that the signal stays a bit longer even after the repair is completed [235].

Built on the results of this chapter we could suggest that the balance between error-prone TLS and error-free template switching is influenced by a combination of the cell cycle phase, the damage load, and the type of lesion. However, with this narrow experimental view, it is challenging to draw a fine border between the subpathways of damage bypass. Hence, additional experiments with various methodologies would help to solve another corner of the puzzling question.

4.3.7 Other potential uses of the Ub-PCNA probes

Throughout this chapter, I showed that the Ub-PCNA probes are indeed multi-tool gadgets. On the one hand, they are capable of acting as inhibitors to manipulate the damage bypass pathways. On the other hand, they can serve as fluorescent sensors to visualise PCNA ubiquitylation in live cells. In both cases, the tools are highly specific to PCNA modifications with some minor off-target effects of the inhibitor function. Switching between the inhibitor and sensor functions is achieved by tuning the expression levels of the tools.The inhibitor function of the probes can be utilised in genetic screens to identify yet unknown factors involved in DNA damage bypass and to study genetic interactions between bypass factors and other repair factors. The sensor function helps to dissect in minute details the passage of a replication fork through a damaged DNA via analysing the colocalisation of the sensors with different repair factors and replication tracts. Moreover, the sensors have the potential to be used in genomics approaches and help to create a genome-wide map of ubiquitylated PCNA. In the next chapters, I will test, discuss, show the pros and cons, and demonstrate the possibility of using the Ub-PCNA probes in various methods aiming to add more functions to these multi-tools.

Chapter 5

Appearance of PCNA ubiquitylation in space and time

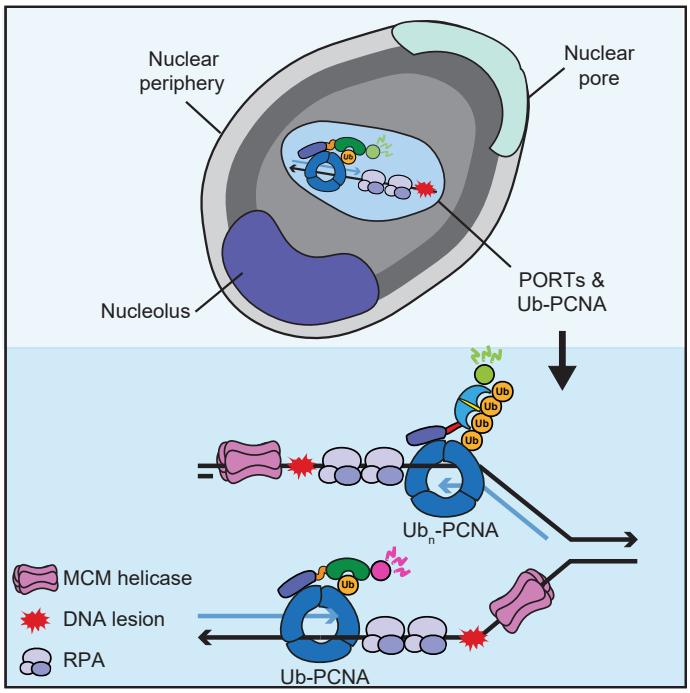

In a nutshell

This chapter intends to investigate the exact timing and location of PCNA ubiquitylation via colocalisation analysis with replisomes and PORTs.
It aims as well to explore the association of PCNA ubiquitylation with known repair centres and the likelihood of bypass events within recombination devoid nucleoli.

Highlights

- Overexpression of Ub-PCNA probes interferes with RPA foci resolution
- PCNA ubiquitylation is activated in replicated regions closer to postreplicative repair territories
- Ubiquitylated PCNA is not concentrated at nuclear pores and the nuclear periphery
- Nucleoli mostly refrain from PCNA ubiquitylation

5.1 Prologue II

Mechanistic analysis of ubiquitin-dependent DNA damage bypass revealed that stalled replication intermediates that include stretches of ssDNA gaps are prerequisite for efficient activation of the pathway [128, 350]. In this context, the rate-limiting E3 of PCNA ubiquitylation, Rad18, interacts directly with the ssDNA binding protein complex RPA. Correspondingly, depletion of RPA prevents damage-induced PCNA ubiquitylation in S phase [128]. During unperturbed replication in budding yeast, RPA forms small speckles associated with replication centres. In contrast, in response to genotoxic stress RPA accumulates in larger foci that colocalise with factors of homologous recombination [351]. Recently, our lab has gained detailed insight into the genesis and resolution of ssDNA tracts during replication of damaged DNA by tracing fluorescent RPA complex [163]. Under conditions of tolerable replication stress induced by polymerase-blocking lesions (MMS and UV), RPA foci serve as markers of DNA damage bypass. These foci are primarily resolved by both error-prone TLS and error-free template switching but also complemented by the salvage pathway. Unlike to DSB- or collapsed replication fork-induced HR foci, RPA foci do not overlap with known repair centres such as nuclear pores, the nuclear periphery or intra-nuclear quality control (INQ) centres [163]. Moreover, analysing the temporal and spatial relation of RPA foci to replisomes and postreplicative chromatin by means of EdU labelling revealed that RPA foci arise predominantly within replicated regions of chromatin. Consequently, the term postreplicative repair territories (PORTs) was proposed for these RPA coated ssDNA tracts.
In this chapter, following the footsteps of the findings mentioned above, I was interested in discovering the exact timing and location of ubiquitylated PCNA, which would help to better fit PCNA ubiquitylation in the proposed model of damage bypass. To this end, first, I used the Ub-PCNA sensors to investigate the temporal and spatial relation of PCNA ubiquitylation to replisomes and PORTs. Next, I interrogated the association of PCNA ubiquitylation with other known repair centres, like the nuclear pore and the nuclear periphery. Finally, I analysed the likelihood of bypass events within the nucleolus because this compartment is devoid of recombination factors.

5.2 Results II

5.2.1 Temporal appearance of PCNA ubiquitylation

5.2.1.1 Interfering with PCNA ubiquitylation inhibits the resolution of RPA foci

Wong *et al.*, 2020 [163] reported that in a strain expressing *RAD18* under control of an inducible promoter [350, 204], RPA foci were not efficiently resolved unless *RAD18* expression was induced. Besides, they demonstrated that the resolution of RPA foci in *ubc13Δ* mutants exhibited a mild delay in comparison to wild type cells [163]. In section (4.2.2.3), I showed that overexpression of Ub-PCNA probes rendered cells sensitive to DNA damage by interfering with signalling downstream of ubiquitylated PCNA. According to their binding properties, overexpression of PIP-monoUBD mimics a *RAD18* deficient situation, whereas overexpression of PIP-polyUBD1 is comparable to *UBC13* deletion. Therefore, we were interested in investigating if overexpression of Ub-PCNA probes would also interfere with the resolution of RPA foci. To this end, Dr Ronald Wong analysed the appearance and resolution of $Rfa1^{GFP}$ foci in cells overexpressing either PIP-monoUBD, PIP-polyUBD1, or a corresponding empty

vector. In all tested strains, accumulation of Rfa1^{GFP} foci showed a similar kinetics starting at the onset of replication and reaching a maximum around the completion of S phase (Figure 5.2.1). Whereas the empty vector contacting strain was able to resolve Rfa1^{GFP} foci effectively (Figure 5.2.1 A), cells overexpressing PIP-monoUBD were incapable of foci resolution and exhibited a delay in cell cycle progression, resembling the condition of *RAD18* absence (Figure 5.2.1 B). In contrast, cells overexpressing PIP-polyUBD1 were able to resolve Rfa1^{GFP} foci; however, with a slower kinetics supporting the previous findings in *ubc13Δ* cells (Figure 5.2.1 C). These results indicate that overproduction of Ub-PCNA probes inhibits DNA damage bypass at the level of PCNA ubiquitylation and resolution of RPA foci. Hence, it is necessary to use the inducible expression of the Ub-PCNA sensors to study the temporal and spatial details of PCNA ubiquitylation.

5.2.1.2 Appearance of PCNA ubiquitylation relative to PORTs

In order to examine the distribution of damage-induced PCNA ubiquitylation throughout the cell cycle and its temporal relation to PORTs, I inducibly expressed PIP-monoUBD^{GFP} in yeast cells carrying Rfa1^{mRuby}. Yeast cultures synchronised in the G1 phase were exposed to a single dose of MMS and monitored upon their release into S phase in the absence of the damaging agent. The appearance of both Ub-PCNA sensor and Rfa1 foci coincided with entry into S phase, reaching a maximum around the end of replication (Figure 5.2.2). In contrast to the overexpression conditions, the number Rfa1^{mRuby} foci declined slowly at the later stages of the cell cycle when the number of PIP-monoUBD^{GFP} foci was also decreased (Figure 5.2.2 B-C).
Throughout the cell cycle, the pattern of RPA signal changed from multiple small foci to a few bright spots (Figure 5.2.2 A). Interestingly, the pattern of the sensor foci followed similar changes, and the degree of overlap between the two factors increased gradually with the progression into the cell cycle (Figure 5.2.2 A-B). These observations suggest that PCNA ubiquitylation emerges and resolves in parallel to RPA foci predominantly in a postreplicative manner.

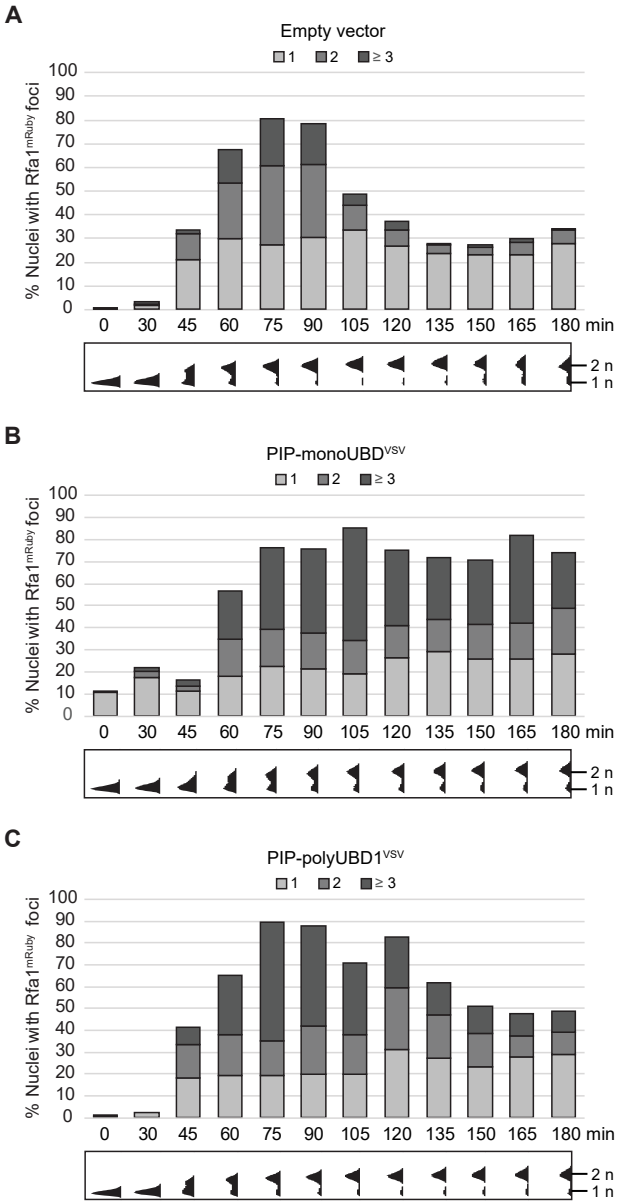

Figure 5.2.1: Overexpression of Ub-PCNA probes interfere with RPA foci resolution. Quantification of $Rfa1^{GFP}$ foci in yeast strains carrying an empty vector (A), overexpressing 1xNLS-PIP-monoUBD^{VSV} (B), or 1xNLS-PIP-polyUBD1^{VSV} (C) under control of a constitutively active *ADH1* promoter. Cells were synchronised with α-factor for 90 min then damaged with 0.02% MMS for 30 min. Then, cells were washed and released from G1 arrest, and images of live cells were taken each 15 minutes. The number of foci in each time point was quantified at least from 100 cells. The cell cycle phase was determined by FACS analysis. These experiments and image analysis were performed by Dr Ronald Wong.

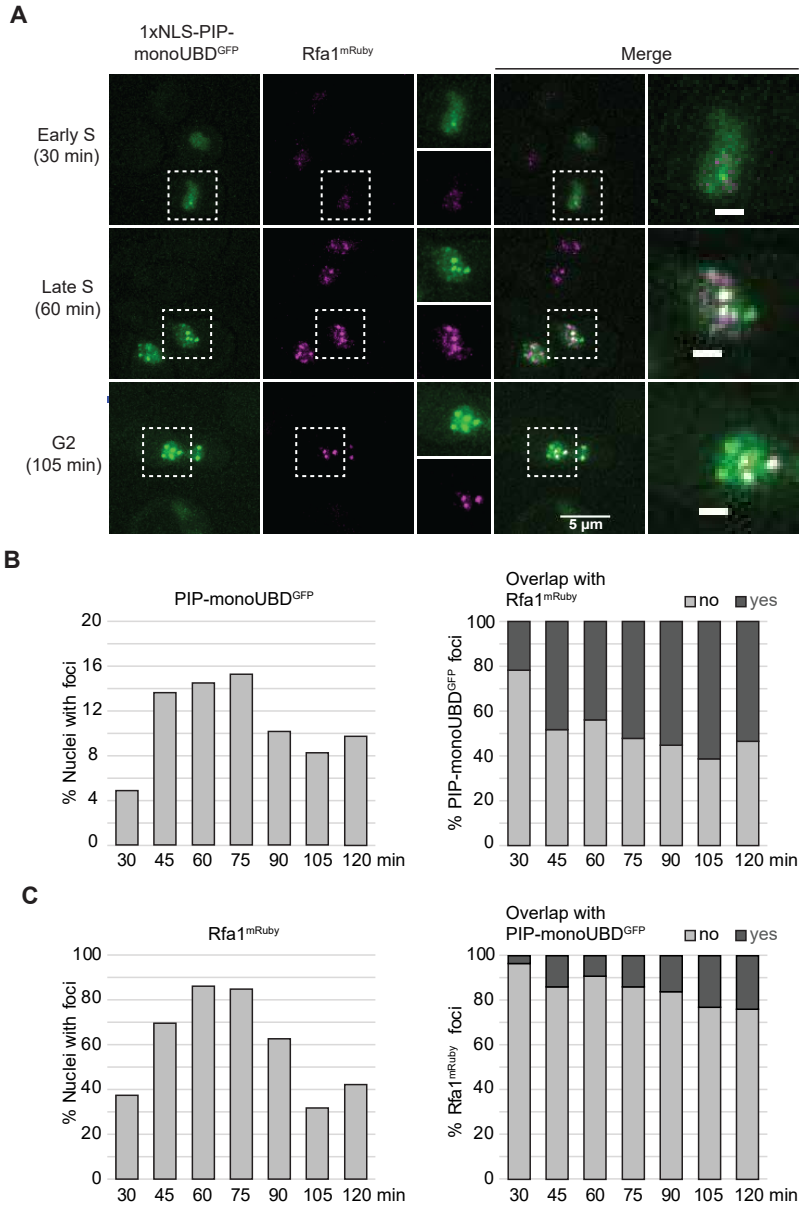

Figure 5.2.2: PCNA ubiquitylation appears in parallel to RPA foci and partly overlaps with PORTs. (A) Ubiquitylated PCNA colocalises with RPA foci. Cells harbouring Rfa1^{mRuby} (magenta) and TET-ON-1xNLS-PIP-monoUBD^{GFP} (green) were synchronised with α-factor, and the expression of the sensor was induced with 2 μg/mL doxycycline for 90 min. Cells were exposed to 0.02% MMS for 30 min before release into the cell cycle without MMS. Then, cells were subjected to live-cell fluorescence microscopy at the indicated time points. The scale bars in the magnified pictures equal to 1 μm. (B) Quantification of 1xNLS-PIP-monoUBD^{GFP} foci (left) and their overlap with Rfa1^{mRuby} (right). (C) Quantification of Rfa1^{mRuby} foci (left) and their overlap with 1xNLS-PIP-monoUBD^{GFP} (right). At least 200 cells were quantified per time point.

5.2.1.3 Appearance of PCNA ubiquitylation relative to replisomes

The partial rather than full overlap between PIP-monoUBD and RPA foci prompted us to assess the spatial relation of PCNA ubiquitylation to replisomes and analyse if the sensor foci precede RPA foci formation. In budding yeast, the core component of the replicative helicase, MCM complex, is loaded onto replication origins directly after mitosis. During S phase, however, the MCM complex leaves the chromatin and is exported out of the nucleus [352]. Tracing replisomes by means of Mcm4^{4GFP} showed a speckled pan-nuclear pattern in early S phase that turned into distinct foci in mid/late S phase and dissolved mostly in G2/M phase (Figure 5.2.3 A and C). As was reported for RPA foci [163], PIP-monoUBD^{mRuby} foci formed predominantly in regions eroded of Mcm4 (Figure 5.2.3 A) and the degree of overlap between the two factors was very little in all the analysed time points (Figure 5.2.3 B). This observation suggests that PCNA ubiquitylation is activated mainly behind ongoing replication forks and closer to the PORTs.

5.2.2 Spatial appearance of PCNA ubiquitylation relative to nuclear organisation

When DSBs, collapsed replication forks, and eroded telomeres are not repaired rapidly, their termini gain mobility and relocate to the nuclear periphery. Once at the periphery, these structures anchor to the nuclear pores and the nuclear envelope, where availability of repair factors and homologous sequences promote repair of the damage [292, 293, 353, 354]. Wong *et al.*, 2020 concluded that RPA foci representing DNA damage bypass tracts do not coincide with any of the known repair centres, such as the nuclear pore and the nuclear periphery [163]. Having seen that foci of ubiquitylated PCNA followed a similar pattern to that of RPA foci and mainly overlapped with PORTs, I was interested in analysing the colocalisation of the Ub-PCNA sensors with the other known repair centres as well.

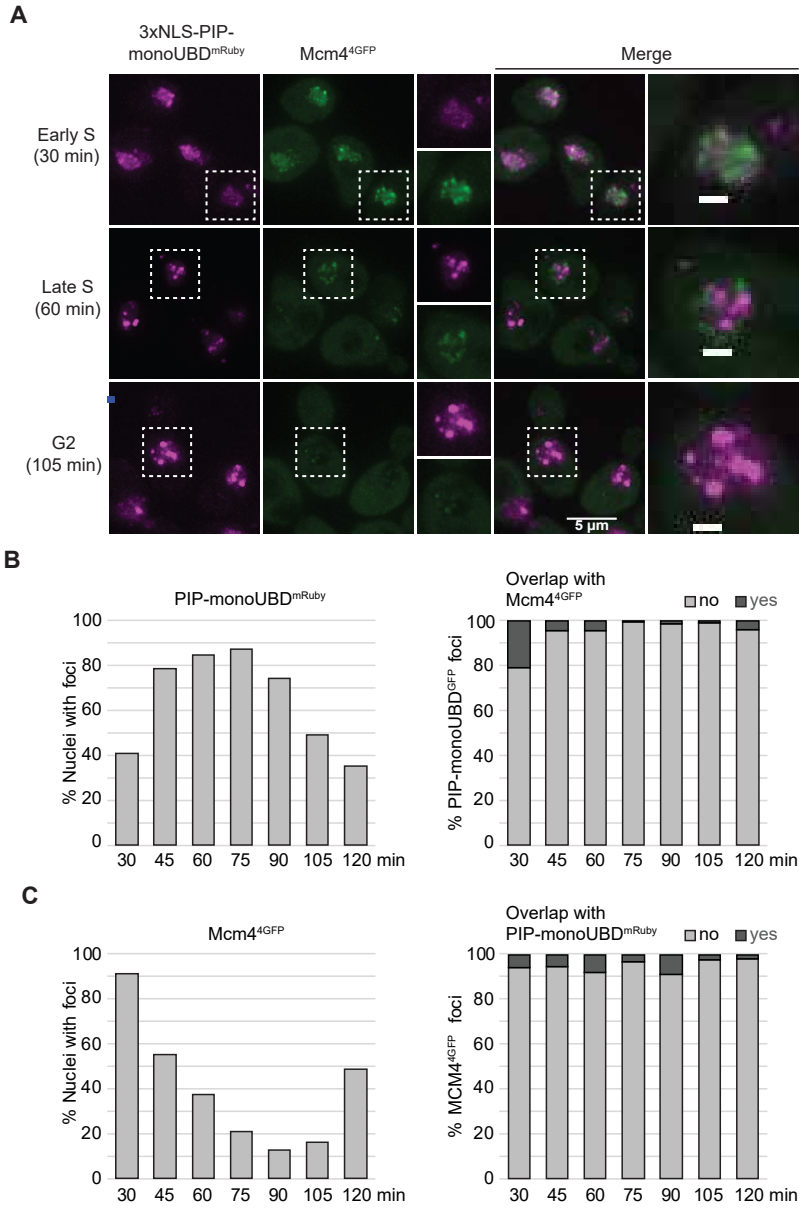

Figure 5.2.3: PCNA ubiquitylation is activated mostly in a postreplicative manner. (A) Ubiquitylated PCNA does not colocalise with replisomes. Cells harbouring Mcm4^{4GFP} (green) and TET-ON-3xNLS-PIP-monoUBD^{mRuby} (magenta) were synchronised with α-factor, and the expression of the sensor was induced with 2 μg/mL doxycycline for 90 min. Cells were exposed to 0.02% MMS for 30 min before release into the cell cycle without MMS. Then, cells were subjected to live-cell fluorescence microscopy at the indicated time points. The scale bars in the magnified pictures equal to 1 μm. (B) Quantification of 3xNLS-PIP-monoUBD^{mRuby} foci (left) and their overlap with Mcm4^{4GFP} (right). (C) Quantification of Mcm4^{4GFP} foci (left) and their overlap with 3xNLS-PIP-monoUBD^{mRuby} (right). At least 100 cells were quantified per time point.These experiments and image analysis were performed by Dr Ronald Wong.

5.2.2.1 PCNA ubiquitylation does not reside at nuclear pores

To investigate colocalisation of Ub-PCNA sensors with nuclear pores, I endogenously tagged a nuclear pore subunit, *NIC96*, with CFP [355], in a strain background carrying a truncated allele of another nuclear pore subunit, *nup133ΔN*. This truncation shifts all nuclear pores into one large but functional cluster (Figure 5.2.4 A) [356, 357]. In asynchronous cultures, the colocalisation values of Nic96^{CFP} with either PIP-monoUBD^{YFP} or PIP-polyUBD2^{YFP} upon exposure to MMS were close to the value expected from a random distribution of the sensors' foci in the nucleus (Figure 5.2.4 B). These results infer that DNA damage bypass tracts marked by ubiquitylated PCNA are not concentrated at nuclear pores.

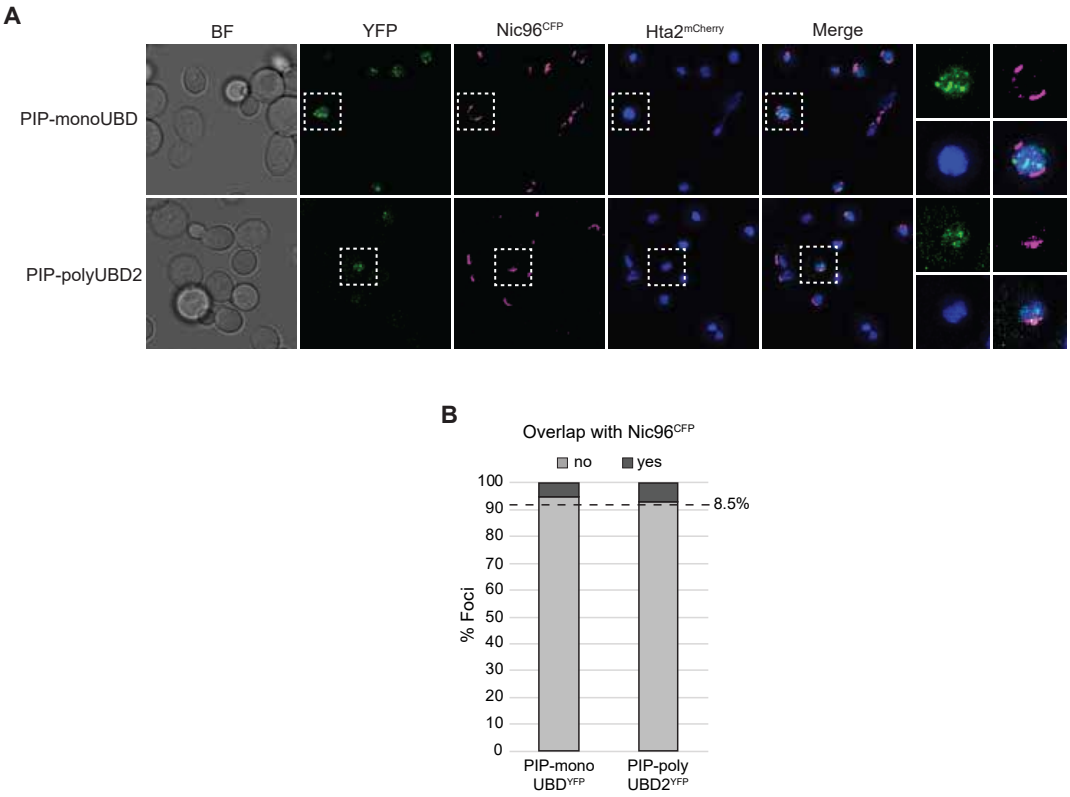

Figure 5.2.4: Ubiquitylated PCNA does not anchor to nuclear pores. (A) Cells carrying Nic96^{CFP} (magenta), Hta2^{mCherry} (a histone subunit, blue), and either TET-ON-1xNLS-PIP-monoUBD^{YFP} or TET-ON-1xNLS-PIP-polyUBD2^{YFP} (green) were exposed to 0.02% MMS, and the expression of the sensors was induced with 2 μg/mL doxycycline for 90 min. Then, cells were subjected to fluorescence microscopy. The scale bars in the magnified pictures equal to 1 μm. (B) Quantification of the overlap between Nic96^{CFP} and TET-ON-1xNLS-PIP-monoUBD^{YFP} or TET-ON-1xNLS-PIP-polyUBD2^{YFP}. The dashed line indicates the percentage of overlap (8.5%) expected for random distribution, calculated based on the relative volumes of the Nic96^{CFP} patch and the nucleus.

5.2.2.2 PCNA ubiquitylation does not accumulate at the nuclear periphery

To evaluate the colocalisation of Ub-PCNA sensors with the nuclear periphery, I utilised a nuclear zoning analysis developed in our lab by Dr Ronald Wong. In this procedure, the nuclei of yeast cells were marked by the fluorescent signal of Hta2^{mCherry}. Then, the nuclei were divided into three layers of equal volume (Figure 5.2.5 A) [357, 163]. Upon exposure of asynchronous cultures to MMS, neither PIP-

monoUBD^{GFP} nor PIP-polyUBD2^{GFP} showed enrichment in the outer zone. Strikingly, both sensors instead got concentrated in the more central zones (Figure 5.2.5 B). Thus, this data exclude a role for the nuclear periphery in processing damaged DNA marked with ubiquitylated PCNA.

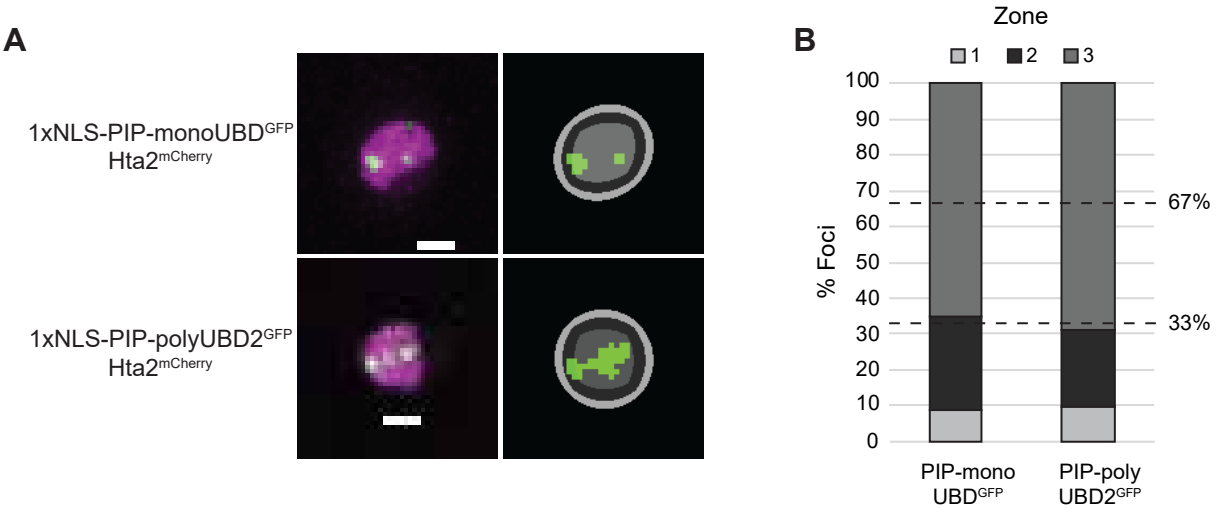

Figure 5.2.5: Ubiquitylated PCNA does not relocate to the nuclear periphery. (A) Cells harbouring Hta2^{mCherry} (a histone subunit, magenta) and either TET-ON-1xNLS-PIP-monoUBD^{GFP} or TET-ON-1xNLS-PIP-polyUBD2^{GFP} (green) were exposed to 0.02% MMS, and the expression of the sensors was induced with 2 μg/mL doxycycline for 90 min. Then, cells were subjected to fluorescence microscopy. Representative images of sensor^{GFP} and Hta2^{mCherry} (left) and the segmentation of these images into sensor^{GFP} foci (green) and nuclear zones of equal volume (gray shades). The scale bars equal to 1 μm. (B) Distribution of sensor^{GFP} foci within the three zones. Dashed lines indicate values expected for random distribution in the nucleus.

5.2.2.3 PCNA ubiquitylation is infrequent in nucleoli

In budding yeast, repair of a DSB in the repetitive ribosomal DNA (rDNA) by recombination requires the transient relocalisation of the lesion from the nucleolus to the nucleus, where the recombination machinery is available [291]. However, such a relocation of stressed replication forks to extranucleolar sites is not yet reported. For better maintenance of the genome integrity, it is beneficial to avoid recombination-like template switching in the repetitive regions of rDNA. Hence, to investigate the distribution of PCNA ubiquitylation in nucleoli, I tagged a nucleolar protein Nop1 with mCherry. Tagging a subunit of the histone core complex, Hta2 , with CFP served to create a nuclear mask (Figure 5.2.6 A). In asynchronous cultures exposed to MMS, the colocalisation values of Nop1^{mCherry} with either PIP-monoUBD^{YFP} or PIP-polyUBD2^{YFP} were lower than the value expected from a random distribution of the sensors' foci in the nucleus (Figure 5.2.6 B). It is worth to mention that the colocalisation of PIP-polyUBD2^{YFP} with the nucleolar marker was even lower in comparison to PIP-monoUBD^{YFP} foci. Altogether, these observations suggest a possible exclusion of PCNA ubiquitylation from nucleoli.

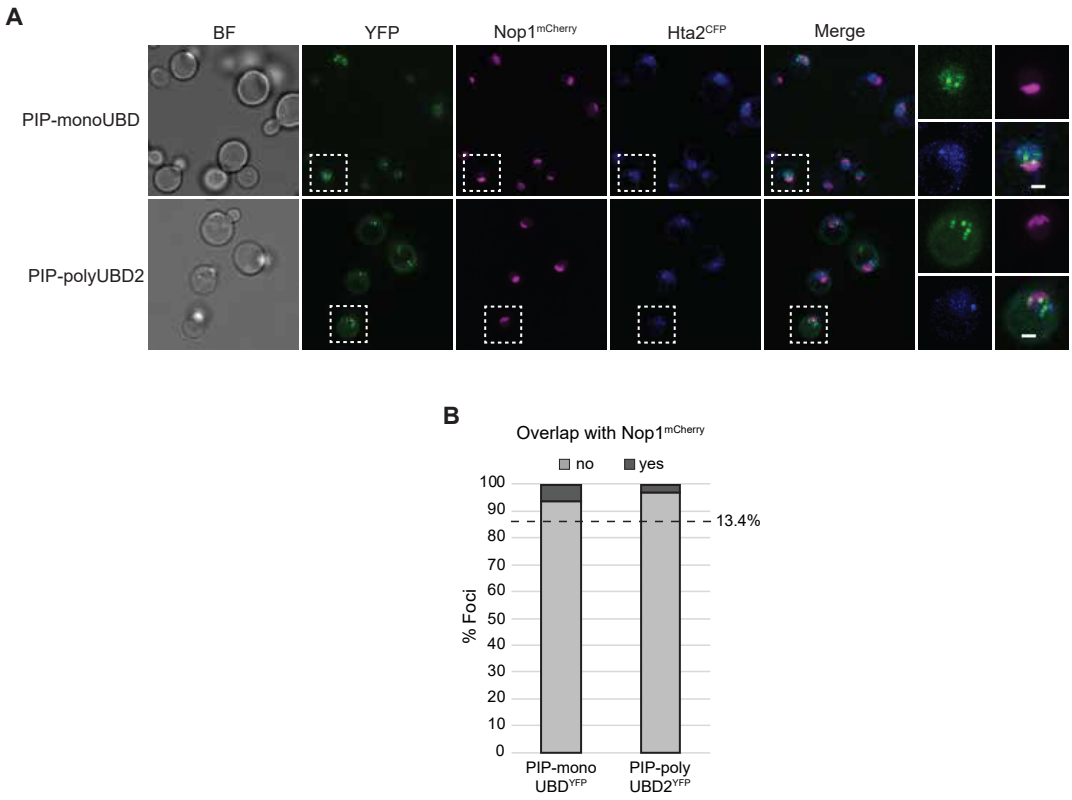

Figure 5.2.6: The ribosome factory, nucleolus, rarely hosts ubiquitylated PCNA. (A) Cells expressing Nop1^{mCherry}, Hta2^{CFP} (a histone subunit, blue) and either TET-ON-1xNLS-PIP-monoUBD^{YFP} or TET-ON-1xNLS-PIP-polyUBD2^{YFP} (green) were exposed to 0.02% MMS, and the expression of the sensors was induced with 2 μg/mL doxycycline for 90 min. Then, cells were subjected to fluorescence microscopy. The scale bars in the magnified pictures equal to 1 μm. (B) Quantification of the overlap between Nop1^{mCherry} and 1xNLS-PIP-monoUBD^{YFP} or 1xNLS-PIP-polyUBD2^{YFP}. The dashed line indicates the percentage of overlap (13.4%) expected for random distribution, calculated based on the relative volumes of Nop1^{mCherry} (nucleolus) and Hta2^{CFP} (nucleus) masks.

5.3 Epilogue and discussion II

Having seen that the Ub-PCNA sensors form discrete nuclear foci upon replication stress encouraged me to investigate the appearance and resolution of these foci in relation to the nuclear organisation, replication clusters, and known DNA repair centres, unravelling new aspects in regulating PCNA ubiquitylation. These analyses demonstrated that modification of PCNA is activated predominantly in a postreplicative manner and accumulate in parallel and close to POTRs. Besides, PCNA ubiquitylation appeared to be infrequent in well-characterised repair centres of DSBs and nucleoli.

5.3.1 PCNA ubiquitylation when and where?

Although the accumulation of RPA is a prerequisite for PCNA ubiquitylation, growing evidence hints to a role of PCNA ubiquitylation in recruiting endonucleases to expand the ssDNA gaps and thereby accumulate more RPA. I addressed this hen and egg situation by investigating the relation of ubiquitylated

PCNA with RPA foci that serve as markers of DNA damage bypass tracts. I showed that overexpression of the Ub-PCNA probes did not inhibit the appearance of RPA foci. In contrast, the probes interfered with the resolution of RPA foci mimicking genetic deficiencies in PCNA ubiquitylation, like in *rad18Δ* and *ubc13Δ* mutants. These observations support the findings that RPA accumulation at ssDNA gaps triggers PCNA ubiquitylation, which in turn involves in the resolution of RPA foci. In an attempt to discover the precise location and time of PCNA ubiquitylation on the road between replication forks and the PORTs, I utilised the inducible Ub-PCNA sensors, which showed that ubiquitylation of PCNA was activated mostly behind replication forks and closer to the sites of RPA covered ssDNA. However, in this stage, it is challenging to build a concrete conclusion since the experiments were done in different batches using sensors tagged with different fluorophores. It is recommended, therefore, to use strains carrying sensors with similar tags and perform the time-lapse imaging in a pairwise manner. Here, I only addressed the regulation of PCNA ubiquitylation at the level of PORTs and upstream of them. To build a full picture of the bypass events, it would be exciting to investigate the colocalisation of PCNA ubiquitylation with downstream recombination centres as well, like Rad52 foci. Moreover, pinpointing the exact timing of PCNA ubiquitylation at the postreplicative tracts would add valuable information to the mechanism of damage bypass events. Such precise measurements are possible by performing EdU pulse and chase experiments to trace the gap-filling in nascent strands and analyse their correlation with Ub-PCNA sensors.

5.3.2 Rather stay in the centre

Cells have evolved an internal organisation to manage the repair and resolution of different DNA lesions by distributing the task into specialised centres. The nuclear envelope protects irreparable DSBs [293], nuclear pores anchor collapsed forks and critically short telomeres [292, 354], whereas PORTs accommodate DNA damage bypass tracts [163]. Investigating the colocalisation of Ub-PCNA sensors with a subunit of the nuclear pore and distribution of the sensors relative to the nuclear volume inferred that PCNA ubiquitylation was enriched neither at nuclear pores nor at the nuclear periphery. Instead, ubiquitylated PCNA overlaped largely with PORTs in the centre of nuclei, excluding an involvement of the nuclear periphery in processing lesions marked with ubiquitylated PCNA.

5.3.3 Faultless manners are not always welcome

Recombination in the centre of nucleoli is rare because recombination factors are restricted to perinucleolar regions [291]. By investigating the likelihood of bypass events within the nucleolus, I demonstrated that nucleoli mostly refrained from PCNA ubiquitylation. This observation might be relevant for nucleolar stability by preventing hyperrecombination of the repetitive rDNA via template switching. In the analysis, I only took into consideration if PCNA ubiquitylation appeared inside or outside of nucleoli. It would be interesting to categorise the foci of ubiquitylated PCNA that appear inside the nucleoli into central and peripheral ones to evaluate if DNA damage bypass, like HR, is also restricted to perinucleolar regions.

Chapter 6

Analysing the distribution of PCNA ubiquitylation along the genome

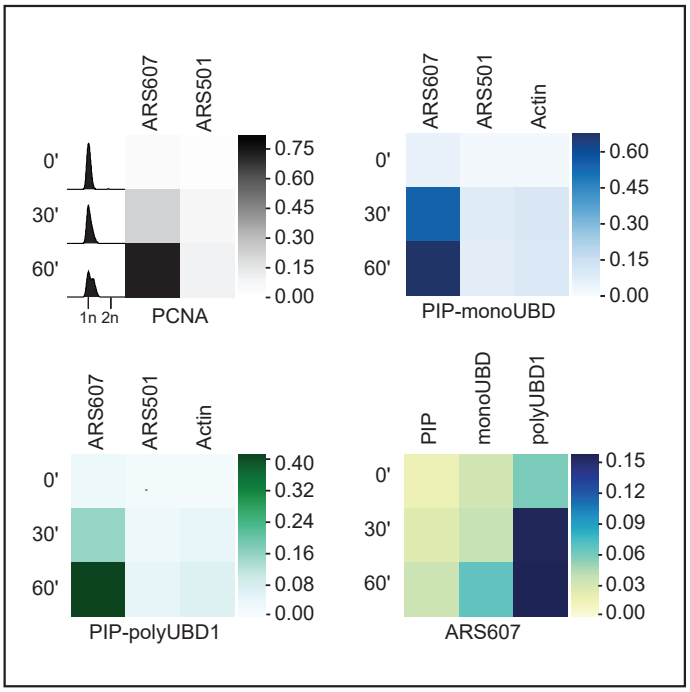

In a nutshell

This chapter aims to gain a global view of PCNA ubiquitylation by using the Ub-PCNA probes in microscopy and genomics.
Analysing the genome-wide distribution of PCNA mono- and polyubiquitylation may unravel any tendency in the genome towards one of the bypass pathways.

Highlights

- Detection of Ub-PCNA sensors at genomic features and loci by microscopy is challenging
- The Ub-PCNA probes accumulate at stressed replication forks detected by ChIP
- Unspecific results accompany the Ub-PCNA probes in ChIP
- UBDs of the Ub-PCNA probes accumulate at stressed replication forks independently of ubiquitylated PCNA

6.1 Prologue III

In chapter 4, I discussed and studied the role of various factors in the decision-making of DNA damage bypass choice. Most of these factors, like the type of the lesion and the responsible repair proteins, lie in close vicinity of the damaged DNA environment, making them elementary regulators of the bypass choice. However, when we zoom out of the nano-environment of a DNA lesion, several other factors may come into play, for example, the DNA sequence up and downstream of the damaged DNA, the chromatin state surrounding the damage, the subnuclear compartment containing the DNA lesion, etc. During the past few decades, numerous reports have indicated that repetitive DNA sequences, like telomers, and difficult to replicate DNA structures, like RNA-DNA hybrids and G-quadruplexes, are hotspots of replication stress and prone to cause genome instability [358, 359, 144]. There is also growing evidence about the importance of chromatin organisation in DNA repair efficiency and its role in the choice of repair mechanism [121]. A possible contribution of some of these factors in modulating DNA damage bypass modes is summarised below.

Repetitive elements: Telomeres and centromeres are non-coding tandem sequences that are repeated in a head to tail orientation [359]. Telomers resides at the end of the chromosomes and protect them from end-to-end fusion and recognition by the DSB repair machinery [360, 361, 362], whereas centromeres play an essential role in sister chromatid cohesion and kinetochore establishment [363]. Despite their vital role in genome maintenance, the secondary structures present at these repetitive regions pose a challenge on replisomes and elevate replication stress [364, 365]. The ribosomal DNA (rDNA) is another example of such repetitive sequences. Although not all rDNA repeats replicate at the same time [366], the secondary structures accumulated by high transcription rates create replication stress [367]. The involvement of PCNA ubiquitylation in the resolution of replication stress at repetitive elements remains poorly characterised**.**

Strand bias: The semi-conservative and unidirectional replication (5' to 3') of the genome, as well as the transcription of genes only from one strand of DNA, exert different challenges for replisomes on the leading and lagging strands [368, 369]. Genome-wide repair maps of UV-induced damage revealed that repair by transcription-coupled nucleotide excision repair (TC-NER) happens earlier on the transcribed strand than on the non-transcribed strand (NTS). Moreover, TC-NER shows a 5' to 3' directional bias within actively transcribed genes where lesions in transcription start sites (TSS) are repaired before the ones in transcription end sites (TES) [370, 371, 372]. Ubp10 and Ubp12 are DUBs that counteract PCNA ubiquitylation. Ubp10 efficiently deubiquitylates both mono- and polyubiquitylated PCNA whereas Ubp12 cleaves only polyubiquitin chains from PCNA. A genome-wide localisation study showed that Ubp10 and Ubp12 engage differently with leading and lagging strands. Under replication stress conditions, Ubp12 resides at early replication origins, whereas the association of Ubp10 to stalled replication forks is evident upon inhibition of PCNA unloading from lagging strands. These observations indicate that Ubp10 and Ubp12 divide the workload of PCNA deubiquitylation between them in a strand-specific manner at stalled replication forks [170].

Challenging DNA structures: RNA-DNA hybrids form when nascent RNA transcripts base pair with the DNA template. The displaced stretches of ssDNA are known as R-loops [144]. These transcriptional by-products contribute to genome instability mainly by colliding with progressing replication forks and inducing replication stress [373, 374]. So far, there is no direct evidence for the resolution of transcription-replication conflicts (TRCs) by DNA damage bypass and PCNA ubiquitylation. Nevertheless, a report showed that RECQ5, a DNA helicase that binds to RNA polymerase II, promotes PCNA ubiquitylation at TRC sites [375]. G-quadruplexes (G4s) are stable DNA secondary structures that consist of multiple stacked guanine quartets. These high order features are usually resolved during replication by Pif1 family helicases; however, unresolved G4 structures elevate replication fork stalling [142]. Most of the G4 resolving helicases associate with replication forks via their interaction with PCNA [208, 376]. Although Pif1 acts downstream of ubiquitylated PCNA [208], the involvement of G4s in inducing PCNA ubiquitylation needs to be investigated further.

Chromatin organisation: The plasticity of chromatin structure and ATP-dependent chromatin remodelers play a significant role in DNA replication and repair. For example, in *S. cerevisiae*, the INO80 chromatin remodelling complex is involved in replication restart and progression of MMS-stalled replication forks [294] but it is not necessary for recovery from UV- or HU-induced replication stress [294, 377]. Rsc2 and its human orthologue BAF180 are chromatin remodellers that enhance PCNA ubiquitylation after UV-, HU-, and MMS-induced DNA damage [377]. Interestingly, BAF180 is also involved in the bypass of UV-induced damage independently of its chromatin remodelling activity [378]. A genome-wide study showed that the repair of MMS-induced alkylated bases by BER happens faster in nucleosome depleted regions, in contrast to the slower repair kinetics at the central dyads of nucleosomes [371]. Interestingly, a more recent study indicated that MMS and UV-induced mutational rates in several species show a periodic pattern that correlates with the orentation of the minor groove of DNA. Such a periodicity may arise from an unequal DNA damage and repair at minor grooves facing towards and away from histones [379].

Nuclear compartmentalisation: Recently, several sub-nuclear repair centres were described intensively, indicating a vital role of nuclear organisation in DNA repair and genome maintenance. For example, persistent DSBs, collapsed replication forks, and eroded telomeres relocate to the nuclear periphery and reside at nuclear pores for efficient recombination [292, 293, 353]. In contrast, stressed replication forks coated by RPA do not relocate to the nuclear periphery, rather they accumulate in postreplicative repair territories (PORTs) [163]. In *S.cerevisiae*, repair of a DSB in the repetitive rDNA by recombination requires the transient relocalisation of the lesion from the nucleolus to the nucleus where the recombination machinery is available [291]. It is unclear whether an analogous mechanism may apply to stressed replication forks in the nucleolus.

I speculate that to improve their chance of survival, cells should avoid template switching in repetitive regions of the genome, like telomeres and rDNA. Avoiding translesion synthesis in the gene body of essential genes may also be another survival advantage. Thus, with the work described in this chapter, I aimed to create and optimise microscopy and genomics approaches based on the Ub-PCNA probes (1) to explore how cells may regulate the choice of DNA damage bypass pathways across the genome and (2)

to analyse if some of the factors mentioned above may be involved in regulating DNA damage bypass. My main goal was to create a genome-wide map of PCNA mono- and polyubiquitylation in a dynamic time-lapse manner.

6.2 Results III

6.2.1 Detection of ubiquitylated PCNA at repetitive elements and R-loops

Having seen that the Ub-PCNA sensors are excellent tools to visualise PCNA ubiquitylation in live cells, I set out to use them in several fluorescently tagged or mutant yeast strains to analyse their localisation at different genomic regions and features, such as telomeres, centromeres, and RNA-DNA hybrids.

First, I wanted to investigate a possible role of PCNA ubiquitylation at telomeres. Rap1 is a protein that binds to yeast telomeric sequences, recruits Rif1 and Rif2 to protect chromosome ends and to regulate telomerase activity [380, 381, 382, 383]. Tagging Rap1 with a fluorescent protein allows the detection of telomeric loci in senescing yeast cells [384]. To detect PCNA ubiquitylation at telomeres, I expressed the GFP tagged Ub-PCNA sensors in a strain carrying Rap1^{mRuby} and analysed the colocalisation between the two proteins after MMS-induced replication stress. Rap1^{mRuby} formed multiple nuclear foci regardless of MMS damage (data not shown), and the percentages of PIP-monoUBD^{GFP} or PIP-polyUBD2^{GFP} foci overlapping with Rap1^{mRuby} were similar (Figure 6.2.1 A-B). The fact that the extent of overlap for the two Ub-PCNA sensors and Rap1^{mRuby} is similar means that either PCNA is equally mono- and polyubiquitylated at telomeres or Rap1^{mRuby} is not the best telomeric marker to be used in this experimental setup because Rap1 functions as a transcriptional regulator as well [380].

Second, I investigated whether PCNA ubiquitylation could be detected at centromeres. The centromeric repeats in yeast are usually detected by fluorescent *in situ* hybridisation (FISH) techniques [385]. However, we lack useful markers to identify centromeres in live cells. Therefore, as an alternative, I fluorescently tagged several centromere associated proteins. Tagging Cse4, a centromeric histone H3 variant [386], with mRuby gave a pan nuclear signal rather than punctate structures (data not shown). Although a subunit of the centromere binding factor [387], Cbf1^{mRuby}, formed detectable foci, they were not bright enough to perform colocalisation image analysis (Figure 6.2.1 C). Thus, I stopped addressing this question any further.

Third, I was interested in exploring whether ubiquitylated PCNA may colocalise with R-loops. The rapidly growing body of research and knowledge about RNA-DNA hybrids and R-loops [144] relies mainly on experiments that employ the S9.6 antibody, which recognises RNA-DNA hybrids [388]. Despite the widespread use of this antibody in various methods, it is not suitable for live-cell imaging. In yeast, most of the RNA-DNA hybrids are resolved by the nucleases, RNase H1 and H2, and the helicase Sen1 [389]. Because antibodies are not suitable for live-cell imaging, I made use of a nuclease-dead point mutant of RNase H1 (*rnh1-D193N*) to visualise R-loops in live cells. This mutant of RNase H1 binds to R-loops without degrading them [390]. As in the case of Ub-PCNA sensors, I used the TET-ON system to control the expression of *rnh1-D193N*^{mRuby} (R-loop sensor). Moreover, to increase the

abundance of R-loops and consequently improve their detection, I deleted the endogenous RNase H1 and H2 enzymes (*rnh1Δ rnh201Δ*). In these cells, the signal of the R-loop sensor was mainly nuclear with a brighter crescent-shaped signal. These brighter regions likely represent the nucleoli, where a higher transcriptional burden of R-loops is expected (Figure 6.2.1 D). Occasionally, bright dots of the R-loop sensor appeared outside of the nucleoli, on the opposite "pole" of nuclei. Because the R-loop sensor did not form any defined foci, as one would have expected, performing colocalisation analysis with the foci of Ub-PCNA sensors would rather be inconclusive. Therefore, I did not continue pursuing this question (Figure 6.2.1 D).

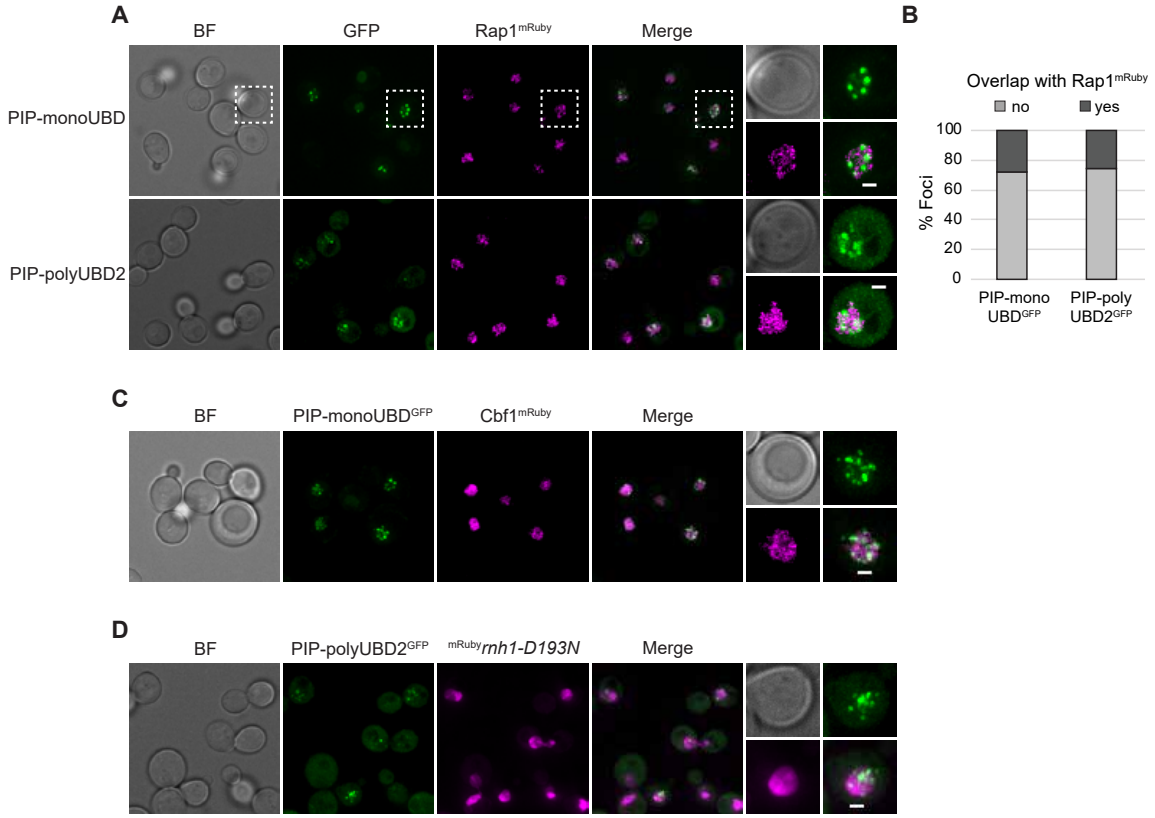

Figure 6.2.1: Microscopy markers to detect PCNA ubiquitylation at different genomic regions. (A) Microscopic images of yeast strains carrying Rap1^{mRuby} and expressing either TET-ON-1xNLS-monoUBD^{GFP} or TET-ON-1xNLS-polyUBD2^{GFP}. Cells were incubated with 2 μg/mL doxycycline and 0.02% MMS, and images were taken after 90 minutes. (B) Colocalisation analysis of the images in A. The percentage of overlap between the sensors and Rap1^{mRuby} is indicated. (C) Microscopic images of yeast strain harbouring Cbf1^{mRuby} and expressing TET-ON-1xNLS-monoUBD^{GFP}. Incubation and imaging conditions were the same as in A. (D) Microscopic images of *rnh1Δ rnh201Δ* strain expressing TET-ON-^{mRuby}*rnh1-D193N* and TET-ON-1xNLS-monoUBD^{GFP}. Incubation and imaging conditions were the same as in A. The scale bars in the magnified pictures equal to 1 μm.

Last, I investigated whether ubiquitylated PCNA may localise at G-quadrulexes. In order to address this question, I expressed the Ub-PCNA sensors in *pif1Δ* cells; however, I could not detect any apparent foci formation in unchallenged *pif1Δ* cells (data not shown). These results indicate that either PCNA ubiquitylation is not involved in resolving G4 structures or that the microscopy approach is not optimal and needs further adjustments, such as using chemicals (e.g. Telomestatin) that stabilises G4s.

Having seen the shortcomings and restrictions of the microscopy approach to gain a global view of PCNA ubiquitylation along the genome, I decided to tackle this question in an alternative genomics approach .

6.2.2 Experimental design to use the Ub-PCNA probes in chromatin immunoprecipitation (ChIP)

The association of proteins with a moving replication fork can be examined by chromatin immunoprecipitation coupled to quantitative PCR (ChIP-qPCR) [391, 392]. Given that the Ub-PCNA sensors selectively marked the sites of ubiquitylated PCNA (see chapter 4), I expected that they could serve as tools to detect where in the genome, the two different modes of DNA damage bypass occur. Such an analysis is carried out by: (1) collecting chromatin samples at different time points after releasing G1 synchronised cells into S phase, (2) crosslinking proteins to DNA by formaldehyde, (3) immunoprecipitating the tagged probes/sensors, and (4) analysing the enrichment of PCNA mono- and polyubiquitylation at genomic loci of interest, such as early and late replicating origins, by qPCR. In addition, the genome-wide localisation of these probes could be analysed by next-generation sequencing (NGS). Analysis of replication fork dynamics by ChIP in yeast generally involves releasing G1-synchronised cells into HU-containing media to slow down S phase, making it easier to capture fork-associated proteins [392]. By using this technique and immunoprecipitating PCNA with a polyclonal antibody, I could recapitulate previously reported results [176]. PCNA was enriched at the early replication origin ARS607 after 20 minutes of cells being released into S phase. At the later time points, PCNA levels dropped, indicating that replication forks moved away from ARS607 (Figure 6.2.2 A-B). In subsection (4.2.3.7), I showed that exposure to HU induced preferentially PCNA monoubiquitylation, rather than PCNA polyubiquitylation. To avoid any lesion dependent bias in the genome-wide analysis, I repeated the ChIP-qPCR protocol by releasing the synchronised cultures into MMS rather than HU. MMS also slows down the progression of replication forks and activates the DNA damage checkpoint response [393, 394]. The efficiency of ChIP was checked by several quality controls at different steps of the protocol, like the immunoprecipitation efficiency of PCNA and the size of DNA fragments used for qPCR (Figure 6.2.2 D-E). Unlike what I observed for HU-treated cells, when cells were replicated in the presence of MMS, PCNA peaked at ARS607 at 20 minutes but remained high also in the later time points (Figure 6.2.2 C). It is worth to mention that cells progressed through S phase more quickly when grown in the presence of MMS than they did when grown in HU, as determined by the cell cycle profiles of the relevant cultures (Figure 6.2.2 B-C). Having seen that PCNA can be captured at replication forks by releasing cells into MMS, I decided to use this alternative experimental setup to create an unbiased map of PCNA mono- and polyubiquitylation along the genome.

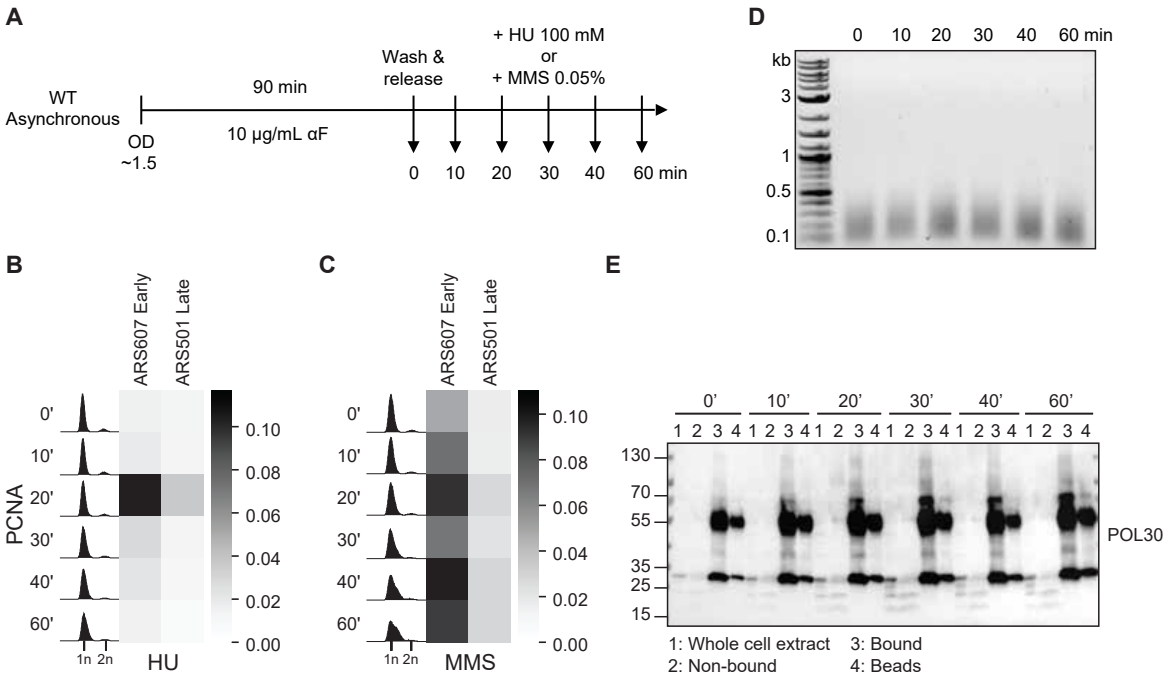

Figure 6.2.2: Setting the stage for Ub-PCNA probes in ChIP. (A) Experimental scheme. Cells were arrested in G1 phase with α-factor for 90 minutes, then washed and released into the cell cycle in the presence of 100 mM HU or 0.05% MMS. Samples for ChIP were collected at the indicated time points. (B-C) The ChIP-qPCR results of PCNA are shown as heatmaps. Cultures were released in HU (B) or MMS (C). Enrichment of PCNA on the chromatin was analysed at an early (ARS607) or late (ARS501) replicating origins. The cell cycle profiles of the cultures are represented on the left side of the heatmaps. (D) Before the qPCR step, the purified DNA samples were run on 1% agarose gel to check for the fragmentation efficiency. Majority of the DNA fragments were within the optimal range of 100-500 bp. (E) The different fractions of ChIP were analysed by SDS-PAGE and blotting for PCNA. Because PCNA runs at the same size as the light chain of the antibody, a heavy chain specific secondary antibody was used to detect PCNA (~29 kDa).

6.2.3 ChIP of ubiquitylated PCNA by *in vivo* expressed Ub-PCNA probes

6.2.3.1 Overexpressed Ub-PCNA probes accumulate at early replicating origins

To capture sufficient amounts of ubiquitylated PCNA at stressed replication forks, I decided to overexpress the Ub-PCNA probes and performed ChIP as described above (see subsection 6.2.2). I used WT yeast strains that constitutively express either 1xNLS-PIP-monoUBD^{VSV} or 1xNLS-PIP-polyUBD1^{VSV} from a multicopy plasmid. The probes were immunoprecipitated using a VSV antibody. To correlate between the enrichments of modified and unmodified PCNA, I performed ChIP of total PCNA in parallel. In WT yeast strains and under MMS damage conditions, both PIP-monoUBD and PIP-polyUBD1 showed enrichment at the early replicating origin, ARS607, at 30 and 60 minutes, whereas their enrichments were negligible at a later origin of replication (ARS501), or an origin-independent control (*ACT1*) (Figure 6.2.3 A). The enrichment profiles of PCNA and ubiquitylated PCNA were very similar (Figure 6.2.3 A). To confirm that the accumulation of the probes at the early origin corresponds to ubiquitylated PCNA, I performed ChIP of PCNA and the probes in *rad18Δ* mutant. Surprisingly, in *rad18Δ* cells, I detected a similar enrichment profile to the WT strains, in which the probes accumulated close to the early origin at 30 and 60 minutes. The unspecific signal detected in *rad18Δ* cells could be a consequence of the high abundance of the probes by their overexpression.

6.2.3.2 Inducible Ub-PCNA sensors are recruited to stalled replication forks

To circumvent the shortcomings of overexpressing the probes in the ChIP experiments (Subsection 6.2.3.1) and the growth defects detected under chronic MMS conditions (Subsection 4.2.2.3), I placed the probes under the control of the TET-ON inducible expression system. This system allowed a tight control over the probes to act as sensors. In these experiments, the expression of the sensors was turned on during the synchronisation period. Then, the cultures were released into S phase in the presence of MMS and the sensors. The rest of the experimental setup was unchanged. Similar to the previous results, immunoprecipitation of the inducible sensors in WT cells showed time-dependent enrichment at the early origin ARS607, which correlated well with the pattern observed for PCNA (Figure 6.2.4 A). Surprisingly, using the TET-ON sensors did not eliminate their Ub-PCNA independent accumulation at ARS607 in *rad18Δ* cells (Figure 6.2.4 B). In chapter 4, I demonstrated that overexpression of the probes unexpectedly rescued the MMS sensitivity of *rad18Δ* cells (Subsection 4.2.2.3). Moreover, I tested the specificity of the sensors and how well they formed foci in different bypass mutants but not in *rad18Δ* cells. Therefore, to check for any off-target binding, I analysed foci formation of the GFP-tagged Ub-PCNA sensors in *rad18Δ* cells. In comparison to WT cells, there were not any detectable foci in *rad18Δ* cells at two different MMS doses (0.02 and 0.05%). These observations indicated that in the absence of crosslinking, the sensors did not bind unspecifically to chromatin in *rad18Δ* cells (data not shown).

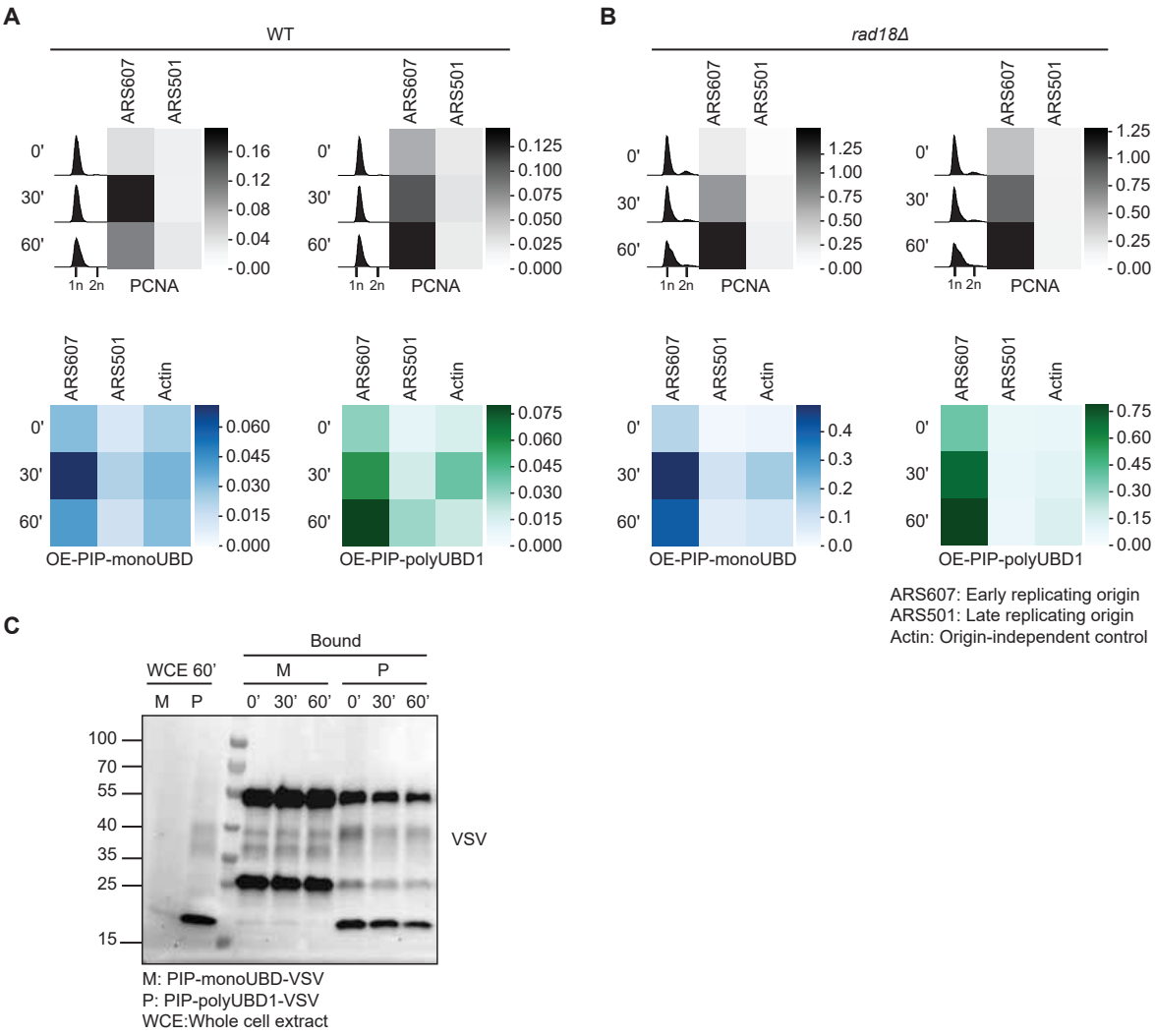

Figure 6.2.3: ChIP of overexpressed Ub-PCNA probes in wild type and *rad18Δ* cells. (A) The ChIP-qPCR results of PCNA, *pADH1*-1xNLS-monoUBD^{VSV}, and *pADH1*-1xNLS-polyUBD1^{VSV} in WT strains are shown as heatmaps. Cells were synchronised in G1 phase with α-factor for 90 minutes then washed and released into 0.05% MMS. Enrichment of PCNA and the probes on the chromatin was analysed at an early (ARS607) and late (ARS501) replicating origins as well as at an origin-independent control, actin (*ACT1*). The cell cycle profiles of the cultures are represented on the left side of the heatmaps. (B) Same as in A for ChIP-qPCR in *rad18Δ* cells. (E) The different ChIP fractions of the probes were analysed by SDS-PAGE and blotting for VSV. The probes' specific bands are ~18 kDa.

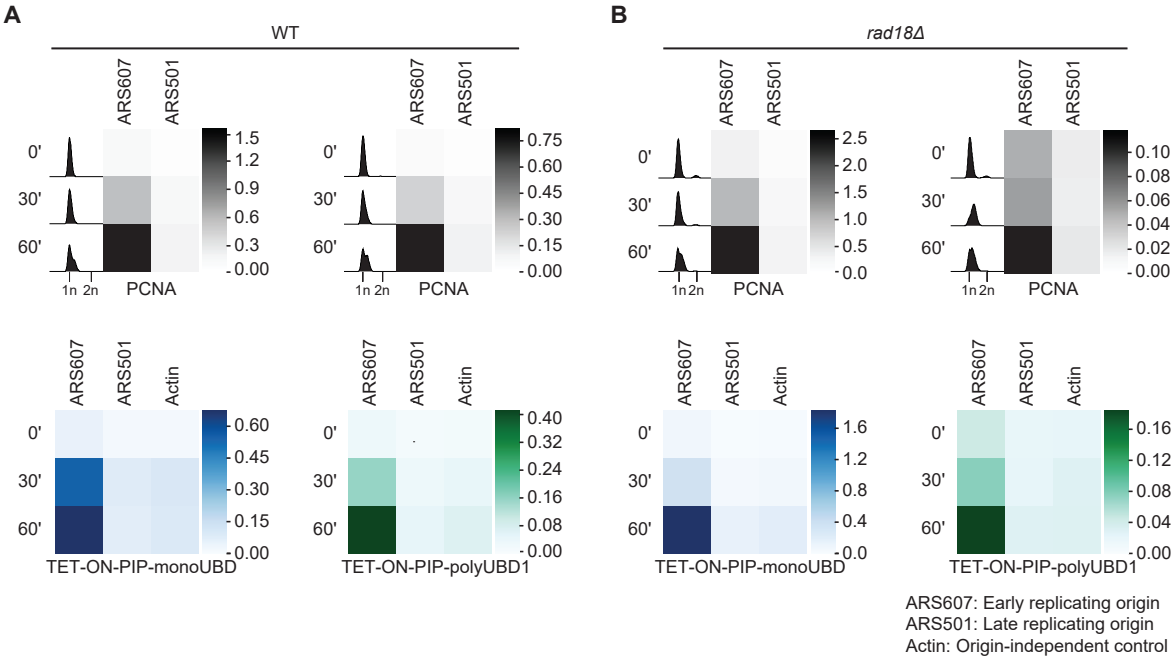

Figure 6.2.4: ChIP of inducible Ub-PCNA sensors in wild type and *rad18Δ* cells. (A) The ChIP-qPCR results of PCNA, TET-ON-1xNLS-PIP-monoUBD^{VSV}, and TET-ON-1xNLS-PIP-polyUBD1^{VSV} in WT cells are shown as heatmaps. Cells were synchronised in G1 phase with α-factor, and the expression of the sensors was induced by addition of 2 μg/mL doxycycline for 90 minutes. Cells then were washed and released into media containing 2 μg/mL doxycycline and 0.05% MMS. Enrichment of PCNA and the sensors on the chromatin was analysed at an early (ARS607) or late (ARS501) replicating origins as well as at an origin-independent control, actin (*ACT1*). The cell cycle profiles of the cultures are represented on the left side of the heatmaps. (B) Same as in A for ChIP-qPCR in *rad18Δ* cells.

To avoid any possible off-target effects of the TET-ON sensors in *rad18Δ* cells, I decided to use *ubc13Δ* strain for the ChIP-qPCR experiments. By performing parallel ChIP experiments in WT and *ubc13Δ* strains using the TET-ON sensors, I detected a similar enrichment pattern of PIP-monoUBD and PIP-polyUBD1 in both WT and *ubc13Δ* cells (Figure 6.2.5 A-B). This was also the case in *rad18Δ* cells (Figure 6.2.4 A-B). These results suggest that the Ub-PCNA probes/sensors may recognise other ubiquitylated proteins at stalled replication forks, possibly due to crosslinking by formaldehyde. It is also possible that the weak affinity of the PIP box is enough to bring the probes close to PCNA, leading to the ubiquitin-independent enrichment of the probes on chromatin.

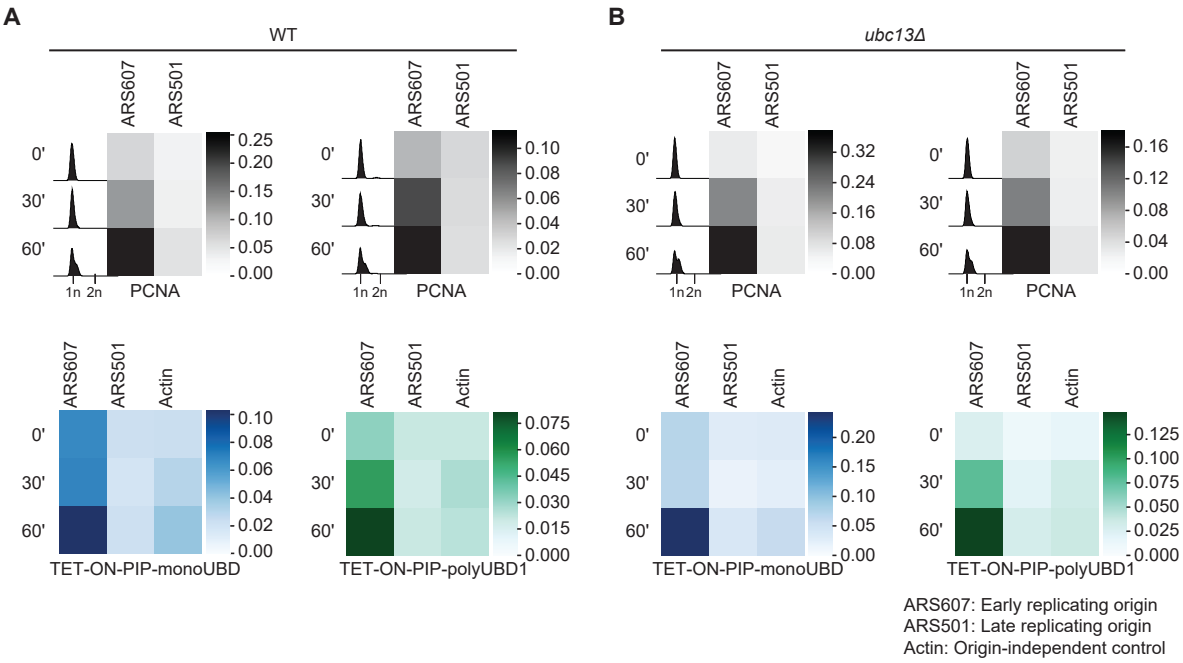

Figure 6.2.5: ChIP of inducible Ub-PCNA sensors in wild type and *ubc13Δ* cells. (A) The ChIP-qPCR results of PCNA, TET-ON-1xNLS-PIP-monoUBD^{VSV}, and TET-ON-1xNLS-PIP-polyUBD1^{VSV} in WT cells are shown as heatmaps. Cells were synchronised in G1 phase with α-factor, and the expression of the sensors was induced by addition of 2 μg/mL doxycycline for 90 minutes. Cells then were washed and released into media containing 2 μg/mL doxycycline and 0.05% MMS. Enrichment of PCNA and the sensors on the chromatin was analysed at an early (ARS607) or late (ARS501) replicating origins as well as at an origin-independent control, actin (*ACT1*). The cell cycle profiles of the cultures are represented on the left side of the heatmaps. (B) Same as in A for ChIP-qPCR in *ubc13Δ* cells.

6.2.3.3 The unspecific enrichment of the Ub-PCNA probes/sensors on chromatin arise mainly from their UBDs

To explore which domains may be responsible for the Ub-PCNA independent accumulation of the probes/sensors at stalled early replication origins, I carried out ChIP experiments using the constituent domains of the Ub-PCNA sensors (i.e. PIP, monoUBD, and polyUBD1). These constructs were constitutively expressed and tagged with VSV. Similar to the previous experiment, I performed ChIP of PCNA in parallel. All the tested single domains were enriched at the early ARS607 when cells entered S phase in a similar pattern observed for PCNA (Figure 6.2.6 A). Although the enrichment values of PIP and monoUBD (Figure 6.2.6 A) were lower than the values of the full-length probes (Figure 6.2.3 A), polyUBD1 showed a reasonable signal (Figure 6.2.6 A). Moreover, a side-to-side comparison of each domain at ARS607 revealed that polyUBD1 is the domain with the highest stickiness (Figure 6.2.6 B). These observations indicate that the unspecific accumulation of Ub-PCNA probes/sensors on damaged chromatin is caused largely by their UBDs.

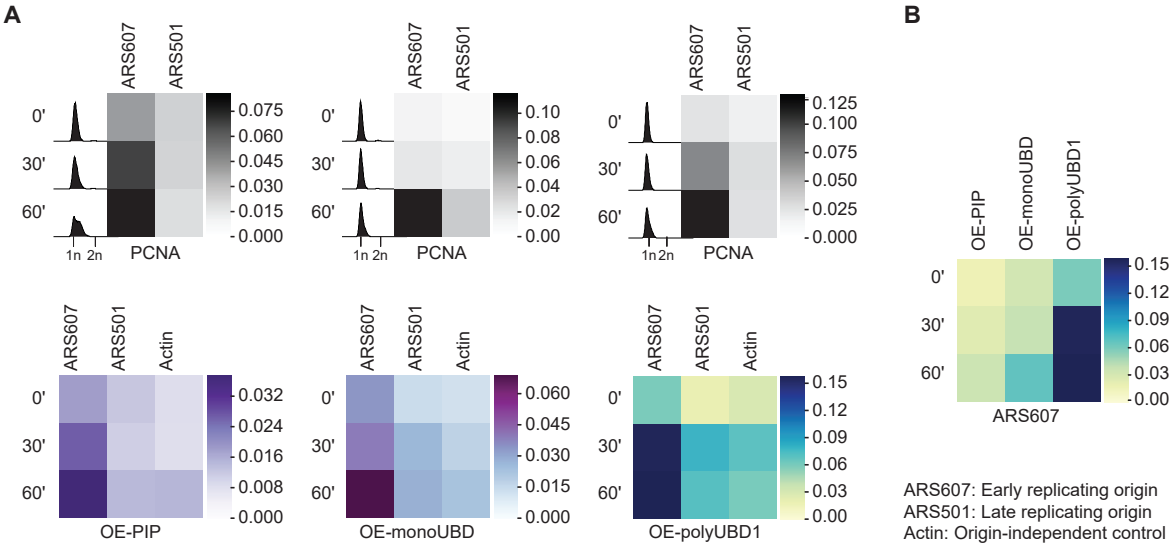

Figure 6.2.6: ChIP of overexpressed single domains in wild type cells. (A) The ChIP-qPCR results of PCNA, *pADH1*-1xNLS-PIP^{VSV}, *pADH1*-1xNLS-monoUBD^{VSV}, and *pADH1*-1xNLS-polyUBD1^{VSV} in WT cells are shown as heatmaps. Cells were synchronised in G1 phase with α-factor for 90 minutes. Cells then were washed and released into media containing 0.05% MMS. Enrichment of PCNA and the single domains on the chromatin was analysed at an early (ARS607) or late (ARS501) replicating origins as well as at an origin-independent control, actin (*ACT1*). The cell cycle profiles of the cultures are represented on the left side of the heatmaps. (B) Side-to-side comparison of the single domains and their enrichment at the early ARS607.

6.2.3.4 The low-affinity Ub-PCNA sensor is recruited to stalled replication forks

In the previous subsection 6.2.3.3, I showed that the UBDs caused accumulation of the Ub-PCNA probes/sensors at stalled replication forks in a manner independent of PCNA ubiquitylation. Therefore, I made use of the low-affinity probe, PIP-polyUBD3 (Table 3.2.1), expecting that its lower affinity would reduce the unspecific signal in the ChIP experiments. To analyse the enrichment of this low-affinity probe at origins under replication stress conditions, I preformed ChIP of both constitutively and inducibly expressed 1xNLS-PIP-polyUBD3^{VSV} in WT and *ubc13Δ* cells. The over- and inducibly expressed PIP-polyUBD3 were both enriched at the early origin ARS607 in a time-dependent manner (Figure 6.2.7 A). Like WT cells, *ubc13Δ* cells showed enrichment of the low-affinity probe/sensor at the early replicating origin (Figure 6.2.7 B). These observations indicate that in addition to the affinity of the UBDs, other constituents also contribute to the accumulation of the Ub-PCNA probes/sensors at stalled replication forks in a Ub-PCNA-independent manner.

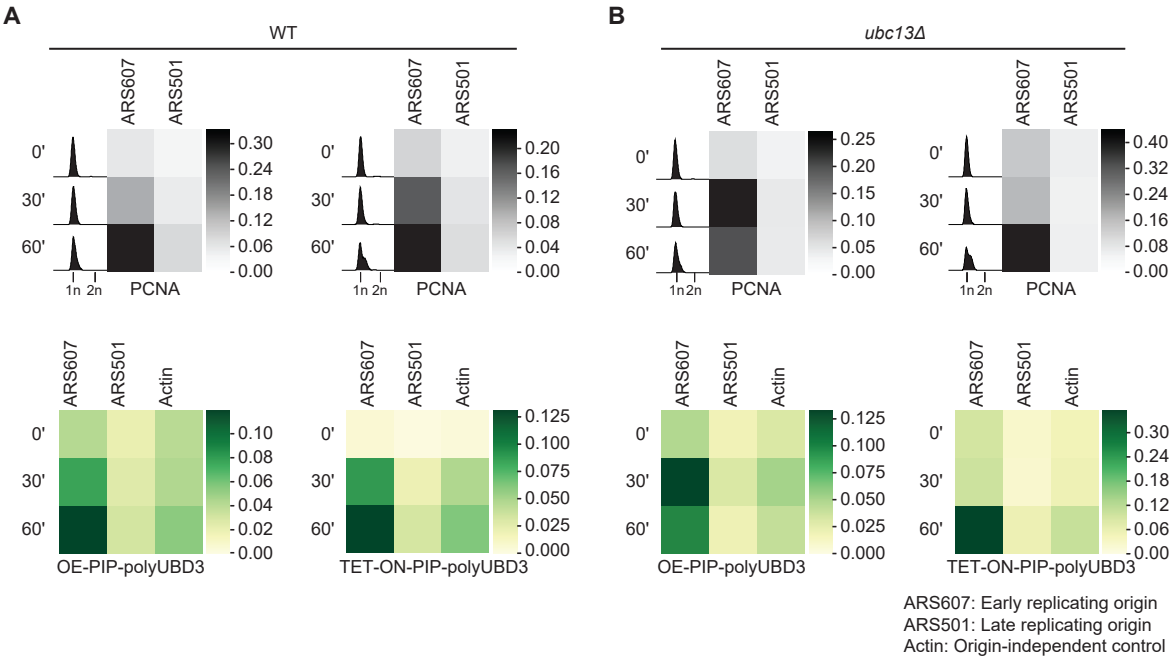

Figure 6.2.7: ChIP of low-affinity Ub-PCNA sensor in wild type and *ubc13Δ* cells. (A) The ChIP-qPCR results of PCNA, *pADH1*-1xNLS-PIP-polyUBD3^{VSV}, and TET-ON-1xNLS-PIP-polyUBD3^{VSV} in WT cells are shown as heatmaps. Cells were synchronised in G1 phase with α-factor, and the expression of the probe/sensor was wither constitutive or induced by addition of 2 μg/mL doxycycline for 90 minutes. Cells then were washed and released into media containing 0.05% MMS and with or without 2 μg/mL doxycycline. Enrichment of PCNA and the probe/sensor on the chromatin was analysed at an early (ARS607) or late (ARS501) replicating origins as well as at an origin-independent control, actin (*ACT1*). The cell cycle profiles of the cultures are represented on the left side of the heatmaps. (B) Same as in A for ChIP-qPCR in *ubc13Δ* cells.

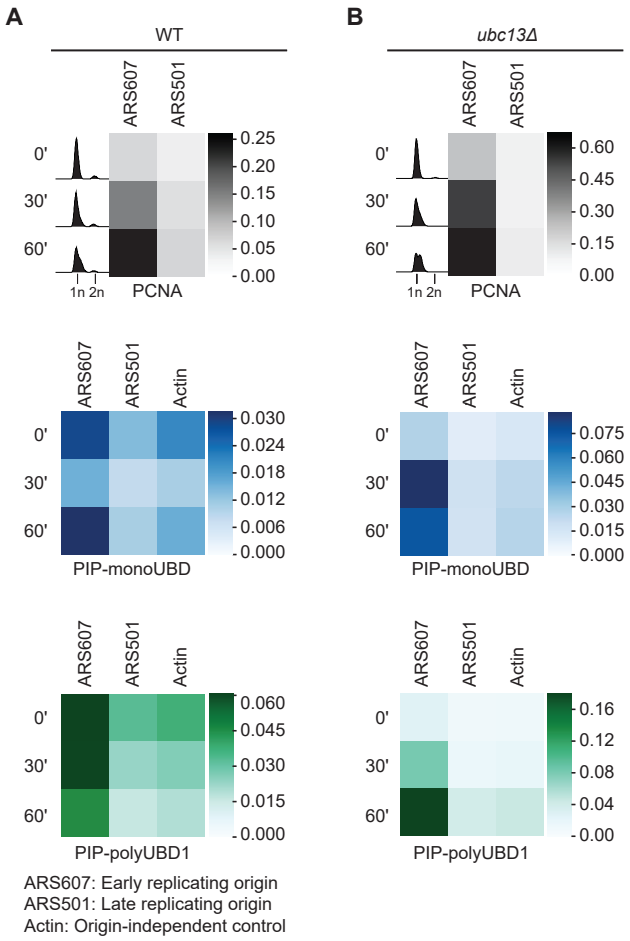

Figure 6.2.8: ChIP of purified Ub-PCNA probes in wild type and *ubc13Δ* cells. (A) The ChIP-qPCR results of PCNA, ^{Flag}PIP-monoUBD, and ^{Flag}PIP-polyUBD1 in WT cells are shown as heatmaps. Cells were synchronised in G1 phase with α-factor, for 90 minutes then washed and released into media containing 0.05% MMS. The purified Flag-tagged probes were used as affinity reagents in immunoprecipitations. Enrichment of PCNA and the probes on the chromatin was analysed at an early (ARS607) or late (ARS501) replicating origins as well as at an origin-independent control, actin (*ACT1*). The cell cycle profiles of the cultures are represented on the left side of the heatmaps. (B) Same as in A for ChIP-qPCR in *ubc13Δ* cells.

6.2.4 Purified Ub-PCNA probes as affinity reagents for ChIP of ubiquitylated PCNA

To exclude the possibility that the unspecific accumulation of the Ub-PCNA probes/sensors on the chromatin may arise from the formaldehyde crosslinking step in the ChIP procedure, I collected samples from WT and *ubc13Δ* cells and carried out the crosslinking step in the absence of the probes. Then, ubiquitylated PCNA was immunoprecipitated from the cell lysates using the Flag-tagged purified probes as affinity reagents (Subsection 4.2.1). The rest of the experimental setup was unchanged. In WT cells, the enrichment of the probes at the early ARS607 appeared to be random, independent of time, and very low compared to the PCNA ChIP signals (Figure 6.2.8 A). Interestingly, in *ubc13Δ* cells, ^{Flag}PIP-polyUBD1 showed a time-dependent enrichment at ARS607 (Figure 6.2.8 B) similar to the inducibly

expressed conditions (Figure 6.2.5 B). In contrast, no significant enrichment over the background was observed for ^{Flag}PIP-monoUBD (Figure 6.2.8 B). These results and the ones from the previous subsections suggest that the crosslinking step may mask or expose ubiquitin surfaces in the vicinity of stalled replication forks, which in turn might be recognised by the Ub-PCNA probes.

6.3 Epilogue and discussion III

Apart from the local factors that may play a role in the bypass choice, several other global factors could contribute to channelling damage bypass to one of its modes. For example, R-loops and G-quadruplexes are DNA secondary structures abundant at repetitive elements, like telomeres, centromeres, and rDNA. These structures challenge replisomes and elevate replication stress [364, 365, 367]. Nucleotide and base excision repair (NER and BER) resolve damaged bases before these lesions collide with the replication machinery; however, NER and BER have a biased repair efficiency. NER is more active on the transcribed strands, whereas BER of lesions in nucleosome depleted regions is faster than in histone packed heterochromatin [370, 379, 371, 372]. Moreover, replisomes on leading and lagging strands are equipped with different accessory proteins that may affect the bypass choice [170]. With the experiments described in this chapter, I tried to gain a global view and study a possible contribution of some of the factors mentioned above in modulating PCNA ubiquitylation and consequently involving in the choice of damage bypass.

6.3.1 Capturing PCNA ubiquitylation with replication troublemakers

To detect the accumulation of ubiquitylated PCNA at different genomic features and loci, I created microscopy-based systems to visualise telomeres, centromeres, and R-loops. However, it was not possible to determine whether any of these structures colocalised with ubiquitylated PCNA because each system had a shortcoming, such as background signal or undefined patterns (Figure 6.2.1). Therefore, I established an alternative genomics approach to gain a genome-wide view of PCNA ubiquitylation.

6.3.2 Shortcomings of the Ub-PCNA probes for genome-wide association analysis

In a complementary approach, using the Ub-PCNA probes, I aimed to determine the locus-specific and genome-wide distribution of mono- and polyubiquitylated PCNA. I analysed the enrichment of unmodified and modified PCNA at early and late replicating origins when cells were grown in the presence of MMS to induce replication stress. In PCNA ubiquitylation proficient (WT) and deficient strains (*rad18Δ* and *ubc13Δ*), the constitutively and inducibly expressed Ub-PCNA probes/sensor were equally enriched at an early replicating origin. These observations suggest that the probes/sensors are recruited to stalled replication forks in a Ub-PCNA-independent manner (Figures 6.2.3 and 6.2.5). Interestingly, the UBDs of the Ub-PCNA probes likely were the underlying cause of the unspecific signal (Figure 6.2.6). One of the low-affinity Ub-PCNA probes did not abolish this unspecific signal (Figure 6.2.7) suggesting the contribution of other factors in the stickiness of the probes. To examine if crosslinking could negatively affect the sensors expressed *in vivo*, the purified probes were used as affinity reagents after the crosslinking step. Under these experimental conditions, I still observed unspecific enrichment of the probes at an early origin detected in *ubc13Δ* cells. These observations indicate a

possible role of the crosslinking step in altering the specificity of the Ub-PCNA probes.
It would be interesting to investigate if this unspecific enrichment of the probes depends on K63 ubiquitin chains or not. This could be done by performing ChIP experiments in Ub-K63R yeast strain. On the one hand, if the unspecific signal is Ub-K63 dependent, it is worth to identify the modified target that accumulates at stalled replication forks because such substrates are poorly studied in yeast. On the other hand, if the background signal is Ub-K63 independent, it is better to further optimise the affinity of the UBDs to K63-linked ubiquitin chains.

6.3.3 Converting the Ub-PCNA probes into alternative genomics tools

Enrichment of the Ub-PCNA probes at stalled replication forks independently of ubiquitylated PCNA could possibly suggest that after crosslinking the probes bind to other ubiquitylated factors at stressed forks. Therefore, the Ub-PCNA probes may not be suitable for conventional ChIP-qPCR or ChIP-Seq experiments. However, this does not mean that creating a genome-wide map of ubiquitylated PCNA is impossible. There are several other methods to study the genome-wide association of proteins with chromatin.
One such alternative approach is DamID profiling of protein-DNA interactions. Briefly, in DamID profiling, a protein of interest is fused to DNA adenine methyltransferase (Dam) from *E.coli* that adds methyl groups to the N6 position of adenines in the sequence GATC [395]. Then the genomic DNA is extracted and digested with the methylation-sensitive restriction enzyme DpnI. Finally, the DNA fragments are ligated to sequencing adapters and sequenced by next-generation sequencing (NGS) platforms [396]. Similarly, Ub-PCNA probes can be fused to Dam and the genomic distribution of PCNA mono- and polyubiquitylation could be analysed by DamID profiling. Because MMS itself adds methyl groups on adenines and guanines [123], this approach requires careful optimisation and performing several control experiments in parallel. Besides, the resolution of DamID is limited by the distribution of GATC sites.
CUT&RUN is another alternative genomics method without a crosslinking step. It is an antibody-targeted system that cleaves protein-DNA complexes in a controlled manner. In a nutshell, a primary antibody recognises a chromatin-bound protein of interest via a tag. Then, Protein A coupled to micrococcal nuclease (MNase) cleaves the protein-DNA complex, where the addition of calcium controls the activity of MNase. In the final step, libraries of the DNA fragments are prepared and sequenced by NGS [397]. This method was best optimised for transcription factors that usually binds tightly to DNA. To use the Ub-PCNA probes in CUT&RUN setup, additional optimisations are required because the interaction of ubiquitylated PCNA with DNA is not as strong as transcription factors and the ubiquitin chains are subjected to cleavage by DUBs.

Chapter 7

Genetic screens to identify readers of polyubiquitylated PCNA

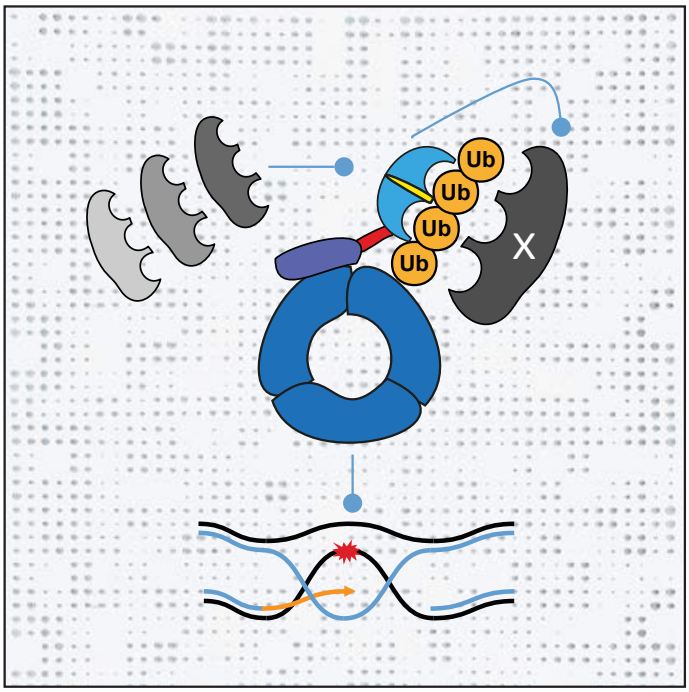

In a nutshell

This chapter aims to discover yet unknown interactors of polyubiquitylated PCNA using the Ub-PCNA probes in genetic screens. These screens rely on the inhibitory effects of PIP-polyUBD1 to find factors that could compete with the probe by selectively binding to K63-linked ubiquitin chains on PCNA.

Highlights

- A novel genetic overexpression screen is carried out to identify receptors of polyubiquitylated PCNA
- Additivity and MMS sensitivity screens are performed to categorise the candidates
- Extensive genetic characterisation reveals many false-positive candidates
- Rad5's ligase function competes with PIP-polyUBD1

7.1 Prologue IV

Initiation of the error-prone translesion synthesis (TLS) by PCNA monoubiquitylation and the downstream repair processes are well-characterised. In spite of the fact that K63-linked polyubiquitin chains on PCNA activate the error-free branch of damage bypass, we lack reliable evidence about the molecular details of template switching and the factors that bind preferentially to polyubiquitylated PCNA. Here, I will briefly touch upon some of the contradicting scenarios and factors that have been suggested to act downstream of PCNA polyubiquitylation.

Proteasomal degradation: Despite the well-known function of K48-linked and to some degree K63-linked ubiquitin chains in triggering proteasomal degradation [36, 398], polyubiquitylation of PCNA with K63-linked chains do not target the replication clamp for degradation. Instead, these ubiquitin chains decrease the mutagenic effects of TLS [399, 400], suggesting the involvement of K63-linked polyubiquitin chains on PCNA in triggering error-free damage bypass.

Promotion of TLS: Several studies reported an impact of PCNA polyubiquitylation factors in regulating the activity of the error-prone TLS. This TLS-promoting action depends mainly on the multi-functional protein Rad5 and its human homologues (HLTF and SHPRH). On the one hand, Rad5, independent of its ubiquitin ligase function, engages in and promotes TLS via direct physical interaction with Rev1 to repair abasic sites and (6-4 TT) photoproducts [263, 264, 401, 265]. More recently, Grant Brown's lab showed that Rad5 forms nuclear foci in unperturbed S-phase cells, travels with replication forks under mild replication stress conditions, and recruits TLS polymerases to replication forks even in the absence of base lesions, thereby promoting the repair of ssDNA gaps [**?**]. On the other hand, TLS-promoting roles of K63-linked ubiquitin chains on PCNA were also reported. TLS polymerases interact preferentially with monoubiquitylated PCNA via their UBDs. Interestingly, some TLS polymerases contain multiple UBDs allowing them to bind to polyubiquitylated PCNA as well. For example, Pol η has only one UBD, whereas Pol ι and Pol κ have two UBDs [80]. There is evidence that Pol κ binds preferentially to polyubiquitylated PCNA after MMS-induced damage, thereby displacing Pol η that is more suited for the repair of UV-induced damage [254]. Using a plasmid-based mutagenesis reporter assay in *S.pombe*, Coulon *et al*., 2010 showed that TLS of UV lesions requires factors needed for PCNA polyubiquitylation, indicating a role for K63-linked ubiquitin chains on PCNA in recruiting several TLS polymerases via their UBDs [223]. Despite all these findings about PCNA polyubiquitylation in promoting TLS, there is clear evidence of synergy between *tlsΔ* and *mms2Δ*, *ubc13Δ*, and *rad5Δ* mutants [216, 306, 315], suggesting an additional TLS-independent function of K63-linked ubiquitin chains on PCNA.

Inhibition of TLS: Another proposed role of polyubiquitin chains on PCNA is the inhibition of TLS polymerases, thereby activation of the error-free template switching. In an *in vitro* study, chemically produced ubiquitylated PCNA was used to analyse the effect of PCNA polyubiquitylation on the action of TLS polymerases. This analysis revealed that with increasing ubiquitin chain length, Pol η binds more tightly to PCNA; however, it shows reduced TLS activity pass abasic sites because the distal ubiquitin moieties trap the TLS polymerase in a non-productive state [402]. Similarly, based on evidence from mammalian cultures, few labs suggested that the enhanced binding of Pol ι and Pol

η to polyubiquitylated PCNA might dissociate the TLS polymerases from the stalled primer terminus either by cleaving the polymerase-bound ubiquitin chains or trapping the polymerases in an unproductive mode [403, 399]. In contrast, using genetically engineered mimics of polyubiquitylated PCNA our lab has recently shown that K63-chain assembled on a permanent ubiquitin-PCNA fusion can trigger template switching independently of TLS polymerases [104], suggesting that PCNA polyubiquitylation has a fundamental function other than acting against or in the favour of TLS polymerases.

Readers of K63-polyubiquitylated PCNA and activators of template switching: Based on substantial genetic and biochemical evidence, the most coherent function of K63-linked polyubiquitin chains on PCNA is the recruitment of a linkage-selective receptor of polyubiquitylated PCNA that initiates template switching. Such a receptor portion would ideally carry one or multiple UBDs and a PCNA recognition sequence. A cohort of factors has been reported to contribute directly or indirectly in template switching [340, 207, 194]. For example, the ATPase Mgs1 involves in damage bypass in multiple ways [404]. Yet, Mgs1 shows affinity to mono- and K63-linked polyubiquitylated PCNA as well as to PCNA with linear ubiquitin chain fusions [405, 104]. Likewise, in higher eukaryotes, the ATPase ZRANB3 is implicated in error-free damage bypass through an affinity to polyubiquitylated PCNA. ZRANB3 is proposed to protect stalled replication forks by promoting fork reversal. However, ZRANB3 lacks a *bona fide* yeast homologue [221, 83]. The damage bypass pathways are highly conserved from budding yeast to human [406]. Therefore, it is unlikely that the downstream factors have evolved very differently. An alternative model that would not require a UBD containing receptor postulated that K63-linked polyubiquitin chains directly interact with DNA and activate template switching [407].

Several other factors are implicated in the promotion and resolution of template switching intermediates. These factors include the 9-1-1 checkpoint clamp; the PCNA unloader Elg1 and RFC complex; the replicative polymerase δ; strand invasion and homologous recombination proteins Rad51, Rad52, Rad55, Rad57, and the Shu complex; helicases Sgs1 and Mph1; resolvases Esc2 and Smc5/6 complex; and the DNA bending factor Hmo1 [196, 197, 198, 193, 194]. Recently, our lab has shown that DNA damage bypass operates predominantly in a postreplicative manner and is not restricted to stalled replication forks [204, 163]. Both in yeast and higher eukaryotes, the postreplicative action of damage bypass requires repriming downstream of the damage site, which serves as an initiation point for template switching [205, 201, 206, 202]. Our lab also speculated the involvement of nucleases and helicases in some steps of template switching. Deletion of the nuclease Exo1 and the helicase Pif1 sharply reduce the damage-dependent accumulation of single-stranded regions in newly replicated DNA [208, 204]. Despite their important roles in error-free damage bypass, evidence for the aforementioned factors in directly binding polyubiquitylated PCNA is still lacking.

In a systematic approach using genetically engineered mimics of polyubiquitylated PCNA in bypass mutants, a former member of our lab, Dr Tomio Takahashi, identified the critical properties of polyubiquitin chains on PCNA that are required for the activation of template switching: (1) Linear, non-cleavable polyubiquitin chain mimics fused to PCNA fails to complement the defects in PCNA polyubiquitylation. (2) A K63-polyubiquitin chain at a non-native position on PCNA promotes template switching. (3) A single K63-junction provides an efficient activation of the pathway, (4) Mgs1 and ZRANB3, two known binders of polyubiquitylated PCNA, efficiently interact with the linear mimics [104].

All these findings suggest the existence of a yet unidentified receptor of polyubiquitylated PCNA that triggers template switching. The UBD of this putative receptor must be highly selective for the K63-linkage. Hence, the identification of factors that directly recognise polyubiquitylated PCNA would be a significant milestone in the fields of post-translational modification and DNA repair. Therefore, with the experiments in this chapter, I aimed to identify, validate, and characterise effector receptors of polyubiquitylated PCNA through novel genetic screening approaches.

7.2 Results IV

7.2.1 Finding suppressors of PIP-polyUBD1 via an overexpression genetic screen

In chapter 3 (subsection 4.2.2.3), I showed that overexpression of the PIP-polyUBD probes inhibit template switching and render cells sensitive to DNA damage, likely by competing with factors that would otherwise bind to polyubiquitylated PCNA (Figure 4.2.3). This genetic trick allows tackling the long-standing question of "What is the factor X?". Therefore, I utilised PIP-polyUBD1 in a genome-wide overexpression screen to search for binders of polyubiquitylated PCNA. I expected that such an effector protein would compete with the probe and suppress its DNA damage sensitising effects (Figure 7.2.1 A).

7.2.1.1 Design of the genome-wide overexpression screen

To carry out the genetic screen, I used an overexpression library that consists of around 5000 yeast open reading frames (ORFs) under the control of an inducible galactose (*GAL1*) promoter. The strategy of the high-throughput screen was based on crossing the overexpression library, which had the mating-type a (*MATa*), with an *MAT*α strain overexpressing PIP-polyUBD1. Then, the fitness of the resulting diploid (a/α) cells was compared in quadruples under replication stress and control conditions after activating the overexpression of the library. Any ORF that rescued the probe sensitivity might have been involved in template switching. Each step of the screen is depicted in figure (7.2.1 B). For more details, see (2.11.13.1). To judge if a particular ORF suppressed the effect of the probe, I included two different controls in the library arrays. A neutral control expressed the probe but did not contain any ORF (+probe/-ORF). The colony size of this control represented the sickness under damage conditions, when template switching was compromised. In contrast, the positive control neither expressed the probe nor an ORF (-probe/-ORF). Thus, it reflected the growth under damage conditions when template switching was functional. Hence, an ORF was considered as suppressor if it grew better than the neutral control and equal to or less than the positive control.

7.2.1.2 Optimising the experimental conditions for the genetic screen

Sensitising effects of the probes: To find the most suitable probe for the screen, I overexpressed the three PIP-polyUBD constructs with different affinities (Table 3.2.1) in a WT yeast strain under the control of the constitutively active *ADH1* promoter. PIP-polyUBD1 showed the highest inhibitory effect under MMS-induced damage conditions without affecting the cell growth under control conditions (Figure 4.2.3 A). Therefore, I decided to use this probe for the high-throughput genetic screen.

The specificity of the probe for template switching: In subsection (4.2.2), I showed that the single domains of the probe, i.e. PIP and polyUBD1, were incapable of sensitising cells to MMS treatment (Figure 4.2.3 A). Moreover, the sensitising effect of PIP-polyUBD1 was likely due to specific inhibition of template switching indicated by the epistasis seen with *mms2Δ* and *ubc13Δ* (Figure 4.2.4).

Creating the query strain: I constructed the *MATα* strain by switching the mating type of library's *MATa* strain through transient induction of the HO endonuclease [278]. The resulting *MATα* strain was transformed with *pADH1*-1xNLS-PIP-polyUBD1^{VSV} expressed from an episomal plasmid.

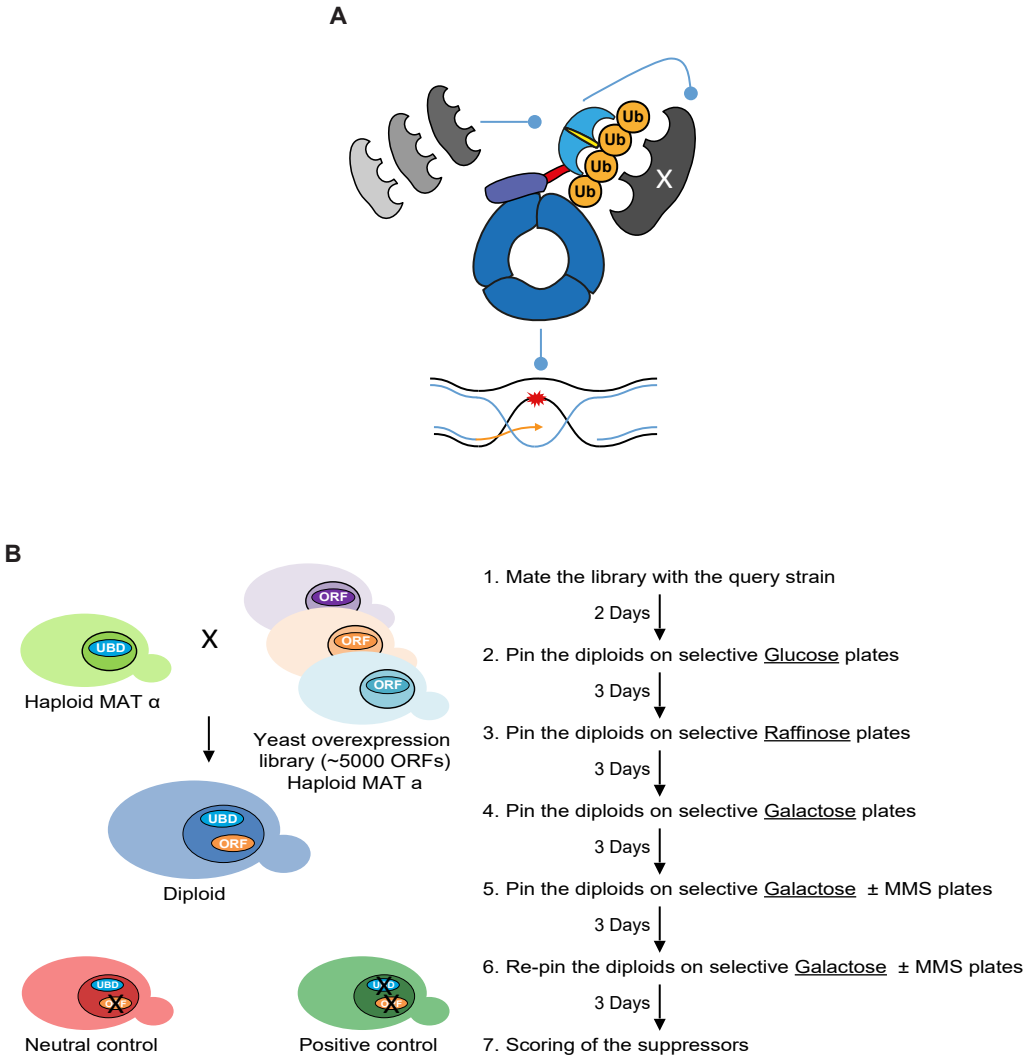

Figure 7.2.1: A genetic overexpression screen to find receptors of polyubiquitylated PCNA. (A) A cartoon of the basic principle behind the genetic screen. (B) A schematic of the overexpression screen. The growth and selection conditions in each step of the screen are indicated. For more details, check the main text (subsection 2.11.13.1).

7.2.1.3 Scoring, thresholding, and identifying suppressors

To analyse the images of the screening plates and identify suppressors of the probe, I utilised a free online tool known as SGAtools [408]. This tool is shaped to study synthetic genetic interactions between single and double gene deletions. Based on the raw colony size that reflects a colony's fitness, this tool scores the growth differences between control and treatment conditions. Moreover, the SGAtools normalises the growth differences between and within different plates taking into consideration the location of each colony on the plate, competition between neighbouring colonies, different batches of plates, and the edge effect of the plates where colonies have more access to nutrients. Overexpression of the library itself caused a great variation in colony size, making the scoring with SGAtools difficult. The filters mentioned above excluded the majority of the colonies from the scoring analysis. Therefore, I used the raw colony size measured by SGAtools in a simple calculation to create a score. I divided each colony size on the MMS plates by the respective colony size on the control plates (Formula 7.2.1), then made an average of the quadruples and used the average value as a score (S) of the fitness (Formula 7.2.2). The scores ranged from 0.0 to 1.95, where the neutral control had a score of (0.72) and the positive control (1.38). It was surprising to see that some scores were lower or higher than the controls themselves. The lower scores could arise when overexpression of a particular ORF made the cells sensitive to MMS. In contrast, the ORFs with higher scores than the positive control conferred resistance to MMS. Scores of the neutral controls varied between different locations on the plates and from one plate to another. To consider these variations and set a threshold, I added the standard deviation of the scores of all the neutral controls (0.17) to the average score of the neutral control (0.72) setting the threshold to (0.89). Any ORF that had an S value equivalent or higher than the calculated threshold was considered as a possible candidate or hit. This cut off identified 229 suppressors as potential candidates for template switching (Figure 7.2.2 B).

$$\chi = \frac{Raw\ colony\ size\ 0.01\%\ MMS}{Raw\ colony\ size\ 0\%\ MMS} \tag{7.2.1}$$

$$S = \overline{\chi} \tag{7.2.2}$$

Interestingly, *RAD5* itself was one of the suppressors with a high score, indicating that the screening approach was reliable and informative. Moreover, several other factors that are involved in DNA repair, like *APN1*, *RAD14*, *RFC5*, *UPF3*, *SMC1*/*SMC3*, and others were also among the suppressors. This might indicate that their overexpression could rescue the MMS sensitivity caused by the probe. Despite using a stringent threshold, the number of the identified suppressors was very high. To narrow down the number of the suppressors and perform additional validation steps, I created a gene list of all the 229 suppressors using the *Saccharomyces* genome database (SGD) and analysed the enrichment of several gene ontology (GO) terms. For example, cellular compartments, biological processes, and functions. Majority of the suppressors were either cytosolic or fell into the categories of the unknown cellular compartment, unknown biological processes, and anonymous functions (Figure 7.2.2 C). Because of the ambiguity of the suppressors, I decided to perform secondary screens to withdraw any false-positive suppressors that were identified in the initial overexpression screen.

7.2.2 Secondary screens: Additivity and MMS sensitivity screens

The overexpression screen identified too many candidates making it difficult to analyse their involvement in template switching systematically. Therefore, I set out to reduce the number of candidates by secondary screens based on the assumption that there are three possible categories, in which a suppressor could rescue the MMS sensitivity caused by overexpression of PIP-polyUBD1.

Category 1: The suppressor binds directly to K63-linked polyubiquitylated PCNA, recruits downstream factors required for the initiation of template switching, and bypass the lesion in a Ub-PCNA dependent manner.

Category 2: The suppressor initiates template switching downstream of K63-linked polyubiquitylated PCNA through recruitment to the lesion sites by an unknown factor. This scenario is also dependent on Ub-PCNA.

Category 3: The suppressor belongs to another repair pathway that compensates and removes the lesions independently of Ub-PCNA.

The unknown factor X that I was looking for would belong to category 1. However, suppressors belonging to category 2 would also be interesting because they might somehow involve in template switching. As long as suppressors from any of the categories repair MMS-caused damage, their deletion may lead to MMS sensitivity. Besides, the removal of suppressors belonging to category 1 and 2 might not cause additional sickness to overexpression of PIP-polyUBD1. Therefore, secondary screens for epistasis or additivity to PIP-polyUBD1 and sensitivity to MMS could pinpoint the candidates and verify the ones that were truly involved in template switching.

7.2.2.1 Design of the secondary screens

To discover any sensitivity or additivity features of the identified suppressors and assign them to the categories mentioned above, I carried out secondary screens. The general scheme of the screens was similar to the initial overexpression screen. The major difference was that I used a yeast knockout library of non-essential genes instead of an overexpression library. In order to deliver the plasmid overexpressing PIP-polyUBD1 or the empty parental vector, I utilised a high-throughput plasmid transfer method known as selective ploidy ablation that relied on a universal donor strain (UDS) [271]. Each step of the screen is depicted in figure (7.2.3). For more details, see (2.11.13.2).

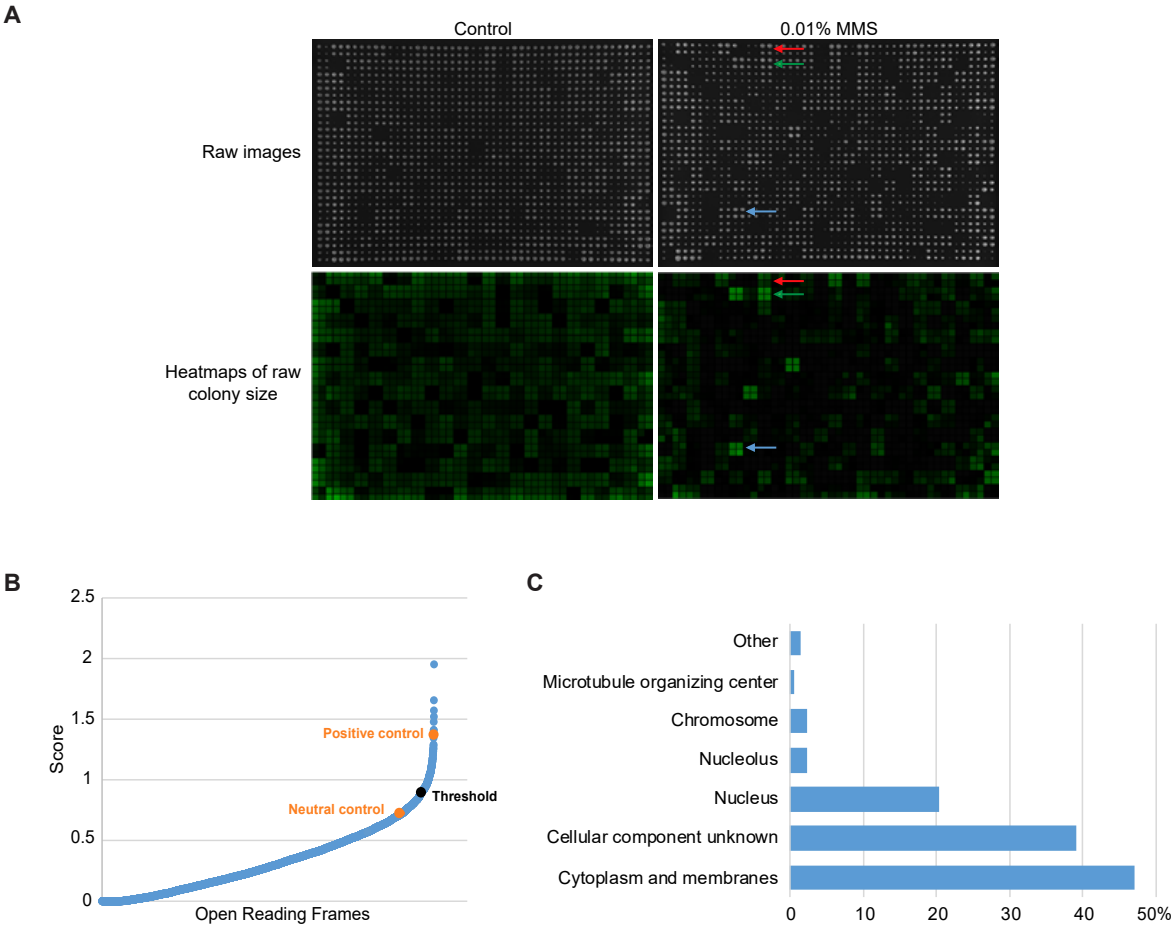

Figure 7.2.2: Outcomes of the overexpression genetic screen. (A) Example of raw images of the screening plates at the finale step. Corresponding heatmaps are shown below each plate. The red arrow indicates a neutral control, the green arrow a positive control, and the blue arrow points to a possible hit (*UPF3*). (B) Score distribution of single ORFs. The scores of the controls are indicated in orange and the threshold in black. (C) Frequency of the GO terms and enrichment analysis of suppressors according to SGD. Some genes are both cytosolic and nuclear, making the total frequency to add up to more than 100%.

7.2.2.2 Scoring, thresholding, and categorising the suppressors

In the MMS sensitivity screen, I crossed the arrayed knockout library with a UDS containing an empty vector and selected for the haploids as mentioned above and in figure (7.2.3). Then, I used the SGAtools, to analyse the images of the plates and score for the fitness. In this screen, the growth variation between the different deletions was minimal, making it possible to use the filters, thresholds, and scoring that are set by the SGAtools. Comparing the fitness of the colonies between plus and minus MMS conditions, allowed me to identify gene deletions that cause MMS sensitivity (Figure 7.2.4 A). This screen identified 232 MMS sensitive deletions out of ~4700 gene deletions, including *rev1Δ*, *ubc13Δ*, and *rad52Δ*. Based on the sensitivity screen, eight out of the 229 suppressor ORFs were sensitive to MMS upon their deletion (Figure 7.2.4 B).

For the additivity screen, the knockout library was mated with a UDS overexpressing 1xNLS-PIP-polyUBD1^{VSV} and selected for the haploids. Then, the fitness of knockouts containing the empty vector was compared to the ones overexpressing the probe under MMS conditions. With this analysis, I discovered gene deletions that caused additional effects to the probe. To validate the additivity screen, I looked for some known genetic interactions with error-free damage bypass. For example, *rev1Δ* and *ubc13Δ* are both sensitive to MMS. Overexpression of the probe made *rev1Δ* cells more sensitive to MMS, whereas *ubc13Δ* did not cause any additional sensitivity, meaning that *ubc13Δ* and the probe were epistatic (Figure 7.2.4 A). Like *ubc13Δ*, majority of the gene deletions in the knockout library did not show any additivity to the probe (Figure 7.2.4 C).

By combining the results of all the three screens, I found eight suppressors that fulfilled the previously mentioned requirements (Figure 7.2.5 A). One of the eight identified suppressors was *RAD5*, which served as an independent internal control in the screens. There were also other DNA repair factors like *RAD14* that is involved in NER and *APN1* in BER, as well as additional factors with unknown functions (Table 7.2.1).

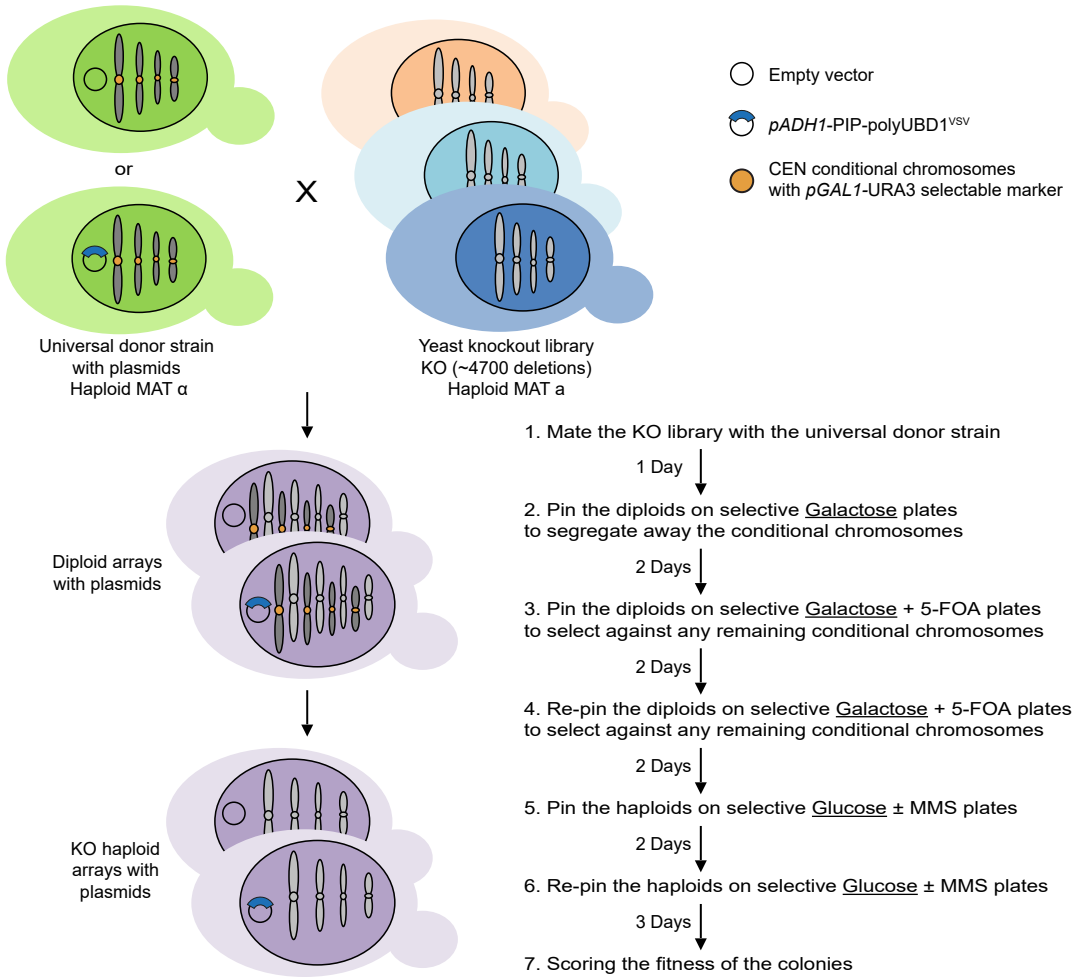

Figure 7.2.3: Genetic screens for sensitivity to MMS and additivity to PIP-polyUBD1. A cartoon of the basic principle behind the genetic screens. The growth and selection conditions in each step of the screens are indicated. For more details, check the main text (2.11.13.2).

Common ORFs	Function	Localisation
RAD5	DNA helicase/Ubiquitin ligase	Nucleus, cytoplasm, chromosome
RAD14	Binds damaged DNA during NER	Nucleus
APN1	Apurinic/apyrimidinic endonuclease	Nucleus, cytoplasm, mitochondrion
SRB5	Subunit of the RNA polymerase II mediator complex	Nucleus
YGR045C	Dubious open reading frame	Membrane
YGL072C	Dubious open reading frame	Unknown
YKL222C	Protein of unknown function; sensitive to caffeine	Nucleus, cytoplasm, ribosome, cytoskeleton
YJR128W	Dubious open reading frame	Unknown

Table 7.2.1: A list of the eight suppressor genes: The eight common ORFs between the overexpression, sensitivity, and additivity screens. Information about the function and localisation of the ORFs were obtained from SGD.

7.2.2.3 Validation of the screening results via correlation analysis

The outcome of the screens could have been affected by several factors, like the nonhomogeneous growth, competition between neighbouring colonies, or even the scoring and defining the thresholds. For this reason, I correlated the results of my screens with comparable published data. The overexpression screen had a unique setup, making it challenging to compare with any other study. I could partly correlate the MMS sensitivity screen with Kapitzky *et al.,* 2010, where they analysed the MMS sensitivity of 500 gene deletions [409]. Because these two screens relied on different scoring and thresholds, I used the Z-score conversion for the correlation analysis. This analysis identified a positive correlation (r=0.59) between the two screens (Figure 7.2.4 D). Based on the data of my thesis, overexpression of PIP-polyUBD1 has similar effects on template switching as *UBC13* deletion. In Guénolé *et al.*, 2013 [410], they studied the additive impact of *ubc13Δ* on a group of gene deletions. A Z-score analysis between the additivity screen and the one from Guénolé *et al.,* 2013 [410] (Figure 7.2.4 E), discovered a very little correlation between the two screens (r = 0.096). The variation seen between these two screens might arise from different genetic backgrounds and treatment conditions. Because overexpression of PIP-polyUBD1 had some off-target effect in different mutant backgrounds (Figures 4.2.4, 4.2.5, 4.2.6, and 4.2.7), it is also possible that overexpression of the probe and deletion of *UBC13* are not 100% comparable.

The yeast knockout library contains only deletions of non-essential genes. However, in the overexpression screen, I also identified 30 essential suppressors. Based on published data, five out of these 30 essential suppressors cause MMS sensitivity upon their conditional deletion by using decreased abundance by mRNA perturbation (DAmP) alleles, and are epistatic with *ubc13Δ*. Rest of the essential suppressors lack information about MMS sensitivity and additivity to *ubc13Δ*. These gene might have been not well studied because lack of viable mutants. Therefore, in future, it is worth to analyse the involvement of these essential suppressors in error-free damage bypass.

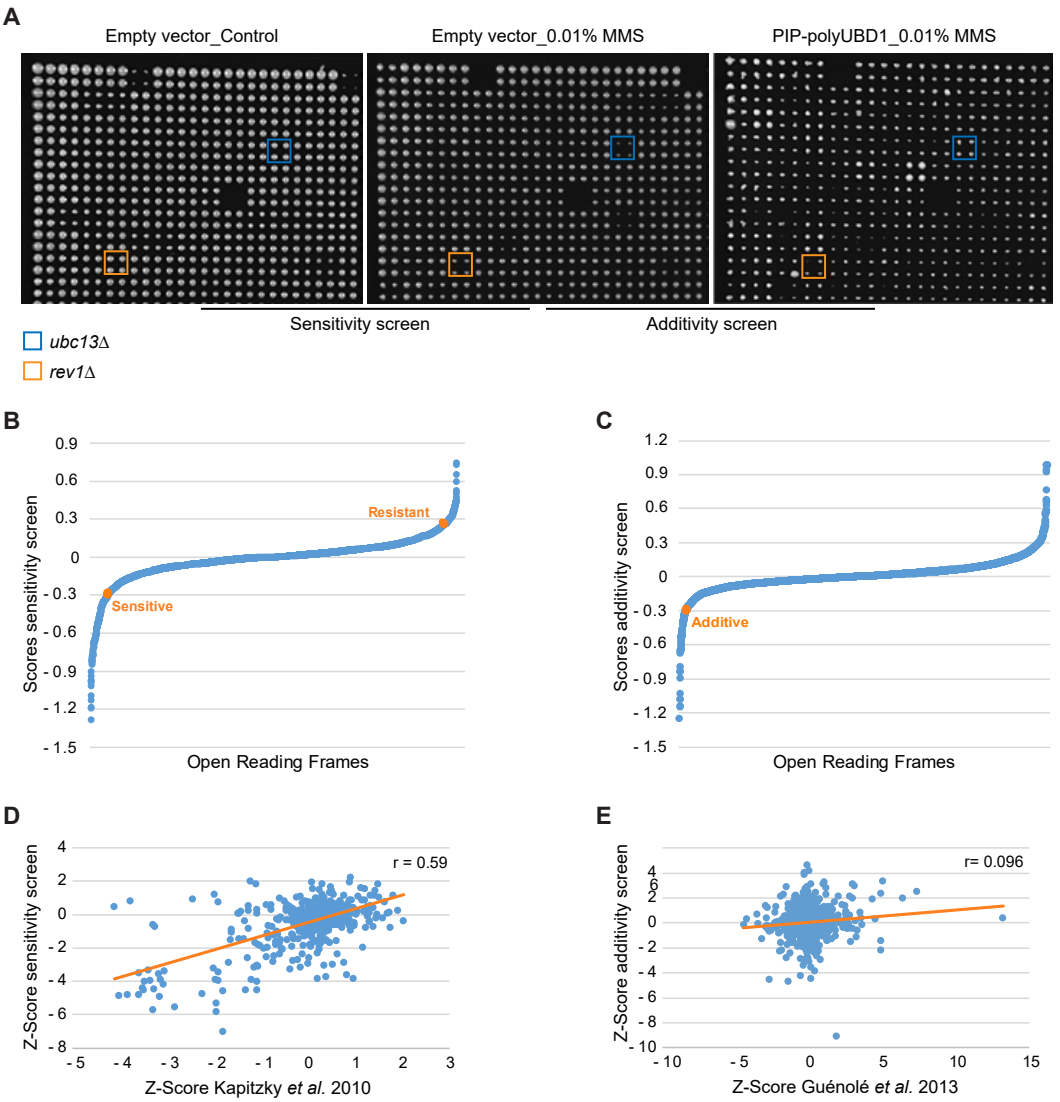

Figure 7.2.4: Outcomes of the sensitivity and additivity screens. (A) An example of raw images of the screening plates at the finale step. In the MMS sensitivity screen, the knockout library containing the empty vector was compared between undamaged and MMS damage conditions. In the additivity screen, the fitness of knockout libraries containing either the empty vector or *pADH1*-1xNLS-PIP-polyUBD1^{VSV} was compared under MMS damage conditions. The blue square refers to *ubc13Δ*, an MMS sensitive and not additive deletion. The orange square refers to *rev1Δ*, an MMS sensitive and additive deletion. (B) Score distribution of the sensitivity screen. The thresholds for MMS sensitivity and MMS resistance are indicated in orange. (C) Score distribution of the additivity screen. The orange dot defines the threshold between deletions that are additive (< -0.28) or epistatic and positive with PIP-polyUBD1 (> -0.28). (D) A dot graph showing the correlation between the MMS sensitivity screens performed in this study and in Kapitzky *et al.*, 2010 [409]. The r value refers to a positive correlation. (E) A dot graph showing the correlation between the additivity screen performed in this study and the synthetic genetic interaction screen of *ubc13Δ* with a panel of ~ 2000 gene deletions in Guénolé *et al.*, 2013 [410]. The r value refers to a very weak correlation.

7.2.3 Confirming and characterising the suppressors of PIP-polyUBD1

The colonies in the overexpression screen showed a significant variation in growth and colony size. Moreover, the format and the manipulation conditions of the arrayed high-throughput screens might have identified some false-positive suppressors. To eliminate such false-positive suppressors, I repeated the sensitivity and additivity tests for four (*rad14Δ*, *apn1Δ*, *ykl222Δ*, *yjr128*w*Δ*) out of the eight identified candidate ORFs in a classical spot assay. Because *rad23Δ* is additive to defects in DNA damage bypass, I used *rad23Δ* cells as a control. Unfortunately, the four tested ORFs showed additivity to the probe (Figure 7.2.5 B). This observation indicates that these suppressors belong to category 3 and repair the damage independently of polyubiquitylated PCNA. Having seen that the false-positive rate between the suppressors was very high, I set out to systematically reevaluate all the 229 suppressors by repeating the overexpression screen in a small-scale, analysing the regulation and involvement of some of the factors in template switching, and their interaction with ubiquitylated PCNA.

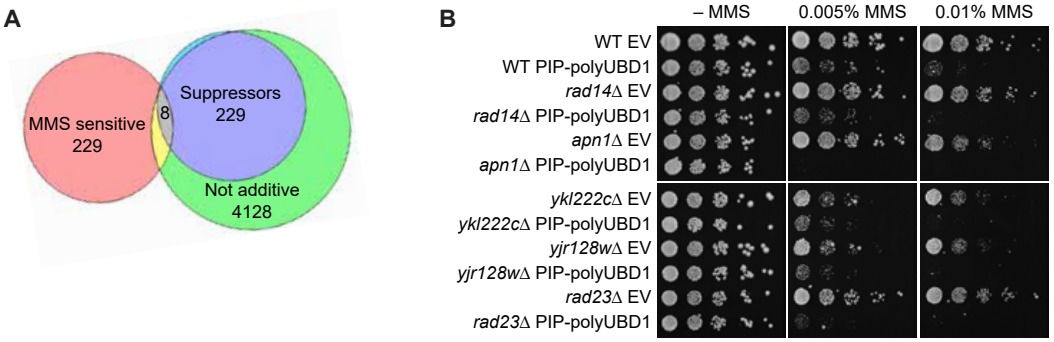

Figure 7.2.5: Combined outcomes of the overexpression, sensitivity, and additivity screens. (A) A Venn-diagram representing the overlap between the ORFs that were identified in the three parallel screens. Eight out of the 229 suppressors met the requirements of a putative factor X. (B) Spot assay to confirm some of the identified candidates. *rad23Δ* cells were used as a control for additivity. The indicated strains were spotted on synthetic complete agar plates containing increasing doses of MMS. All the tested ORFs were synergistic to overexpression of *pADH1*-1xNLS-PIP-polyUBD1^{VSV}.

7.2.3.1 Are all the identified suppressors true suppressors of PIP-polyUBD1?

To reanalyse and confirm all the 229 suppresses, I performed classical spot assays following similar steps as in the initial overexpression screen. Surprisingly, the suppression effects of the ORFs in the spot assays were not as strong and prominent as in the array format. Nevertheless, I could confirm some of the suppressors and sort them depending on their suppression strength (Figure 7.2.6 A). Here, the ORF of *LEU2* had the most potent effect probably by segregating away the *LEU2* plasmid that carried PIP-polyUBD1. Similar to the array format, *RAD5* could suppress the probe efficiently (Figure 7.2.6 A). Because most of the suppressors showed marginal effects, I chose the three strongest ones (*ECM32*, *YBL036C*, and *UPF3*) to analyse their involvement in template switching by various experiments. Ecm32 is an ATP-dependent DNA and RNA helicase that belongs to the Dna2-like family. It is stimulated by RPA and has similar domains as Mgs1, Rfc3, and Smc4 [411, 412, 413, 414]. Ybl036c is a racemase that binds pyridoxal 5' phosphate. However, the molecular function and genetic interactions of Ybl036c is poorly studied [415]. Upf3 forms a heterotrimer with Upf2 and the ubiquitin ligase Upf1. This complex has

a well-established role in nonsense-mediated mRNA decay (NMD). Interestingly, functions in telomere maintenance and DNA recombination are assigned to Upf1-Upf3 that are independent of Upf2 [416].

7.2.3.2 How do the suppressors behave during the cell cycle and after replication stress?

To gain a general view about the regulation, localisation, and function of the suppressors, I either deleted or tagged the three candidates (*ECM32*, *YBL036C*, and *UPF3*) with GFP on their C-termini. Deletion of *ybl036cΔ* and *upf3Δ* rendered cells sensitive to high doses of MMS (Figure 7.2.6 B). The cellular localisation of the factors was analysed by fluorescent microscopy, to asses any tendency in nuclear accumulation after replication stress. Asynchronously growing cells were incubated with or without 0.02% MMS for 90 min. MMS-induced damage did not cause any changes in localisation or intensity of Ecm32^{GFP} and Upf3^{GFP}, whereas the signal of Ybl036c^{GFP} was sharply reduced in MMS treated cells (Figure 7.2.6 C). Next, to analyse the cell cycle regulation of these factors, cultures were synchronised in G1 phase by (αF), incubated with or without 0.02% MMS, then released into the cell cycle. This experiment revealed that Ecm32^{GFP} persist in G2, whereas Upf3^{GFP} accumulate mainly in G1, and MMS damage did not lead to significant changes in their regulation apart from the delay in the cell cycle. Ybl036c^{GFP} did not show any cell cycle-dependent regulation. However, a decrease in the protein abundance after MMS damage detected by microscopy was also reflected in the western blot (Figure 7.2.6 D).

7.2.3.3 Do the suppressors bind to polyubiquitylated PCNA?

The three identified suppressors may belong to one of the categories mentioned earlier and thus take part in template switching. If these factors belong to category 1, they are expected to bind to polyubiquitylated PCNA directly and thereby compete with the probe. The yeast two-hybrid assay (Y2H) provides a powerful system to study protein-protein interactions. Briefly, one of the proteins of interest is fused to Gal4 DNA-binding domain (BD) and the other protein to Gal4 transcriptional activation domain (AD). If the two proteins of interest interact with each other, the Gal4 transcription factor is reconstituted and drives the expression of a downstream reporter gene [417, 418, 419]. Using the Y2H system, I analysed interaction of the three ORFs with PCNA, PCNA-monoubiquitin fusion, and PCNA-polyubiquitin fusion. Ecm32 and Upf3 showed a weak interaction only with PCNA-monoubiquitin fusion (Figure 7.2.7 A). This observation indicates that the suppressors do not bind directly to polyubiquitylated PCNA instead they might be involved in template switching downstream of polyubiquitylated PCNA.

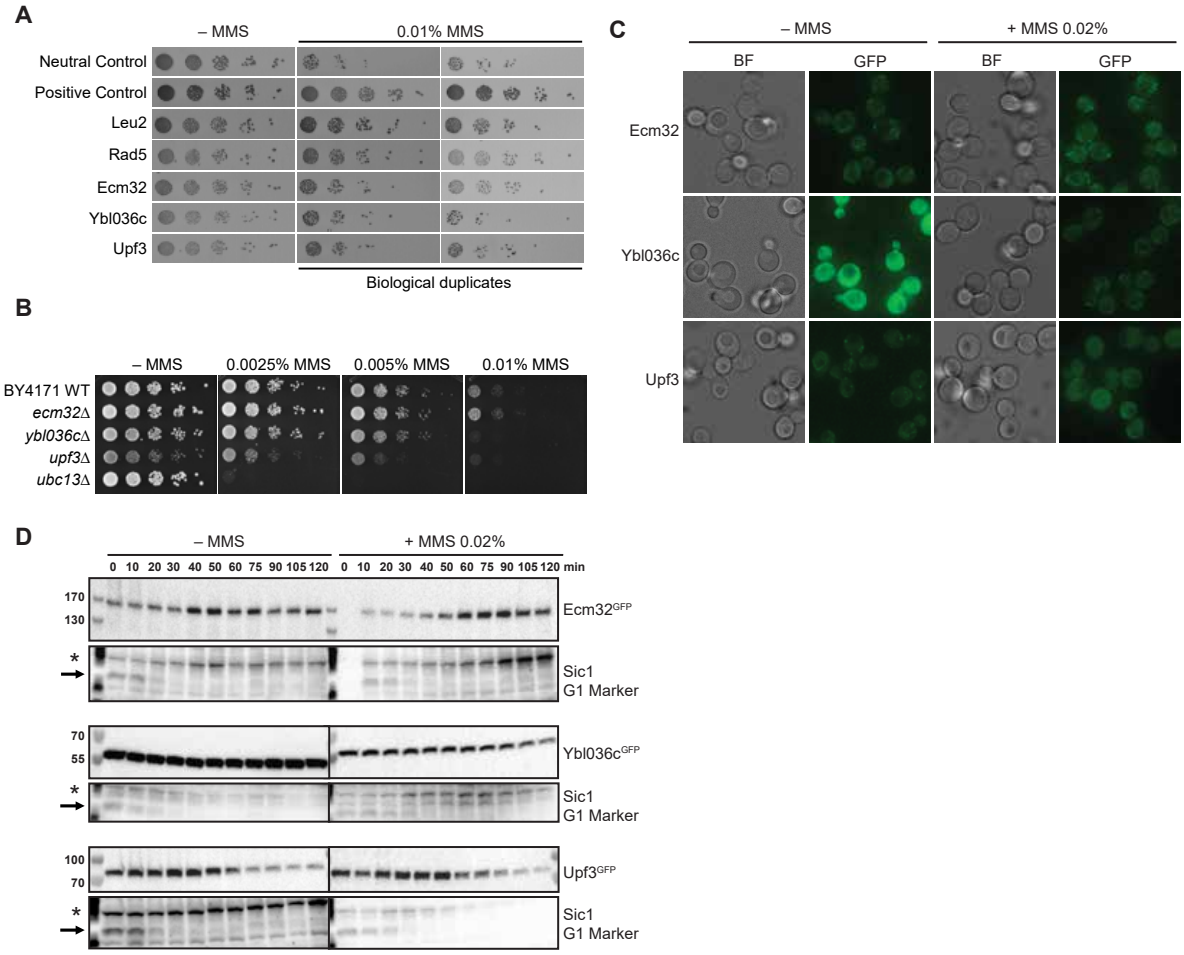

Figure 7.2.6: Validating the suppressors of PIP-polyUBD1. (A) Spot assays to confirm the 229 suppressors from the overexpression screen. Expression of the ORFs was activated as in the high-throughput format, and the suppression effects were validated in two biological replicates. The suppressors are arranged from top to bottom according to their degree of suppression. (B) Spot assay showing the MMS sensitivity of cells when the indicated genes are deleted. (C) Asynchronous cultures of $Ecm32^{GFP}$, $Ybl036c^{GFP}$, and $Upf3^{GFP}$ were incubated with or without 0.02% MMS for 90 min. The localisation of the fluorescent proteins was analysed by microscopy. (D) Cell cycle analysis of $Ecm32^{GFP}$, $Ybl036c^{GFP}$, and $Upf3^{GFP}$. Cultures were synchronised in G1 by (αF) for 90 min, incubated with or without 0.02% MMS for 30 min, then washed and released into the cell cycle. Protein samples were collected each 10 min for two hours and analysed by SDS-PAGE and western blotting for GFP. The G1 marker, Sic1, was used to track the cell cycle stage. The arrow points to the Sic1 specific band, whereas the asterisk is an unspecific band.

7.2.3.4 Are the suppressors involved in template switching?

In the previous subsection, I showed that the three suppressors do not belong to category 1 and do not interact with polyubiquitylated PCNA. Deletion of many well-characterised template switching factors is epistatic with deletion of *UBC13* or *MMS2*. To test whether the suppressors are involved in template switching downstream of polyubiquitylated PCNA, I analysed their genetic interaction with *ubc13Δ* and *mms2Δ*. Deletion of *UPF3* made the cells sick even in the absence of any cellular stress. Because Upf1 and Upf3 have mutual functions in genome maintenance and *UPF1* was also in the list of suppressors, I included *UPF1* as well in the following experiments. Surprisingly, deletion of all the three suppressors *ecm32Δ*, *ybl036cΔ*, and *upf1Δ* showed synergistic effects with *ubc13Δ* and *mms2Δ* (Figure 7.2.8). Alternative proxies to confirm that a gene plays a role in template switching is to study the gene's potential in rescuing the cold sensitivity of *pol32Δ* mutant and the DNA damage sensitivity of *smc6-56* mutant. Pol32 is a non-essential subunit of polymerase δ, and mutants of template switching rescue the cold sensitivity of *pol32Δ* cells via so far an unknown mechanism [247, 208, 192]. Genetic interactions with the mutants of structural maintenance of chromosomes 6 (Smc6) allows investigating the role of a gene in recombination-dependent damage bypass. The Smc5/6 is an essential complex, which resolves X-shaped DNA structures that arise during recombination [191, 420, 421]. The hypomorphic allele *smc6-56* accumulates toxic cruciform DNA molecules making the cells sensitive to replication stress. Deletion of template switching factors suppresses the DNA damage sensitivity of *smc6-56* mutants by inhibiting the formation of toxic recombination structures at the first place [420, 421, 422, 198]. Compared to *ubc13Δ*, neither *ecm32Δ* nor *ybl036cΔ* could rescue the sensitivity of *pol32Δ* or *smc6-56* mutants (Figure7.2.7 B and C). All these results indicate that these three ORFs suppress the probe independently of polyubiquitylated PCNA disqualifying them to be the factor X.

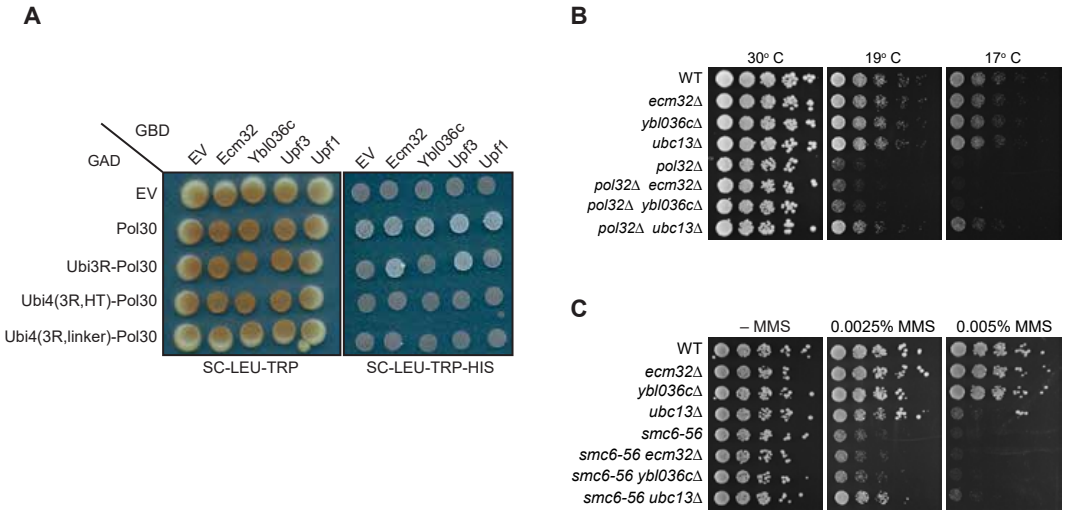

Figure 7.2.7: Analysing the role of the suppressors in DNA damage bypass. (A) Yeast two-hybrid assay to investigate the potential interaction of the indicated ORFs with PCNA, PCNA-monoubiquitin fusion, and PCNA-polyubiquitin fusion. (B) Rescue experiments of *pol32Δ* cold sensitivity. The strains were spotted on synthetic complete agar plates and cells were grown at the indicated temperatures for four days. (C) Rescue experiments of *smc6-56* MMS sensitivity. The strains were spotted on synthetic complete agar plates containing increasing doses of MMS. The cells were grown at 30° C for three days. In B and C, *ubc13Δ* strains were used as controls for comparison of the rescue effects.

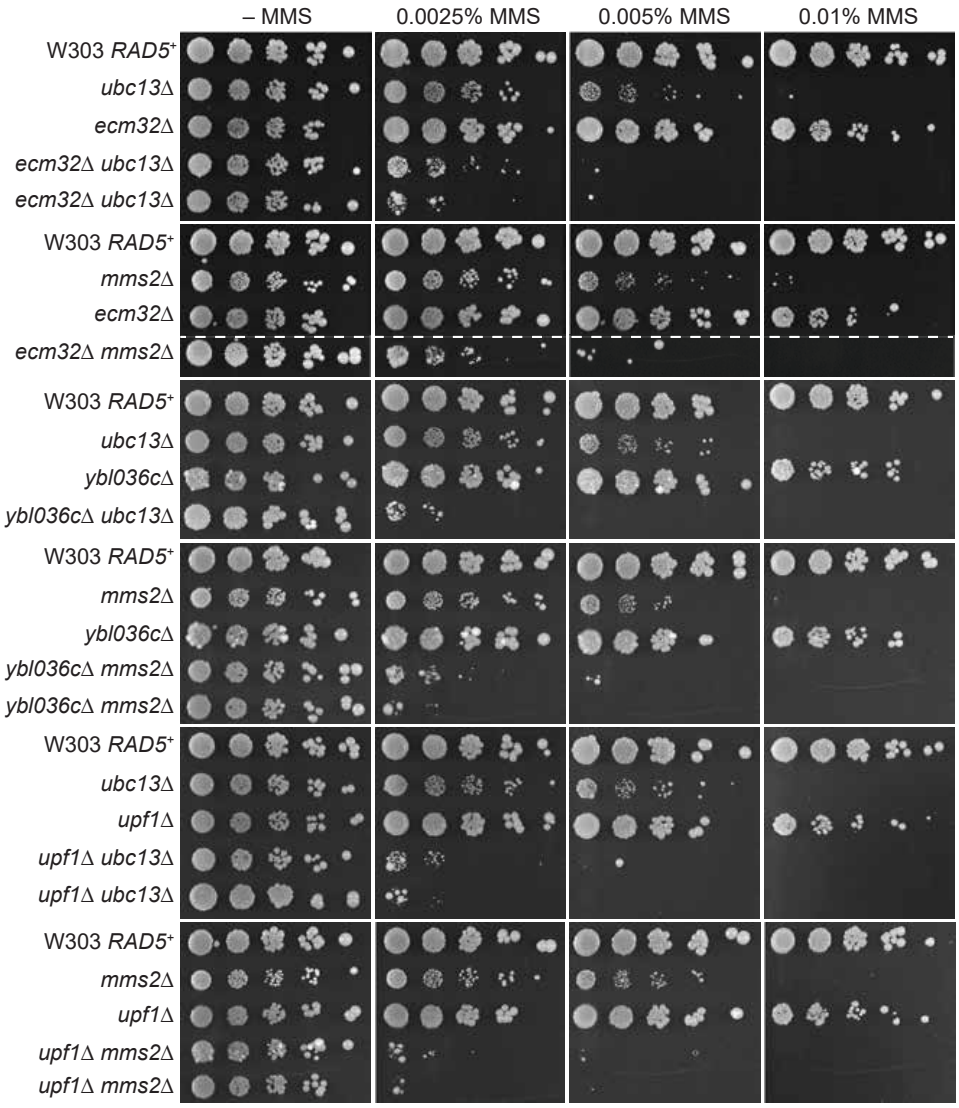

Figure 7.2.8: The candidate suppressors are synergistic with *ubc13Δ* and *mms2Δ*. Spot assay of single and double mutants for genetic interaction analysis. The strains were spotted on synthetic complete agar plates containing increasing doses of MMS. For some of the double mutants, more than one clone was analysed.

7.2.4 Rad5 as a suppressor of PIP-polyUBD1

In contrast to the above tested suppressors (Figure 7.2.7), it is reported that mutants of *RAD5* rescue the sensitivities of *pol32Δ* and *smc6-56* [247]. Besides, given that *RAD5* overexpression counteracted the inhibitory effects of PIP-polyUBD1 in a Ub-PCNA dependent manner (Figure 7.2.6 A), I got interested in knowing how Rad5 can achieve this suppression. Rad5 is a complex protein with several functional domains; DNA binding, ATPase/helicase, RING-ubiquitin ligase (E3), and Rev1 interaction domain [247, 423**?**]. Rad5's ligase activity is responsible for PCNA polyubiquitylation [166, 18], its helicase function is required for the recombination-dependent and independent lesion bypass [247], and its interaction with Rev1 promotes TLS during unperturbed replication [**?**]. Therefore, *RAD5* overexpression could suppress the probe in at least three possible ways. Either it builds more K63-linked

polyubiquitin chains on PCNA, thereby titrating away the probe, its helicase function promotes lesion bypass up- or downstream of polyubiquitylated PCNA, or it channels the repair of the lesion to TLS. In the following subsections, I tested all the mentioned hypotheses.

7.2.4.1 Rad5's ligase activity counteracts PIP-polyUBD1

To pinpoint the domain or the function of Rad5 that suppresses the inhibitory effects of PIP-polyUBD1, I overexpressed different mutants of *RAD5*, which carry a point mutation either in the ligase (*rad5-I916A*), helicase (*rad5-Q1106D*), or Rev1-interaction (*rad5-FN13-14AA*) domains, as well as their double and triple mutant combinations. As indicated in figure (7.2.9), mainly *rad5* mutants that carry a functional E3 activity could rescue the MMS sensitivity of PIP-polyUBD1 overexpression to a similar degree as WT *RAD5*. Interestingly, the ligase-dead mutants conferred some dominant-negative effects, indicating that the mutant *rad5-I916A* blocks the accessibility of other repair factors to the sites of lesions. These observations suggest that Rad5's ligase function is the most potent function that counteracts the probe. Therefore, in future, it would be interesting to analyse PCNA ubiquitylation levels in each of these mutants by pull-down assays to confirm that building more ubiquitin chains on PCNA is one of the ways to suppress the probe.

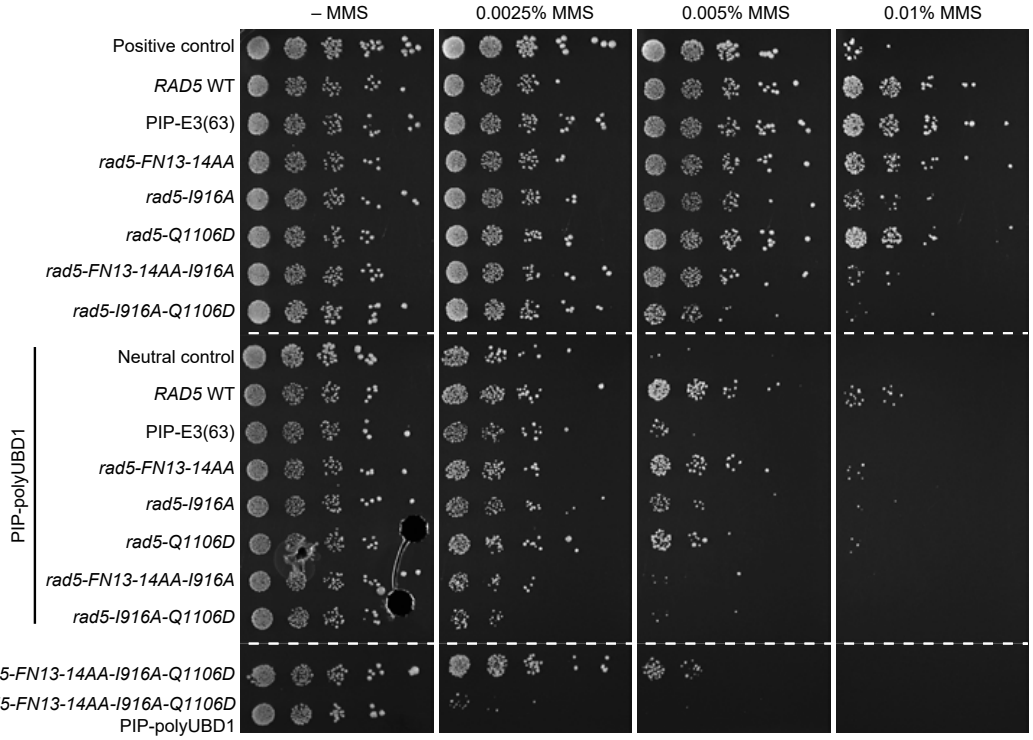

Figure 7.2.9: Rad5's ubiquitin ligase function is required to neutralise PIP-polyUBD1. Spot assay of yeast strains overexpressing single, double, or triple mutants of *RAD5* from an episomal plasmid under the control of *GAL1* promoter. *rad5-I916A*, ligase-dead; *rad5-Q1106D*, helicase-dead; *rad5-FN13-14AA*, Rev1-interaction mutant. In addition, the strians contain either an empty vector or a plasmid overexpressing 1xNLS-PIP-poyUBD1^{VSV} under the control of *ADH1* promoter. The strains were spotted on selective synthetic complete agar plates containing increasing doses of MMS. The cells were grown at 30^{o} C for five days.

7.2.4.2 PIP-E3(63), a Rad5 mimicking ligase, partly suppresses PIP-polyUBD1

Considering that Rad5 competes with PIP-polyUBD1 mainly via its ubiquitin ligase activity, I expected that building K63-linked polyubiquitin chains on PCNA by other means might also suppress the probe. To address this hypothesis, I analysed the antagonising effects of a tailor-made Rad5-mimicking ubiquitin ligase. A former PhD student in our lab, Dr Sabrina Wegmann, engineered tailor-made ligases that put linkage-specific ubiquitin chains on PCNA. One of these PCNA-directed and linkage-specific ligases, PIP-E3(63), can modify monoubiquitylated PCNA with K63-linked polyubiquitin chains *in vivo* and replace the requirement for Rad5 under replication stress conditions. In similar experiments as for *RAD5* mutants, I tested if PIP-E3(63) is capable of suppressing PIP-polyUBD1. In control cells, inducible overexpression of PIP-E3(63) by the *GAL1* promoter conferred MMS resistant that was comparable to overexpression of the full-length *RAD5*. Surprisingly, in cells that overexpressed PIP-polyUBD1, the tailor-made ligase could not suppress the probe as good as the ligase efficient mutants of *RAD5* (Figure 7.2.9). Such observations could result from technical and biological differences.
On the one hand, by *in vitro* experiments, Dr Sabrina Wegmann showed that PIP-E3(63) is a bit less active than Rad5 in catalysing the ubiquitylation reaction. Besides, the expression and stability of Rad5 and the tailor-made ligase may differ upon their overexpression. On the other hand, better suppression of the probe by full-length *RAD5*could arise from the contribution of the helicase and the Rev1-interaction domains.

7.3 Discussion and epilogue IV

7.3.1 The enigmatic role of PCNA polyubiquitylation in template switching

The role of PCNA polyubiquitylation in triggering template switching is well established [166]. However, the underlying molecular mechanism involved in the activation of the error-free bypass is puzzling. Several hypotheses have been suggested and debated for the function of K63-linked ubiquitin chains on PCNA. The option that polyubiquitylation of PCNA activates its proteasomal degradation is off the table [36, 399, 400, 398]. The synergy that exists between error-prone TLS and error-free template switching factors argue against an essential function of PCNA polyubiquitylation in promoting or inhibiting TLS [216, 306, 80, 403, 223, 402, 399]. More recent evidence from our lab has established a better view of the critical properties of polyubiquitin chains on PCNA. Linear, non-cleavable polyubiquitin chain mimics are not sufficient in activating template switching, whereas a single K63-junction at a non-native position on PCNA promotes error-free damage bypass. Interestingly, the few known binders of polyubiquitylated PCNA, Mgs1 and ZRANB3, efficiently recognize the linear mimics as well [104]. These findings narrow down the role of PCNA polyubiquitylation to the recruitment of a novel receptor that is highly selective for the K63-linkage and triggers template switching in a yet unknown molecular function. Here, using a set of genome-wide genetic screens and interaction analysis, I aimed to identify factors that directly recognise polyubiquitylated PCNA.

7.3.2 On a journey to find the factor X

Discovering and characterising factors that directly recognise polyubiquitylated PCNA would be a significant turning point in our knowledge about DNA damage bypass. On a journey to find the factor X, I utilised PIP-polyUBD1 in a genetic overexpression screen to identify factors that suppress and rescue the damage sensitivity caused by the probe. The overexpression genetic screen identified 229 suppressors that could compete with PIP-polyUBD1. Many DNA repair factors, like *RAD5*, *RAD14*, *RFC5*, *UPF3*, *SMC1*/*SMC3* were among the suppressors. However, the screen also identified dozens of other factors, making it difficult to speculate on the novel receptor of polyubiquitylated PCNA. This ambiguity of the suppressors, made me perform additional screens for additivity and MMS sensitivity. These secondary screens and classical spot assays helped to withdraw many false-positive suppressors that were identified in the initial overexpression screen.

7.3.3 Possible causes of failure of the genetic screen in identifying receptors of polyubiquitylated PCNA

The additivity and MMS sensitivity screens and the classical spot assays helped me to reduce the number of the identified candidates to three (*ECM32*, *YBL036C*, and *UPF3*). I further analysed and characterised the involvement of these factors in template switching. However, performing various experiments, like cell cycle regulation, microscopy, MMS sensitivity, physical interaction with ubiquitylated PCNA, epistasis with *ubc13Δ* and *mms2Δ* suggested that these three factors repair DNA lesions independently of polyubiquitylated PCNA.
The overexpression screen might have failed in identifying factor X for several reasons:

- The substantial growth variation between the colonies upon overexpression of the ORFs may cause miscalculations in the scores and the thresholds.
- Overexpression of some ORFs, such as nucleases, is toxic to the cells, making it difficult to score for suppression.
- Some factors exert their biological function as co-factors of a particular protein or as subunits of a larger functional complex. Hence, the overexpression of a single ORF or factor could not rescue the dominant-negative effects of PIP-polyUBD1.

7.3.4 Rad5: the prodigy factor of damage bypass

In all the genetic screens and the downstream validation experiments, Rad5 was one of the most prominent suppressors of PIP-polyUBD1. Rad5 is the E3 responsible for PCNA polyubiquitylation. However, its helicase function and interaction with TLS polymerases contribute to both error-free and error-prone damage bypass. Using different mutants of *RAD5*, I demonstrated that mainly *rad5* mutants with a functional E3 activity could compete with PIP-polyUBD1 most probably by building more ubiquitin chains on PCNA. Interestingly, a Rad5 mimicking ligase, PIP-E3(63), was unable to compete with the probe as good as the full-length *RAD5*. A better suppression of the probe by full-length *RAD5* could arise from the contribution of the helicase and the Rev1-interaction domains. It is also possible that there are yet undiscovered functions or domains of Rad5. One such envision is that Rad5 itself

carries a UBD/UIM and a PIP box. Once Rad5's E3 builds K63-linked polyubiquitin chain on PCNA, the combined avidity of the PIP box and UBD/UIM initiates the binding of Rad5 to polyubiquitylated PCNA and stimulates its helicase function. In mammals, RNF125 (TRAC1), RNF138, and RNF166 are examples of E3s with UBDs/UIMs. They are involved in various biological processes, like T-cell activation, autophagy, and DSB repair. Nevertheless, the function of their UIMs is not well studied [424, 425, 426]. The assumption that Rad5 contains a PIP box and a UBD/UIM can be checked by Y2H experiments using PCNA and PCNA-ubiquitin fusions as binding partners.

7.3.5 Beginning of another journey: Using Ub-PCNA probes in alternative methods to find the factor X

7.3.5.1 Microscopy-based methods

The Ub-PCNA probes perform very well as sensors for ubiquitylated PCNA in live cells using fluorescent microscopy. Therefore, it is worth to develop a microscopy-based screening system to discover factor X. These screens can be done on a genome-wide scale with a high-throughput microscopy approach or on a small-scale candidate-oriented screen. In both cases, the involvement of a factor in template switching can be judged by monitoring the appearance, persistence, and resolution of the Ub-PCNA foci [427].
Recently, a yeast library with N-terminal split-Venus (YFP) tag was created [428]. This library provides another microscopy-based approach to identify receptors of polyubiquitylated PCNA. Briefly, a query yeast strain is created that contains PIP-polyUBD1 fused to one half of Venus. Then, this query strain is simply crossed to the yeast library carrying ORFs tagged with the other half of Venus. In the resulted diploids, any interaction between the probe and a possible factor X would reconstitute the fluorescent signal of Venus. Performing high-throughput imaging allows the identification of factors that come into proximity with polyubiquitylated PCNA. Moreover, in a similar fluorescent reconstitution screen, fusing only the polyUBD1 domain of the probe to a fragment of Venus could identify any K63-linked polyubiquitylated substrates at stalled replication forks. In the microscopy screens, the scoring depends on direct detection of polyubiquitylated PCNA at very early stages of damage bypass signalling. In contrast, the overexpression screen relies on the fitness of colonies, which requires several rounds of replication to form detectable colonies. Therefore, the microscopy-based approaches would give more reliable results than the fitness-based overexpression screen.

7.3.5.2 Proteomics-based methods

To discover receptors of polyubiquitylated PCNA through proteomic analysis, the GFP or VSV tagged PIP-polyUBD can be used as bait in immunoprecipitation experiments. Then the protein complexes can be analysed by SILAC-based (stable isotope labelling with amino acids in cell culture) mass-spectrometry [429]. Another alternative and elegant way to identify the factor X is the proteomic-based BioID profiling. Briefly, a mutant version of the bacterial biotin ligase (BirA*) is fused to the Ub-PCNA probe and used to detect any protein-protein interactions via proximity-dependent biotinylation [430, 431]. Three different conditions can be compared to get more accurate results. Undamaged vs damaged, WT vs $pol30^{K164R}$, and tagged probe vs tag only samples. However, these proteomic approaches need additional optimisation of the probes because the experiments require using special yeast strains and media.

Chapter 8

General conclusions and future perspectives

8.1 Limitations of the Ub-PCNA probes

Throughout this work, I demonstrated that the Ub-PCNA probes are multitasking tools. Upon overexpression, they act as pathway-specific inhibitors, whereas an inducible expression system turns them into sensors to visualise PCNA ubiquitylation in live cells. Both functions showed to be very useful in dissecting mechanistic and genetic details of DNA damage bypass in the budding yeast. However, defining the boundaries between the inhibitor and the sensor functions requires careful optimisation. Therefore, caution should be taken when utilising the Ub-PCNA probes in other model organisms. For example, transient transfection of mammalian cells with the inducible fluorescent sensors would most probably act as inhibitors because of multiple copies of the plasmid per cell and substantial heterogeneity in the culture. The limited use of the probes only for PCNA is yet another drawback. Several dozens of other proteins are decorated by different ubiquitin modifications. It would be fascinating to generalise the use of such multi-tools for any protein of interest in a broad range of applications. The substrate specificity of the probes can be changed by using a different dimerisation system instead of the PIP box. For instance, the substrate can be fused with a small tag such as Myc or SPOT-tag, whereas the fluorescently tagged UBD can be fused to a respective nanobody. However, such systems need optimisation because the affinities of nanobodies are much higher than the PIP box mediated interactions. These may lead to avidity/UBD independent recognition of the substrate. A chemically inducible dimerisation system that relies on rapamycin and the FRB/FKBP dimerisation domains might be used in targeting the probes to the desired substrate. Nonetheless, it is difficult to switch off the signal because rapamycin is usually not released from its binding proteins [432].

8.2 Potential implications of the Ub-PCNA probes

8.2.1 Exploring undiscovered aspects of DNA damage bypass

Dissecting the bypass events in minute details

Live-cell imaging of Ub-PCNA sensors helped to gain new insights into the spatial and temporal regulation of PCNA ubiquitylation. There is still a window of opportunity to further pinpoint the exact timing of PCNA ubiquitylation at the postreplicative tracts, which would add valuable information to the mechanism of damage bypass. Such precise measurements are possible by performing EdU pulse and chase experiments followed by chromatin spread, antibody staining, and Click reaction to trace the gap-filling of nascent strands and analyse their correlation with Ub-PCNA sensors.

Gaining a global view of PCNA ubiquitylation

Partial instead of full colocalisation between the two sensors (i.e. PIP-monoUBD and PIP-polyUBD2), suggests a task distributing between the two bypass modes throughout the genome. Unfortunately, the ChIP approach failed to build a genome-wide view of PCNA ubiquitylation because of the chromatin crosslinking step. However, Ub-PCNA probes can be used in several alternative genomics approaches. One such method is DamID profiling that makes use of DNA adenine methyltransferase to mark the regions of protein-DNA interaction with methyl groups. Then, DNA fragments created by DpnI digestion are analysed by NGS [396]. CUT&RUN is another method without a crosslinking step. It is an antibody-targeted system that uses the MNase to cleave protein-DNA complexes, followed by NGS of the resulting DNA fragments [397]. For more details about these techniques, see (6.3.3).

Discovering yet unknown factors of template switching

Identifying the factors that bind to polyubiquitylated PCNA is of great scientific interest. Recent unpublished results carried out by Dr Néstor García-Rodríguez in our lab indicated that the endonuclease, Exo1, might be such a factor. By performing several biochemical and genetic analysis, Dr Néstor García-Rodríguez showed that the PIP-box of Exo1 is necessary for interaction with PCNA and that Exo1 involves in template switching in a pathway-specific manner. However, it is unclear if Exo1 contains a UBD. The overexpression screen that I performed to identify interactors of polyubiquitylated PCNA relied on the fitness of yeast cells, which required several rounds of replication to form detectable colonies. This experimental setup excluded Exo1 as a potential interactor because its overexpression was toxic to cells even without external damaging agents. Other potential factors might also have been eliminated for similar reasons. The Ub-PCNA sensors performed very well in fluorescent microscopy. Therefore, it is worth to develop a microscopy-based screening to discover factor X either in a high-throughput format or on a small-scale candidate-oriented screen. In both cases, the involvement of a factor in template switching can be judged by monitoring the appearance, persistence, and resolution of the sensors' foci [427].

Alternatively, a fluorescent reconstitution screen might help to identify receptors of polyubiquitylated PCNA. In such a screen, the Ub-PCNA probe would be fused to one half of a fluorescent protein, and then expressed in a yeast library carrying ORFs tagged with the other half of the fluorophore [428]. Any factor that comes into proximity with polyubiquitylated PCNA would reconstitute the fluorescent signal. Moreover, fusing only the polyUBD1 domain of the probe to a fragment of the fluorophore could identify

any K63-linked polyubiquitylated substrates at stalled replication forks. For more details, see (7.3.5.1). Proteomic-based BioID profiling is another option to find new interactors of polyubiquitylated PCNA. In such experiments, the Ub-PCNA probe fused to the biotin ligase (BirA*) could be used to detect any protein-protein interactions via proximity-dependent biotinylation [430, 431].

8.2.2 Studying role of PCNA ubiquitylation in other biological processes

Many lines of evidence suggested the involvement of TLS polymerases in the resolution of DNA interstrand crosslinks. However, there are discrepancies in the requirement for PCNA ubiquitylation for this process [433, 434]. Ub-PCNA sensors provide a convenient tool to address when and in which step of ICL repair PCNA ubiquitylation and TLS polymerases might be involved.
Telomerase inactivation induces replication stress at telomeres. It is suggested that under moderate replication stress, activation of Mrc1 and counteracting replication stress by recombination delay the onset of senescence. Template switching is one of the proposed mechanism of recombination at telomeres depending on the observations that deletion of *RAD5* accelerates senescence and accumulation of X-shaped structures at telomeres during senescence [242, 192, 435]. It would be interesting to analyse and determine the exact time window in which telomerase negative cells rely on replication stress to induce recombination and to what degree PCNA ubiquitylation is required to delay senescence. In this aspect of telomere biology, use of the Ub-PCNA sensors would allow obtaining critical knowledge of telomerase-independent immortalisation seen in yeast survivors and 15% of human cancer.

8.2.3 Diagnosis and treatment

If optimised well, Ub-PCNA sensors might be used for diagnostic and therapeutic purposes. Several established diagnostic pipelines use antibody staining of PCNA to categorise tumour types [436]. Besides, a cohort of cancer types shows an increase in expression of different TLS polymerases, like POL η, POL ζ, and REV1, which in turn associates with increased frequency of mutations, poor prognosis, and survival [437, 438]. However, there is no direct evidence of an increase in PCNA ubiquitylation in such cancer cells. Developing cell-permeable Ub-PCNA probes may serve as diagnostic markers. One possibility would be to fuse the probes with a cell-penetrating peptide, derived from the HIV-1 trans-activator of transcription (TAT) that helps to deliver the probes into live cells. Such a cell-permeable reagent that contains a PIP box was described before [439]. Moreover, transient inhibition of TLS could be synthetically lethal to tumour cells that rely on TLS to accumulate more mutations. Human cells contain at least eleven different TLS polymerases, which can act redundantly. Instead of developing specific inhibitors for each of these TLS polymerases, using Ub-PCNA probes to inhibit and mask the signal of ubiquitylated PCNA would save cost and time.

8.3 Upgrading the Ub-PCNA probes

In the ChIP experiments, Ub-PCNA probes enriched at stalled replication forks independently of ubiquitylated PCNA. This observation suggests that the probes bind to other ubiquitylated factors at stressed forks upon crosslinking. Such an off-target binding might happen because the domains of the probes are obtained either from yeast or mammalian proteins. Nevertheless, using synthetic peptides

may increase the specificity of the probes. Designed ankyrin repeat proteins (DARPins) [440], affimers [441], and nanobodies [442] offer different options for such synthetic proteins. Libraries of these entities are screened to find high-affinity binders of the desired protein. In collaboration with Plückthun lab, Dr Christian Renz and Tina Strauch in our lab initiated a DARPins-screen to identify binders of K63-linked polyubiquitin chains. Once a high-affinity and specific DARPin for this type of ubiquitin chain is characterised, it can replace the polyUBD domain of the Ub-PCNA probe aiming for a better avidity to polyubiquitylated PCNA. The Yeast surface display for selective nanobodies provides an even better option for the creation of next-generation Ub-PCNA probes. A previous member of our lab, Dr Sabrina Wegmann, has created tailor-made ubiquitin ligases to produce K63-linked polyubiquitylated PCNA *in vitro*. This *in vitro* ubiquitylated PCNA could be used as a substrate for nanobody screen using the yeast surface display to identify specific binders of K63-polyubiquitylated PCNA. Because yeast is used as an expression system, identified nanobodies would be internally selected against binding to unmodified PCNA. However, the risk of not finding any specific binder or off-target effect of the identified ones should be taken into consideration.

Chapter 9

Appendix

9.1 Abbreviations

4-6 PP	4-6 photoproducts
4-NQO	4-nitroquinoline oxide
53BP1	p53-binding protein 1
8-Oxo-G	8-oxoguanine
9-1-1	Rad9, Hus1, Rad1
aa	Amino acid
AD	Activation domain
AP	Abasic site
APC/C	Anaphase promoting complex/cyclosome
APIM	AlkB homolog 2 PCNA-interaction motif
AQUA	Absolute quantification
ATG8	Autophagy-related protein 8
ATP	Adenosine-5'-triphosphate
BD	Binding domain
BER	Base excision repair
BRCA1/2	Breast cancer susceptibility protein type 1/2
BrdU	5-bromo-2-deoxyuridine
CEN	Centromere
CPD	Cyclobutane-pyrimidine dimer
CPT	Camptothecin
CRL	Cullin-RING ligase
DAmP	Decreased abundance by mRNA perturbation
DARPins	Designed ankyrin repeat proteins
DDB2	Damage specific DNA binding protein 2
DDR	DNA damage response
D-loop	Displacement-loop
DNA	Deoxyribonucleic acid

dNTP	Deoxyribonucleotide triphosphate
Dox	Doxycycline
DSB	Double-strand break
dsDNA	Double-stranded DNA
DDT	DNA damage tolerance
E1	Ubiquitin-activating enzyme
E2	Ubiquitin-conjugating enzyme
E3	Ubiquitin-ligating enzyme (Ubiquitin ligase)
EGFR	Epidermal growth factor receptor
EM	Electron microscopy
ER	Endoplasmatic reticulum
ERAD	ER-associated degradation
EV	Empty vector
FANCD2	Fanconi anemia complementation group D2
FISH	Fluorescent *in situ* hybridisation
FKBP	FK506 binding protein
FRB	FKBP and rapamycin binding
GFP	Green fluorescent protein
HECT	Homology to E6AP C-terminus
HIRAN	HIP116 and Rad5p N-terminal
HJ	Holliday junction
HLTF	Helicase-like transcription factor
HO	Homothallic switching
HR	Homologous Recombination
HU	Hydroxyurea
ICL	Interstrand DNA crosslink
IMAC	Immobilised metal ion affinity chromatography
INQ	Intra-nuclear quality control
IR	Ionising radiation
ISG15	Interferon stimulated gene 15
IsoT	Isopeptidase T
JAMM	JAB1/MPN/Mov34 metalloenzyme
LOH	Loss of heterozygosity
LUBAC	Linear ubiquitin chain assembly complex
MBT	Mid-blastula transition
MCM	Minichromosome maintenance
MGS1	Maintenance of genome stability 1
MIU	Motif interacting with ubiquitin
MJD	Machado-Josephin domain
MMR	Mismatch repair
MS	Mass-spectrometry
MSH2	MutS homolog

N6-MeA	N6-methyladenine
NEDD8	Neural precursor cell expressed, developmentally down-regulated 8
NEM	N-ethylmaleimide
NEMO	Nuclear factor-kB (NF-kB) essential modulator
NER	Nucleotide excision repair
NF-kB	Nuclear factor kappa-light-chain-enhancer of activated B cells
NHEJ	Non-homologous end-joining
NLS	Nuclear localisation signal
NMD	Nonsense-mediated mRNA decay
NZFL	Nuclear protein localisation 4 ZnF
O6-meG	O6-methylguanine
ORFs	Open reading frames
OTU	Ovarian tumour domain
PAD	Polymerase-associated domain
PCNA	Proliferating cell nuclear antigen
PCR	Polymerase chain reaction
PH	Pleckstrin homology
PIP	PCNA interacting peptide
Pol	Polymerase
PORTs	Postreplicative repair territories
PTM	Posttranslational modification
RAD5	Radiation sensitive 5
RAP80	Receptor associated protein 80
RBR	RING-in-between-RING
REV1/3/7	Revisionless1/3/7
RFP	Red fluorescent protein
RING	Really interesting new gene
RMI1	RecQ mediated genome instability 1
RNF8	RING finger protein 8
RNR	Ribonucleotide excision repair
rNTP	Rribonucleotide triphosphate
ROS	Reactive oxygen species
RPA	Replication protein A
RSP5	Reverses Spt- Phenotype 5
S5a	Subunit of the 26S proteasome
SC	Synthetic complete
SCJ	Sister chromatid junction
SDS	Sodium dodecyl sulfate
SGS1	Slow growth suppressor 1
SILAC	Stable isotope labelling with amino acids in cell culture
SIM	SUMO-interaction motif
SIZ1/2	SAP and mIZ-finger domain 1/2

SLD	SUMO-like domain
SMC1/3/5/6	Structural maintenance of chromosomes 1/3/5/6
SRS2	Suppressor of rad six-2
SSB	Single strand break
ssDNA	Single-stranded DNA
STUbL	SUMO-targeted ubiquitin ligase
SUMO	Small ubiquitin-like modifier
TAT	Trans-activator of transcription
TCA	Trichloroacetic acid
TetO	Tetracycline-inducible promoter/operator
TetR	Tetracycline-inducible repressor
TLS	Translesion synthesis
TMT	Tandem mass tag
TOP1/3	Topoisomerase 1/3
TS	Template switching
TUBEs	Tandem-repeated ubiquitin-binding entities
tUIM	Tandem ubiquitin-interacting motif
UBA	Ubiquitin-associated
UBAN	Ubiquitin binding in ABIN and NEMO
UBC9	Ubiquitin conjugating 9
UBD	Ubiquitin binding domain
UbiCRest	Ubiquitin chain restriction
UBL	Ubiquitin-like protein
UBZ	Ubiquitin-binding zinc finger
UCH	Ubiquitin C-terminal hydrolase
UDR	Ubiquitination-dependent recruitment
UDS	Universal doner strain
UFD	Ubiquitin-fusion-degradation
UIM	Ubiquitin-interacting motif
ULP	Ubl-specific protease
USP2	Ubiquitin-specific protease 2
UV	Ultraviolet light
VPS27	Vacuolar protein sorting 27
WCE	Whole-cell extract
XPC	Xeroderma pigmentosum complementation group C
XPV	Xeroderma pigmentosum variant
yeGFP	Yeast enhanced green fluorescent protein
YP	Yeast peptone
YPD	Yeast peptone glucose
ZRANB3	Zinc Finger RANBP2-Type Containing 3

9.2 Supplementary information

The following supplementary information is included on the DVD-ROM, placed on the last page of this thesis:

9.2.1 *In vivo* optimisation of the Ub-PCNA probes

- Uncropped microscopy images of the experiments in chapter 4. A ReadMe file in each folder contains details about the used filter sets and channels.
- Uncropped images of the spotting assays in chapter 4.
- ImageJ scripts used to analyse colocalisation in the experiments of chapter 4.

9.2.2 Spatial and temporal appearance of PCNA ubiquitylation

- Uncropped microscopy images of the experiments in chapter 5. A ReadMe file in each folder contains details about the used filter sets and channels.
- ImageJ scripts used to analyse colocalisation in the experiments of chapter 5.

9.2.3 Detection of PCNA ubiquitylation by ChIP-qPCR

- Raw Ct values of the qPCR results and the calculated percent input values for the experiments of chapter 6.

9.2.4 Ub-PCNA probes in high-throughput genetic screens

- Images of plates from the overexpression genetic screen in each step of library activation and MMS damage.
- Complete list of the ORFs with their respective raw colony size and calculated scores.
- Images of plates from the MMS sensitivity and additivity genetic screens.
- Complete list of gene deletions with their respective MMS sensitivity scores.
- Complete list of gene deletions with their respective scores of additivity to PIP-polyUBD1.

9.3 Publications

Lockhart A, Pires VB, Bento F, Kellner V, Luke-Glaser S, Yakoub G, et al. RNase H1 and H2 Are Differentially Regulated to Process RNA-DNA Hybrids. 2019 Cell Reports;29(9):2890–2900.e5.

9.4 Curriculum vitae

References

[1] Lothrop AP, Torres MP, Fuchs SM. Deciphering Post-Translational Modification Codes. 2013 FEBS Letters;587(8):1247–1257.

[2] Alfano C, Faggiano S, Pastore A. The Ball and Chain of Polyubiquitin Structures. 2016 Trends in Biochemical Sciences;41(4):371–385.

[3] Komander D, Rape M. The Ubiquitin Code. 2012 Annual Review of Biochemistry;81(1):203–229.

[4] Goldstein G, Scheid M, Hammerling U, Schlesinger DH, Niall HD, Boyse EA. Isolation of a Polypeptide That Has Lymphocyte-Differentiating Properties and Is Probably Represented Universally in Living Cells. 1975 Proceedings of the National Academy of Sciences of the United States of America;72(1):11–15.

[5] Ozkaynak E, Finley D, Solomon MJ, Varshavsky A. The Yeast Ubiquitin Genes: A Family of Natural Gene Fusions. 1987 The EMBO Journal;6(5):1429–1439.

[6] Archibald JM, Teh EM, Keeling PJ. Novel Ubiquitin Fusion Proteins: Ribosomal Protein P1 and Actin. 2003 Journal of Molecular Biology;328(4):771–778.

[7] Song C, Feodorova Y, Guy J, Peichl L, Jost KL, Kimura H, et al. DNA Methylation Reader MECP2: Cell Type- and Differentiation Stage-Specific Protein Distribution. 2014 Epigenetics & Chromatin;7(1):1–17.

[8] Vijay-Kumar S, Bugg CE, Cook WJ. Structure of Ubiquitin Refined at 1.8Åresolution. 1987 Journal of Molecular Biology;194(3):531–544.

[9] Schlesinger DH, Goldstein G, Niall HD. Complete Amino Acid Sequence of Ubiquitin, an Adenylate Cyclase Stimulating Polypeptide Probably Universal in Living Cells. 1975 Biochemistry;14(10):2214–2218.

[10] Hurley JH, Lee S, Prag G. Ubiquitin-Binding Domains. 2006 Biochemical Journal;399(3):361–372.

[11] Komander D. The Emerging Complexity of Protein Ubiquitination. 2009 Biochemical Society Transactions;37(5):937–953.

[12] Ronau JA, Beckmann JF, Hochstrasser M. Substrate Specificity of the Ubiquitin and Ubl Proteases. 2016 Cell Research;26(4):441–456.

[13] Cook WJ, Jeffrey LC, Carson M, Chenlal Z. Structure of a Diubiquitin Conjugate and a Model for Interaction with Ubiquitin Conjugating Enzyme(E2). 1992 The Journal of Biological Chemistry;267(23):16467–1647.

[14] Komander D, Reyes-Turcu F, Licchesi JDF, Odenwaelder P, Wilkinson KD, Barford D. Molecular Discrimination of Structurally Equivalent Lys 63-Linked and Linear Polyubiquitin Chains. 2009 EMBO Reports;10(5):466–473.

[15] Deshaies RJ, Joazeiro CAP. RING Domain E3 Ubiquitin Ligases. 2009 Annual Review of Biochemistry;78(1):399–434.

[16] Dikic I, Wakatsuki S, Walters KJ. Ubiquitin-Binding Domains — from Structures to Functions. 2009 Nature Reviews Molecular Cell Biology;10(10):659–671.

[17] Ye Y, Rape M. Building Ubiquitin Chains: E2 Enzymes at Work. 2009 Nature reviews Molecular cell biology;10(11):755–764.

[18] Hoege C, Pfander B, Moldovan GL, Pyrowolakis G, Jentsch S. RAD6 -Dependent DNA Repair Is Linked to Modification of PCNA by Ubiquitin and SUMO. 2002 Nature;419(6903):135–141.

[19] Haglund K, Sigismund S, Polo S, Szymkiewicz I, Di Fiore PP, Dikic I. Multiple Monoubiquitination of RTKs Is Sufficient for Their Endocytosis and Degradation. 2003 Nature Cell Biology;5(5):461–466.

[20] Hicke L. Protein Regulation by Monoubiquitin. 2001 Nature Reviews Molecular Cell Biology;2(3):195–201.

[21] Boname JM, Thomas M, Stagg HR, Xu P, Peng J, Lehner PJ. Efficient Internalization of MHC I Requires Lysine-11 and Lysine-63 Mixed Linkage Polyubiquitin Chains. 2010 Traffic (Copenhagen, Denmark);11(2):210–220.

[22] Ohtake F, Saeki Y, Ishido S, Kanno J, Tanaka K. The K48-K63 Branched Ubiquitin Chain Regulates NF-κB Signaling. 2016 Molecular Cell;64(2):251–266.

[23] Swatek KN, Komander D. Ubiquitin Modifications. 2016 Cell Research;26(4):399–422.

[24] Xu P, Duong DM, Seyfried NT, Cheng D, Xie Y, Robert J, et al. Quantitative Proteomics Reveals the Function of Unconventional Ubiquitin Chains in Proteasomal Degradation. 2009 Cell;137(1):133–145.

[25] Matsumoto ML, Castellanos ER, Zeng YJ, Kirkpatrick DS. Interpreting the Language of Polyubiquitin with Linkage-Specific Antibodies and Mass Spectrometry. In: Mayor T, Kleiger G, editors. The Ubiquitin Proteasome System: Methods and Protocols. Methods in Molecular Biology; 2018. p. 385–400.

[26] Kim W, Bennett EJ, Huttlin EL, Guo A, Li J, Possemato A, et al. Systematic and Quantitative Assessment of the Ubiquitin-Modified Proteome. 2011 Molecular Cell;44(2):325–340.

[27] Chau V, Tobias JW, Bachmair A, Marriott D, Ecker DJ, Gonda DK, et al. A Multiubiquitin Chain Is Confined to Specific Lysine in a Targeted Short-Lived Protein. 1989 Science;243(4898):1576–1583.

[28] Petroski MD, Deshaies RJ. Function and Regulation of Cullin–RING Ubiquitin Ligases. 2005 Nature Reviews Molecular Cell Biology;6(1):9–20.

[29] Kim HC, Huibregtse JM. Polyubiquitination by HECT E3s and the Determinants of Chain Type Specificity. 2009 Molecular and Cellular Biology;29(12):3307–3318.

[30] Peng J, Schwartz D, Elias JE, Thoreen CC, Cheng D, Marsischky G, et al. A Proteomics Approach to Understanding Protein Ubiquitination. 2003 Nature Biotechnology;21(8):921–926.

[31] Jin L, Williamson A, Banerjee S, Philipp I, Rape M. Mechanism of Ubiquitin-Chain Formation by the Human Anaphase-Promoting Complex. 2008 Cell;133(4):653–665.

[32] Matsumoto ML, Wickliffe KE, Dong KC, Yu C, Bosanac I, Bustos D, et al. K11-Linked Polyubiquitination in Cell Cycle Control Revealed by a K11 Linkage-Specific Antibody. 2010 Molecular Cell;39(3):477–484.

[33] Verma R, Chen S, Feldman R, Schieltz D, Yates J, Dohmen J, et al. Proteasomal Proteomics: Identification of Nucleotide-Sensitive Proteasome-Interacting Proteins by Mass Spectrometric Analysis of Affinity-Purified Proteasomes. 2000 Molecular Biology of the Cell;11(10):3425–3439.

[34] Seeger M, Hartmann-Petersen R, Wilkinson CRM, Wallace M, Samejima I, Taylor MS, et al. Interaction of the Anaphase-Promoting Complex/Cyclosome and Proteasome Protein Complexes with Multiubiquitin Chain-Binding Proteins. 2003 Journal of Biological Chemistry;278(19):16791–16796.

[35] Johnson ES, Ma PCM, Ota IM, Varshavsky A. A Proteolytic Pathway That Recognizes Ubiquitin as a Degradation Signal. 1995 Journal of Biological Chemistry;270(29):17442–17456.

[36] Saeki Y, Kudo T, Sone T, Kikuchi Y, Yokosawa H, Toh-e A, et al. Lysine 63-Linked Polyubiquitin Chain May Serve as a Targeting Signal for the 26S Proteasome. 2009 The EMBO Journal;28(4):359–371.

[37] Finley D, Ulrich HD, Sommer T, Kaiser P. The Ubiquitin–Proteasome System of Saccharomyces Cerevisiae. 2012 Genetics;192(2):319–360.

[38] Mukhopadhyay D, Riezman H. Proteasome-Independent Functions of Ubiquitin in Endocytosis and Signaling. 2007 Science;315(5809):201–205.

[39] Terrell J, Shih S, Dunn R, Hicke L. A Function for Monoubiquitination in the Internalization of a G Protein–Coupled Receptor. 1998 Molecular Cell;1(2):193–202.

[40] Huang F, Kirkpatrick D, Jiang X, Gygi S, Sorkin A. Differential Regulation of EGF Receptor Internalization and Degradation by Multiubiquitination within the Kinase Domain. 2006 Molecular Cell;21(6):737–748.

[41] Moldovan GL, D'Andrea AD. How the Fanconi Anemia Pathway Guards the Genome. 2009 Annual Review of Genetics;43(1):223–249.

[42] Spence J, Gali RR, Dittmar G, Sherman F, Karin M, Finley D. Cell Cycle–Regulated Modification of the Ribosome by a Variant Multiubiquitin Chain. 2000 Cell;102(1):67–76.

[43] Schwertman P, Bekker-Jensen S, Mailand N. Regulation of DNA Double-Strand Break Repair by Ubiquitin and Ubiquitin-like Modifiers. 2016 Nature Reviews Molecular Cell Biology;17(6):379–394.

[44] Komander D, Clague MJ, Urbé S. Breaking the Chains: Structure and Function of the Deubiquitinases. 2009 Nature Reviews Molecular Cell Biology;10(8):550–563.

[45] Li M. Mono- Versus Polyubiquitination: Differential Control of P53 Fate by Mdm2. 2003 Science;302(5652):1972–1975.

[46] Winston JT, Strack P, Beer-Romero P, Chu CY, Elledge SJ, Harper JW. The SCFβ-TRCP–Ubiquitin Ligase Complex Associates Specifically with Phosphorylated Destruction Motifs in IκBα and β-Catenin and Stimulates IκBα Ubiquitination in Vitro. 1999 Genes & Development;13(3):270–283.

[47] Palombella VJ, Rando OJ, Goldberg AL, Maniatis T. The Ubiquitinproteasome Pathway Is Required for Processing the NF-κB1 Precursor Protein and the Activation of NF-κB. 1994 Cell;78(5):773–785.

[48] Rahighi S, Ikeda F, Kawasaki M, Akutsu M, Suzuki N, Kato R, et al. Specific Recognition of Linear Ubiquitin Chains by NEMO Is Important for NF-κB Activation. 2009 Cell;136(6):1098–1109.

[49] Wang C, Deng L, Hong M, Akkaraju GR, Inoue Ji, Chen ZJ. TAK1 Is a Ubiquitin-Dependent Kinase of MKK and IKK. 2001 Nature;412(6844):346–351.

[50] McGrath JP, Jentsch S, Varshavsky A. UBA 1: An Essential Yeast Gene Encoding Ubiquitin-Activating Enzyme. 1991 The EMBO Journal;10(1):227–236.

[51] Ghaboosi N, Deshaies RJ. A Conditional Yeast E1 Mutant Blocks the Ubiquitin–Proteasome Pathway and Reveals a Role for Ubiquitin Conjugates in Targeting Rad23 to the Proteasome. 2007 Molecular Biology of the Cell;18(5):1953–1963.

[52] Jin J, Li X, Gygi SP, Harper JW. Dual E1 Activation Systems for Ubiquitin Differentially Regulate E2 Enzyme Charging. 2007 Nature;447(7148):1135–1138.

[53] Schulman BA, Wade Harper J. Ubiquitin-like Protein Activation by E1 Enzymes: The Apex for Downstream Signalling Pathways. 2009 Nature Reviews Molecular Cell Biology;10(5):319–331.

[54] Eletr ZM, Huang DT, Duda DM, Schulman BA, Kuhlman B. E2 Conjugating Enzymes Must Disengage from Their E1 Enzymes before E3-Dependent Ubiquitin and Ubiquitin-like Transfer. 2005 Nature Structural & Molecular Biology;12(10):933–934.

[55] Johnson ES, Blobel G. Ubc9p Is the Conjugating Enzyme for the Ubiquitin-like Protein Smt3p. 1997 Journal of Biological Chemistry;272(43):26799–26802.

[56] Liakopoulos D, Doenges G, Matuschewski K, Jentsch S. A Novel Protein Modification Pathway Related to the Ubiquitin System. 1998 The EMBO Journal;17(8):2208–2214.

[57] Goebl MG, Yochem J, Jentsch S, McGrath JP, Varshavsky A, Byers B. The Yeast Cell Cycle Gene CDC34 Encodes a Ubiquitin-Conjugating Enzyme. 1988 Science;241(4871):1331–1335.

[58] Stewart MD, Ritterhoff T, Klevit RE, Brzovic PS. E2 Enzymes: More than Just Middle Men. 2016 Cell Research;26(4):423–440.

[59] Scheffner M, Nuber U, Huibregtse JM. Protein Ubiquitination Involving an E1–E2–E3 Enzyme Ubiquitin Thioester Cascade. 1995 Nature;373(6509):81–83.

[60] Huang L, Kinnucan E, Wang G, Beaudenon S, Howley PM, Huibregtse JM, et al. Structure of an E6AP-UbcH7 Complex: Insights into Ubiquitination by the E2-E3 Enzyme Cascade. 1999 Science;286(5443):1321–1326.

[61] Zheng N, Wang P, Jeffrey PD, Pavletich NP. Structure of a C-Cbl–UbcH7 Complex: RING Domain Function in Ubiquitin-Protein Ligases. 2000 Cell;102(4):533–539.

[62] Metzger MB, Pruneda JN, Klevit RE, Weissman AM. RING-Type E3 Ligases: Master Manipulators of E2 Ubiquitin-Conjugating Enzymes and Ubiquitination. 2014 Biochimica et biophysica acta;1843(1):47–60.

[63] Pesin JA, Orr-Weaver TL. Regulation of APC/C Activators in Mitosis and Meiosis. 2008 Annual Review of Cell and Developmental Biology;24(1):475–499.

[64] McLean JR, Chaix D, Ohi MD, Gould KL. State of the APC/C: Organization, Function, and Structure. 2011 Critical Reviews in Biochemistry and Molecular Biology;46(2):118–136.

[65] Duda DM, Scott DC, Calabrese MF, Zimmerman ES, Zheng N, Schulman BA. Structural Regulation of Cullin-RING Ubiquitin Ligase Complexes. 2011 Current Opinion in Structural Biology;21(2):257–264.

[66] Wenzel DM, Lissounov A, Brzovic PS, Klevit RE. UBCH7 Reactivity Profile Reveals Parkin and HHARI to Be RING/HECT Hybrids. 2011 Nature;474(7349):105–108.

[67] Wenzel DM, Klevit RE. Following Ariadne's Thread: A New Perspective on RBR Ubiquitin Ligases. 2012 BMC Biology;10(1):24–31.

[68] Hicke L, Schubert HL, Hill CP. Ubiquitin-Binding Domains. 2005 Nature Reviews Molecular Cell Biology;6(8):610–621.

[69] Sato Y, Yoshikawa A, Mimura H, Yamashita M, Yamagata A, Fukai S. Structural Basis for Specific Recognition of Lys 63-Linked Polyubiquitin Chains by Tandem UIMs of RAP80. 2009 The EMBO Journal;28(16):2461–2468.

[70] Sims JJ, Cohen RE. Linkage-Specific Avidity Defines the Lysine 63-Linked Polyubiquitin-Binding Preference of Rap80. 2009 Molecular Cell;33(6):775–783.

[71] Swanson KA, Kang RS, Stamenova SD, Hicke L, Radhakrishnan I. Solution Structure of Vps27 UIM–Ubiquitin Complex Important for Endosomal Sorting and Receptor Downregulation. 2003 The EMBO Journal;22(18):4597–4606.

[72] Newton K, Matsumoto ML, Wertz IE, Kirkpatrick DS, Lill JR, Tan J, et al. Ubiquitin Chain Editing Revealed by Polyubiquitin Linkage-Specific Antibodies. 2008 Cell;134(4):668–678.

[73] Lo YC, Lin SC, Rospigliosi CC, Conze DB, Wu CJ, Ashwell JD, et al. Structural Basis for Recognition of Diubiquitins by NEMO. 2009 Molecular Cell;33(5):602–615.

[74] Varadan R, Assfalg M, Raasi S, Pickart C, Fushman D. Structural Determinants for Selective Recognition of a Lys48-Linked Polyubiquitin Chain by a UBA Domain. 2005 Molecular Cell;18(6):687–698.

[75] Trempe JF, Brown NR, Lowe ED, Gordon C, Campbell ID, Noble ME, et al. Mechanism of Lys48-Linked Polyubiquitin Chain Recognition by the Mud1 UBA Domain. 2005 The EMBO Journal;24(18):3178–3189.

[76] Kulathu Y, Akutsu M, Bremm A, Hofmann K, Komander D. Two-Sided Ubiquitin Binding Explains Specificity of the TAB2 NZF Domain. 2009 Nature Structural & Molecular Biology;16(12):1328–30.

[77] Bosanac I, Wertz IE, Pan B, Yu C, Kusam S, Lam C, et al. Ubiquitin Binding to A20 ZnF4 Is Required for Modulation of NF-κB Signaling. 2010 Molecular Cell;40(4):548–557.

[78] Reyes-Turcu FE, Ventii KH, Wilkinson KD. Regulation and Cellular Roles of Ubiquitin-Specific Deubiquitinating Enzymes. 2009 Annual Review of Biochemistry;78(1):363–397.

[79] Ouyang H, Ali YO, Ravichandran M, Dong A, Qiu W, MacKenzie F, et al. Protein Aggregates Are Recruited to Aggresome by Histone Deacetylase 6 via Unanchored Ubiquitin C Termini. 2012 The Journal of Biological Chemistry;287(4):2317–2327.

[80] Bienko M. Ubiquitin-Binding Domains in Y-Family Polymerases Regulate Translesion Synthesis. 2005 Science;310(5755):1821–1824.

[81] Yuan J, Ghosal G, Chen J. The HARP-like Domain-Containing Protein AH2/ZRANB3 Binds to PCNA and Participates in Cellular Response to Replication Stress. 2012 Molecular Cell;47(3):410–421.

[82] Weston R, Peeters H, Ahel D. ZRANB3 Is a Structure-Specific ATP-Dependent Endonuclease Involved in Replication Stress Response. 2012 Genes & Development;26(14):1558–1572.

[83] Ciccia A, Nimonkar AV, Hu Y, Hajdu I, Achar YJ, Izhar L, et al. Polyubiquitinated PCNA Recruits the ZRANB3 Translocase to Maintain Genomic Integrity after Replication Stress. 2012 Molecular Cell;47(3):396–409.

[84] MacKay C, Déclais AC, Lundin C, Agostinho A, Deans AJ, MacArtney TJ, et al. Identification of KIAA1018/FAN1, a DNA Repair Nuclease Recruited to DNA Damage by Monoubiquitinated FANCD2. 2010 Cell;142(1):65–76.

[85] Fradet-Turcotte A, Canny MD, Escribano-Díaz C, Orthwein A, Leung CCY, Huang H, et al. 53BP1 Is a Reader of the DNA-Damage-Induced H2A Lys 15 Ubiquitin Mark. 2013 Nature;499(7456):50–54.

[86] Verma R, Aravind L, Oania R, McDonald WH, Yates JR, Koonin EV, et al. Role of Rpn11 Metalloprotease in Deubiquitination and Degradation by the 26S Proteasome. 2002 Science;298(5593):611–615.

[87] Yao T, Cohen RE. A Cryptic Protease Couples Deubiquitination and Degradation by the Proteasome. 2002 Nature;419(6905):403–407.

[88] Henry KW, Wyce A, Lo WS, Duggan LJ, Emre NCT, Kao CF, et al. Transcriptional Activation via Sequential Histone H2B Ubiquitylation and Deubiquitylation, Mediated by SAGA-Associated Ubp8. 2003 Genes & Development;17(21):2648–2663.

[89] Amerik A, Sindhi N, Hochstrasser M. A Conserved Late Endosome–Targeting Signal Required for Doa4 Deubiquitylating Enzyme Function. 2006 Journal of Cell Biology;175(5):825–835.

[90] Luhtala N, Odorizzi G. Bro1 Coordinates Deubiquitination in the Multivesicular Body Pathway by Recruiting Doa4 to Endosomes. 2004 Journal of Cell Biology;166(5):717–729.

[91] Kinner A, Kölling R. The Yeast Deubiquitinating Enzyme Ubp16 Is Anchored to the Outer Mitochondrial Membrane. 2003 FEBS Letters;549(1-3):135–140.

[92] Hanna J, Hathaway NA, Tone Y, Crosas B, Elsasser S, Kirkpatrick DS, et al. Deubiquitinating Enzyme Ubp6 Functions Noncatalytically to Delay Proteasomal Degradation. 2006 Cell;127(1):99–111.

[93] Dikic I. Proteasomal and Autophagic Degradation Systems. 2017 Annual Review of Biochemistry;86(1):193–224.

[94] Finley D, Özkaynak E, Varshavsky A. The Yeast Polyubiquitin Gene Is Essential for Resistance to High Temperatures, Starvation, and Other Stresses. 1987 Cell;48(6):1035–1046.

[95] Finley D, Bartel B, Varshavsky A. The Tails of Ubiquitin Precursors Are Ribosomal Proteins Whose Fusion to Ubiquitin Facilitates Ribosome Biogenesis. 1989 Nature;338(6214):394–401.

[96] Baker RT, Board PG. The Human Ubiquitin-52 Amino Acid Fusion Protein Gene Shares Several Structural Features with Mammalian Ribosomal Protein Genes. 1991 Nucleic Acids Research;19(5):1035–1040.

[97] Wiborg O, Pedersen Ms, Wind A, Berglund Le, Marcker Ka, Vuust J. The Human Ubiquitin Multigene Family: Some Genes Contain Multiple Directly Repeated Ubiquitin Coding Sequences. 1985 The EMBO Journal;4(3):755–759.

[98] Turner GC, Varshavsky A. Detecting and Measuring Cotranslational Protein Degradation in Vivo. 2000 Science;289(5487):2117–2120.

[99] Leggett DS, Hanna J, Borodovsky A, Crosas B, Schmidt M, Baker RT, et al. Multiple Associated Proteins Regulate Proteasome Structure and Function. 2002 Molecular Cell;10(3):495–507.

[100] Kee Y, Lyon N, Huibregtse JM. The Rsp5 Ubiquitin Ligase Is Coupled to and Antagonized by the Ubp2 Deubiquitinating Enzyme. 2005 The EMBO Journal;24(13):2414–2424.

[101] Wang T, Yin L, Cooper EM, Lai MY, Dickey S, Pickart CM, et al. Evidence for Bidentate Substrate Binding as the Basis for the K48 Linkage Specificity of OTUBAIN 1. 2009 Journal of molecular biology;386(4):1011.

[102] Bremm A, Freund SMV, Komander D. Lys11-Linked Ubiquitin Chains Adopt Compact Conformations and Are Preferentially Hydrolyzed by the Deubiquitinase Cezanne. 2010 Nature Structural & Molecular Biology;17(8):939–947.

[103] Deng L, Wang C, Spencer E, Yang L, Braun A, You J, et al. Activation of the IκB Kinase Complex by TRAF6 Requires a Dimeric Ubiquitin-Conjugating Enzyme Complex and a Unique Polyubiquitin Chain. 2000 Cell;103(2):351–361.

[104] Takahashi TS, Wollscheid HP, Lowther J, Ulrich HD. Effects of Chain Length and Geometry on the Activation of DNA Damage Bypass by Polyubiquitylated PCNA. 2020 Nucleic Acids Research;48(6):3024–3052.

[105] Xu M, Skaug B, Zeng W, Chen ZJ. A Ubiquitin Replacement Strategy in Human Cells Reveals Distinct Mechanisms of IKK Activation by TNFα and IL-1β. 2009 Molecular Cell;36(2):302–314.

[106] Matsumoto ML, Dong KC, Yu C, Phu L, Gao X, Hannoush RN, et al. Engineering and Structural Characterization of a Linear Polyubiquitin-Specific Antibody. 2012 Journal of Molecular Biology;418(3):134–144.

[107] Sims JJ, Scavone F, Cooper EM, Kane LA, Youle RJ, Boeke JD, et al. Polyubiquitin-Sensor Proteins Reveal Localization and Linkage-Type Dependence of Cellular Ubiquitin Signaling. 2012 Nature Methods;9(3):303–309.

[108] Hjerpe R, Aillet F, Lopitz-Otsoa F, Lang V, England P, Rodriguez MS. Efficient Protection and Isolation of Ubiquitylated Proteins Using Tandem Ubiquitin-Binding Entities. 2009 EMBO reports;10(11):1250–1258.

[109] Yoshida Y, Saeki Y, Tsuchiya H, Tanaka K. Detection of Ubiquitination Activity and Identification of Ubiquitinated Substrates Using TR-TUBE. In: Methods in Enzymology. vol. 618. Elsevier; 2019. p. 135–147.

[110] van Wijk SJL, Fiskin E, Putyrski M, Pampaloni F, Hou J, Wild P, et al. Fluorescence-Based Sensors to Monitor Localization and Functions of Linear and K63-Linked Ubiquitin Chains in Cells. 2012 Molecular Cell;47(5):797–809.

[111] Hospenthal MK, Mevissen TET, Komander D. Deubiquitinase-Based Analysis of Ubiquitin Chain Architecture Using Ubiquitin Chain Restriction (UbiCRest). 2015 Nature Protocols;10(2):349–361.

[112] Tiede C, Tang AAS, Deacon SE, Mandal U, Nettleship JE, Owen RL, et al. Adhiron: A Stable and Versatile Peptide Display Scaffold for Molecular Recognition Applications. 2014 Protein Engineering, Design and Selection;27(5):145–155.

[113] Hughes DJ, Tiede C, Penswick N, Tang AAS, Trinh CH, Mandal U, et al. Generation of Specific Inhibitors of SUMO1- and SUMO2/3-Mediated Protein-Protein Interactions Using Affimer (Adhiron) Technology. 2017 Science signaling;10(505):1–13.

[114] Ordureau A, Münch C, Harper JW. Quantifying Ubiquitin Signaling. 2015 Molecular Cell;58(4):660–676.

[115] Thompson A, Schäfer J, Kuhn K, Kienle S, Schwarz J, Schmidt G, et al. Tandem Mass Tags: A Novel Quantification Strategy for Comparative Analysis of Complex Protein Mixtures by MS/MS. 2003 Analytical Chemistry;75(8):1895–1904.

[116] Ong SE, Blagoev B, Kratchmarova I, Kristensen DB, Steen H, Pandey A, et al. Stable Isotope Labeling by Amino Acids in Cell Culture, SILAC, as a Simple and Accurate Approach to Expression Proteomics. 2002 Molecular & Cellular Proteomics;1(5):376–386.

[117] Kirkpatrick DS, Gerber SA, Gygi SP. The Absolute Quantification Strategy: A General Procedure for the Quantification of Proteins and Post-Translational Modifications. 2005 Methods;35(3):265–273.

[118] Bustos D, Bakalarski CE, Yang Y, Peng J, Kirkpatrick DS. Characterizing Ubiquitination Sites by Peptide-Based Immunoaffinity Enrichment. 2012 Molecular & Cellular Proteomics;11(12):1529–1540.

[119] Jackson SP, Bartek J. The DNA-Damage Response in Human Biology and Disease. 2009 Nature;461(7267):1071–1078.

[120] Harper JW, Elledge SJ. The DNA Damage Response: Ten Years After. 2007 Molecular Cell;28(5):739–745.

[121] Nair N, Shoaib M, Sørensen CS. Chromatin Dynamics in Genome Stability: Roles in Suppressing Endogenous DNA Damage and Facilitating DNA Repair. 2017 International Journal of Molecular Sciences;18(7):1486–1507.

[122] Chatterjee N, Walker GC. Mechanisms of DNA Damage, Repair and Mutagenesis. 2017 Environmental and molecular mutagenesis;58(5):235–263.

[123] Beranek DT. Distribution of Methyl and Ethyl Adducts Following Alkylation with Monofunctional Alkylating Agents. 1990 Mutation Research/Fundamental and Molecular Mechanisms of Mutagenesis;231(1):11–30.

[124] Drabløs F, Feyzi E, Aas PA, Vaagbø CB, Kavli B, Bratlie MS, et al. Alkylation Damage in DNA and RNA—Repair Mechanisms and Medical Significance. 2004 DNA Repair;3(11):1389–1407.

[125] Sinha RP, Häder DP. UV-Induced DNA Damage and Repair: A Review. 2002 Photochemical & Photobiological Sciences;1(4):225–236.

[126] Krakoff IH, Brown NC, Reichard P. Inhibition of Ribonucleoside Diphosphate Reductase by Hydroxyurea. 1968 Cancer Research;28(8):1559–1565.

[127] Branzei D, Foiani M. The DNA Damage Response during DNA Replication. 2005 Current Opinion in Cell Biology;17(6):568–575.

[128] Davies AA, Huttner D, Daigaku Y, Chen S, Ulrich HD. Activation of Ubiquitin-Dependent DNA Damage Bypass Is Mediated by Replication Protein A. 2008 Molecular Cell;29(5):625–636.

[129] Liu LF, Desai SD, Li TK, Mao Y, Sun M, Sim SP. Mechanism of Action of Camptothecin. 2000 Annals of the New York Academy of Sciences;922(1):1–10.

[130] Povirk LF, Wübker W, Köhnlein W, Hutchinson F. DNA Double-Strand Breaks and Alkali-Labile Bonds Produced by Bleomycin. 1977 Nucleic Acids Research;4(10):3573–3580.

[131] Chankova SG, Dimova E, Dimitrova M, Bryant PE. Induction of DNA Double-Strand Breaks by Zeocin in Chlamydomonas Reinhardtii and the Role of Increased DNA Double-Strand Breaks Rejoining in the Formation of an Adaptive Response. 2007 Radiation and Environmental Biophysics;46(4):409–416.

[132] Manova V, Gruszka D. DNA Damage and Repair in Plants – from Models to Crops. 2015 Frontiers in Plant Science;6(885):1–26.

[133] Masai H, Matsumoto S, You Z, Yoshizawa-Sugata N, Oda M. Eukaryotic Chromosome DNA Replication: Where, When, and How? 2010 Annual Review of Biochemistry;79(1):89–130.

[134] Woodward AM, Göhler T, Luciani MG, Oehlmann M, Ge X, Gartner A, et al. Excess Mcm2–7 License Dormant Origins of Replication That Can Be Used under Conditions of Replicative Stress. 2006 The Journal of Cell Biology;173(5):673–683.

[135] McIntosh D, Blow JJ. Dormant Origins, the Licensing Checkpoint, and the Response to Replicative Stresses. 2012 Cold Spring Harbor Perspectives in Biology;4(10):1–10.

[136] Pacek M, Walter JC. A Requirement for MCM7 and Cdc45 in Chromosome Unwinding during Eukaryotic DNA Replication. 2004 The EMBO Journal;23(18):3667–3676.

[137] Zeman MK, Cimprich KA. Causes and Consequences of Replication Stress. 2014 Nature Cell Biology;16(1):2–9.

[138] Bester AC, Roniger M, Oren YS, Im MM, Sarni D, Chaoat M, et al. Nucleotide Deficiency Promotes Genomic Instability in Early Stages of Cancer Development. 2011 Cell;145(3):435–446.

[139] Dalgaard JZ. Causes and Consequences of Ribonucleotide Incorporation into Nuclear DNA. 2012 Trends in Genetics;28(12):592–597.

[140] Sparks JL, Chon H, Cerritelli SM, Kunkel TA, Johansson E, Crouch RJ, et al. RNase H2-Initiated Ribonucleotide Excision Repair. 2012 Molecular Cell;47(6):980–986.

[141] Kim JC, Mirkin SM. The Balancing Act of DNA Repeat Expansions. 2013 Current Opinion in Genetics & Development;23(3):280–288.

[142] Bochman ML, Paeschke K, Zakian VA. DNA Secondary Structures: Stability and Function of G-Quadruplex Structures. 2012 Nature Reviews Genetics;13(11):770–780.

[143] Aguilera A, García-Muse T. R Loops: From Transcription Byproducts to Threats to Genome Stability. 2012 Molecular Cell;46(2):115–124.

[144] Niehrs C, Luke B. Regulatory R-Loops as Facilitators of Gene Expression and Genome Stability. 2020 Nature Reviews Molecular Cell Biology;21:167–178.

[145] Jackson SP, Durocher D. Regulation of DNA Damage Responses by Ubiquitin and SUMO. 2013 Molecular Cell;49(5):795–807.

[146] Yates M, Maréchal A. Ubiquitylation at the Fork: Making and Breaking Chains to Complete DNA Replication. 2018 International Journal of Molecular Sciences;19(10):2909.

[147] García-Rodríguez N, Wong RP, Ulrich HD. Functions of Ubiquitin and SUMO in DNA Replication and Replication Stress. 2016 Frontiers in Genetics;7(87):1–28.

[148] Povlsen LK, Beli P, Wagner SA, Poulsen SL, Sylvestersen KB, Poulsen JW, et al. Systems-Wide Analysis of Ubiquitylation Dynamics Reveals a Key Role for PAF15 Ubiquitylation in DNA-Damage Bypass. 2012 Nature Cell Biology;14(10):1089–1098.

[149] Elia AEH, Boardman AP, Wang DC, Huttlin EL, Everley RA, Dephoure N, et al. Quantitative Proteomic Atlas of Ubiquitination and Acetylation in the DNA Damage Response. 2015 Molecular Cell;59(5):867–881.

[150] Dungrawala H, Rose KL, Bhat KP, Mohni KN, Glick GG, Couch FB, et al. The Replication Checkpoint Prevents Two Types of Fork Collapse without Regulating Replisome Stability. 2015 Molecular Cell;59(6):998–1010.

[151] Maréchal A, Li JM, Ji XY, Wu CS, Yazinski SA, Nguyen HD, et al. PRP19 Transforms into a Sensor of RPA-ssDNA after DNA Damage and Drives ATR Activation via a Ubiquitin-Mediated Circuitry. 2014 Molecular Cell;53(2):235–246.

[152] Dubois JC, Yates M, Gaudreau-Lapierre A, Clément G, Cappadocia L, Gaudreau L, et al. A Phosphorylation-and-Ubiquitylation Circuitry Driving ATR Activation and Homologous Recombination. 2017 Nucleic Acids Research;45(15):8859–8872.

[153] de Moura TR, Mozaffari-Jovin S, Szabó CZK, Schmitzová J, Dybkov O, Cretu C, et al. Prp19/Pso4 Is an Autoinhibited Ubiquitin Ligase Activated by Stepwise Assembly of Three Splicing Factors. 2018 Molecular Cell;69(6):979–992.e6.

[154] Lin YC, Wang Y, Hsu R, Giri S, Wopat S, Arif MK, et al. PCNA-Mediated Stabilization of E3 Ligase RFWD3 at the Replication Fork Is Essential for DNA Replication. 2018 Proceedings of the National Academy of Sciences;115(52):13282–13287.

[155] Elia AEH, Wang DC, Willis NA, Boardman AP, Hajdu I, Adeyemi RO, et al. RFWD3-Dependent Ubiquitination of RPA Regulates Repair at Stalled Replication Forks. 2015 Molecular Cell;60(2):280–293.

[156] Inano S, Sato K, Katsuki Y, Kobayashi W, Tanaka H, Nakajima K, et al. RFWD3-Mediated Ubiquitination Promotes Timely Removal of Both RPA and RAD51 from DNA Damage Sites to Facilitate Homologous Recombination. 2017 Molecular Cell;66(5):622–634.e8.

[157] Parker JL, Bielen AB, Dikic I, Ulrich HD. Contributions of Ubiquitin- and PCNA-Binding Domains to the Activity of Polymerase Eta in Saccharomyces Cerevisiae. 2007 Nucleic Acids Research;35(3):881–889.

[158] Skoneczna A, McIntyre J, Skoneczny M, Policinska Z, Sledziewska-Gojska E. Polymerase Eta Is a Short-Lived, Proteasomally Degraded Protein That Is Temporarily Stabilized Following UV Irradiation in Saccharomyces Cerevisiae. 2007 Journal of Molecular Biology;366(4):1074–1086.

[159] Trujillo KM, Osley MA. A Role for H2B Ubiquitylation in DNA Replication. 2012 Molecular Cell;48(5):734–746.

[160] Scrima A, Fischer ES, Lingaraju GM, Böhm K, Cavadini S, Thomä NH. Detecting UV-Lesions in the Genome: The Modular CRL4 Ubiquitin Ligase Does It Best! 2011 FEBS Letters;585(18):2818–2825.

[161] Lehner K, Jinks-Robertson S. Shared Genetic Pathways Contribute to the Tolerance of Endogenous and Low-Dose Exogenous DNA Damage in Yeast. 2014 Genetics;198(2):519–530.

[162] Ulrich HD. Timing and Spacing of Ubiquitin-Dependent DNA Damage Bypass. 2011 FEBS Letters;585(18):2861–2867.

[163] Wong RP, García-Rodríguez N, Zilio N, Hanulová M, Ulrich HD. Processing of DNA Polymerase-Blocking Lesions during Genome Replication Is Spatially and Temporally Segregated from Replication Forks. 2020 Molecular Cell;77(1):3–16.e4.

[164] Lehmann A, Niimi A, Ogi T, Brown S, Sabbioneda S, Wing J, et al. Translesion Synthesis: Y-Family Polymerases and the Polymerase Switch. 2007 DNA Repair;6(7):891–899.

[165] Stelter P, Ulrich HD. Control of Spontaneous and Damage-Induced Mutagenesis by SUMO and Ubiquitin Conjugation. 2003 Nature;425(6954):188–191.

[166] Parker JL, Ulrich HD. Mechanistic Analysis of PCNA Poly-Ubiquitylation by the Ubiquitin Protein Ligases Rad18 and Rad5. 2009 The EMBO Journal;28(23):3657–3666.

[167] Branzei D, Foiani M. Maintaining Genome Stability at the Replication Fork. 2010 Nature Reviews Molecular Cell Biology;11(3):208–219.

[168] Neelsen KJ, Chaudhuri AR, Follonier C, Herrador R, Lopes M. Visualization and Interpretation of Eukaryotic DNA Replication Intermediates In Vivo by Electron Microscopy. In: Stockert JC, Espada J, Blázquez-Castro A, editors. Functional Analysis of DNA and Chromatin. vol. 1094. Totowa, NJ: Humana Press; 2014. p. 177–208.

[169] Branzei D. Ubiquitin Family Modifications and Template Switching. 2011 FEBS Letters;585(18):2810–2817.

[170] Álvarez V, Frattini C, Sacristán MP, Gallego-Sánchez A, Bermejo R, Bueno A. PCNA Deubiquitylases Control DNA Damage Bypass at Replication Forks. 2019 Cell Reports;29(5):1323–1335.e5.

[171] Huang TT, Nijman SMB, Mirchandani KD, Galardy PJ, Cohn MA, Haas W, et al. Regulation of Monoubiquitinated PCNA by DUB Autocleavage. 2006 Nature Cell Biology;8(4):341–347.

[172] Parker JL, Bucceri A, Davies AA, Heidrich K, Windecker H, Ulrich HD. SUMO Modification of PCNA Is Controlled by DNA. 2008 The EMBO Journal;27(18):2422–2431.

[173] Krejci L, Van Komen S, Li Y, Villemain J, Reddy MS, Klein H, et al. DNA Helicase Srs2 Disrupts the Rad51 Presynaptic Filament. 2003 Nature;423(6937):305–309.

[174] Pfander B, Moldovan GL, Sacher M, Hoege C, Jentsch S. SUMO-Modified PCNA Recruits Srs2 to Prevent Recombination during S Phase. 2005 Nature;436(7049):428–433.

[175] Veaute X, Jeusset J, Soustelle C, Kowalczykowski SC, Le Cam E, Fabre F. The Srs2 Helicase Prevents Recombination by Disrupting Rad51 Nucleoprotein Filaments. 2003 Nature;423(6937):309–312.

[176] Papouli E, Chen S, Davies AA, Huttner D, Krejci L, Sung P, et al. Crosstalk between SUMO and Ubiquitin on PCNA Is Mediated by Recruitment of the Helicase Srs2p. 2005 Molecular Cell;19(1):123–133.

[177] Armstrong AA, Mohideen F, Lima CD. Recognition of SUMO-Modified PCNA Requires Tandem Receptor Motifs in Srs2. 2012 Nature;483(7387):59–63.

[178] Parker JL, Ulrich HD. A SUMO-Interacting Motif Activates Budding Yeast Ubiquitin Ligase Rad18 towards SUMO-Modified PCNA. 2012 Nucleic Acids Research;40(22):11380–11388.

[179] Sale JE. Translesion DNA Synthesis and Mutagenesis in Eukaryotes. 2013 Cold Spring Harbor Perspectives in Biology;5(3):a012708.

[180] Pagès V, Fuchs RP. How DNA Lesions Are Turned into Mutations within Cells? 2002 Oncogene;21(58):8957–8966.

[181] Waters LS, Walker GC. The Critical Mutagenic Translesion DNA Polymerase Rev1 Is Highly Expressed during G2/M Phase Rather than S Phase. 2006 Proceedings of the National Academy of Sciences;103(24):8971–8976.

[182] Yamada A, Masutani C, Iwai S, Hanaoka F. Complementation of Defective Translesion Synthesis and UV Light Sensitivity in Xeroderma Pigmentosum Variant Cells by Human and Mouse DNA Polymerase η. 2000 Nucleic Acids Research;28(13):52.

[183] Wang Y, Woodgate R, McManus TP, Mead S, McCormick JJ, Maher VM. Evidence That in Xeroderma Pigmentosum Variant Cells, Which Lack DNA Polymerase η, DNA Polymerase ι Causes the Very High Frequency and Unique Spectrum of UV-Induced Mutations. 2007 Cancer Research;67(7):3018–3026.

[184] Washington MT, Minko IG, Johnson RE, Haracska L, Harris TM, Lloyd RS, et al. Efficient and Error-Free Replication Past a Minor-Groove N2-Guanine Adduct by the Sequential Action of Yeast Rev1 and DNA Polymerase ζ. 2004 Molecular and Cellular Biology;24(16):6900–6906.

[185] Washington MT, Minko IG, Johnson RE, Wolfle WT, Harris TM, Lloyd RS, et al. Efficient and Error-Free Replication Past a Minor-Groove DNA Adduct by the Sequential Action of Human DNA Polymerases ι and κ. 2004 Molecular and Cellular Biology;24(13):5687–5693.

[186] Korzhnev DM, Hadden MK. Targeting the Translesion Synthesis Pathway for the Development of Anti-Cancer Chemotherapeutics. 2016 Journal of Medicinal Chemistry;59(20):9321–9336.

[187] de Groote FH, Jansen JG, Masuda Y, Shah DM, Kamiya K, de Wind N, et al. The Rev1 Translesion Synthesis Polymerase Has Multiple Distinct DNA Binding Modes. 2011 DNA Repair;10(9):915–925.

[188] Quinet A, Lerner LK, Martins DJ, Menck CFM. Filling Gaps in Translesion DNA Synthesis in Human Cells. 2018 Mutation Research/Genetic Toxicology and Environmental Mutagenesis;836:127–142.

[189] Branzei D, Sollier J, Liberi G, Zhao X, Maeda D, Seki M, et al. Ubc9- and Mms21-Mediated Sumoylation Counteracts Recombinogenic Events at Damaged Replication Forks. 2006 Cell;127(3):509–522.

[190] Wu L, Hickson ID. The Bloom's Syndrome Helicase Suppresses Crossing over during Homologous Recombination. 2003 Nature;426(6968):870–874.

[191] Liberi G, Maffioletti G, Lucca C, Chiolo I, Baryshnikova A, Cotta-Ramusino C, et al. Rad51-Dependent DNA Structures Accumulate at Damaged Replication Forks in Sgs1 Mutants Defective in the Yeast Ortholog of BLM RecQ Helicase. 2005 Genes & Development;19(3):339–350.

[192] Karras GI, Jentsch S. The RAD6 DNA Damage Tolerance Pathway Operates Uncoupled from the Replication Fork and Is Functional Beyond S Phase. 2010 Cell;141(2):255–267.

[193] Karras GI, Fumasoni M, Sienski G, Vanoli F, Branzei D, Jentsch S. Noncanonical Role of the 9-1-1 Clamp in the Error-Free DNA Damage Tolerance Pathway. 2013 Molecular Cell;49(3):536–546.

[194] Gonzalez-Huici V, Szakal B, Urulangodi M, Psakhye I, Castellucci F, Menolfi D, et al. DNA Bending Facilitates the Error-Free DNA Damage Tolerance Pathway and Upholds Genome Integrity. 2014 The EMBO Journal;33(4):327–340.

[195] Ortiz-Bazán MÁ, Gallo-Fernández M, Saugar I, Jiménez-Martín A, Vázquez MV, Tercero JA. Rad5 Plays a Major Role in the Cellular Response to DNA Damage during Chromosome Replication. 2014 Cell Reports;9(2):460–468.

[196] Ball LG, Zhang K, Cobb JA, Boone C, Xiao W. The Yeast Shu Complex Couples Error-Free Post-Replication Repair to Homologous Recombination. 2009 Molecular Microbiology;73(1):89–102.

[197] Vanoli F, Fumasoni M, Szakal B, Maloisel L, Branzei D. Replication and Recombination Factors Contributing to Recombination-Dependent Bypass of DNA Lesions by Template Switch. 2010 PLOS Genetics;6(11):e1001205.

[198] Choi K, Szakal B, Chen YH, Branzei D, Zhao X. The Smc5/6 Complex and Esc2 Influence Multiple Replication-Associated Recombination Processes in Saccharomyces Cerevisiae. 2010 Molecular Biology of the Cell;21(13):2306–2314.

[199] Prakash L. Characterization of Postreplication Repair in Saccharomyces Cerevisiae and Effects of Rad6, Rad18, Rev3 and Rad52 Mutations. 1981 Molecular and General Genetics MGG;184(3):471–478.

[200] Majka J, Binz SK, Wold MS, Burgers PMJ. Replication Protein A Directs Loading of the DNA Damage Checkpoint Clamp to 5′-DNA Junctions. 2006 Journal of Biological Chemistry;281(38):27855–27861.

[201] Lopes M, Foiani M, Sogo JM. Multiple Mechanisms Control Chromosome Integrity after Replication Fork Uncoupling and Restart at Irreparable UV Lesions. 2006 Molecular Cell;21(1):15–27.

[202] Giannattasio M, Zwicky K, Follonier C, Foiani M, Lopes M, Branzei D. Visualization of Recombination–Mediated Damage-Bypass by Template Switching. 2014 Nature structural & molecular biology;21(10):884–892.

[203] Daigaku Y, Davies AA, Ulrich HD. Ubiquitin-Dependent DNA Damage Bypass Is Separable from Genome Replication. 2010 Nature;465(7300):951–955.

[204] García-Rodríguez N, Morawska M, Wong RP, Daigaku Y, Ulrich HD. Spatial Separation between Replisome- and Template-induced Replication Stress Signaling. 2018 The EMBO Journal;37(9):e98369.

[205] Heller RC, Marians KJ. Replication Fork Reactivation Downstream of a Blocked Nascent Leading Strand. 2006 Nature;439(7076):557–562.

[206] Elvers I, Johansson F, Groth P, Erixon K, Helleday T. UV Stalled Replication Forks Restart by Re-Priming in Human Fibroblasts. 2011 Nucleic Acids Research;39(16):7049–7057.

[207] Fumasoni M, Zwicky K, Vanoli F, Lopes M, Branzei D. Error-Free DNA Damage Tolerance and Sister Chromatid Proximity during DNA Replication Rely on the Polα/Primase/Ctf4 Complex. 2015 Molecular Cell;57(5):812–823.

[208] García-Rodríguez N, Wong RP, Ulrich HD. The Helicase Pif1 Functions in the Template Switching Pathway of DNA Damage Bypass. 2018 Nucleic Acids Research;46(16):8347–8356.

[209] Branzei D, Szakal B. DNA Damage Tolerance by Recombination: Molecular Pathways and DNA Structures. 2016 DNA Repair;44:68–75.

[210] Blastyák A, Pintér L, Unk I, Prakash L, Prakash S, Haracska L. Yeast Rad5 Protein Required for Postreplication Repair Has a DNA Helicase Activity Specific for Replication Fork Regression. 2007 Molecular Cell;28(1):167–175.

[211] Bugreev DV, Rossi MJ, Mazin AV. Cooperation of RAD51 and RAD54 in Regression of a Model Replication Fork. 2011 Nucleic Acids Research;39(6):2153–2164.

[212] Xue X, Choi K, Bonner J, Chiba T, Kwon Y, Xu Y, et al. Restriction of Replication Fork Regression Activities by a Conserved SMC Complex. 2014 Molecular Cell;56(3):436–445.

[213] Zellweger R, Dalcher D, Mutreja K, Berti M, Schmid JA, Herrador R, et al. Rad51-Mediated Replication Fork Reversal Is a Global Response to Genotoxic Treatments in Human Cells. 2015 Journal of Cell Biology;208(5):563–579.

[214] Quinet A, Lemaçon D, Vindigni A. Replication Fork Reversal: Players and Guardians. 2017 Molecular Cell;68(5):830–833.

[215] Johnson RE, Henderson ST, Petes TD, Prakash S, Bankmann M, Prakash L. Saccharomyces Cerevisiae RAD5-Encoded DNA Repair Protein Contains DNA Helicase and Zinc-Binding Sequence Motifs and Affects the Stability of Simple Repetitive Sequences in the Genome. 1992 Molecular and Cellular Biology;12(9):3807–3818.

[216] Ulrich HD, Jentsch S. Two RING Finger Proteins Mediate Cooperation between Ubiquitin-Conjugating Enzymes in DNA Repair. 2000 The EMBO Journal;19(13):3388–3397.

[217] Kile AC, Chavez DA, Bacal J, Eldirany S, Korzhnev DM, Bezsonova I, et al. HLTF's Ancient HIRAN Domain Binds 3′ DNA Ends to Drive Replication Fork Reversal. 2015 Molecular Cell;58(6):1090–1100.

[218] Ball LG, Xu X, Blackwell S, Hanna MD, Lambrecht AD, Xiao W. The Rad5 Helicase Activity Is Dispensable for Error-Free DNA Post-Replication Repair. 2014 DNA Repair;16:74–83.

[219] Chen S, Davies AA, Sagan D, Ulrich HD. The RING Finger ATPase Rad5p of Saccharomyces Cerevisiae Contributes to DNA Double-Strand Break Repair in a Ubiquitin-Independent Manner. 2005 Nucleic Acids Research;33(18):5878–5886.

[220] Sogo JM, Lopes M, Foiani M. Fork Reversal and ssDNA Accumulation at Stalled Replication Forks Owing to Checkpoint Defects. 2002 Science;297(5581):599–602.

[221] Vujanovic M, Krietsch J, Raso MC, Terraneo N, Zellweger R, Schmid JA, et al. Replication Fork Slowing and Reversal upon DNA Damage Require PCNA Polyubiquitination and ZRANB3 DNA Translocase Activity. 2017 Molecular Cell;67(5):882–890.e5.

[222] Zhuang Z, Johnson RE, Haracska L, Prakash L, Prakash S, Benkovic SJ. Regulation of Polymerase Exchange between Poleta and Poldelta by Monoubiquitination of PCNA and the Movement of DNA Polymerase Holoenzyme. 2008 Proceedings of the National Academy of Sciences of the United States of America;105(14):5361–5366.

[223] Coulon S, Ramasubramanyan S, Alies C, Philippin G, Lehmann A, Fuchs RP. Rad8Rad5/Mms2–Ubc13 Ubiquitin Ligase Complex Controls Translesion Synthesis in Fission Yeast. 2010 The EMBO Journal;29(12):2048–2058.

[224] Okada T, Sonoda E, Yamashita YM, Koyoshi S, Tateishi S, Yamaizumi M, et al. Involvement of Vertebrate Polκ in Rad18-Independent Postreplication Repair of UV Damage. 2002 Journal of Biological Chemistry;277(50):48690–48695.

[225] Edmunds CE, Simpson LJ, Sale JE. PCNA Ubiquitination and REV1 Define Temporally Distinct Mechanisms for Controlling Translesion Synthesis in the Avian Cell Line DT40. 2008 Molecular Cell;30(4):519–529.

[226] Acharya N, Yoon JH, Hurwitz J, Prakash L, Prakash S. DNA Polymerase η Lacking the Ubiquitin-Binding Domain Promotes Replicative Lesion Bypass in Humans Cells. 2010 Proceedings of the National Academy of Sciences;107(23):10401–10405.

[227] Hendel A, Krijger PHL, Diamant N, Goren Z, Langerak P, Kim J, et al. PCNA ubiquitination is important, but not essential for translesion DNA synthesis in mammalian cells. 2011 PLoS Genetics;7(9):e1002262.

[228] Wit N, Buoninfante OA, van den Berk PCM, Jansen JG, Hogenbirk MA, de Wind N, et al. Roles of PCNA Ubiquitination and TLS Polymerases κ and η in the Bypass of Methyl Methanesulfonate-Induced DNA Damage. 2015 Nucleic Acids Research;43(1):282–294.

[229] Motegi A, Liaw HJ, Lee KY, Roest HP, Maas A, Wu X, et al. Polyubiquitination of Proliferating Cell Nuclear Antigen by HLTF and SHPRH Prevents Genomic Instability from Stalled Replication Forks. 2008 Proceedings of the National Academy of Sciences;105(34):12411–12416.

[230] Krijger PHL, Lee KY, Wit N, van den Berk PCM, Wu X, Roest HP, et al. HLTF and SHPRH Are Not Essential for PCNA Polyubiquitination, Survival and Somatic Hypermutation: Existence of an Alternative E3 Ligase. 2011 DNA Repair;10(4):438–444.

[231] Kannouche PL, Wing J, Lehmann AR. Interaction of Human DNA Polymerase η with Monoubiquitinated PCNA: A Possible Mechanism for the Polymerase Switch in Response to DNA Damage. 2004 Molecular Cell;14(4):491–500.

[232] Frampton J, Irmisch A, Green CM, Neiss A, Trickey M, Ulrich HD, et al. Postreplication Repair and PCNA Modification in *Schizosaccharomyces Pombe*. 2006 Molecular Biology of the Cell;17(7):2976–2985.

[233] Watanabe K, Tateishi S, Kawasuji M, Tsurimoto T, Inoue H, Yamaizumi M. Rad18 Guides Polη to Replication Stalling Sites through Physical Interaction and PCNA Monoubiquitination. 2004 The EMBO Journal;23(19):3886–3896.

[234] Kashiwaba Si, Kanao R, Masuda Y, Kusumoto-Matsuo R, Hanaoka F, Masutani C. USP7 Is a Suppressor of PCNA Ubiquitination and Oxidative-Stress-Induced Mutagenesis in Human Cells. 2015 Cell Reports;13(10):2072–2080.

[235] Niimi A, Brown S, Sabbioneda S, Kannouche PL, Scott A, Yasui A, et al. Regulation of Proliferating Cell Nuclear Antigen Ubiquitination in Mammalian Cells. 2008 Proceedings of the National Academy of Sciences;105(42):16125–16130.

[236] Hishida T, Kubota Y, Carr AM, Iwasaki H. RAD6 – RAD18 – RAD5 -Pathway-Dependent Tolerance to Chronic Low-Dose Ultraviolet Light. 2009 Nature;457(7229):612–615.

[237] Huang D, Piening BD, Paulovich AG. The Preference for Error-Free or Error-Prone Postreplication Repair in Saccharomyces Cerevisiae Exposed to Low-Dose Methyl Methanesulfonate Is Cell Cycle Dependent. 2013 Molecular and Cellular Biology;33(8):1515–1527.

[238] Bi X, Barkley LR, Slater DM, Tateishi S, Yamaizumi M, Ohmori H, et al. Rad18 Regulates DNA Polymerase κ and Is Required for Recovery from S-Phase Checkpoint-Mediated Arrest. 2006 Molecular and Cellular Biology;26(9):3527–3540.

[239] Kermi C, Prieto S, van der Laan S, Tsanov N, Recolin B, Uro-Coste E, et al. RAD18 Is a Maternal Limiting Factor Silencing the UV-Dependent DNA Damage Checkpoint in Xenopus Embryos. 2015 Developmental Cell;34(3):364–372.

[240] Liefshitz B, Steinlauf R, Friedl A, Eckardt-Schupp F, Kupiec M. Genetic Interactions between Mutants of the 'error-Prone' Repair Group of Saccharomyces Cerevisiae and Their Effect on Recombination and Mutagenesis. 1998 Mutation Research/DNA Repair;407(2):135–145.

[241] Minesinger BK, Jinks-Robertson S. Roles of RAD6 Epistasis Group Members in Spontaneous Polζ-Dependent Translesion Synthesis in Saccharomyces Cerevisiae. 2005 Genetics;169(4):1939–1955.

[242] Branzei D, Vanoli F, Foiani M. SUMOylation Regulates Rad18-Mediated Template Switch. 2008 Nature;456(7224):915–920.

[243] Stamatoyannopoulos JA, Adzhubei I, Thurman RE, Kryukov GV, Mirkin SM, Sunyaev SR. Human Mutation Rate Associated with DNA Replication Timing. 2009 Nature Genetics;41(4):393–395.

[244] Koren A, Polak P, Nemesh J, Michaelson JJ, Sebat J, Sunyaev SR, et al. Differential Relationship of DNA Replication Timing to Different Forms of Human Mutation and Variation. 2012 The American Journal of Human Genetics;91(6):1033–1040.

[245] Lang GI, Murray AW. Mutation Rates across Budding Yeast Chromosome VI Are Correlated with Replication Timing. 2011 Genome Biology and Evolution;3:799–811.

[246] Unk I, Hajdú I, Blastyák A, Haracska L. Role of Yeast Rad5 and Its Human Orthologs, HLTF and SHPRH in DNA Damage Tolerance. 2010 DNA Repair;9(3):257–267.

[247] Choi K, Batke S, Szakal B, Lowther J, Hao F, Sarangi P, et al. Concerted and Differential Actions of Two Enzymatic Domains Underlie Rad5 Contributions to DNA Damage Tolerance. 2015 Nucleic Acids Research;43(5):2666–2677.

[248] Fan Q, Xu X, Zhao X, Wang Q, Xiao W, Guo Y, et al. Rad5 Coordinates Translesion DNA Synthesis Pathway by Recognizing Specific DNA Structures in Saccharomyces Cerevisiae. 2018 Current Genetics;64(4):889–899.

[249] MacKay C, Toth R, Rouse J. Biochemical Characterisation of the SWI/SNF Family Member HLTF. 2009 Biochemical and Biophysical Research Communications;390(2):187–191.

[250] Hofmann RM, Pickart CM. Noncanonical MMS2-Encoded Ubiquitin-Conjugating Enzyme Functions in Assembly of Novel Polyubiquitin Chains for DNA Repair. 1999 Cell;96(5):645–653.

[251] Broomfield S, Chow BL, Xiao W. MMS2, Encoding a Ubiquitin-Conjugating-Enzyme-like Protein, Is a Member of the Yeast Error-Free Postreplication Repair Pathway. 1998 Proceedings of the National Academy of Sciences;95(10):5678–5683.

[252] Moraes TF, Edwards RA, McKenna S, Pastushok L, Xiao W, Glover JNM, et al. Crystal Structure of the Human Ubiquitin Conjugating Enzyme Complex, hMms2–hUbc13. 2001 Nature Structural Biology;8(8):669–673.

[253] Motegi A, Sood R, Moinova H, Markowitz SD, Liu PP, Myung K. Human SHPRH Suppresses Genomic Instability through Proliferating Cell Nuclear Antigen Polyubiquitination. 2006 The Journal of Cell Biology;175(5):703–708.

[254] Lin JR, Zeman MK, Chen JY, Yee MC, Cimprich KA. SHPRH and HLTF Act in a Damage-Specific Manner to Coordinate Different Forms of Postreplication Repair and Prevent Mutagenesis. 2011 Molecular Cell;42(2):237–249.

[255] Iyer LM, Babu M, Aravind L. The HIRAN Domain and Recruitment of Chromatin Remodeling and Repair Activities to Damaged DNA. 2006 Cell Cycle;5(7):775–782.

[256] Hishiki A, Hara K, Ikegaya Y, Yokoyama H, Shimizu T, Sato M, et al. Structure of a Novel DNA-Binding Domain of Helicase-like Transcription Factor (HLTF) and Its Functional Implication in DNA Damage Tolerance. 2015 Journal of Biological Chemistry;290(21):13215–13223.

[257] Burkovics P, Sebesta M, Balogh D, Haracska L, Krejci L. Strand Invasion by HLTF as a Mechanism for Template Switch in Fork Rescue. 2014 Nucleic Acids Research;42(3):1711–1720.

[258] Achar YJ, Balogh D, Neculai D, Juhasz S, Morocz M, Gali H, et al. Human HLTF Mediates Postreplication Repair by Its HIRAN Domain-Dependent Replication Fork Remodelling. 2015 Nucleic Acids Research;43(21):10277–10291.

[259] Masuda Y, Mitsuyuki S, Kanao R, Hishiki A, Hashimoto H, Masutani C. Regulation of HLTF-Mediated PCNA Polyubiquitination by RFC and PCNA Monoubiquitination Levels Determines Choice of Damage Tolerance Pathway. 2018 Nucleic Acids Research;46(21):11340–11356.

[260] Gallo D, Brown GW. Post-Replication Repair: Rad5/HLTF Regulation, Activity on Undamaged Templates, and Relationship to Cancer. 2019 Critical Reviews in Biochemistry and Molecular Biology;0(0):1–32.

[261] Blastyák A, Hajdú I, Unk I, Haracska L. Role of Double-Stranded DNA Translocase Activity of Human HLTF in Replication of Damaged DNA. 2010 Molecular and Cellular Biology;30(3):684–693.

[262] Ćejka P, Vondrejs V, Storchová Z. Dissection of the Functions of the Saccharomyces Cerevisiae RAD6 Postreplicative Repair Group in Mutagenesis and UV Sensitivity. 2001 Genetics;159(3):953–963.

[263] Pagès V, Bresson A, Acharya N, Prakash S, Fuchs RP, Prakash L. Requirement of Rad5 for DNA Polymerase ζ-Dependent Translesion Synthesis in Saccharomyces Cerevisiae. 2008 Genetics;180(1):73–82.

[264] Kuang L, Kou H, Xie Z, Zhou Y, Feng X, Wang L, et al. A Non-Catalytic Function of Rev1 in Translesion DNA Synthesis and Mutagenesis Is Mediated by Its Stable Interaction with Rad5. 2013 DNA Repair;12(1):27–37.

[265] Xu X, Lin A, Zhou C, Blackwell SR, Zhang Y, Wang Z, et al. Involvement of Budding Yeast Rad5 in Translesion DNA Synthesis through Physical Interaction with Rev1. 2016 Nucleic Acids Research;44(11):5231–5245.

[266] Liboska R, Ligasová A, Strunin D, Rosenberg I, Koberna K. Most Anti-BrdU Antibodies React with 2′-Deoxy-5-Ethynyluridine — The Method for the Effective Suppression of This Cross-Reactivity. 2012 PLOS ONE;7(12):e51679.

[267] Janke C, Magiera MM, Rathfelder N, Taxis C, Reber S, Maekawa H, et al. A Versatile Toolbox for PCR-Based Tagging of Yeast Genes: New Fluorescent Proteins, More Markers and Promoter Substitution Cassettes. 2004 Yeast;21(11):947–962.

[268] Lee S, Lim WA, Thorn KS. Improved Blue, Green, and Red Fluorescent Protein Tagging Vectors for S. Cerevisiae. 2013 PLOS ONE;8(7):e67902.

[269] Brachmann CB, Davies A, Cost GJ, Caputo E, Li J, Hieter P, et al. Designer Deletion Strains Derived from Saccharomyces Cerevisiae S288C: A Useful Set of Strains and Plasmids for PCR-Mediated Gene Disruption and Other Applications. 1998 Yeast;14(2):115–132.

[270] James P, Halladay J, Craig EA. Genomic Libraries and a Host Strain Designed for Highly Efficient Two-Hybrid Selection in Yeast. 1996 Genetics;144(4):1425–1436.

[271] Reid RJD, González-Barrera S, Sunjevaric I, Alvaro D, Ciccone S, Wagner M, et al. Selective Ploidy Ablation, a High-Throughput Plasmid Transfer Protocol, Identifies New Genes Affecting Topoisomerase I–Induced DNA Damage. 2011 Genome Research;21(3):477–486.

[272] Thomas BJ, Rothstein R. Elevated Recombination Rates in Transcriptionally Active DNA. 1989 Cell;56(4):619–630.

[273] Gelperin DM, White MA, Wilkinson ML, Kon Y, Kung LA, Wise KJ, et al. Biochemical and Genetic Analysis of the Yeast Proteome with a Movable ORF Collection. 2005 Genes & Development;19(23):2816–2826.

[274] Rothstein RJ. [12] One-Step Gene Disruption in Yeast. In: Methods in Enzymology. vol. 101 of Recombinant DNA Part C. Academic Press; 1983. p. 202–211.

[275] Pace CN, Vajdos F, Fee L, Grimsley G, Gray T. How to measure and predict the molar absorption coefficient of a protein. 1995 Protein Science;4(11):2411–2423.

[276] Bradford MM. A Rapid and Sensitive Method for the Quantitation of Microgram Quantities of Protein Utilizing the Principle of Protein-Dye Binding. 1976 Analytical Biochemistry;72(1):248–254.

[277] Morawska M, Ulrich HD. An Expanded Tool Kit for the Auxin-Inducible Degron System in Budding Yeast: A Tool Kit for the AID System. 2013 Yeast;30(9):341–351.

[278] Haber JE. Mating-Type Genes and MAT Switching in Saccharomyces Cerevisiae. 2012 Genetics;191(1):33–64.

[279] Choe KN, Moldovan GL. Forging Ahead through Darkness: PCNA, Still the Principal Conductor at the Replication Fork. 2017 Molecular Cell;65(3):380–392.

[280] Xu H, Zhang P, Liu L, Lee MYWT. A Novel PCNA-Binding Motif Identified by the Panning of a Random Peptide Display Library. 2001 Biochemistry;40(14):4512–4520.

[281] Xu M, Qin J, Wang L, Lee HJ, Kao CY, Liu D, et al. Nuclear Receptors Regulate Alternative Lengthening of Telomeres through a Novel Noncanonical FANCD2 Pathway. 2019 Science Advances;5(10):eaax6366.

[282] Moldovan GL, Pfander B, Jentsch S. PCNA, the Maestro of the Replication Fork. 2007 Cell;129(4):665–679.

[283] Young P, Deveraux Q, Beal RE, Pickart CM, Rechsteiner M. Characterization of Two Polyubiquitin Binding Sites in the 26 S Protease Subunit 5a. 1998 Journal of Biological Chemistry;273(10):5461–5467.

[284] Wang Q, Young P, Walters KJ. Structure of S5a Bound to Monoubiquitin Provides a Model for Polyubiquitin Recognition. 2005 Journal of Molecular Biology;348(3):727–739.

[285] Albrecht AC. Polarizations and Assignments of Transitions: The Method of Photoselection. 1961 Journal of Molecular Spectroscopy;6:84–108.

[286] Chin J, Längst G, Becker PB, Widom J. Fluorescence Anisotropy Assays for Analysis of ISWI-DNA and ISWI-Nucleosome Interactions. In: Methods in Enzymology. vol. 376 of Chromatin and Chromatin Remodeling Enzymes, Part B. Academic Press; 2003. p. 3–16.

[287] Kim H, Chen J, Yu X. Ubiquitin-Binding Protein RAP80 Mediates BRCA1-Dependent DNA Damage Response. 2007 Science;316(5828):1202–1205.

[288] Sobhian B, Shao G, Lilli DR, Culhane AC, Moreau LA, Xia B, et al. RAP80 Targets BRCA1 to Specific Ubiquitin Structures at DNA Damage Sites. 2007 Science;316(5828):1198–1202.

[289] Wang B, Matsuoka S, Ballif BA, Zhang D, Smogorzewska A, Gygi SP, et al. Abraxas and RAP80 Form a BRCA1 Protein Complex Required for the DNA Damage Response. 2007 Science;316(5828):1194–1198.

[290] Yan J, Kim YS, Yang XP, Li LP, Liao G, Xia F, et al. The Ubiquitin-Interacting Motif–Containing Protein RAP80 Interacts with BRCA1 and Functions in DNA Damage Repair Response. 2007 Cancer Research;67(14):6647–6656.

[291] Torres-Rosell J, Sunjevaric I, De Piccoli G, Sacher M, Eckert-Boulet N, Reid R, et al. The Smc5–Smc6 Complex and SUMO Modification of Rad52 Regulates Recombinational Repair at the Ribosomal Gene Locus. 2007 Nature Cell Biology;9(8):923–931.

[292] Nagai S, Dubrana K, Tsai-Pflugfelder M, Davidson MB, Roberts TM, Brown GW, et al. Functional Targeting of DNA Damage to a Nuclear Pore-Associated SUMO-Dependent Ubiquitin Ligase. 2008 Science;322(5901):597–602.

[293] Oza P, Jaspersen SL, Miele A, Dekker J, Peterson CL. Mechanisms That Regulate Localization of a DNA Double-Strand Break to the Nuclear Periphery. 2009 Genes & Development;23(8):912–927.

[294] Falbo KB, Alabert C, Katou Y, Wu S, Han J, Wehr T, et al. Involvement of a Chromatin Remodeling Complex in Damage Tolerance during DNA Replication. 2009 Nature Structural & Molecular Biology;16(11):1167–1172.

[295] Porath J, Carlsson J, Olsson I, Belfrage G. Metal Chelate Affinity Chromatography, a New Approach to Protein Fractionation. 1975 Nature;258(5536):598–599.

[296] Porath J, Olin B. Immobilized Metal Affinity Adsorption and Immobilized Metal Affinity Chromatography of Biomaterials. Serum Protein Affinities for Gel-Immobilized Iron and Nickel Ions. 1983 Biochemistry;22(7):1621–1630.

[297] Gaberc-Porekar V, Menart V. Perspectives of Immobilized-Metal Affinity Chromatography. 2001 Journal of Biochemical and Biophysical Methods;49(1):335–360.

[298] Partow S, Siewers V, Bjørn S, Nielsen J, Maury J. Characterization of Different Promoters for Designing a New Expression Vector in Saccharomyces Cerevisiae. 2010 Yeast;27(11):955–964.

[299] Vernet T, Dignard D, Thomas DY. A Family of Yeast Expression Vectors Containing the Phage F1 Intergenic Region1. 1987 Gene;52(2):225–233.

[300] Klapisz E, Sorokina I, Lemeer S, Pijnenburg M, Verkleij AJ, en Henegouwen PMPvB. A Ubiquitin-Interacting Motif (UIM) Is Essential for Eps15 and Eps15R Ubiquitination. 2002 Journal of Biological Chemistry;277(34):30746–30753.

[301] Shih SC, Prag G, Francis SA, Sutanto MA, Hurley JH, Hicke L. A Ubiquitin-Binding Motif Required for Intramolecular Monoubiquitylation, the CUE Domain. 2003 The EMBO Journal;22(6):1273–1281.

[302] Polo S, Sigismund S, Faretta M, Guidi M, Capua MR, Bossi G, et al. A Single Motif Responsible for Ubiquitin Recognition and Monoubiquitination in Endocytic Proteins. 2002 Nature;416(6879):451–455.

[303] Oldham CE, Mohney RP, Miller SLH, Hanes RN, O'Bryan JP. The Ubiquitin-Interacting Motifs Target the Endocytic Adaptor Protein Epsin for Ubiquitination. 2002 Current Biology;12(13):1112–1116.

[304] Uchiki T, Kim HT, Zhai B, Gygi SP, Johnston JA, O'Bryan JP, et al. The Ubiquitin-Interacting Motif Protein, S5a, Is Ubiquitinated by All Types of Ubiquitin Ligases by a Mechanism Different from Typical Substrate Recognition. 2009 Journal of Biological Chemistry;284(19):12622–12632.

[305] Seufert W, McGrath JP, Jentsch S. UBC1 Encodes a Novel Member of an Essential Subfamily of Yeast Ubiquitin-Conjugating Enzymes Involved in Protein Degradation. 1990 The EMBO Journal;9(13):4535–4541.

[306] Brusky J, Zhu Y, Xiao W. UBC13, a DNA-Damage-Inducible Gene, Is a Member of the Error-Free Postreplication Repair Pathway in Saccharomyces Cerevisiae. 2000 Current Genetics;37(3):168–174.

[307] Lemontt JF. Mutants of Yeast Defective in Mutation Induced by Ultraviolet Light. 1971 Genetics;68(1):21–33.

[308] Larimer FW, Perry JR, Hardigree AA. The REV1 Gene of Saccharomyces Cerevisiae: Isolation, Sequence, and Functional Analysis. 1989 Journal of Bacteriology;171(1):230–237.

[309] Nelson JR, Lawrence CW, Hinkle DC. Thymine-Thymine Dimer Bypass by Yeast DNA Polymerase ζ. 1996 Science;272(5268):1646–1649.

[310] McDonald JP, Levine AS, Woodgate R. The Saccharomyces Cerevisiae Rad30 Gene, a Homologue of Escherichia Coli Dinb and Umuc, Is DNA Damage Inducible and Functions in a Novel Error-Free Postreplication Repair Mechanism. 1997 Genetics;147(4):1557–1568.

[311] Johnson RE, Prakash S, Prakash L. Efficient Bypass of a Thymine-Thymine Dimer by Yeast DNA Polymerase, Polη. 1999 Science;283(5404):1001–1004.

[312] Haracska L, Kondratick CM, Unk I, Prakash S, Prakash L. Interaction with PCNA Is Essential for Yeast DNA Polymerase η Function. 2001 Molecular Cell;8(2):407–415.

[313] Johnson RE, Yu SL, Prakash S, Prakash L. Yeast DNA Polymerase Zeta (ζ) Is Essential for Error-Free Replication Past Thymine Glycol. 2003 Genes & Development;17(1):77–87.

[314] Prakash S, Johnson RE, Prakash L. Eukaryotic Translesion Synthesis DNA Polymerases: Specificity of Structure and Function. 2005 Annual Review of Biochemistry;74(1):317–353.

[315] Torres-Ramos CA, Prakash S, Prakash L. Requirement of RAD5 and MMS2 for Postreplication Repair of UV-Damaged DNA in Saccharomyces Cerevisiae. 2002 Molecular and Cellular Biology;22(7):2419–2426.

[316] Davies AA, Ulrich HD. Detection of PCNA Modifications in Saccharomyces Cerevisiae. In: Bjergbæk L, editor. DNA Repair Protocols. Methods in Molecular Biology. Totowa, NJ: Humana Press; 2012. p. 543–567.

[317] Lawrence CW, Christensen RB. Metabolic Suppressors of Trimethoprim and Ultraviolet Light Sensitivities of Saccharomyces Cerevisiae Rad6 Mutants. 1979 Journal of Bacteriology;139(3):866–876.

[318] Xu G, Paige JS, Jaffrey SR. Global Analysis of Lysine Ubiquitination by Ubiquitin Remnant Immunoaffinity Profiling. 2010 Nature Biotechnology;28(8):868–873.

[319] Hottiger T, Fürst P, Pohlig G, Heim J. Physiological Characterization of the Yeast Metallothionein (CUP1) Promoter, and Consequences of Overexpressing Its Transcriptional Activator, ACE1. 1994 Yeast;10(3):283–296.

[320] Winge DR. Copper-Regulatory Domain Involved in Gene Expression. In: Moldave K, editor. Progress in Nucleic Acid Research and Molecular Biology. vol. 58. Academic Press; 1997. p. 165–195.

[321] Garí E, Piedrafita L, Aldea M, Herrero E. A Set of Vectors with a Tetracycline-Regulatable Promoter System for Modulated Gene Expression in Saccharomyces Cerevisiae. 1997 Yeast;13(9):837–848.

[322] Johnston M. A Model Fungal Gene Regulatory Mechanism: The GAL Genes of Saccharomyces Cerevisiae. 1987 Microbiological Reviews;51(4):458–476.

[323] Matsuyama T, Yamanishi M, Takahashi H. Improvement of Galactose Induction System in Saccharomyces Cerevisiae. 2011 Journal of Bioscience and Bioengineering;111(2):175–177.

[324] Weinhandl K, Winkler M, Glieder A, Camattari A. Carbon Source Dependent Promoters in Yeasts. 2014 Microbial Cell Factories;13:5.

[325] Mountain HA, Byström AS, Larsen JT, Korch C. Four Major Transcriptional Responses in the Methionine/Threonine Biosynthetic Pathway of Saccharomyces Cerevisiae. 1991 Yeast;7(8):781–803.

[326] Mao X, Hu Y, Liang C, Lu C. MET3 Promoter: A Tightly Regulated Promoter and Its Application in Construction of Conditional Lethal Strain. 2002 Current Microbiology;45(1):37–40.

[327] Rothkamm K, Barnard S, Moquet J, Ellender M, Rana Z, Burdak-Rothkamm S. DNA Damage Foci: Meaning and Significance. 2015 Environmental and Molecular Mutagenesis;56(6):491–504.

[328] Gossen M, Freundlieb S, Bender G, Muller G, Hillen W, Bujard H. Transcriptional Activation by Tetracyclines in Mammalian Cells. 1995 Science;268(5218):1766–1769.

[329] Chen CF, Li S, Chen Y, Chen PL, Sharp ZD, Lee WH. The Nuclear Localization Sequences of the BRCA1 Protein Interact with the Importin-α Subunit of the Nuclear Transport Signal Receptor. 1996 Journal of Biological Chemistry;271(51):32863–32868.

[330] Yano Ki, Morotomi K, Saito H, Kato M, Matsuo F, Miki Y. Nuclear Localization Signals of the BRCA2 Protein. 2000 Biochemical and Biophysical Research Communications;270(1):171–175.

[331] Burich R, Lei M. Two Bipartite NLSs Mediate Constitutive Nuclear Localization of Mcm10. 2003 Current Genetics;44(4):195–201.

[332] Masuda Y, Suzuki M, Kawai H, Suzuki F, Kamiya K. Asymmetric Nature of Two Subunits of RAD18, a RING-Type Ubiquitin Ligase E3, in the Human RAD6A–RAD18 Ternary Complex. 2012 Nucleic Acids Research;40(3):1065–1076.

[333] Lam AJ, St-Pierre F, Gong Y, Marshall JD, Cranfill PJ, Baird MA, et al. Improving FRET Dynamic Range with Bright Green and Red Fluorescent Proteins. 2012 Nature Methods;9(10):1005–1012.

[334] Bajar BT, Wang ES, Lam AJ, Kim BB, Jacobs CL, Howe ES, et al. Improving Brightness and Photostability of Green and Red Fluorescent Proteins for Live Cell Imaging and FRET Reporting. 2016 Scientific Reports;6(1):1–12.

[335] Naryzhny SN, Lee H. The Post-Translational Modifications of Proliferating Cell Nuclear Antigen Acetylation, Not Phosphorylation, Plays an Important Role in the Regulation of Its Function. 2004 Journal of Biological Chemistry;279(19):20194–20199.

[336] Naryzhny SN, Lee H. Proliferating Cell Nuclear Antigen in the Cytoplasm Interacts with Components of Glycolysis and Cancer. 2010 FEBS letters;584(20):4292–4298.

[337] Shaner NC, Campbell RE, Steinbach PA, Giepmans BNG, Palmer AE, Tsien RY. Improved Monomeric Red, Orange and Yellow Fluorescent Proteins Derived from Discosoma Sp. Red Fluorescent Protein. 2004 Nature Biotechnology;22(12):1567–1572.

[338] Bellí G, Garí E, Piedrafita L, Aldea M, Herrero E. An Activator/Repressor Dual System Allows Tight Tetracycline-Regulated Gene Expression in Budding Yeast. 1998 Nucleic Acids Research;26(4):942–947.

[339] Daigaku Y, Etheridge TJ, Nakazawa Y, Nakayama M, Watson AT, Miyabe I, et al. PCNA Ubiquitylation Ensures Timely Completion of Unperturbed DNA Replication in Fission Yeast. 2017 PLOS Genetics;13(5):e1006789.

[340] Ulrich HD, Takahashi T. Readers of PCNA Modifications. 2013 Chromosoma;122(4):259–274.

[341] Burkovics P, Sebesta M, Sisakova A, Plault N, Szukacsov V, Robert T, et al. Srs2 Mediates PCNA-SUMO-Dependent Inhibition of DNA Repair Synthesis. 2013 The EMBO Journal;32(5):742–755.

[342] Kubota T, Nishimura K, Kanemaki MT, Donaldson AD. The Elg1 Replication Factor C-like Complex Functions in PCNA Unloading during DNA Replication. 2013 Molecular Cell;50(2):273–280.

[343] Parnas O, Zipin-Roitman A, Pfander B, Liefshitz B, Mazor Y, Ben-Aroya S, et al. Elg1, an Alternative Subunit of the RFC Clamp Loader, Preferentially Interacts with SUMOylated PCNA. 2010 The EMBO Journal;29(15):2611–2622.

[344] Burgess RC, Rahman S, Lisby M, Rothstein R, Zhao X. The Slx5-Slx8 Complex Affects Sumoylation of DNA Repair Proteins and Negatively Regulates Recombination. 2007 Molecular and Cellular Biology;27(17):6153–6162.

[345] Cook CE, Hochstrasser M, Kerscher O. The SUMO-Targeted Ubiquitin Ligase Subunit Slx5 Resides in Nuclear Foci and at Sites of DNA Breaks. 2009 Cell Cycle;8(7):1080–1089.

[346] Cal-Bąkowska M, Litwin I, Bocer T, Wysocki R, Dziadkowiec D. The Swi2–Snf2-like Protein Uls1 Is Involved in Replication Stress Response. 2011 Nucleic Acids Research;39(20):8765–8777.

[347] Kramarz K, Litwin I, Cal-Bąkowska M, Szakal B, Branzei D, Wysocki R, et al. Swi2/Snf2-like Protein Uls1 Functions in the Sgs1-Dependent Pathway of Maintenance of rDNA Stability and Alleviation of Replication Stress. 2014 DNA Repair;21:24–35.

[348] Kramarz K, Mucha S, Litwin I, Barg-Wojas A, Wysocki R, Dziadkowiec D. DNA Damage Tolerance Pathway Choice Through Uls1 Modulation of Srs2 SUMOylation in Saccharomyces Cerevisiae. 2017 Genetics;206(1):513–525.

[349] Poulsen SL, Hansen RK, Wagner SA, van Cuijk L, van Belle GJ, Streicher W, et al. RNF111/Arkadia Is a SUMO-Targeted Ubiquitin Ligase That Facilitates the DNA Damage Response. 2013 The Journal of Cell Biology;201(6):797–807.

[350] Daigaku Y, Davies AA, Ulrich HD. Ubiquitin-Dependent DNA Damage Bypass Is Separable from Genome Replication. 2010 Nature;465(7300):951–955.

[351] Burgess RC, Lisby M, Altmannova V, Krejci L, Sung P, Rothstein R. Localization of Recombination Proteins and Srs2 Reveals Anti-Recombinase Function in Vivo. 2009 Journal of Cell Biology;185(6):969–981.

[352] Yan H, Merchant AM, Tye BK. Cell Cycle-Regulated Nuclear Localization of MCM2 and MCM3, Which Are Required for the Initiation of DNA Synthesis at Chromosomal Replication Origins in Yeast. 1993 Genes & Development;7(11):2149–2160.

[353] Su XA, Dion V, Gasser SM, Freudenreich CH. Regulation of Recombination at Yeast Nuclear Pores Controls Repair and Triplet Repeat Stability. 2015 Genes & Development;29(10):1006–1017.

[354] Churikov D, Charifi F, Eckert-Boulet N, Silva S, Simon MN, Lisby M, et al. SUMO-Dependent Relocalization of Eroded Telomeres to Nuclear Pore Complexes Controls Telomere Recombination. 2016 Cell Reports;15(6):1242–1253.

[355] Khadaroo B, Teixeira MT, Luciano P, Eckert-Boulet N, Germann SM, Simon MN, et al. The DNA Damage Response at Eroded Telomeres and Tethering to the Nuclear Pore Complex. 2009 Nature Cell Biology;11(8):980–987.

[356] Doye V, Wepf R, Hurt Ec. A Novel Nuclear Pore Protein Nup133p with Distinct Roles in Poly(A)+ RNA Transport and Nuclear Pore Distribution. 1994 The EMBO Journal;13(24):6062–6075.

[357] Schober H, Ferreira H, Kalck V, Gehlen LR, Gasser SM. Yeast Telomerase and the SUN Domain Protein Mps3 Anchor Telomeres and Repress Subtelomeric Recombination. 2009 Genes & Development;23(8):928–938.

[358] Sabouri N, Capra JA, Zakian VA. The Essential Schizosaccharomyces Pombe Pfh1 DNA Helicase Promotes Fork Movement Past G-Quadruplex Motifs to Prevent DNA Damage. 2014 BMC Biology;12(1):101.

[359] Padeken J, Zeller P, Gasser SM. Repeat DNA in Genome Organization and Stability. 2015 Current Opinion in Genetics & Development;31:12–19.

[360] Vaziri H, Dragowska W, Allsopp RC, Thomas TE, Harley CB, Lansdorp PM. Evidence for a Mitotic Clock in Human Hematopoietic Stem Cells: Loss of Telomeric DNA with Age. 1994 Proceedings of the National Academy of Sciences;91(21):9857–9860.

[361] Karlseder J, Broccoli D, Dai Y, Hardy S, de Lange T. P53- and ATM-Dependent Apoptosis Induced by Telomeres Lacking TRF2. 1999 Science;283(5406):1321–1325.

[362] Zalzman M, Meltzer WA, Portney BA, Brown RA, Gupta A. The Role of Ubiquitination and SUMOylation in Telomere Biology. 2020 Current Issues in Molecular Biology;(35):85–98.

[363] Bernard P, Maure JF, Partridge JF, Genier S, Javerzat JP, Allshire RC. Requirement of Heterochromatin for Cohesion at Centromeres. 2001 Science;294(5551):2539–2542.

[364] Barra V, Fachinetti D. The Dark Side of Centromeres: Types, Causes and Consequences of Structural Abnormalities Implicating Centromeric DNA. 2018 Nature Communications;9(1):1–17.

[365] Billard P, Poncet DA. Replication Stress at Telomeric and Mitochondrial DNA: Common Origins and Consequences on Ageing. 2019 International Journal of Molecular Sciences;20(19):4959.

[366] Dimitrova DS. DNA Replication Initiation Patterns and Spatial Dynamics of the Human Ribosomal RNA Gene Loci. 2011 Journal of Cell Science;124(16):2743–2752.

[367] Warmerdam DO, Wolthuis RMF. Keeping Ribosomal DNA Intact: A Repeating Challenge. 2019 Chromosome Research;27(1):57–72.

[368] Watson JD, Crick FHC. Genetical Implications of the Structure of Deoxyribonucleic Acid. 1953 Nature;171(4361):964–967.

[369] Okazaki R, Okazaki T, Sakabe K, Sugimoto K, Kainuma R, Sugino A, et al. In Vivo Mechanism of DNA Chain Growth. 1968 Cold Spring Harbor Symposia on Quantitative Biology;33:129–143.

[370] Hu J, Adebali O, Adar S, Sancar A. Dynamic Maps of UV Damage Formation and Repair for the Human Genome. 2017 Proceedings of the National Academy of Sciences of the United States of America;114(26):6758–6763.

[371] Mao P, Brown AJ, Malc EP, Mieczkowski PA, Smerdon MJ, Roberts SA, et al. Genome-Wide Maps of Alkylation Damage, Repair, and Mutagenesis in Yeast Reveal Mechanisms of Mutational Heterogeneity. 2017 Genome Research;27(10):1674–1684.

[372] Li W, Adebali O, Yang Y, Selby CP, Sancar A. Single-Nucleotide Resolution Dynamic Repair Maps of UV Damage in *Saccharomyces Cerevisiae* Genome. 2018 Proceedings of the National Academy of Sciences;115(15):E3408–E3415.

[373] Hamperl S, Cimprich KA. Conflict Resolution in the Genome: How Transcription and Replication Make It Work. 2016 Cell;167(6):1455–1467.

[374] Hamperl S, Bocek MJ, Saldivar JC, Swigut T, Cimprich KA. Transcription-Replication Conflict Orientation Modulates R-Loop Levels and Activates Distinct DNA Damage Responses. 2017 Cell;170(4):774–786.e19.

[375] Urban V, Dobrovolna J, Hühn D, Fryzelkova J, Bartek J, Janscak P. RECQ5 Helicase Promotes Resolution of Conflicts between Replication and Transcription in Human Cells. 2016 J Cell Biol;214(4):401–415.

[376] Lerner LK, Sale JE. Replication of G Quadruplex DNA. 2019 Genes;10(2):95.

[377] Niimi A, Chambers A, Downs J, Lehmann A. A Role for Chromatin Remodellers in Replication of Damaged DNA. 2012 Nucleic acids research;40(15):7393–403.

[378] Niimi A, Hopkins SR, Downs JA, Masutani C. The BAH Domain of BAF180 Is Required for PCNA Ubiquitination. 2015 Mutation Research/Fundamental and Molecular Mechanisms of Mutagenesis;779:16–23.

[379] Pich O, Muiños F, Sabarinathan R, Reyes-Salazar I, Gonzalez-Perez A, Lopez-Bigas N. Somatic and Germline Mutation Periodicity Follow the Orientation of the DNA Minor Groove around Nucleosomes. 2018 Cell;175(4):1074–1087.e18.

[380] Hardy CF, Sussel L, Shore D. A RAP1-Interacting Protein Involved in Transcriptional Silencing and Telomere Length Regulation. 1992 Genes & Development;6(5):801–814.

[381] Wotton D, Shore D. A Novel Rap1p-Interacting Factor, Rif2p, Cooperates with Rif1p to Regulate Telomere Length in Saccharomyces Cerevisiae. 1997 Genes & Development;11(6):748–760.

[382] Teixeira MT, Arneric M, Sperisen P, Lingner J. Telomere Length Homeostasis Is Achieved via a Switch between Telomerase- Extendible and -Nonextendible States. 2004 Cell;117(3):323–335.

[383] Bonetti D, Clerici M, Anbalagan S, Martina M, Lucchini G, Longhese MP. Shelterin-Like Proteins and Yku Inhibit Nucleolytic Processing of Saccharomyces Cerevisiae Telomeres. 2010 PLOS Genetics;6(5):e1000966.

[384] Graf M, Bonetti D, Lockhart A, Serhal K, Kellner V, Maicher A, et al. Telomere Length Determines TERRA and R-Loop Regulation through the Cell Cycle. 2017 Cell;170(1):72–85.e14.

[385] Heun P, Laroche T, Raghuraman MK, Gasser SM. The Positioning and Dynamics of Origins of Replication in the Budding Yeast Nucleus. 2001 The Journal of Cell Biology;152(2):385–400.

[386] Cheng H, Bao X, Gan X, Luo S, Rao H. Multiple E3s Promote the Degradation of Histone H3 Variant Cse4. 2017 Scientific Reports;7(1):8565.

[387] Cai M, Davis RW. Yeast Centromere Binding Protein CBF1, of the Helix-Loop-Helix Protein Family, Is Required for Chromosome Stability and Methionine Prototrophy. 1990 Cell;61(3):437–446.

[388] Boguslawski SJ, Smith DE, Michalak MA, Mickelson KE, Yehle CO, Patterson WL, et al. Characterization of Monoclonal Antibody to DNA · RNA and Its Application to Immunodetection of Hybrids. 1986 Journal of Immunological Methods;89(1):123–130.

[389] Lockhart A, Pires VB, Bento F, Kellner V, Luke-Glaser S, Yakoub G, et al. RNase H1 and H2 Are Differentially Regulated to Process RNA-DNA Hybrids. 2019 Cell Reports;29(9):2890–2900.e5.

[390] Zimmer AD, Koshland D. Differential Roles of the RNases H in Preventing Chromosome Instability. 2016 Proceedings of the National Academy of Sciences of the United States of America;113(43):12220–12225.

[391] Tanaka T, Nasmyth K. Association of RPA with Chromosomal Replication Origins Requires an Mcm Protein, and Is Regulated by Rad53, and Cyclin- and Dbf4-Dependent Kinases. 1998 The EMBO Journal;17(17):5182–5191.

[392] Cobb JA, Bjergbaek L, Shimada K, Frei C, Gasser SM. DNA Polymerase Stabilization at Stalled Replication Forks Requires Mec1 and the RecQ Helicase Sgs1. 2003 The EMBO Journal;22(16):4325–4336.

[393] Tercero JA, Diffley JFX. Regulation of DNA Replication Fork Progression through Damaged DNA by the Mec1/Rad53 Checkpoint. 2001 Nature;412(6846):553–557.

[394] Sheu YJ, Kinney JB, Stillman B. Concerted Activities of Mcm4, Sld3, and Dbf4 in Control of Origin Activation and DNA Replication Fork Progression. 2016 Genome Research;26(3):315–330.

[395] Lebrun E, Fourel G, Defossez PA, Gilson E. A Methyltransferase Targeting Assay Reveals Silencer-Telomere Interactions in Budding Yeast. 2003 Molecular and Cellular Biology;23(5):1498–1508.

[396] Vogel MJ, Peric-Hupkes D, van Steensel B. Detection of *in Vivo* Protein–DNA Interactions Using DamID in Mammalian Cells. 2007 Nature Protocols;2(6):1467–1478.

[397] Skene PJ, Henikoff S. An Efficient Targeted Nuclease Strategy for High-Resolution Mapping of DNA Binding Sites. 2017 eLife;6:e21856.

[398] Ohtake F, Tsuchiya H, Saeki Y, Tanaka K. K63 Ubiquitylation Triggers Proteasomal Degradation by Seeding Branched Ubiquitin Chains. 2018 Proceedings of the National Academy of Sciences of the United States of America;115(7):1401–1407.

[399] Chiu RK, Brun J, Ramaekers C, Theys J, Weng L, Lambin P, et al. Lysine 63-Polyubiquitination Guards against Translesion Synthesis–Induced Mutations. 2006 PLOS Genetics;2(7):e116.

[400] Zhao S, Ulrich HD. Distinct Consequences of Posttranslational Modification by Linear versus K63-Linked Polyubiquitin Chains. 2010 Proceedings of the National Academy of Sciences;107(17):7704–7709.

[401] Gangavarapu V, Haracska L, Unk I, Johnson RE, Prakash S, Prakash L. Mms2-Ubc13-Dependent and -Independent Roles of Rad5 Ubiquitin Ligase in Postreplication Repair and Translesion DNA Synthesis in Saccharomyces Cerevisiae. 2006 Molecular and Cellular Biology;26(20):7783–7790.

[402] Yang K, Gong P, Gokhale P, Zhuang Z. Chemical Protein Polyubiquitination Reveals the Role of a Noncanonical Polyubiquitin Chain in DNA Damage Tolerance. 2014 ACS Chemical Biology;9(8):1685–1691.

[403] Plosky BS, Vidal AE, de Henestrosa ARF, McLenigan MP, McDonald JP, Mead S, et al. Controlling the Subcellular Localization of DNA Polymerases ι and η via Interactions with Ubiquitin. 2006 The EMBO Journal;25(12):2847–2855.

[404] Hishida T, Ohno T, Iwasaki H, Shinagawa H. Saccharomyces Cerevisiae MGS1 Is Essential in Strains Deficient in the RAD6-Dependent DNA Damage Tolerance Pathway. 2002 The EMBO journal;21(8):2019–2029.

[405] Saugar I, Parker JL, Zhao S, Ulrich HD. The Genome Maintenance Factor Mgs1 Is Targeted to Sites of Replication Stress by Ubiquitylated PCNA. 2012 Nucleic Acids Research;40(1):245–257.

[406] Ulrich HD. Regulating Post-Translational Modifications of the Eukaryotic Replication Clamp PCNA. 2009 DNA Repair;8(4):461–469.

[407] Liu P, Gan W, Su S, Hauenstein AV, Fu Tm, Brasher B, et al. K63-Linked Polyubiquitin Chains Bind to DNA to Facilitate DNA Damage Repair. 2018 Science Signaling;11(533).

[408] Wagih O, Usaj M, Baryshnikova A, VanderSluis B, Kuzmin E, Costanzo M, et al. SGAtools: One-Stop Analysis and Visualization of Array-Based Genetic Interaction Screens. 2013 Nucleic Acids Research;41(W1):W591–W596.

[409] Kapitzky L, Beltrao P, Berens TJ, Gassner N, Zhou C, Wüster A, et al. Cross-Species Chemogenomic Profiling Reveals Evolutionarily Conserved Drug Mode of Action. 2010 Molecular Systems Biology;6:451.

[410] Guénolé A, Srivas R, Vreeken K, Wang ZZ, Wang S, Krogan NJ, et al. Dissection of DNA Damage Responses Using Multiconditional Genetic Interaction Maps. 2013 Molecular Cell;49(2):346–358.

[411] Biswas EE, Chen PH, Leszyk J, Biswas SB. Biochemical and Genetic Characterization of a Replication Protein A-Dependent DNA Helicase from the Yeast, Saccharomyces Cerevisiae. 1995 Biochemical and Biophysical Research Communications;206(3):850–856.

[412] Bean DW, Matson SW. Identification of the Gene Encoding scHelI, a DNA Helicase from Saccharomyces Cerevisiae. 1997 Yeast;13(15):1465–1475.

[413] Kamimura YI, Kawasaki Y, Ohara T, Sugino A. DNA Helicase III of *Saccharomyces Cerevisiae*, Encoded by YER176w (*HEL1*), Highly Unwinds Covalently Closed, Circular DNA in the Presence of a DNA Topoisomerase and yRF-A. 1999 The Journal of Biochemistry;125(2):236–244.

[414] Czaplinski K, Majlesi N, Banerjee T, Peltz SW. Mtt1 Is a Upf1-like Helicase That Interacts with the Translation Termination Factors and Whose Overexpression Can Modulate Termination Efficiency. 2000 RNA;6(5):730–743.

[415] Eswaramoorthy S, Gerchman S, Graziano V, Kycia H, Studier FW, Swaminathan S. Structure of a Yeast Hypothetical Protein Selected by a Structural Genomics Approach. 2003 Acta Crystallographica Section D Biological Crystallography;59(1):127–135.

[416] Takahashi S, Araki Y, Ohya Y, Sakuno T, Hoshino SI, Kontani K, et al. Upf1 Potentially Serves as a RING-Related E3 Ubiquitin Ligase via Its Association with Upf3 in Yeast. 2008 RNA;14(9):1950–1958.

[417] Chien CT, Bartel PL, Sternglanz R, Fields S. The Two-Hybrid System: A Method to Identify and Clone Genes for Proteins That Interact with a Protein of Interest. 1991 Proceedings of the National Academy of Sciences of the United States of America;88(21):9578–9582.

[418] Zhu L. Yeast GAL4 Two-Hybrid System. In: Tuan RS, editor. Recombinant Protein Protocols: Detection and Isolation. Methods in Molecular Biology™. Totowa, NJ: Humana Press; 1997. p. 173–196.

[419] Guo D, Rajamäki ML, Valkonen J. Protein–Protein Interactions: The Yeast Two-Hybrid System. In: Foster GD, Johansen IE, Hong Y, Nagy PD, editors. Plant Virology Protocols: From Viral Sequence to Protein Function. Methods in Molecular Biology™. Totowa, NJ: Humana Press; 2008. p. 421–439.

[420] Sollier J, Driscoll R, Castellucci F, Foiani M, Jackson SP, Branzei D. The Saccharomyces Cerevisiae Esc2 and Smc5-6 Proteins Promote Sister Chromatid Junction-Mediated Intra-S Repair. 2009 Molecular Biology of the Cell;20(6):1671–1682.

[421] Chen YH, Choi K, Szakal B, Arenz J, Duan X, Ye H, et al. Interplay between the Smc5/6 Complex and the Mph1 Helicase in Recombinational Repair. 2009 Proceedings of the National Academy of Sciences;106(50):21252–21257.

[422] Mankouri HW, Ngo HP, Hickson ID. Esc2 and Sgs1 Act in Functionally Distinct Branches of the Homologous Recombination Repair Pathway in Saccharomyces Cerevisiae. 2009 Molecular Biology of the Cell;20(6):1683–1694.

[423] Shin S, Hyun K, Kim J, Hohng S. ATP Binding to Rad5 Initiates Replication Fork Reversal by Inducing the Unwinding of the Leading Arm and the Formation of the Holliday Junction. 2018 Cell Reports;23(6):1831–1839.

[424] Ismail IH, Gagné JP, Genois MM, Strickfaden H, McDonald D, Xu Z, et al. The RNF138 E3 Ligase Displaces Ku to Promote DNA End Resection and Regulate DNA Repair Pathway Choice. 2015 Nature Cell Biology;17(11):1446–1457.

[425] Heath RJ, Goel G, Baxt LA, Rush JS, Mohanan V, Paulus GLC, et al. RNF166 Determines Recruitment of Adaptor Proteins during Antibacterial Autophagy. 2016 Cell Reports;17(9):2183–2194.

[426] Giannini AL, Gao Y, Bijlmakers MJ. T Cell Regulator RNF125/TRAC-1 Belongs to a Novel Family of Ubiquitin Ligases with Zinc Fingers and an Ubiquitin-Binding Domain. 2008 The Biochemical journal;410(1):101–111.

[427] Styles EB, Founk KJ, Zamparo LA, Sing TL, Altintas D, Ribeyre C, et al. Exploring Quantitative Yeast Phenomics with Single-Cell Analysis of DNA Damage Foci. 2016 Cell Systems;3(3):264–277.e10.

[428] Weill U, Yofe I, Sass E, Stynen B, Davidi D, Natarajan J, et al. Genome-Wide SWAp-Tag Yeast Libraries for Proteome Exploration. 2018 Nature methods;15(8):617–622.

[429] de Godoy LMF. SILAC Yeast: From Labeling to Comprehensive Proteome Quantification. In: Martins-de-Souza D, editor. Shotgun Proteomics: Methods and Protocols. Methods in Molecular Biology. New York, NY: Springer; 2014. p. 81–109.

[430] Choi-Rhee E, Schulman H, Cronan JE. Promiscuous Protein Biotinylation by Escherichia Coli Biotin Protein Ligase. 2004 Protein Science;13(11):3043–3050.

[431] Williams CC, Jan CH, Weissman JS. Targeting and Plasticity of Mitochondrial Proteins Revealed by Proximity-Specific Ribosome Profiling. 2014 Science;346(6210):748–751.

[432] Putyrski M, Schultz C. Protein Translocation as a Tool: The Current Rapamycin Story. 2012 FEBS Letters;586(15):2097–2105.

[433] Sarkar S, Davies AA, Ulrich HD, McHugh PJ. DNA Interstrand Crosslink Repair during G1 Involves Nucleotide Excision Repair and DNA Polymerase ζ. 2006 The EMBO Journal;25(6):1285–1294.

[434] Hicks JK, Chute CL, Paulsen MT, Ragland RL, Howlett NG, Guéranger Q, et al. Differential Roles for DNA Polymerases Eta, Zeta, and REV1 in Lesion Bypass of Intrastrand versus Interstrand DNA Cross-Links. 2010 Molecular and Cellular Biology;30(5):1217–1230.

[435] Simon MN, Churikov D, Géli V. Replication Stress as a Source of Telomere Recombination during Replicative Senescence in Saccharomyces Cerevisiae. 2016 FEMS Yeast Research;16(7).

[436] Juríková M, Danihel Ľ, Polák Š, Varga I. Ki67, PCNA, and MCM Proteins: Markers of Proliferation in the Diagnosis of Breast Cancer. 2016 Acta Histochemica;118(5):544–552.

[437] Ceppi P, Novello S, Cambieri A, Longo M, Monica V, Iacono ML, et al. Polymerase η mRNA Expression Predicts Survival of Non–Small Cell Lung Cancer Patients Treated with Platinum-Based Chemotherapy. 2009 Clinical Cancer Research;15(3):1039–1045.

[438] Xie K, Doles J, Hemann MT, Walker GC. Error-Prone Translesion Synthesis Mediates Acquired Chemoresistance. 2010 Proceedings of the National Academy of Sciences;107(48):20792–20797.

[439] Herce HD, Rajan M, Lättig-Tünnemann G, Fillies M, Cardoso MC. A Novel Cell Permeable DNA Replication and Repair Marker. 2014 Nucleus;5(6):590–600.

[440] Plückthun A. Designed Ankyrin Repeat Proteins (DARPins): Binding Proteins for Research, Diagnostics, and Therapy. 2015 Annual Review of Pharmacology and Toxicology;55(1):489–511.

[441] Michel MA, Swatek KN, Hospenthal MK, Komander D. Ubiquitin Linkage-Specific Affimers Reveal Insights into K6-Linked Ubiquitin Signaling. 2017 Molecular Cell;68(1):233–246.e5.

[442] McMahon C, Baier AS, Pascolutti R, Wegrecki M, Zheng S, Ong JX, et al. Yeast Surface Display Platform for Rapid Discovery of Conformationally Selective Nanobodies. 2018 Nature Structural & Molecular Biology;25(3):289–296.